ICMRM 2009

10th International Conference on Magnetic Resonance Microscopy

"The Heidelberg Conference"

& the 9th Colloquium on Mobile NMR

Book of Abstracts

www.icmrm10.montana.edu

Agenda for Sunday, August 30th

9 AM	Bus departs from Grantree Inn, Bozeman and arrives 11am Holiday Inn, West Yellowstone			
10 AM	REGISTRATION OPENS			Holiday Inn
11.30 AM	Buffet Lunch			Holiday Inn

Time	Session (Chair)	No.	Presenter	Title
12:30 - 2:30 PM	**Tutorials I** (Sarah Codd)			
40 min		Tu1	Louis Bouchard	Introduction To Modern NMR Experiments
40 min		Tu2	Siegfried Stapf	Excuse Me, Can You Take A Picture Of Me?
40 min		Tu3	Martin Hürlimann	2D Correlation Measurements Of Relaxation And Diffusion
3 - 5 PM	**Tutorials II** (Sarah Codd)			
40 min		Tu4	Luisa Ciobanu	Introduction To Flow And Diffusion Magnetic Resonance Measurements With Application In Micro-Environments
40 min		Tu5	Mike Johns	Rapid Measurement Of Flow And Diffusion Using Magnetic Resonance
40 min		Tu6	Peter Blümler	Mobile NMR
5:30 - 8 PM	**Welcome Reception and Talk Sponsored by:**		Eiichi Fukushima	**Union Pacific Dining Hall**

Agenda for Monday, August 31st

7 - 8:45 AM   Continental Breakfast

8:45 - 9 AM   Welcome Address by Sarah Codd

Time	Session (Chair)	No.	Presenter	Title
9 - 10:30 AM	**High Field I** (Paul Callaghan)			
25 min		T1	Lynn Gladden	Imaging Flows: From Microns To Metres Per Second
25 min		T2	Bruce Balcom	Materials MRI With Pure Phase Encode Spin Echoes
20 min		T3	Steve Beyea	Spiral In Vs. Out: It's All About The Journey
20 min		T4	Nadia Amor	Low-Power MRI By Polyphase Perfect Sequence Excitation
11 - 12:35 PM	**High Field II** (Paul Majors)			
25 min		**T5**	Ute Goerke	Novel Approaches To Functional Magnetic Resonance Imaging At Ultra-High Magnetic Field Strength
25 min		T6	Federico Casanova	Flow Imaging Employing A Single-Shot Encoding: The FLIESSEN Sequence
25 min		T7	Melanie Britton	Applications Of Magnetic Resonance Imaging To Visualise Chemistry
20 min		T8	D. van Dusschoten	NMR Microscopy T2 Mapping At High Resolution
12:35 - 2 PM	Buffet Lunch			Executive Committee Meeting
2 - 3:30 PM	**Material Science Applications** (Steven Beyea)			
25 min		T9	Igor Koptyug	MRI Of The Preparation Of Supported Catalysts
25 min		T10	Jeffrey Reimer	Hyperpolarized 13C NMR In Diamond Via Optical Pumping
20 min		T11	Sergey Dvinskikh	MRI Of Swelling, Sedimenting, Adsorbing And Drying Materials
20 min		T12	Nikolaus Nestle	Gaining Practical Profile: NMR Profiling Of Industrial Polymer Composites

4 - 6 PM   **Poster Session 1**

6 - 8 PM   Light Evening Meal

Agenda for Tuesday, September 1st

7 - 9 AM   Continental Breakfast

Time	Session (Chair)	No.	Presenter	Title
9 - 10:30 AM	**Flow/Diffusion** (Joseph Seymour)			
25 min		T13	Ben Newling	Phase Encoding Phast Phlows
25 min		T14	Steve Altobelli	Searching For Flow Disturbances High And Low
25 min		T15	Andrew Sederman	Rapid Measurement Of Transient Velocity Evolution Using GERVAIS
15 min		T16	Mark Hunter	Measurement And Simulation Of The Non-Local Dispersion Tensor In Porous Media
11 - 12:30 AM	**In-Vivo/Biological/Biomedical Applications I** (Peter Basser)			
25 min		T17	Henk Van As	Laurel MRI: Flow Characteristics And Exchange In Complex Biological Systems As Observed By PFG-MRI
25 min		T18	Russell Jacobs	Simultaneous μPET And μMRI
20 min		T19	Mark Henkelman	Finding Phenotypes By High Throughput MR Microscopy
20 min		T20	Yang Xia	T2 Anisotropy In The Superficial Articular Cartilage
12:30 - 2 PM	Buffet Lunch			Division Committee Meeting
2 - 3:30 PM	**In-Vivo/Biological/Biomedical Applications II** (Peter Basser)			
25 min		T21	Stephen Blackband	MR Microscopy At The Mammalian Cell Level
25 min		T22	Evren Özarslan	Characterization Of Tissue Microstructure Using Porous Media Concepts
20 min		T23	Subramanian, Sankaran	Electron Paramagnetic Resonance Imaging Of Tumor Oxygen Status In Vivo
20 min		T24	Hadassah Shinar	2H Double Quantum Filtered NMR Studies Of Water Compartmentation In Sciatic And Optic Nerves

4 - 6 PM   **Poster Session 2**

6 - 8 PM   Light Evening Meal

Agenda for Wednesday, September 2nd

7 - 8:30 AM   Continental Breakfast

Time	Session (Chair)	No.	Presenter	Title
8:30-10:15 AM	**Mobile/Low Field NMR I** (Bruce Balcom)			
25 min	25	T25	Bernhard Blümich	The NMR Machine: A Convenience Tool?
25 min	25	T26	Andrew McDowell	Living With Ultracompact NMR Magnets
20 min	20	T27	Lizhi Xiao	A Two-Dimensional NMR Method Of Probing The Internal Field Gradients In Rocks
20 min	20	T28	Meghan Halse	Quantitative Analysis Of Earth's Field NMR Spectra Of Tightly-Coupled Heteronuclear Systems
15 min	15	T29	Kristl L. Adams	ON-Line Coupling Of Capillary Electrophoresis With Portable NMR Detection For Pharmaceutical And Environmental Exposure Applications
10:40-12:15 P	**Mobile/Low Field NMR II** (Bernhard Blümich)			
20 min		T30	Vasiliki Demas	Portable Magnetic Resonance For Medical Diagnostics
20 min		T31	Katsumi Kose	Development Of A Portable MRI System For Fruits And Trees
20 min		T32	Stephan Appelt	New Developments Of Low Field NMR
20 min		T33	Dimitris Sakellariou	Permanent Magnets For NMR And MRI
15 min		T34	Carel Windt	The NMR-CUFF: From Concept To Portable Plant Imager

12:15 PM   Packed Lunches available for pickup

12:30-7 PM   Excursion to Yellowstone Park

7 - 9 PM   **Western BBQ Buffet
Sponsored by:**

Agenda for Thursday, September 3rd

8 - 10:30 AM **Poster Session 3** w/ Hot Buffet Breakfast

Time	Session (Chair)	No.	Presenter	Title
10:30-12:30 A	**Young Investigators** (Kevin Minard)			
20 min		T35	Tyler Brosten	Characterization Of Complex Cellular Structures Through Displacement Correlations Measured Using PGSE NMR
20 min		T36	Ernesto Danieli	Compact Magnet Array For High-Resolution NMR And MRI With Portable Sensors
20 min		T37	Stefan Gloeggler	High-Resolution-NMR Below 200 Khz
20 min		T38	Daniel Holland	Velocity Imaging Using Compressed Sensing
20 min		T39	Prodromos Parasoglou	Accurate Reconstruction Of Under-Sampled Images With Compressed Sensing And Dynamic Filtering
20 min		T40	Chunqi Qian	Broadband Volume Coil For MR Microscopy At 900 MHz

12:30 - 2 PM Buffet Lunch

Time	Session (Chair)	No.	Presenter	Title
2 - 3:35 PM	**Polarisation Enhancement Techniques and Applications** (Lynn Gladden)			
25 min		T41	David Lurie	Polarisation Manipulation In MRI By Magnetic Field-Cycling And DNP
25 min		T42	Gil Navon	Enhancement Of CEST And DNP By Idqc
15 min		T43	Vadim Zotev	Microtesla MRI With Dynamic Nuclear Polarization
15 min		T44	Mark Lingwood	Continuous Flow Dynamic Nuclear Polarization Of Water Under Ambient Conditions For In-Vivo Perfusion MRI
15 min		T45	Sandra Garcia	Overhauser Dynamic Nuclear Polarization At 0.04T

Time	Session (Chair)	No.	Presenter	Title
4 - 5:20 PM	**2D Relaxation and Diffusion Correlation Experiments** (Melanie Britton)			
25 min		T46	Paul Callaghan	A Brief History Of Double Wave-Vector Encoding
25 min		T47	Yi-Qiao Song	2D NMR And Laplace Inversion
15 min		T48	Jonathan Mitchell	Determining Pore Sizes From T2-T2 Exchange Measurements
15 min		T49	Kathryn Washburn	Characterization Of Rock Cores By Sodium NMR

5:20 - 5:50 PM **General Meeting**
6:30 - 10 PM **Conference Dinner**

Agenda for Friday, September 4th

	Happy Trails to You (Until We Meet Again)
4 AM	**Early bus departs Holiday Inn for 5:45 AM Bozeman Airport arrival**
8 AM	**Later bus departs Holiday Inn for 9:45 AM Bozeman Airport arrival**

Corporate Sponsorship of the 10th ICMRM

We gratefully acknowledge financial support from:

Gold Level:

MSU Vice President for Research
http://www.montana.edu

National Institute for Biomedical Imaging & Bioengineering
http://www.nibib.nih.gov

ACS Petroleum Research Fund
http://portal.acs.org

Silver Level:

Bruker Biospin
http://www.bruker-biospin.com

Varian NMR
http://www.varianinc.com

Rapid Biomedical
http://www.rapidbiomed.de

Bronze Level:

Pacific Northwest NATIONAL LABORATORY

magritek

SPiNLOCK MAGNETIC RESONANCE SOLUTIONS

SCANCO MEDICAL

act mobile nmr solutions

tecmag TECHNOLOGY FOR MAGNETIC RESONANCE

Schlumberger

Welcome to Doty Scientific

MRTe

ABQMR Innovations in Magnetic Resonance

T2Biosystems

J S RESEARCH INC. NMR PROBES AND SYSTEMS

m2m imaging

Book Prize Sponsors:

WILEY-VCH

OXFORD UNIVERSITY PRESS

SpringerLink

Westview

Welcome

Welcome to the 10th International Conference on Magnetic Resonance Microscopy (ICMRM10) in West Yellowstone, Montana. The ICMRM is the biennial meeting of the Spatially Resolved Magnetic Resonance (SRMR) Division of the AMPERE (*Atomes et Molécules Par Études Radio-Électrique*) Society. This year's conference represents 20 years of enhancing scientific knowledge, understanding and cooperation in spatially resolved magnetic resonance research. Mutual knowledge, understanding and cooperation, "*Se Connaitre, S'Entendre, S'Entraider*", is the motto of the AMPERE Society as proposed by Prof. René Freymann upon it's establishment in 1952.

The conference series began with "the Heidelberg Conference" in 1991 and 1993, and moved to Würzburg in 1995. Due to the diverse international character of the conference attendees the original Executive Committee of the SRMR Division sought the long term goal of having the conference rotate between Europe, North America and Asia to further the aim of international understanding and cooperation. Since ICMRM4 in Albuquerque (New Mexico) the conference has been held in Heidelberg, Nottingham, Snowbird (Utah), Utsunomiya (Japan), Aachen, returns to North America in Montana this year and is scheduled for Beijing (China) in 2011, fulfilling the goals of the early Division leaders and reflecting the continued international nature of the field. The success of the conference is also evidenced by three edited books published in 1991, 1998 and 2009.

The international character of the field is reflected in this year's conference with 160 attendees from 15 countries, delivering 6 educational tutorials, 49 oral research presentations and 99 poster research presentations. Details of the schedule are found within these pages. Of note is the Young Investigators session whose 6 finalists were chosen by a special committee based on the quality and innovativeness of their submitted abstracts. The winner of the Young Investigator Award will be announced at the Conference Dinner Thursday night.

The local organizers welcome you to Montana to share in mutual knowledge, understanding and cooperation in spatially resolved magnetic resonance science and of the beautiful natural environment surrounding us. Montana is a land of rivers, mountains and wildlife, a place where grizzly bears, wolves and elk still roam free. As part of the American Western frontier, Montana was explored and settled by rugged individualists who knew the necessity of cooperation. Let's consider, here among the unique natural wonders of the Yellowstone ecosystem, in this land that is still a frontier of nature, the frontiers and development of our diverse and active field of research.

"It seems to me that Montana is a great splash of grandeur. The scale is huge but not overpowering. The land is rich with grass and color, and the mountains are the kind I would create if mountains were ever put on my agenda." John Steinbeck, *Travels with Charley, In Search of America*

Division of Spatially Resolved Magnetic Resonance of AMPERE Society

The Division was founded in 1995 during the 3rd meeting on Magnetic Resonance Microscopy. The purpose of the division is to advance the subject of Spatially Resolved Magnetic Resonance by means of the International Conference organized biennially across the world and symposia, summer schools and workshops. The governing organization of the Division consists of the Executive Committee, the Division Committee and the General Membership composed of conference attendees who are automatically members of the AMPERE Society.

Executive Committee Meeting:

The Executive Committee is responsible for the management, administration and finances of the SRMR Division

The following members of the Executive Committee are asked to attend the Executive Committee Meeting

Chair	Bernhard Blümich
Vice Chair	Paul Callaghan
Treasurer	Henk Van As
Secretary General	Joseph Seymour
Vice Secretary General	Igor Koptyug
Past Conference Chair	Peter Bluemler
Conference Chair	Sarah Codd
Past Chair	Eiichi Fukushima
Advisors	Axel Haase, Rainer Kimmich

The meeting will take place in Electric/Faithful room of the Holiday Inn during the Monday lunch break. Lunch will be provided.

Division Committee Meeting:

The Division Committee is responsible for carrying out the business of the Division, including the scientific organization of the conference.

The following members of the Division Committee are asked to attend the Division Committee Meeting.

All above members of the Executive Committee

(2007-2009)	A. Coy	K. Kose	Y. Seo		
(2005-2009)	S. Altobelli	B. Balcom	M. Barbic	P. Blümler	D. Gross
	K. Hayamizu	M. Johns	Y.-Y. Lin	R. Mair	J. Reimer
	K. Saito				
(2003-2009)	S. Beyea	M. Conradi	F. Grinberg	T. Haishi	S.-I. Han
	R. Jacobs	W. Köckenberger		D. Kuethe	P. McDonald
	K. Minard	G. Navon	K. Ogawa	P. Prado	B. Saam
	Y.-Q. Song	S. Stapf	Y. Xia		

The meeting will take place in the Holiday Inn immediately after the morning session at 12.30 on Tuesday. The lunch buffet will be available afterwards.

General Meeting:

The General Meeting has the final authority of the Division. All conference attendees are automatically members of the General Meeting and are encouraged to attend.

The General meeting will take place in the same room as the oral presentations on Thursday afternoon at 5.20 PM

Conference General Information

Organizing Committee:
Sarah Codd (Chair)   Montana State University
Steven Beyea   National Research Council, Halifax, Canada
Paul Majors   Pacific Northwest National Laboratory
Kevin Minard   Pacific Northwest National Laboratory
Joseph Seymour   Montana State University

Montana State University Student Helpers:
Amber Broadbent   Tyler Brosten   Loribeth Evertz   Hilary Fabich
Einar Fridjonsson   Erik Rassi   Sarah Vogt

Staff:
Kristen Griffin   Mountain Destinations, Bozeman
Katie Walters   Mountain Destinations, Bozeman
Austin Jacobs   Montana State University

Venues (see maps also)
> Holiday Inn   Registration, oral sessions, continental breakfast buffet, coffee beaks, lodging, excursion departure, shuttle bus arrival and departure
> Union Pacific Dining Hall   Reception, poster sessions, exhibitors, lunch buffet, dinners and evening socializing
> Yellowstone Lodge   Overflow lodging

Registration desk:
The registration desk will be attended by student helpers throughout the meeting. However registration assistance will only be available during the following times.
Sunday, August 30   10:00am - 5:00pm
Monday, August 31   7:00am - 2:00pm
Tuesday, September 1   7:00am - 9:00am
Wednesday, September 2   7:00am - 8:30am
Thursday, September 3   7:00am - 9:00am

Conference Phone:
There is no specific conference phone. Please call the Holiday Inn front desk 406-646-7365.

Wireless Access:
Wireless is available throughout the Holiday Inn. Instructions should be found in your hotel rooms. For additional assistance please see the Holiday Inn front desk.

Events

Welcome Reception:
The welcome reception has been sponsored by Bruker Biospin and will start at 5.30pm on Sunday Evening in the Union Pacific Dining Hall. There will plenty of H'or Doevres, a bar where you can use cash or redeem your drink tickets, and a talk by Eiichi Fukushima.   Eiichi's talk will start at 6pm.

Meal Locations:
All registered attendees are invited to join all meals, which are included in your registration fees. Daily continental breakfast and coffee breaks will be served in the Electric/Faithful Room at the Holiday Inn.
The Welcome Reception, daily lunches, dinners, BBQ and Conference Dinner will be held at the Union Pacific Dining Hall, directly across the street from the Holiday Inn.
For non-registered guests, a limited number of additional meal tickets are available for purchase from the registration desk for the reception, dinners and BBQ.

Excursion
Busses will depart between 12.30 and 1pm outside the Holiday Inn on Wednesday. Remember to collect your packed lunch from the Holiday Inn before you leave, and an additional snack will be provided on the tour. The tour includes all gratuities and park entrance fees.   Some tickets may still be available from the conference registration desk at $75 each. The tour will return to the Union Pacific Dining Hall in time for a Western BBQ Buffet.

The Conference Dinner
A wonderful locally themed buffet with wine provided will begin at 6.30pm on Thursday evening. All the Young Investigators will be recognized and the winner announced. The winners of the Student Poster Competition and the Image Beauty Competition will be announced. Tickets for non-registered guests can be purchased from the registration desk but only until noon on Monday.

Drink Tickets
Drink tickets have been provided with your name badge. These drink tickets can be transferred amongst participants and can be redeemed each night at the bar in the Union Pacific Dining Hall. These drink tickets include gratuities.
Additional drinks can be purchased at the bar in the Union Pacific Dining Hall and gratuities are included.
Free non-Alcoholic beverages are available at the bar during evening events.

Additional Dining and Bar Options
There are a few additional dining and bar options in West Yellowstone including the Holiday Inn. Please see the hotel front desk. Prices for meals and drinks purchased at restaurants do not include gratuities which in the USA are usually 18%.

Presentation and Competition Instructions

Instructions for Oral Presentations:
The duration of individual talks are listed in the program. Please time your talk so that you allow time for approximately 5 minutes of questions and discussion.   A technical assistant (Austin Jacobs) will be available 30 minutes before sessions if you wish to load your presentation to the communal laptop or test your own laptop for compatibility. Please try and test your presentation the day before your session

Instructions for Posters
Posters can stay up for the whole conference, from 11am Sunday until 1pm on Thursday.
The poster session location is in the Union Pacific Dining Hall directly across the road from the Holiday Inn
The board you have to attach to will be 3 ft wide by 5ft high. However your poster can overflow to one side and above and below this space, but it will not have a surface to attach this overflow to.   Pins are available in the Union Pacific Dining Hall.

Poster Session 1   Odd numbered posters
Poster Session 2   Even numbered posters
Poster Session 3   All posters

Student Poster Competition
Please collect and attach a yellow label identifying your poster as eligible for this competition. You must be a student presenter to be eligible. You must attend your poster during the final poster session 3.

Image Beauty Competition
This is a competition for the most beautiful artwork created from spatially resolved MR data. Submission can be made anonymously at the conference by posting on a designated board in the Union Pacific Dining Hall. . The winner will be announced and receive an award at the conference dinner. Anything goes, artefacts and all - as long as it uses spatially resolved MR data. Don't forget to give your artwork a title.

Instructions for Exhibitors
The exhibit table location is in the Union Pacific Dining Hall directly across the road from the Holiday Inn.
Setup can begin Sunday, August 30 from 10:00am
Tear down must be completed by 5:00pm on Thursday, Sept. 3

Venues
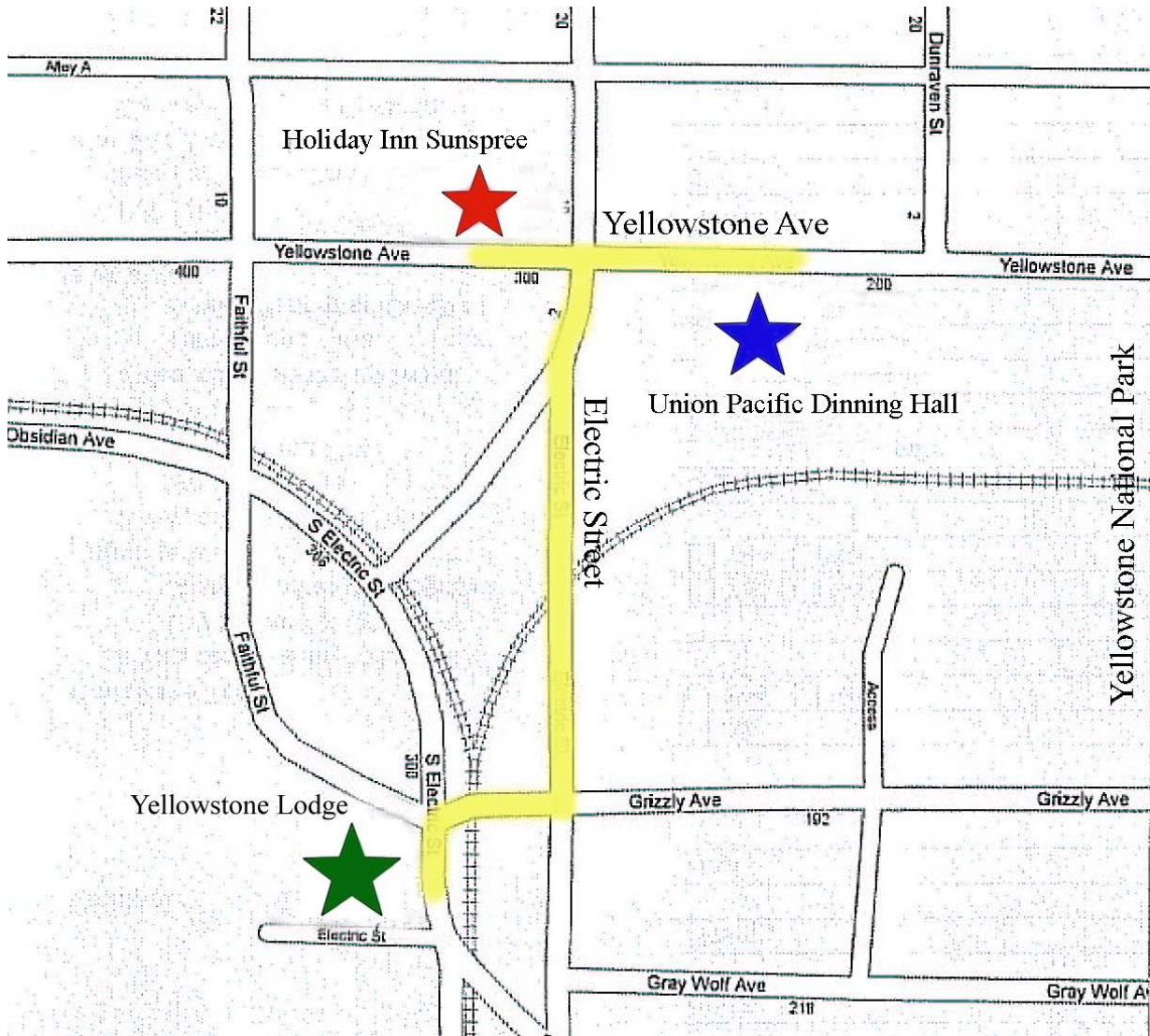
Venues
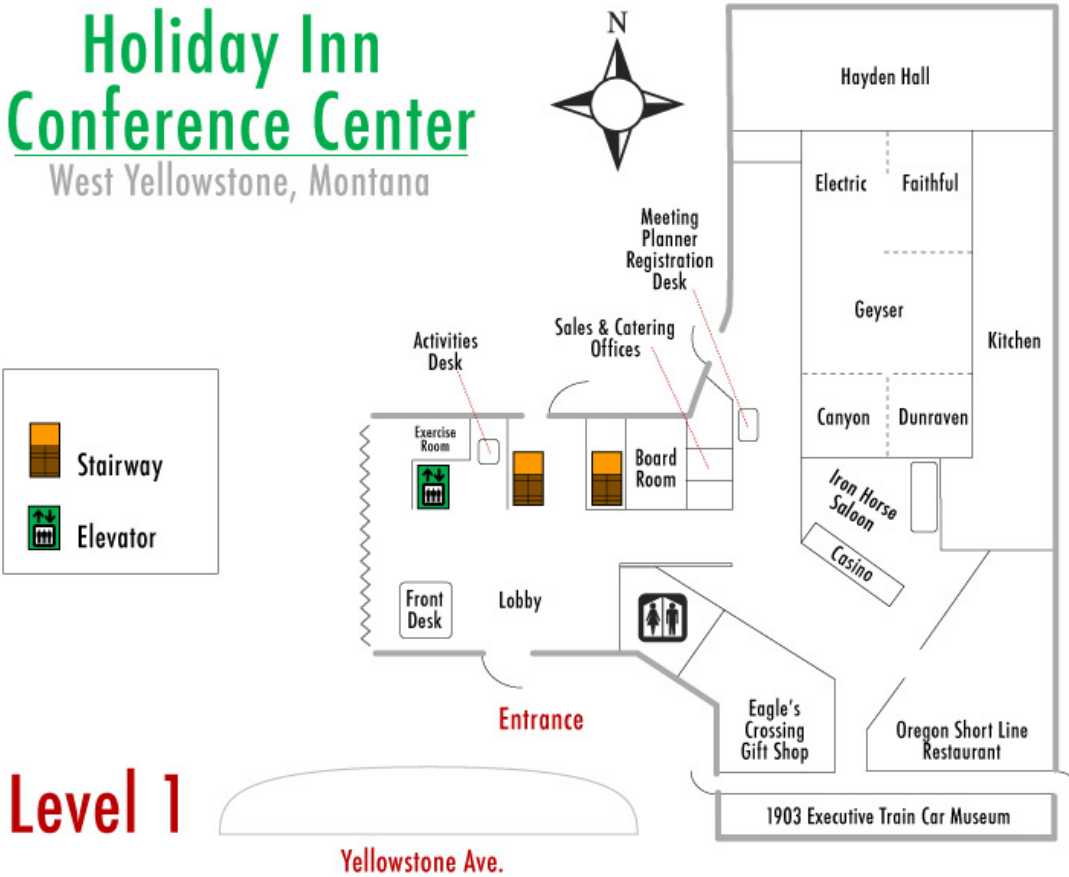
Oral presentations will take place in the Geyser/Canyon/Dunraven rooms

Breakfast and breaks will take place in the Electric/Faithful room.

Opening Reception Talk
Eiichi Fukushima

This is what I wrote out in preparation for a talk at the opening reception at the 10th International Conference on Magnetic Resonance Microscopy. I kept rearranging this talk until the last minute so what is written here is not the talk I gave but forms the ingredients for much of the talk; I took out a fair fraction of this material in order that the talk not ramble too much. Perhaps the readers will find a bit more of the historical material in this written version compared to the actual talk I gave.

These personal (or personally experienced) stories are not just to entertain but also to possibly call your attention to some aspects of our field of magnetic resonance that are not commonly known (or at least not commonly practiced).

By the time I came along, NMR was already established as a sophisticated tool in analytical and organic chemistry albeit of more limited use than now before the advent of pulse-FT NMR. In physics, it was of interest by itself with applications such as ferroelectricity, electronic structure of intermetallic compounds, and various phase transitions.

The first I heard of NMR was at a lecture by Ed Purcell a few years after his Nobel Prize. I also heard a lecture the same year by Polycarp Kusch so naturally thought that Nobel Prizes were commonplace and that the awardees gave very clear talks about their fields. I had no idea that those two lectures would be a significant fraction of all Nobel laureate's' talks that I'd hear in my life and that I would be working in the field of NMR shortly after listening to Purcell's lecture.

When I joined the group of Edwin Uehling as a grad student, there had been a recent paper that discussed the way spin-temperature diffused to paramagnetic impurities in solids. It was claimed that non-exponential spin-lattice relaxation, specifically √t dependence, was observed and Ed expressed doubts about this result and wanted me to double check it. This became my thesis project.

Ed Uehling had been one of George Uehlenbeck's students in the '30s and studied vacuum polarization in the heyday of early modern physics and field theory. He worked on RADAR in the Manhattan Project and was one of many physicists to come out of WW-II ready to apply the newfound knowledge that led to the rapid development of radiofrequency spectroscopy such as NMR and NQR. Hans Dehmelt, a co-inventor of NQR and who won the Nobel prize in 1989 for single electron trapping, was next door so there was a small but solid island of rf spectroscopy in the sea of nuclear physics that was the department at University of Washington.

Interestingly, Ed Uehling, in his 25-30 years as a theoretical physicist, never had a theoretical student until his last student just before he retired. All of us experimental students felt Ed could suggest (which is tantamount to an assignment) a problem that he thought was a good one (and it invariably was) without regard for potential experimental difficulties. Thus, whenever a new student came back from a conference with Ed, the grad students in the group would gather round to see what problem was suggested to him (there

Opening Reception Talk

were no women students when I was there) and offer suggestions on how to tackle it, starting from what equipment needs to be built. [Such conferences were quite infrequent. When I visited the group to see if I wanted to join it, the blackboard had a row of check marks – perhaps a dozen – along the top. Each check represented a visit to the lab by Ed, except for the one with an asterisk which signified the time Ed returned to fetch his glasses.]

This rather unusual arrangement of having a theorist manage experimental students had its plusses and minuses. One thing for sure; students had to became proficient at experimental NMR or else.

The common readings assigned to physics grad students in NMR were by Raymond Andrew, Saha & Das, Nicholas Bloembergen's thesis, as well as the pioneering articles by Bloch, Hansen, & Packard, and Bloembergen, Purcell, & Pound, called BPP. Abragam's book came out during my grad student years and instantly became required reading for all students in our group – and no doubt in other NMR groups, too.

The vast majority of NMR being performed in those years was CW NMR. The phrases bandied about the lab included Pound box (for Pound oscillator), Robinson oscillator, and 304TL. (I leave as an exercise for you to figure out why it was common to hear about 304TLs in NMR labs.) I remember a colleague building a marginal oscillator and having a lot of trouble with noise pick up. The noise had an unusual time dependence that caused someone to suggest connecting a speaker to the receiver and, to everyone's surprise, there was someone being interviewed on the campus radio station. This made no sense because the station was FM and the marginal oscillator had no capability to demodulate FM. My colleague left in disgust only to find the interview taking place immediately outside the lab with a mobile truck nearby to relay (by an AM link) the interview to the station.

My assignment requiring the measurement of non-exponential relaxation of spins needed a pulse NMR apparatus because the only way to measure relaxation with marginal oscillators was by saturating the signal by increasing the B1 field and it was difficult to tell if the recovery was exponential or not. I remember seeing a bibliography of publications relating to pulsed NMR, published by a little known company named Bruker. It was maybe two typewritten pages or less. Imagine that.

I was helped in the task of designing the instruments by Hank Silsbee, who had measured the nuetron magnetic moment with Bill Nuernberg. He would
design a power supply or an amplifier or whatever I asked for on a napkin. He would do this from scratch being familiar with vacuum tube characteristics; when he finished, the design on the napkin was complete – nothing had to be looked up. He helped us all in reducing the mystery of electronic circuits to understandable principles that we learned in classes.

One good thing about the clunky tubes was that you could not put too many on a chassis because of space and power limitations. So, the circuitry never got too complicated. I made a pulse generator that had perhaps enough flip-flops (each requiring two vacuum tubes) to generate a train of pulses as well as separate pulses to block the receiver and a pulse to

Opening Reception Talk

trigger an oscilloscope that constituted the detection system when augmented by a Polaroid camera.

Data acquisition consisted of our staring into the hood of a rather large Tektronix oscilloscope and visually and mentally signal averaging the FIDs. One could get surprisingly good at this task with practice. For more difficult data, for example, with low repetition rates, we would signal average on Polaroid film by turning down the oscilloscope's intensity so a single trace would barely register on the film. Now, if you leave the shutter open for many FIDs, the portions of the traces that landed on the same spots would add to brighten the image so you ended up with an averaged data set. We took so many Polaroid photos that 1) the lab smelled of acetic acid that was in the paste used to fix the prints and 2) the prints invariably curled so there were all these curled prints with parameters written in the back laying around the lab and desks. Minicomputers were unheard of; this was our data bank.

About the time I finished the pulse generator and its power supply, a treatise on how to build a pulse NMR apparatus by Gil Clark appeared in RSI. This was a fantastic coincidence and I built the transmitter and receiver according to Clark. I still remember that the receiver had three shielded tuned stages with ganged air-gap capacitors that gave the physics shop fits. Gil Clark visited the Uehling lab – for some reason, I was absent – and supposedly said I had out-Clark'ed his instrument. I am sure he was being complimentary of a green student but it is also true that it is always much easier to be the second one to do something than the first one.

I was a solid state physics graduate student in an era when NMR was not such a big deal as it became later. In those days, physics graduate student who did NMR had to make most of the components, sometimes including magnets and/or magnet power supplies. Furthermore, NMR was not considered to be a specialty field; those of us who did thesis projects using NMR did not necessarily expect to get jobs in NMR.

I went to Los Alamos and inherited a Varian DP-60 multipurpose CW machine that could do high res or broadband spectroscopy. However, with my inclinations to do T1 measurements, the first paper I published there was of a C-13 T1 measurement of KCN. KCN at room temperature is an ionic crystal with cubic arrangement of K+ and CN- with the nonspherical CN ions undergoing hindered rotations about their fixed positions. As I recall, there was controversy about this and it just happened that someone else in the lab had some C-13 labeled KCN for some other purpose that I could borrow. Even though the DP-60 was not the natural instrument for this purpose, I had to make do.

The DP-60 used a 14kG (=1.4T) electromagnet whose field was swept to produce spectra. There was a power supply that was as tall as I with a big Variac knob and a sweep-width range switch. One could set up the NMR experiment with the field set to somewhere off-center of the sweep width range and move the switch from one range to another to manually (and reproducibly) sweep the field and watch the adiabatic fast passage signal go by on an oscilloscope. The signal would be right-side-up or upside-down depending on the

Opening Reception Talk

delay between the forward and return sweeps. All one needed was a stopwatch to measure T1 provided it was within range of manual operation of the stopwatch.

The magnet itself was a thing of beauty and wonderment. It stood almost as tall as I, weighed many tons, and had pole pieces that were 12 inches in diameter with a gap of ~1-1/2 inches. The Varian service engineer was a big man. I distinctly remember his shimming the magnet using a rubber mallet (essentially a hammer) about the size of a football with a four-foot handle.

I turned over the DP-60 to the chemists after I succeeded in my assigned task to make the instrument useable to them so had to build up my own instrument. By then, I was hooked on my newfound knowledge of CW NMR – yes, about the time pulse NMR was coming into vogue after Ernst and Anderson's amazing scheme to enhance S/N by using minicomputers to do FTNMR – so I built up a CW system based on an excellent tranceiver made by the late Dave Torgeson. It was a significant upgrade of the DO-60 electronics that was designed to use the wideline Varian probes for DP-60.

I learned about mini-computers and bought myself a Data General Nova 1200 computer with 4K of 16-bit memory. (I remember the cost of the 15" square 4K memory board as being $4K.) We designed a stepper motor interface for the Varian magnet power supply called the Fieldial, a field-controlled (rather than current control as the high res magnets were) modern magnet for solid state NMR. We just added a gear to the shaft to the potentiometer that controlled the field sweep to connect the stepper motor. I recall making many measurements of quadrupole satellites and spin-spin coupled lines in appropriate solids with this setup while all other labs were gearing up to do FT NMR but not of broad lines as I was studying.

The Nova 1200 had a chopper stabilized power supply with some big ferrite chokes to filter out the ac. You could actually hear the chopper frequency that depended on the current load which changed a lot because the aforementioned $4K of memory consisted of 4096 ferrite cores with wires running through them and it took a lot of current to read from and write to them. We could tell what the pulse sequence was doing by listening to the computer, much like how you can tell the imaging sequence being run by the sound of the gradient pulses these days.

4K of memory was not enough to run a Fortran compiler so we wrote the programs in assembly language. The Nova had a two-pass assembler that took forever to input. We used a Teletype reader/printer that piled the paper tape on the floor. We got good at gingerly moving a large pile of tape that formed on the floor for each pass to the input side of the Teletype for the next pass. There was even a special tool to rewind such unruly piles of tape but we got pretty good at just arranging the tape in a pile so it would feed nicely without hanging up. The teletype reader checked for the sum of bits every 16 words and stopped when the check failed. We would have to reread such groups of bits and sometime it could take hours to successfully assemble a program. We got good at putting in dummy instructions (called no-ops) so minor changes could be inserted into the program without the need to reassemble.

Opening Reception Talk

I want to finish this welcome ramble with historical descriptions of unusual settings for NMR. Of course, we shall hear more examples during the conference because the use of NMR in extra-laboratory surroundings is increasing and a portion of this conference is devoted to such mobile NMR applications.

The oil industry has been using NMR to log wells for some years. It all started with Bob Brown's Earth's field efforts at Exxon and got a boost when Jasper Jackson proposed lowing permanent magnets downhole.

At past ICMRM meetings, we heard Paul Callaghan describe his trips to Antarctica to measure brine characteristics in sea ice. I don't care how serious the science might be – it still is a fantastic adventure to just go there where very few people ever go and wander around the ice among the penguins and skuas.

A few years ago, I visited Janez Stepisnik's Earth's field MRI "laboratory" in the woods outside Ljubljana. His group chose the idyllic setting of the countryside to get away from culture noise. This they succeeded in; the first MRI in Earth's field is to their credit. An unexpected bonus was to be shown the tank tracks left in the pavement in front of the "lab" – the legacy of the brief skirmish with the Yugoslav army tanks 18 years ago.

Many of us have also seen videos of Stefan Appelt and his co-workers running through the forest with a prepolarized sample to the low field detection apparatus.

Some of you have heard my descriptions of the subsurface NMR measurements with 100 meter diameter surface coils in Siberia, true adventures for me. I shall not repeat that story here but would like to tell you a different NMR adventure story. About 25 years ago, I was sitting at a picnic table at a NMR Gordon Conference when Al Garroway asked if I would be interested in joining him to evaluate an FAA funded project at Southwest Research Institute to build a dynamite detector for checked airline baggage by NMR. It sounded preposterous but Al is a respectable NMR scientist and I agreed.

This was my first exposure to truly extra-laboratory and industrial application of NMR and changed the way I think about NMR. I will tell you a bit about this project because it was very instructive to me. The NMR effort at SwRI had been going on for much longer than we in the academic (or non-industrial) community were aware of. It began with Bill Rollwitz, a very smart electrical engineer, who heard or read about NMR in a popular magazine after learning electronics in the US Army. He tried NMR on his own and built up an industrial NMR/NQR program at Southwest Research Institute in San Antonio, Texas over the years. This group did an amazing amount of development in the use of NMR for industrial applications. They developed, among other things, a one-sided NMR for monitoring drying of concrete, measuring the moisture distribution of farm fields (for NASA!!), and the aforementioned explosives detection.

The objective of this detector was to find dynamite in checked airline baggages. [You have to remember that we are now talking about 1985 or even before.] Bill Rollwitz and

Opening Reception Talk

colleagues decided the best way to do this is by proton NMR of dynamite which is characterized by very long T1 and very short T2. [Of all the materials they surveyed that passengers might carry on an airplane, only cocaine and some forms of silicon rubber overlapped with dynamite in these parameters, as I recall.] So, the detection of dynamite signal took place by rapidly repeating solid and Hahn echoes and subtracting the FIDs which would select short T2 and long T1 signals. Now, imagine doing a solid echo experiment in a suitcase sized sample with 11 microsecond pi/2 pulses. Picture these folks around a table calculating how much power is required to produce those pulses on the backs of envelopes. When the answer comes out to be something like 1.5 million watts, most, if not all, of us in traditional NMR would have dismissed that idea but the SwRI folks just built the transmitter.

This 1.5 million watt transmitter was something to behold. Its final amplifier was an EIMAC tube that was ~10cm diameter and perhaps 20 cm high. I recall that the filament power dissipation was 2kW – the bottom of the ceramic tube glowed white even when the tube was idling! When Al and I first saw the apparatus, it did not produce any NMR signals and we were asked for help in diagnosing it. We finally found out what was wrong when we went back to the lab after dinner one night – the zipper on a softsided suitcase that was in the sample chamber was arcing all the way around with each RF pulse! A Faraday shield around the sample chamber solved this problem and allowed the observation of a good signal.

One more story about this instrument while I am on a roll. For reasons I cannot recall, we asked about the locations of the feedpoints in the parallel rf coil sections along the coil and Armando De Los Santos, the amicable chief engineer told us how to find them by putting our hands into the sample chamber along the walls. Al and I looked at each other while Armando did this and we could hear arcing sounds coming out of the chamber! Even through about 1cm of sulfur hexafluoride gas and the Faraday shield, the transmitter coil was arcing to his finger! It felt like someone slapping your fingers.

Some time later, Al and I spent several days under the terminal at the old Dallas/Ft. Worth airport in August, supposedly observing a reliability test of this apparatus. We could not simply observe while Armando and his assistant labored to run actual passengers' bags through this machine under 40C temperatures of typical Texas summer afternoons so we became temporary baggage handlers, too.

After the final report was written for the FAA, I heard that the machine was sent to Miami where it was tested for cocaine detection in flower boxes being imported from Columbia. I believe this was a Quantum Magnetics project but maybe someone in the audience knows this better.

Bill Rollwitz passed away some years ago and left an office full of papers including a few thousand page manuscript on industrial applications of NMR. I hope it gets published soon.

I wish to close this rambling reminiscence by making a connection to this series of wonderful conferences that is the ICMRM. As some of you remember, it was conceived by

Opening Reception Talk

Bernhard Bluemich and Winfried Kuhn and the first meeting was held in Heidelberg in 1991. I met Paul Callaghan for the first time then, even though we had corresponded earlier, and he introduced us to his great new book. What timing; it gave a big push to this meeting and the general area of spatially resolved NMR. A poignant memory of that meeting for me was the announcement by the session chair at the end of a morning session: Professor Blinc, please go home; your country needs you. Robert got up, left, and Slovenia attained its independence several months later. Everything is connected in this world and we cannot work in isolation.

I wish everyone a wonderful week of international discussion and collaboration.

Sunday August 30th Talks:

Tutorials I

Tutorials II

Tu1

Introduction to modern NMR experiments

Louis Bouchard[1]

[1] Department of Chemistry and Biochemistry, University of California, Los Angeles, CA, USA

Abstract:
I will present an introduction to the NMR experiment and attempt to cover a number of recent topics from the past 20 years which are not normally covered in standard introductory textbooks, such as long-range magnetic interactions, low field detection or techniques for inhomogeneous fields. This presentation will be in the form of an introductory tutorial and discussions during the presentation are welcome.

Tu2

Excuse me, can you take a picture of me?

Siegfried Stapf[1]

[1] Dept. of Technical Physics II, Institute of Physics, TU Ilmenau, Germany

Abstract:

Everybody has probably heard this familiar request. For those who are working in MRI and are dealing with non-MRI experts, the question has a different flavor. There is a general misconception that taking an MR image is about the same as shooting a photo with a 50 $ camera. Our usual answer therefore will not be, "stand over there and smile", but "let me think how I can cover k space appropriately!"

Other questions arising frequently are "why can you not look through metal", "what resolution does your tool give me", and "how long does it take?"

In this tutorial, the problem of traveling through k space (without getting lost) will be addressed from different points of view. Which are the visa requirements to cross from k space into real space (pitfalls of Fourier transformations)? What needs to be done to avoid the MRI version of "blurring" (motion compensation)? How can mysterious, hidden objects (such as metals) still be detected, and how are aliens being dealt with (i.e. which nuclei are accessible by MRI)? Finally, when it comes to taking a nice picture, contrast is everything – the art of MRI is mainly based on generating the desired contrast to highlight your best side.

Tu3

2d Correlation Measurements of Relaxation and Diffusion

Martin D. Hürlimann[1]

[1] Schlumberger – Doll Research, Cambridge MA, U.S.A.

Abstract:

Two dimensional correlation measurements between relaxation (T_1,T_2) and diffusion (D) have become an important technique for the characterization of a wide range of systems, ranging from biological systems to hydrocarbon bearing sedimentary rocks. Examples include the measurement of distribution functions such as T_1-T_2 [1], $T_1/T_2 - T_2$ [2], and $D - T_2$ [3], as well as exchange measurements such as $D - D$ [4], or $T_1 - T_1$ [5] measurements. These measurements probe the dynamics of molecules on the molecular level and are sensitive to the local environment. The techniques are particularly powerful for the characterization of heterogeneous systems. The experimental implementation of relaxation and diffusion measurements is much less demanding than that of conventional spectroscopy, as they do not require magnetic fields of high intensity or homogeneity. They are routinely performed in systems using permanent magnets and at Larmor frequencies in the range of a fraction of MHz to a few tens of MHz. In addition, the measurements are suited for ex-situ applications, i.e. situations where the sample is outside the apparatus.

The measurements are based on pulse sequences that are designed such that the resulting kernels describing the experiments are separable in the parameters of interest. This allows the extraction of multidimensional distribution functions using fast inverse Laplace transforms [6]. Since the inverse Laplace transform is an ill-conditioned problem, this inversion is intrinsically more difficult to perform than the familiar Fourier transform.

This talk will give an overview of the technique, discuss critical aspects of the data analysis, and present a number of applications.
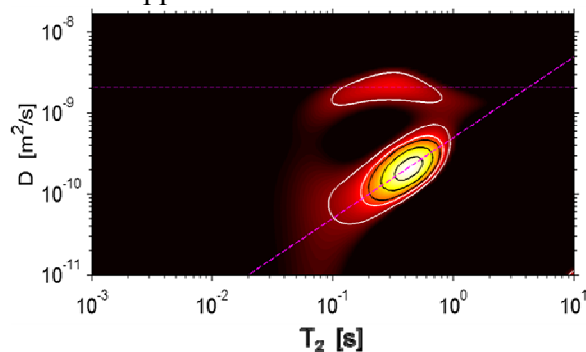
Fig. 1: Example of a diffusion – relaxation distribution function f(D,T_2) measured on a sedimentary rock saturated with a mixture of oil and water.

1. Y. Q. Song et al., *J. Magn. Reson.* **154** (2002) 261-268.
2. J. Mitchell et al. *J. Magn. Reson.* (2009), doi:10.1016/j.jmr.2009.07.002
3. M. D. Hürlimann et al., *J. Magn. Reson.* **157** (2002) 31-42.
4. P. T. Callaghan et al. *J. Chem. Phys.* **120** (2004) 4032-4048.
5. P. J. McDonald et al. *Phys. Rev. E* **72** (2005) 011409.
6. L. Venkataramanan et al. *IEEE Trans. Signal Processing* **50** (2002) 1017-1026.

Tu4

Introduction to Flow and Diffusion Magnetic Resonance Measurements with Application in Micro-Environments

Luisa Ciobanu

[1] NeuroSpin, CEA, Saclay, France

Diffusion and flow can be measured very accurately using NMR/MRI techniques. The study of these two phenomena has led to the development of the powerful techniques currently used in physics, chemistry, material science, biology, and medical science. The essence of diffusion/flow MR methods is that the molecular displacements induced by the presence of magnetic field gradients impart a phase spread to the spin transverse magnetization. Thus, information about molecular motion can be obtained by measuring the changes in the MRI signal due to this phase spread. In 1950 Hahn measured the self-diffusion of molecules for the first time [1], while in 1954 Carr and Purcell showed that NMR can be used to separate self-diffusion and flow [2]. The primary objective of this presentation is to introduce the basic NMR techniques for diffusion and flow measurements, and to give an overview of current and potential applications with emphasis on micro-environments. The second part of the talk is dedicated to the development of two novel diffusion techniques: Diffusion Enhancement of SIgnal and REsolution (DESIRE) [3] and Diffusion functional Magnetic Resonance Imaging (DfMRI) [4]. Once fully developed, these techniques will significantly enhance our understanding of the water diffusion process in biological cells and tissues.

1. Hahn E. L. *Phys. Rev.* **80** (1950) 580.
2. Carr H. Y. and Purcell E. M. *Phys. Rev.* **94** (1954) 630.
3. Ciobanu L., Webb A., Pennington C., *J.Magn.Reson*. **170** (2004) 252.
4. Le Bihan D. et al. *PNAS* **103** (2006) 8263.

Tu5

Rapid Measurement of Flow and Diffusion using Magnetic Resonance

Mike Johns[1]

[1] MRRC, Department of Chemical Engineering and Biotechnology, University of Cambridge

Abstract:

Magnetic resonance (MR) techniques have a unique ability to quantify mass transfer involving a liquid as determined by both convective flow and diffusion. This is predominately achieved by the effects of such transport on the NMR signal phase or phase distribution. By comparison with alternative measurement techniques (e.g. PIV, LDA) however, they conventionally offer a poor temporal resolution which has restricted their application to transient systems. The relatively recent emergence and incorporation of rapid MRI techniques has served to often address this limitation.

In this educational overview, we will discuss various alternatives for acquiring spatially resolved velocimetry data fast. This will focus predominately on both 'single shot' (e.g. EPI based pulse sequences) and usually 'multiple shot' (e.g. Rare based pulse sequences) acquisitions. We will consider the parameter space in which their application is possible and various practical considerations in their implementation. We will also briefly consider attempts to speed up this acquisition using sparse k-space sampling and appropriate image reconstruction. Fast acquisition of displacement propagators (and their moments) and application of MR techniques to fast flows will be discussed.

Fast self-diffusion measurement, both unresolved and spatially resolved, can be achieved using a variety of methods. A range of these will be presented including the use of Difftrain and multiple coherence pathways. Pros and cons of these various approaches will be considered against measurement requirements and desirables, as will practical limitations on their application.

Tu6

Mobile NMR

Peter Blümler

ICG-3: Phytosphere, Forschungszentrum Jülich GmbH, 52425 Jülich, Germany

Abstract:

This tutorial intends to give an overview and introduction to the following topics:

1) History of mobile NMR
2) Application of mobile NMR
3) Design Concepts:
    3.1) Unilateral Designs (Magnets, RF, Gradients)
    3.2) Surrounding Designs (Magnets, RF, Gradients)
    3.3) Dedicated Designs
4) Mobile Spectrometers and Amplifiers
5) Problems to be solved

Monday, August 31st Talks:

High Field I & II
And
Material Science Applications

T1

Imaging Flows: From microns to metres per second

L.F. Gladden , D.J. Holland, M.D. Mantle and A,J, Sederman

University of Cambridge, Department of Chemical Engineering and Biotechnology, Pembroke Street, Cambridge, CB2 3RA, U.K.

Abstract:
Understanding flow fields is of widespread interest and importance in physics, chemistry, biology and engineering. This contribution will report soem novel applications of magnetic resonance imaging to image flow fields in gases, liquids and solids. To address particular questions different approaches to the magnetic resonance data acquisitions are taken, and this talk will highlight the flexibility of magnetic resonance methods to give unique insights into hydrodynamic phenomena. The presentation will also include very recent work in which we have used compressed sensing techniques to increase our data acquisition times by up to an order of magnitude.

- imaging flow fields in single cell plants
- understanding defect formation during solidification
- bifurcation phenomena in laminar and time-dependent flows through a sudden expansion
- granular dynamics in vibro-fluidized beds
- 'speeding up' flow imaging

Materials MRI with Pure Phase Encode Spin Echoes

Bruce Balcom[1]

[1] MRI Research Centre, Department of Physics, University of New Brunswick, 8 Bailey Drive, Fredericton, New Brunswick, Canada, E3B 5A3

Abstract:

MRI is the most powerful and flexible diagnostic imaging method available to clinical medicine. MRI has the prospect of offering similar value to scientific studies in materials science. However, truly successful methods should report both spin density and local relaxation times. In previous work at UNB we have largely avoided the difficulties of multi exponential T_2 decay through pure phase encoded FID measurements with the SPRITE method. It is commonly observed, particularly in porous media, that multi exponential T_2 decay is reduced to single exponential T_2^* decay, with consequent simplification of the image quantification problem.

We continue to favor pure phase encode methods for materials imaging since spatial encoding in this manner is robust to underlying magnetic field gradients, and non-ideal magnetic field gradient waveforms – geometrically correct images are likely. The subject of this lecture will be recent work with pure phase encode, multi echo, spin echo imaging methods, where the echo time is very short (less than 1 msec). These methods permit spatially resolved T_2 mapping, including spatially resolved T_2 distributions, and spin density mapping.

Early stages in the development of these ideas will be reviewed[1,2,3] with an emphasis on recent work with two representative classes of materials. (i) Imaging thin film operational PEM fuel cells[4] and (ii) mapping fluid content in petroleum reservoir core plug samples[5]. In the first case high sensitivity and high resolution (10 micron resolution in less than 2 minutes) is the challenge. In the second case, T_2 distribution measurements of a quality similar to bulk CPMG measurement is the challenge.

1. Beyea, S. D., Balcom, B. J., Mastikhin, I. V., Bremner, T. W., Armstrong, R. L. and Grattan-Bellew, P. E. "Imaging of Heterogeneous Materials with a Turbo Spin Echo Single-Point Imaging Technique", *J. Magn. Reson.* (2000) 144, 255-265.
2. Cheng, Y., MacMillan, M. B., MacGregor, R. P. and Balcom, B. J."Direct Detection of Hydrocarbon Displacement in a Model Porous Soil with Magnetic Resonance Imaging", *Anal. Chem.* (2005) 77, 1824-1830.
3. Ouriadov, A. V., MacGregor, R. P. and Balcom B. J. "Thin Film MRI - High Resolution Depth Imaging with a Local Surface Coil and Spin Echo SPI", *J. Magn. Reson.* (2004) 169, 174-186.
4. Zhang, Z., Martin, J., Wu, J., Wang, H., Promislow, K. and Balcom, B.J."Magnetic Resonance Imaging of Water Content across the Nafion Membrane in an Operational PEM Fuel Cell", *J. Magn. Reson.* (2008) 193, 259-266.
5. Li, L., Han, H. and Balcom, B. J."Spin Echo SPI Methods for Quantitative Analysis of Fluids in Porous Media" *J. Magn. Reson.* (2009) 198, 252–260.

Spiral In vs. Out: It's All About the Journey

K. D. Brewer[1,3], J.R. Rioux[1,3], C. V. Bowen[1-3], and S. D. Beyea[1-3]

Department of Physics[1] & Radiology[2], Dalhousie University, Halifax, Canada,
[3]Institute for Biodiagnostics (Atlantic), National Research Council of Canada, Halifax, Canada,

Abstract:
The presence of large susceptibility-induced field gradients (SFGs) leads to signal loss and image distortions regardless of origin; heterogeneities in porous solids, heavily SPIO loaded cells, or regions of human cortex that are close to the sinuses. This issue is compounded when attempting functional MRI in such regions, given that the rapid image acquisition techniques such as Spiral and EPI required for fMRI are particularly sensitive to off-resonance.

Spiral-In waveforms have been consistently shown to recover significant amounts of signal in SFG regions and their use has been incorporated into several sequences including Spiral-In/Out [1], Spiral-In/In [2], and ASE Spiral [3].   There have been two main theories proposed for explaining why Spiral-In is superior to Spiral-Out for signal recovery but neither completely explains why Spiral-In images are able to recover more signal even when the Spiral-In acquisition window does not begin until after the Spiral-Out acquisition window is finished, nor why distortion patterns are different between Spiral-In and Out (see Fig. 1).
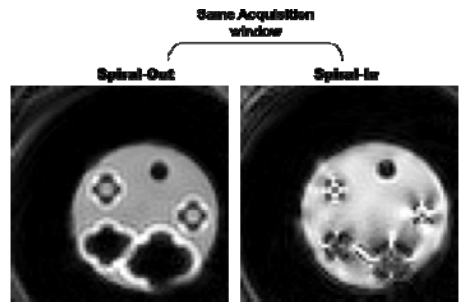
Figure 1: Spiral-In and Spiral-Out images of 5 cylindrical tubes with varying magnetic susceptibility, sitting in a tube of water.

In general, the Spiral-In images exhibit improved signal recovery and decreased signal displacement relative to the Spiral-Out images in regions of high R_2^*. However, even if the Spiral-In acquisition window occurs after the Spiral-Out acquisition window the images exhibit only the expected increase in R_2^* weighting while retaining the overall geometric features of the earlier Spiral-In.

To better understand this phenomenon, computer simulations were performed of a "phantom" made of two concentric tubes containing differing magnetic
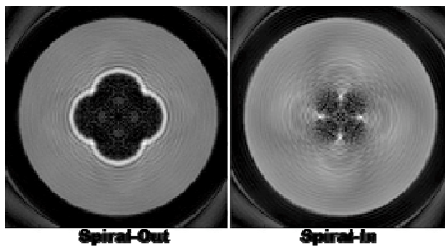
Figure 2: Simulated Spiral-In and Spiral-Out images of a cylindrical tube with a susceptibility equivalent to "air", sitting in a
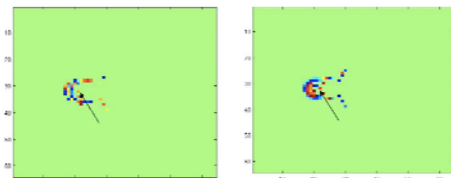
Figure 3: Target Based Phase Maps for a simulated cylindrical phantom. Spiral imaging distortions result in voxels containing signal from a variety of spatial locations, each with a potentially different phase. Colourized phase maps are shown for Spiral-Out (left) and In (right) for all spatial locations contributing to the voxel indicated by the black arrow. Phase coherence is better preserved using Spiral-In, resulting in measurable image intensity at that

susceptibility (Fig. 2). Simulation results indicate that differences between Spiral-In and Out are not due to differences in the amount of signal loss. The distance that real signal is displaced was also not found to be different for both techniques. Instead, the differences appear to be due to constructive and destructive phase interference. As can be seen in Figure 3, the phase sums constructively for Spiral-In, while it sums to zero for Spiral-Out.

References: [1] G.H. Glover & C.S. Law. *Magn Reson. Med.* **46** 515-522 (2001). **[2]** T.Z. Li *et al. Magn. Reson. Med.* **55**, 325-334 (2006). **[3]** K. Brewer *et al. NMR in Biomed.*, in press (2009).

T4

Low-Power MRI by Polyphase Perfect Sequence Excitation

N. Amor[1*], B. Blümich[1], Q. Gong[1], Eimear Byrne[2], and M. Greferath[2]

[1] ITMC, RWTH Aachen University, Germany
[2] School of Mathematical Sciences, University College Dublin, Ireland

Abstract:

A new scheme of NMR excitation is presented which significantly reduces RF peak power and energy [1]. It represents an essential progress for miniaturized NMR due to a possible reduction of the power amplifier and the power supply. Furthermore, the application of the concept to clinical (ultra-) high field MRI permits exploitation of advantages of high magnetic fields such as the intrinsically higher SNR and the resulting higher spatial resolution while still complying to legal regulations given by the SAR (Specific Absorption Rate) limitations. With conventional pulsed high-frequency excitation techniques, absorption of high energy may lead to unwanted tissue heating and local erythema [2].

We propose an excitation scheme employing constant-flip angle pulses with phase modulation resulting in minimum peak excitation power at maximum response peak power (Fig. 1). The method combines advantages of customary pulse NMR, the less prevalent rapid scan NMR [3] in which the spectrum is scanned directly in the frequency domain, and noise excitation [4]. It leads to a reduction of RF power of up to six orders of magnitude and of deposited energy of up to three orders compared to pulsed NMR.

Experimental results including 2D slice selective images using backprojection algorithms are shown, demonstrating the feasibility of the new method and its potential to meet essential needs of medical imaging.
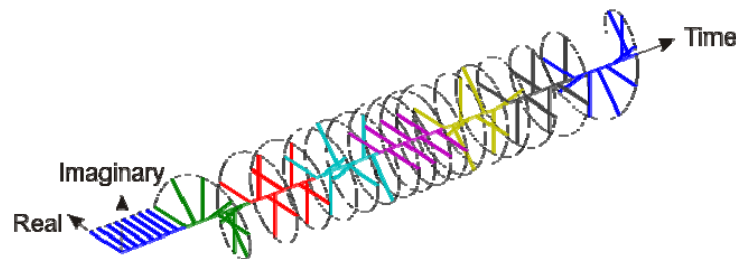
Fig. 1: Pulse scheme of Polyphase Perfect Frank Sequence Excitation: constant-flip angle pulses with phase modulation as a discrete representation of rotating waves with constant amplitude.

1. B. Blümich et al. *JMR* **199** (2009) 18-24.
2. P. A. Bottomley et al. *PMB* **23** (1978) 630–643.
3. J. Jen. *JMR* **45** (1981) 257–269.
4. J. Paff et al. *Phys. Rev. A* **43** (1991) 3640–3644.

Novel Approaches to functional magnetic resonance imaging at ultra-high magnetic field strength

Ute Goerke[1], Michael Garwood[1], Kamil Ugurbil[1]

[1]CMRR/University of Minnesota Medical School, Minneapolis, Minnesota, USA

Functional magnetic resonance imaging (fMRI) is a technique which is successfully used to probe neuronal activation in the human brain. Image contrast is based on the blood oxygenation level dependent (BOLD) response, which is triggered by the physiologic and metabolic responses evoked by alterations in neuronal activity. Depending on blood oxygenation, the magnetic field is distorted near blood vessels containing the paramagnetic deoxyhemoglobin molecule, i.e. capillaries, venules and veins.

Typically, the T_2^*-weighted echo planar imaging (EPI) sequence is used to probe transient changes of the BOLD response related to neural activity as a function of time. Recently, a novel T_2-weighted fast imaging sequence, rapid acquisition with sequential excitation and refocusing (RASER) method, has been proposed (Figure 1).

In RASER, the frequency-swept chirp-pulse pulse sequentially excites isochromates along the time-encoded dimension, G_t. The transverse magnetization is refocused by two 180º pulses and is read out in the presence of a constant gradient G_t in the same temporal order of excitation. Localization is obtained by the steep quadratic profile across each echo, which is generated by the frequency-swept excitation pulse with a high bandwidth time product.

Figure 1: RASER pulse sequence
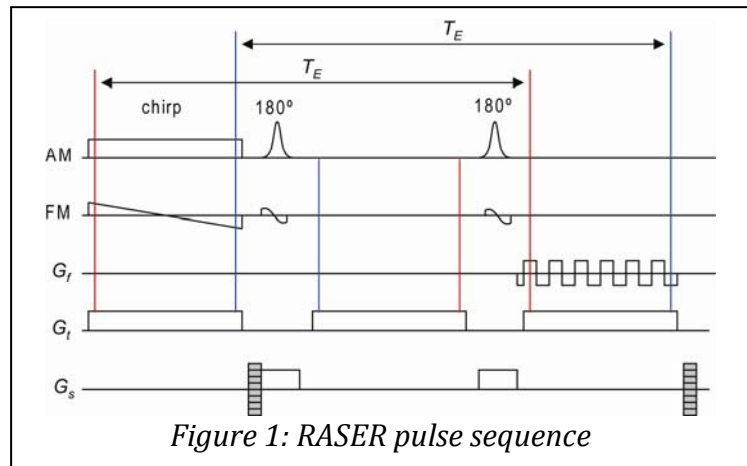
This novel approach for spatial encoding replaces the phase-encoding blips in the conventional EPI scheme. The second spatial dimension is frequency-encoded by an alternating gradient readout train G_f similar to EPI. The third spatial dimension is phase-encoded by incrementing a gradient in subsequent scans (gray shaded gradient pulses). In RASER, all echoes experience exactly the same T_2-weighting, and the BOLD-contrast is based on the diffusion of water molecules in the vicinity of magnetic field gradients of veins, venules, and capillaries.

In this paper, the unique properties of RASER for fMRI at ultrahigh magnetic field strength will be discussed and compared with the conventional EPI approach. The main advantage of RASER is its insensitivity to macroscopic magnetic field inhomogeneities. One example demonstrates that RASER is able to robustly detect the BOLD response in the orbitofrontal cortex, where susceptibility variations at the air/tissue-interface of the sinuses cause signal loss and geometric distortions in EPI images. Another example will show the robustness against modulation of the static magnetic field due to motion, such as chest movements related to breathing.

[1] Chamberlain R *et al*, *MRM* **58**: 794 (2007); Financial support by the grants P41 RR008079 and P30 NS057091, and the MIND Institute is acknowledged.

FLow Imaging Employing a Single-Shot ENcoding: The FLIESSEN sequence

Federico Casanova, Andrea Amar, and Bernhard Blümich

Institute of Technical and Macromolecular Chemistry, RWTH Aachen University, Aachen, Germany

Abstract:
NMR velocimetry has proven to be a remarkably useful tool for non-invasive investigations of fluid dynamics. Among the different approaches developed to spatially resolve velocity distributions, one of the most powerful ones combines displacement encoding in the phase of the NMR signal with the successive application of fast read-out imaging sequences like RARE or EPI. Although such sequences have succeeded to produce reasonable velocity maps, they are limited to the study of systems evolving sufficiently slowly so that displacement during the acquisition of the complete k-space can be neglected. This particular limitation comes from the fact that the velocity is encoded in a period prior to the k-space sampling (Fig. 1b). In this work we present a new multi-echo sequence where the velocity is encoded and decoded before and after the formation of each single echo (Fig. 1c). As the velocity information is refreshed for each echo, velocities almost two orders of magnitude higher than accessible with conventional sequences can be measured. Besides tolerating much higher velocities, the fact that the echoes are independently encoded along the train, allows one to measure velocity maps along all three directions in a single shot. The performance of the sequence was extensively studied by means of numerical simulations, which allowed us to evaluate the efficiency of velocity compensation along read and phase directions, as well as that of velocity encoding. Moreover, the simulations clearly show that, as no phase needs to be preserved during the echo train, the sequence is highly immune to B_1 inhomogeneities, an extremely critical source of distortions even in conventional birdcage resonators.
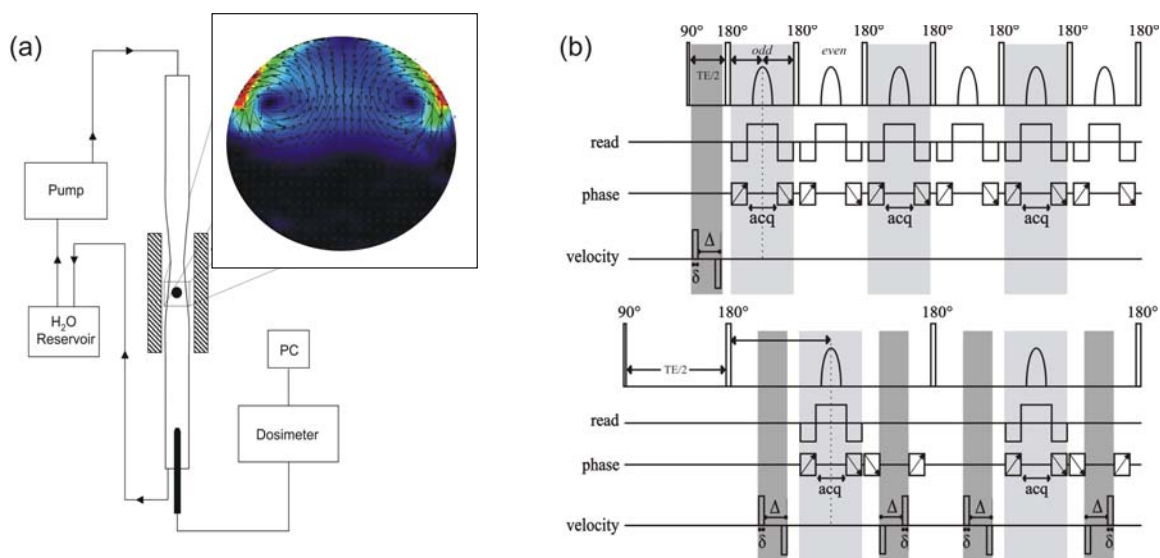
FIGURE 1. (a) Levitated drop setup. **(b)** Standard RARE sequence (top). The velocity encoding (dark grey) is applied during the first period and can be acquired only every other echo in the imaging part (light grey). **(c)** New FLIESSEN sequence with a double pair of velocity gradients and phase compensation in every period that allows to sample all echoes (bottom). T_E is the echo time, δ is the duration of the velocity encoding gradients, and Δ the evolution period.

Applications of Magnetic Resonance Imaging to Visualise Chemistry

Melanie M. Britton[1]

[1] School of Chemistry, University of Birmingham, Edgbaston, Birmingham, B15 2TT, UK.

Abstract:

Our research involves the application and development of MRI techniques to measure and visualise chemistry in a diverse range of applications. MRI has already proven very useful in imaging chemical waves and patterns formed by the Belousov-Zhabotinsky (BZ) reaction[1,2]. However, MRI is capable of more than just being a visualisation technique, it can also provide quantitative information on the concentrations of chemical species[3] during chemical reactions or processes. For example, where there are variations in the concentration of transition metal ions, it is possible to probe their concentration using NMR relaxation measurements. This has allowed us to, not only, image pattern forming chemical reactions, but has also enabled the visualization of chemical processes, for the first time, within corrosive salt solutions during Galvanic corrosion.

We have also applied MRI to studying the chemistry inside microemulsions. Using the variations in both relaxation time and chemical shift it is possible to probe the pH inside water droplets in reverse water-in-oil microemulsions. Using these methods we have been able to observe the propagation of pH fronts in microemulsions, produced by the bromate-sulfite autocatalytic 'clock' reaction. Other reactions imaged inside a microemulsion medium include the BZ reaction, which is able to produce a greater diversity of patterns than in aqueous solution.

An area of particular interest in the group, is in understanding how chemistry and reaction couple. This is of obvious practical interest in chemical engineering, but is also of importance is areas such as biology, geology and physics. Previous work has demonstrated the power of MRI to visualise chemical waves under flowing conditions in packed bed reactors[4]. We have taken this work further and are looking at the coupling between pattern or front forming reactions, with more complex flow environments, such as Taylor-Couette vortices (figure 1).
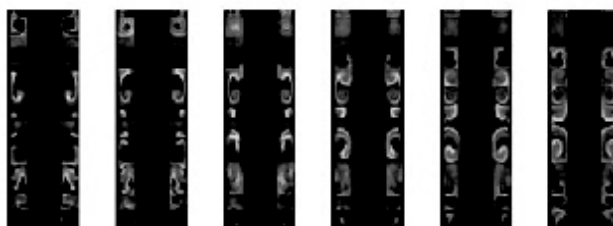
Fig. 1: MR images of chemical waves in Taylor-Couette vortices

1. RL Armstrong, et al., Magnetic Resonance Microscopy: methods and application in materials science, agriculture and biomedicine. VCH, Weinheim, 1992.
2. MM Britton *J. Phys. Chem. A* **107** (2003) 5033-41.
3. MM Britton *J. Phys. Chem. A* **110** (2006) 2579-82.
4. MM Britton, AJ Sederman, A Taylor, SK Scott, LF Gladden *J. Phys. Chem. A* **109** (2005) 8306-13.

NMR microscopy T_2 mapping at high resolution

Dagmar van Dusschoten[1]

[1] ICG-3, Research Center Jülich, Jülich, Germany

Abstract:
One of the useful characteristics of NMR is its ability to assess local water mobility in heterogeneous systems of various nature. Both NMR relaxation and translational diffusion properties can be used to estimate the size of (sub-)compartments of an object and sometimes it is possible to estimate the speed at which these compartments interact. E.g. one can estimate cell compartment sizes from plant cells (like the vacuole and the cytoplasm) and the membrane permeability between the two compartments. This works rather well without spatial resolution as long as the compartments of the object are comparable with regard to size, content and boundary characteristics. In case this condition is not met, NMR imaging is required. Relaxation maps can be obtained at a resolution that comes close to plant cell dimensions, but these maps can normally only be generated for one relaxation component, due to problems associated with multi-echo sequence in imaging mode. At a resolution better than 120 mm the longest T_2 that can be measured reliably is limited by the additional signal attenuation caused by diffusion during a series of gradient pulses used for spatial encoding, primarily the read-out gradient. At a resolution of about 100 mm the upper T_2 limit is about 300 ms [1], unless gradient switching is near instantaneous. At 50 mm the limit is reduced to roughly 80 ms.
Here we demonstrate how this limit can be circumvented by segmentation of $k_{read-out}$-space. In this manner T_2 values up to 500 ms at a spatial resolution of about 65 mm can be obtained. This approach does come with a time penalty identical to the segmentation factor, which is at least three and may rise with increasing resolution. These measurements were performed at 200 MHz in a super wide-bore supercon equipped with 300 mT/m gradients and using a home-build openable, tilted solenoid r.f. coil to achieve the necessary signal to noise. This coil type is described elsewhere [2].

1. H.T. Edzes , D. van Dusschoten, H. Van As, *Magn. Reson. Im.* **16** (1998) 185-196.
2. D. van Dusschoten, N. Hermes, J. Kochs, this conference

T9

MRI of the preparation of supported catalysts

Igor V. Koptyug and Anna A. Lysova

International Tomography Center SB RAS, Novosibirsk, Russia

Abstract:

Many industrial catalytic processes use catalysts comprising nanoparticles of metals (or metal oxides, metal sulfides, etc.) supported on a porous material. A uniform macroscopic distribution of the active phase within the support body can be difficult to achieve in some cases. Besides, in many applications the catalysts perform better if the distribution is non-uniform. Supported catalysts are often prepared by contacting a porous support body with a solution containing the active component precursors (e.g., a metal salt) along with some additives. After the initial impregnation, transport of the solutes within the support body is allowed to continue for some time. Then the solvent is removed by drying, and further processing yields an active catalyst. The drying process can alter the distribution achieved during the preceding stage if adsorption of precursor species is not strong enough. The properties of the support surface and the chemical nature of the species present in the solution can change drastically depending on the conditions of impregnation such as concentrations of key species, solution pH, etc. These changes affect significantly the strength of the interaction between the support and the solutes and therefore modify transport rates and the final distributions achieved. As a result, the optimization of the catalyst preparation requires the ability to monitor these transport processes.

Paramagnetic complexes of metal ions (Ni^{2+}, Co^{2+}, Cu^{2+}) measurably reduce the nuclear spin relaxation times of a solvent (water), therefore their transport in a γ-Al_2O_3 support body was relatively easy to monitor with MRI. With the use of an appropriate calibration procedure, quantitative distributions of the metal ions could be obtained and their evolution in time could be monitored. Interestingly, some diamagnetic additives increase the relaxation times of a solvent in a porous material. This fact was used to monitor the transport of $Mo_7O_{24}^{6-}$, $PtCl_6^{2-}$, $PdCl_4^{2-}$ and citrate anions in γ-Al_2O_3 bodies. Furthermore, the distribution of the paramagnetic and the diamagnetic species could be mapped after the drying stage as well. This was achieved by saturating the porous bodies with a non-polar liquid which did not re-dissolve the species of interest. For the species that contain suitable magnetic nuclei, a direct visualization of distribution and transport dynamics with MRI is possible, as demonstrated for the aqueous solutions of H_3PO_4 (^{31}P MRI) and ^{13}C-labeled citric acid (^{13}C MRI). The feasibility of the direct mapping of metal atoms was demonstrated for ^{95}Mo and ^{195}Pt. The effects of variation of the concentrations and pH of the impregnation solutions were studied in detail. The use of other (e.g., optical) techniques is essential to establish the chemical nature of the species present in the impregnation solution.

1. 1. A.A. Lysova, I.V. Koptyug, R.Z. Sagdeev, V.N. Parmon et al., J.A. Bergwerff, B.M. Weckhuysen, *J. Amer. Chem. Soc.* **127** (2005) 11916-11917.
2. J.A. Bergwerff, A.A. Lysova, L. Espinosa-Alonso, I.V. Koptyug, B.M. Weckhuysen, *Angew. Chem. Int. Ed.* **46** (2007) 7224-7227.
3. J.A. Bergwerff, A.A. Lysova, L. Espinosa-Alonso, I.V. Koptyug, B.M. Weckhuysen, *Chem. Eur. J.* **14** (2008) 2363-2374.
4. L. Espinosa-Alonso, A.A. Lysova, P. Peinder, K.P. de Jong, I.V. Koptyug, B.M. Weckhuysen, *J. Amer. Chem. Soc.* **131** (2009) 6525-6534.

T10

Hyperpolarized ^{13}C NMR in Diamond via Optical Pumping

Jeffrey Reimer[1] , Jonathan King, and Patrick Coles[2]

[1] University of California, Berkeley, USA
[2] Carnegie Mellon University, Pittsburgh USA

Abstract:
We have identified a new method of optical hyper-polarization of carbon-13 nuclei in diamond. When nitrogen-containing diamonds are irradiated with electrons and subsequently annealed, a significant number of nitrogen-vacancy defects are formed. The negatively charged version of this defect has a paramagnetic triplet ground state that can be highly polarized into the Ms=0 spin state by illumination in the phonon-sideband of the optical absorption spectrum. This can be accomplished with the multi-wavelength (457.9nm to 514.5nm) output of our argon ion pump laser. The polarization process has been modeled with a first-principles quantum mechanical treatment in conjunction with a spin diffusion transport model. The mechanism underlying this model is not dependent upon lattice energy (unlike OPNMR in semiconductors), and thus is generalizable to room temperature pumping in bulk and nanopowdered materials, and easily suita ble to polarization transfer to targets.

T11

MRI of swelling, sedimenting, adsorbing and drying materials

Sergey Dvinskikh and István Furó

Department of Chemistry and Industrial NMR Center, Royal Institute of Technology, SE-10044 Stockholm, Sweden

Abstract:

Magnetic resonance imaging, known mostly in clinical and biomedical applications, is becoming integrated also into chemical engineering and material research [1]. While many processes in that area are similar to those addressed in medical applications of MRI, parameters and experimental implementations are often quite different and, in many respects, far more demanding. This hinders direct transfer of existing methods developed for biomedical research, especially when facing the challenging task of obtaining spatially resolved *quantitative* information. Most significant limitations of many current MRI approaches, leading to the losses of quantitative information, can be identified as following: short T_2 times compared to gradient switching and probe dead times; molecular diffusion artifacts; susceptibility artifacts; varying dielectric losses and induced currents in conductive samples; limited dynamic range; blurring artifacts accompanying drive for increasing sensitivity and/or imaging speed.

In this contribution, specific MRI examples from the areas of soil and mineral research and of wood research will be presented. Efforts in developing and adapting MRI approaches to study these kinds of systems will be outlined as well.

Soil and mineral research: Understanding water transport and erosion processes in soils, sediments, minerals, and rocks is one of the key challenges in environmental science. In particular, extensive studies of clay/water interaction have been performed at the Industrial NMR Center in Stockholm in order to provide a quantitative measure of clay distribution in extended samples during different physical processes such as swelling, dissolution, and sedimentation on the time scale from minutes to years [2,3]. Our results have a significant impact for engineering barriers for storage of spent nuclear fuel where clay erosion by low salinity water must be addressed.

Wood research: There is a growing interest in the moisture buffering performance of wood for indoor climate regulation. In contrast to green or water-soaked wood, processed construction wood at ambient conditions is much less suitable for standard MRI because of the very short relaxation times of "bound" water. Hence, solid state MRI methods were applied to assess the moisture buffering capacity of wood. As one result, it was possible to obtain separate radial images of water and macromolecular content and, thus, directly demonstrate a close linear correlation between those parameters [4].

1. S. Stapf and S.-I. Han (Eds.), *NMR imaging in Chemical Engineering*, Wiley, New York, 2006.
2. S.V. Dvinskikh, K. Szutkowski, and I. Furó, *J. Magn. Reson.* **198** (2009) 146-150.
3. L. Liu, L. Moreno, and I. Neretnieks, *Langmuir* **25** (2009) 679-687.
4. S. V. Dvinskikh, M. Henriksson, L. A. Berglund, and I. Furó. Manuscript (2009).

Gaining practical profile: NMR profiling of industrial polymer composites

N. Nestle[1], C. Renner[2], M. Völkel[1], J. Perlo[3], F. Casanova[3]

[1]BASF SE Ludwigshafen, D-67056 Ludwigshafen, Germany,
[2]Elastogran GmbH, D-49440 Lemförde, Germany,
[3]RWTH Aachen and ACT GmbH, D-52074 Aachen, Germany

Abstract:
Low-cost, easy-to-use unilateral NMR profiling equipment which has become commercially available within recent years has opened up a whole range of novel options for studying industrial polymer composites.

The contribution presents a general overview on different applications of NMR profiling on various polymer composite samples. Typical limitations to the achievable depth resolution are discussed as well as the contrast mechanisms observed in different materials. A special emphasis is put on different approaches to evaluate the (intrinsically quite noisy) individual CPMG magnetization decay curves in order to extract information on parameters such as "spin density", "relaxation time" or "heterogeneity" of the material at each depth level. The example in Fig.1 shows a comparison of raw integrated CPMG signal profiles and the relaxation time and signal amplitude determined from fitting binned signal curves on a composite in which migration of a plasticizer component occurs from the region near the surface into the inner material layer. While the integrated signal decay curves suggest a signal amplitude which is almost constant or even increasing over the first material, the extrapolated amplitude indicates a loss of signal near the interface. This is due to a loss of CPMG-detectable signal inside this region (relaxation times too short from loss of plasticizer); at the same time, a very slowly relaxing component seems to form near the interface. This may be attributed to an enrichment of plasticizer there.
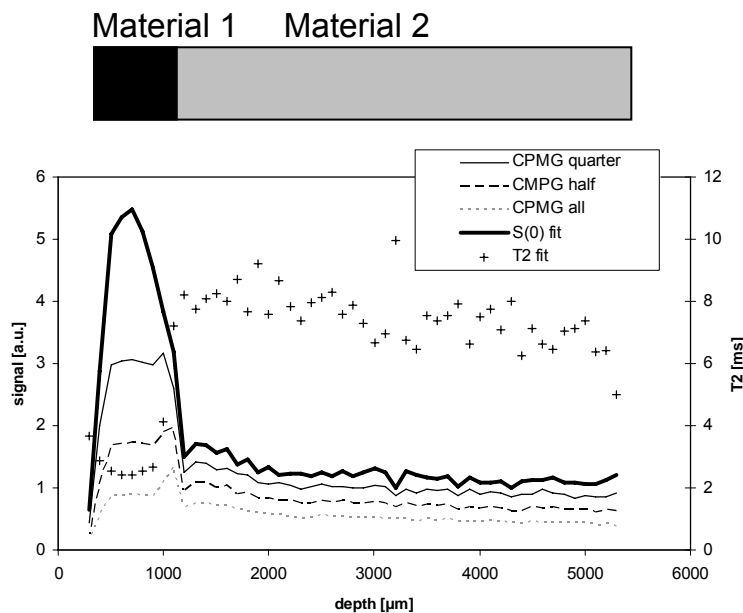
Fig. 1: Profiling NMR results obtained on a polymer composite

Tuesday, September 1st Talks:

Flow/Diffusion

In-Vivo/Biological/Biomedical Applications I

In-Vivo/Biological/Biomedical Applications II

T13

Phase Encoding Phast Phlows

Ben Newling, Olusegun Adegbite, Zhi Yang, Alex Adair and Igor Mastikhin

UNB MRI Centre, Department of Physics, University of New Brunswick, Fredericton, Canada.

Abstract:

Traditional pulsed field gradient (PFG) methods for measuring flow and diffusion have struggled when the flows are faster than *c.* 1 m/s. During the measurement interval (which may be the spin echo time, for example), the fluid can move significantly and, in turbulent flows, may also experience significant acceleration. The measurement interval in purely phase-encoded imaging techniques, such as SPI or SPRITE [1], is typically hundreds of microseconds, which is shorter than in the majority of frequency encoding techniques. Our motion-sensitised version of SPRITE [2] has proven useful in the imaging of turbulent gas or liquid flows. Although the imaging time is on the order of minutes and the method is not a snapshot, averaged flow behaviour is usually most useful in steady, turbulent flows. The motion-sensitisation is in the PFG style, so that the Fourier transform of decaying signal in any image voxel is an averaged propagator [3], which allows us to assess both mean velocity and random fluctuations in the velocity which are caused by turbulence. We will discuss the generation and interpretation of these data.

The SPRITE basis of our flow measurement confers other advantages than the ability to image fast flows. The short measurement interval permits flow measurements even when T_2^* is short. This has been an advantage in studying fluorinated gas flow. Purely phase-encoded imaging is free from distortions due to B_0 inhomogeneity, chemical shift and variations is magnetic susceptibility, because of the *constant* measurement interval [4]. This is a crucial advantage in imaging two-phase flows [5] (Fig. 1), which we will discuss with reference to a couple of application-driven examples.
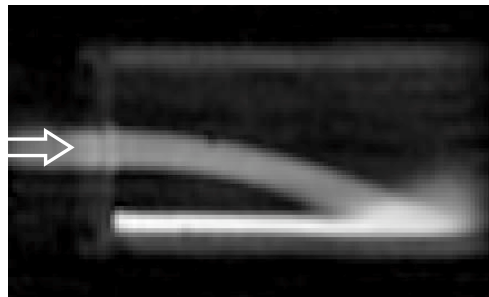
Fig. 1: Water flow (left to right) from a pipe into an open, cylindrical culvert. The plastic material of the culvert can be seen thanks to the short measurement interval. The SPRITE image is undistorted by B_0 inhomogeneity, which means the edges of the jet and even the time-averaged splash are resolved.

1. B. J. Balcom *et al.*, *J. Magn. Reson. A* **123** (1996) 131-134.
2. B. Newling *et al.*, *Phys. Rev. Lett.* **93** (2005) 154503.
3. P. T. Callaghan, *Principles of Nuclear Magnetic Resonance Microscopy*, OUP, Oxford (1991).
4. S. Gravina and D. G. Cory, *J. Magn. Reson. B*, **104** (1994) 53-61.
5. M. Sankey *et al.*, *J. Magn. Reson.* **199** (2009) 126-135.

T14

Searching for flow disturbances high and low

Steve Altobelli[1], Dean Kuethe[1]

[1]New Mexico Resonance, Albuquerque, New Mexico, USA

Abstract:

This paper describes two recent but dissimilar flow studies that involved temporal fluctuations. In the first case, we studied groundwater flow using stimulated-echo spin warp 3d phase mapping. In the second, we used 2d spin echo phase mapping methods with both spin warp (SW) raster scan k-space acquisition and projection imaging (PI) to measure high speed flows of water and air in a variety of cross-sections.

Searching low: Flow in Rocks

Portions of the Biscayne aquifer (near Miami, Florida) are composed of carbonate stone with labyrinthine, centimeter-scale channels made by ancient burrowing shrimp. We recently studied convective/diffusive transport between the carbonate matrix and the channels[1]. The connected channels provide high hydraulic conductance paths for flow and there have been indications that flows in them may become disturbed or even turbulent. We made measurements to look for signs of these flow disturbances and also to validate Lattice Boltzmann (LBM) calculations (by M. Sukop) which are now nearing completion at Florida International University, see figure 1. Peak axial velocities were 0.3 mm/s in this slice, Reynolds number is less than 10. No unsteadiness has been observed so far. In this study we measured three velocity components on a coarse 3d grid; a set of data with NEX 4 took 7.5 hours.

Figure 1. LBM and MRI, axial v, mm/s

Searching high: Bubbly flows

We measured axial velocities and the distribution of water and air in circular, rectangular (10:1 aspect) and triangular cross-sections. Typical velocities in both the air and water phases were 0.7 m/s, giving Reynolds numbers of a few thousand. Figure two shows examples of measurements in the triangular cross-section. On the left is the SW axial velocity image showing the relatively high velocity in the upper mixed phase region and a prominent velocity artifact. In the center the velocity compensated SW fluid-fraction image is shown, the same artifact is present but much reduced. On the right is a fluid fraction PI image, where the unsteady velocity field results only in local blurring of the image.

In a situation where one needs only to confirm or deny the existence of flow disturbances the phase-encoding artifacts in SW experiments are diagnostic. If on the other hand, one desires to suppress the artifact, PI imaging is suggested.
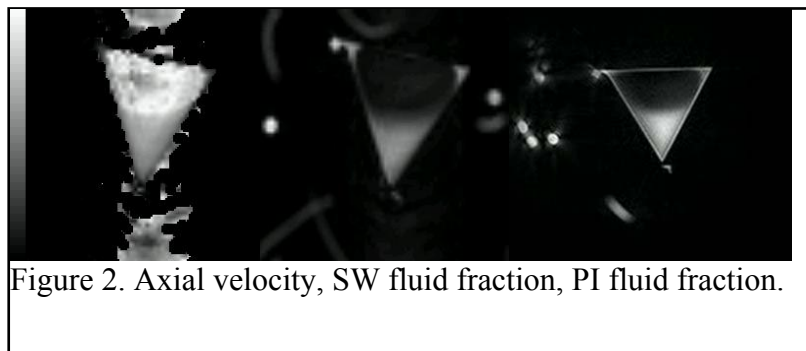
Figure 2. Axial velocity, SW fluid fraction, PI fluid fraction.

1. Florea, Cunningham, Altobelli, *Ground Water* **47**(3) 382-390 (2009).

T15

Rapid Measurement of Transient Velocity Evolution using GERVAIS

Colin J. Davies[1], Andrew J. Sederman[1], Chris J. Pipe[2], Gareth H. McKinley[2], Lynn F. Gladden[1] and Mike L. Johns[1]

[1] MRRC, Department of Chemical Engineering and Biotechnology, University of Cambridge, Cambridge, UK

[2] Hatsopoulos Microfluids Laboratory, Department of Mechanical Engineering, Massachusetts Institute of Technology, Cambridge, MA, 02139, USA

Abstract:

Rapid velocity measurements using GERVAIS (Gradient Echo Recalled Velocity and Acceleration Imaging Sequence), an EPI (Echo Planar Imaging) based technique capable of measuring velocity over an observation time of several milliseconds, are performed on a wide gap couette Rheo-NMR cell. Velocity images were acquired after a variable delay time between a control signal to initiate a transition in flow and the start of the measurement sequence. This allows investigation of the transient evolution of the velocity field following a step change in rotation rate. Both the initiation and the cessation of imposed shear stress have been investigated for (i) a shear banding micellar solution of (CetylPyridiniumChloride) / NaSal (Sodium Salicylate) in brine, and (ii) a viscous Newtonian fluid (polydimethylsiloxane (PDMS)). For the CPyCl micellar solution, an elastic wave is seen to propagate across the cell following the initiation of shear stress whilst an oscillatory 're-coil' is observed following the cessation of shear stress; neither of these phenomena was observed for the Newtonian PDMS. The figure below shows the progression of velocity with delay time across the centre of the couette cell for the CPyCl solution following the cessation of imposed shear. Damped oscillatory flow in the wide gap of the couette is observed while the marker fluid (water) in the centre decreases monotonically.
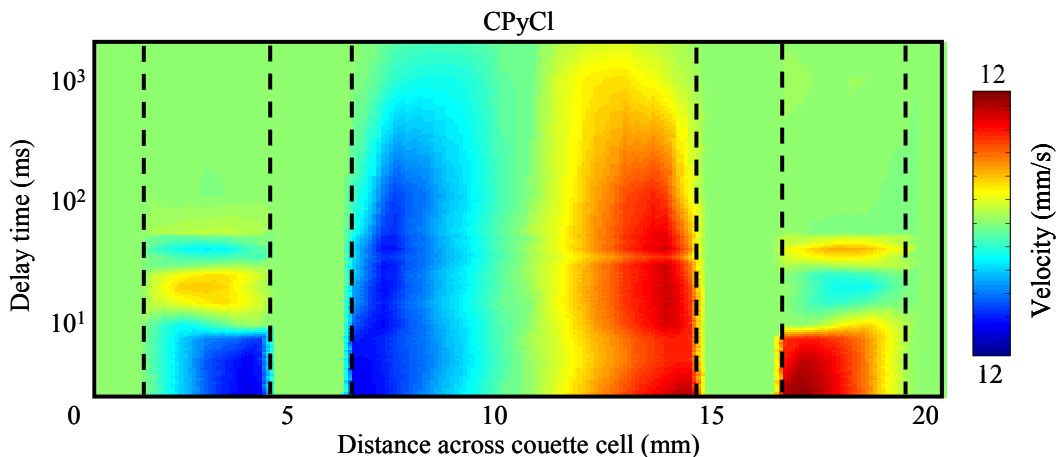
Fig. 1: 2D velocity plots with profile position and time (following cessation of inner cylinder rotation) as axes for a CPyCl / NaSal solution

T16

Measurement and simulation of the non-local dispersion tensor in porous media

<u>Mark Hunter</u>[1] , Andy Jackson[,2] and Paul Callaghan[1]

[1] MacDiarmid Institute for Advanced Materials and Nanotechnology, Victoria University of Wellington, Wellington, New Zealand
[2] SUPA School of Physics, University of Edinburgh, Edinburgh, Scotland

Abstract:

Dispersion describes the phenomenon whereby particles on the same streamline separate during flow. The physics of dispersion is governed by stochastic processes arising from the interplay between advective velocity gradients, molecular diffusion and boundary layer effects[1]. The dispersion tensor, $\mathbf{D}^*$, is a local measurement in the sense that it does not depend on positional relationships and is measured as time asymptotes[2]. For situations where the length- and time-scales on which transport occurs are not much larger than the scale of the fluctuations in the velocity field, a non-local description is required[3].

Pulsed Gradient Spin Echo (PGSE)-NMR provides a wealth of information about the velocity correlations in porous media. Presented here is a set of NMR pulse sequences and a superposition designed to extract the velocity correlations necessary to calculate the dispersion as a function of displacement and hence the non-local dispersion. The experimental method will be tested against the calculable non-local dispersion in a Couette cell[4]. Experiments performed on porous media will be discussed including other tensors and non-local measurements with higher dimensionality[5]. Preliminary measurements on rock cores will also be discussed.

The Lattice-Boltzmann algorithm has been shown to successfully predict the flow field in porous media[6], and has been used to model the flow field through our model porous medium. This flow field is used to simulate a large ensemble of virtual tracer particles, from which numerical estimates for both the local and non-local dispersion can be determined. Our implementation of this approach is presented here along with a comparison between the experimental and computational results. Numerical simulation will also be used to investigate dimensionalities difficult to obtain in experiment.

1. A. A. Khrapitchev and P.T. Callaghan, *Phys. Fluids* **15** (9) pages.
2. J.D. Seymour and P.T. Callaghan, *AIChE J.* **43**
3. D.L. Koch and J.F. Brady *J. Fluid Mech.* **180**
4. M.W. Hunter and P.T. Callaghan *PRL* **99** 210602
5. M.W. Hunter *et. al.* submitted.
6. B. Manz *et. al. AIChE J* **45**

Laurel MRI: Flow characteristics and exchange in complex biological systems as observed by PFG-MRI

Henk Van As, Natalia Homan, Bart Venne, Edo Gerkema, Frank J. Vergeldt

Laboratory of Biophysics and Wageningen NMR Centre, Wageningen University, Wageningen, The Netherlands

Abstract:

Fluid flow and exchange are of great importance in many areas of science and technology, e.g. flow in (woody) plants, and flow in bio(film)-reactors. These systems are of interest from ecophysiological and environmental point of view. They are characterized by complex (dispersive) flow, and exchange between flowing and stagnant fluid pools.

Pulsed field gradient (PFG) MRI propagator methods result in flow visualization spatially resolved. In this way flow characteristics like velocity, volume flow and flow conducting area can be measured per pixel, even in pixels that contain flowing and non-flowing fluid [1,2,3]. This is key information to address plant performance and stress-induced effects like cavitation. Correlated propagator-T_2 MRI can be applied to yield information about the relation between flow, pore size and exchange behavior, and to obtain T_2 corrected volume flow quantification [4].

Propagator measurements have been successfully applied to quantify exchange between the intraparticle pore network and the interparticle void space in chromatographic columns packed with spherical-shaped, porous particles [5]. In realistic (bio-)systems like (woody) plants and biofilm reactors we have to deal with surface relaxation, internal field gradients due to susceptibility differences and differences in relaxation times between exchanging flowing and stagnant water pools. All these effects will differently affect the propagator and signal amplitudes and its subsequent interpretation in the above mentioned flow characteristics. The effect of exchange under these conditions has not yet been investigated systematically.

Here we present results of a systematic study. Water flow through model porous media was studied in the presence of surface relaxation, internal magnetic field gradients and exchange with stagnant water pools with different relaxation behavior, demonstrating how the apparent flow parameters in these situations depend on the observation time. To investigate the water exchange process a two component biofilm reactor was used, before and after a heat treatment to introduce exchange. It is shown that correction of the stagnant fluid signal amplitude for relaxation at increasing observation time using the observed relaxation times reveals the exchange between the two fractions in the system. Further it is demonstrated how this exchange can be quantified. This method was applied to study flow and exchange between flowing and stagnant water in xylem tissue of ring porous (*Quercus robur*, oak) and diffuse porous (*Laurus nobilis,* laurel) trees.

1. T. Scheenen, D. van Dusschoten, P.A. de Jager and H. Van As, *J. Magn. Reson.* **142** (2000) 207 .
2. C.W. Windt, F.J. Vergeldt, P.A. de Jager and H. Van As, *Plant Cell Environ.* **29** (2006) 1715.
3. H. Van As, *J. Exp. Bot.* **58** (2007) 743.
4. C.W. Windt, F.J. Vergeldt and H. Van As, *J. Magn. Reson.* **185** (2007) 230.
5. U. Tallarek, F.J. Vergeldt and H. Van As, *J. Phys. Chem. B* **103** (1999) 7654 .

T18

Simultaneous μPET and μMRI

Thomas Ng[1], Daniel Procissi[1], Yibao Wu[2], Andrew A. Raubitschek[3], Russell E. Jacobs[1]

[1]Beckman Institute, California Institute of Technology, Pasadena, CA USA
[2]Department of Biomedical Engineering, UC Davis, Davis, CA
[3]Dept. of Radioimmunotherapy, Beckman Research Institute, City of Hope National Medical Center, Duarte, CA USA

The millimeter resolution of PET scans makes it crucially important to have an accurate anatomical context within which to interpret the significance of the observed activity in pre-clinical imaging. Methods to co-register PET to MRI work well across multiple subjects and longitudinally for the same subject in the brain because of the constancy of the anatomy and constraint of the skull. In situations where unconstrained anatomy is imaged (*e.g.* cell tracking) and where time dependent information is important (*e.g.* responses to therapy) simultaneous acquisition of PET and MR data allows seamless and efficient cross modal registration over space and time.

We employ the recently constructed MR-compatible micro-PET insert (Catana et. al *PNAS* 105 (10), 3705, 2008) in a 7T MRI scanner to perform pre-clinical studies of the mechanism(s) and efficacy of immunotherapies. Development of a near real-time preliminary data analysis process provides facile feedback between PET and MR imaging, allowing one modality to guide more useful data collection in the other. We present an examination of the consequences of an immunotherapy on tumor characteristics using simultaneous PET/MR imaging and spectroscopy. Heterogeneous 18F-FDG uptake is spatially and temporally compared to: 1) local metabolite concentrations using MRS, 2) ADC's, 3) T2-weighted contrast and 4) Gd-DOTA uptake. In particular, 18F-FDG uptake is used to guide localization of MR spectroscopy scans. 64Cu labeled therapeutics allow us to assess biodistribution simultaneously with efficacy. Significant variation of tumor growth from mouse to mouse, along with the pliability of the local anatomy makes co-registration of sequential scans difficult. Simultaneous *in situ* data acquisition allows almost immediate spatial and temporal co-registration of multimodal anatomic and functional information. Further development of such simultaneous multimodal techniques will open new possibilities to study more intricate physiological mechanisms *in vivo*.

T19

Finding Phenotypes by High Throughput MR Microscopy

R. Mark Henkelman[1], Jason P. Lerch[1]

[1] Mouse Imaging Centre, The Hospital for Sick Children, Toronto, Ontario, Canada

Abstract:

With the completed sequencing of the human and mouse genomes, a major challenge in biomedical research is to identify how genes give rise to the individual and how genes effect diseases of the individual. Because there is a 99.5% ability to recognize mouse analogues of human genes, much of the relationship between genes and phenotype will be worked out in the mouse. The mouse is advantageous because there is a remarkable set of tools for manipulating the genetics, and there are also inbred strains of genetically individual mice. After genetically modified mice are created, the major task of phenotyping can be well addressed by magnetic resonance microscopy and sophisticated statistical analysis.

This presentation will demonstrate the development of parallel sample MR microscopy for phenotyping of live mice, mouse brains, and embryos. Some of the challenges of running 16-parallel spectrometers in a single magnet and gradient without excessive interference will be discussed. RF coils for high quality imaging will be presented.

To identify imaging changes associated with genetic changes requires knowledge of the variation within the inbred strain as well as the variation within the putative mutant. This can be handled with non-linear image registration techniques to find analogous anatomical points in both groups of mice. Once these points have been identified, statistical differences in anatomy and in brain shape between the wild type and mutant group can be recognized and identified.

Examples of genetic changes that give rise to neuroanatomical differences in the brain will be presented. Diseases such as Huntington's disease, schizophrenia, and other rarer mutations will be presented. Finally, brain differences associated with a learning-and-memory task of maze exploration will be shown.
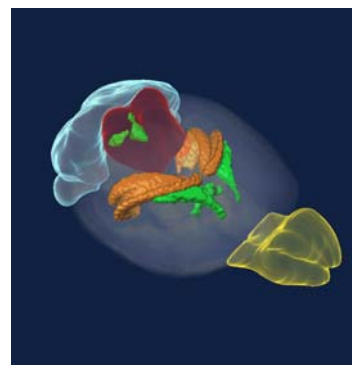
1. N.A. Bock, et al., *Magn Reson Med* **54** (2005) 1311-1316.
2. N. Kovacevic, et al., *Cerebral Cortex* **15** (2005) 639-645.
3. J.P. Lerch, et al., *NeuroImage* **39** (2007) 32-39.

T2 Anisotropy in the Superficial Articular Cartilage

Yang Xia[1] , ShaoKuan Zheng[2]

[1,2]Oakland University, Rochester, MI 48309, USA

As one of the major molecular constituents in articular cartilage, the fine fibrils of collagen have some unique architectural features, which form the criteria in histology to conceptually subdivide the thickness (depth) of articular cartilage into three consecutive zones, namely the superficial, transitional, and radial zones (SZ, TZ, RZ) respectively [1]. Since the fibril integrity of the surface structure of cartilage is of great importance to the load-bearing ability of the tissue, the superficial cartilage has been called the 'skin' of the tissue.

To investigate the fibril architecture of the collage matrix in the superficial zone of articular cartilage non-destructively, NMR microscopy (µMRI) T2 anisotropy technique has been used to image six specimens of canine humeral cartilage that were rotated in such a way (Fig a) that the normal axis of the articular surface of the specimen remained *stationary* and perpendicular to B_0, over a range of 180° and at a step of 15°. At each rotation angle, a quantitative T2 image was constructed at 13µm pixel resolution using a CPMG-SE imaging sequence (Fig b). A Bruker AVANCE II 7-Tesla/89-mm system was used.

A set of complex and depth-dependent patterns was found in the µMRI T2 anisotropy along the depth of the tissue. In the superficial zone, the T2 anisotropy is clearly periodic (Fig c), which demonstrates that the distribution of the collagen fibrils in the superficial zone is not random. In the transitional zone, the periodicity of the T2 anisotropy approximately doubles with respect to that in the superficial zone. In the initial part of the radial zone, the T2 anisotropy is also periodic but inverse to that in the superficial zone. In the deep part of the radial zone, the T2 anisotropy becomes increasingly weaker and eventually disappears.

This work demonstrates that the collagen fibril organization at SZ of cartilage is not random and that the transition of the fibril structure between the zones in articular cartilage is not sudden. An architecture model of collagen fibrils was formulated to interpret the NMR experimental data.
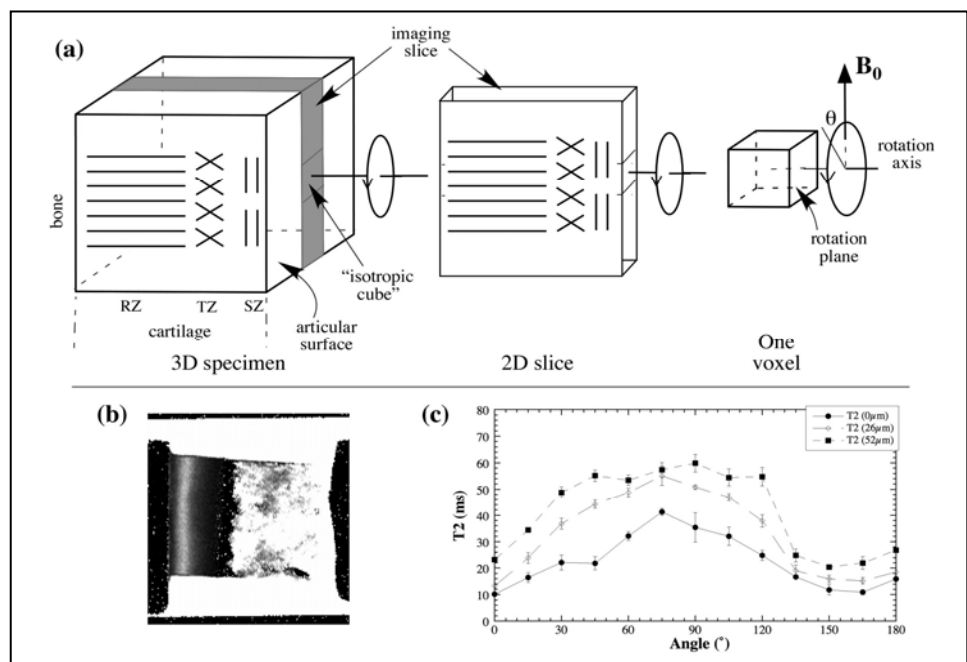
Reference:[1] Y Xia, *Seminars in Arthritis and Rheumatism*, **37** (2008), 317-327.

T21

MR Microscopy at the Mammalian Cell Level.

Stephen J. Blackband[1,3,4,7], Jeremy J. Flint[1,3], Michael Fey[6], Daniel Schmidig[6], Michael A. King[2], Brian Hansen[5], Peter Vestergaard-Poulsen[5].

Departments of [1]Neuroscience, [2]Pharmacology and Therapeutics, and the [3]McKnight Brain Institute and [4]Center for Structural Biology, University of Florida, Gainesville, Florida, USA; [5]Center for Functionally Integrative Neuroscience, Aarhus University, Denmark; [6]Bruker Biospin AG, Switzerland; [7]National High Magnetic Field Laboratory, Tallahassee, Florida, USA.

Abstract:

The pioneers of MRI immediately realized its potential to reach into the microscopic regime, and consequently the spatial resolution of MR has steadily improved over the last ~35 years. For the most part this has been achieved through the use of ever smaller rf coils and ever higher magnetic fields in the search for increased SNR. So far a variety of plant and animal cells have been studied, with the frog ova and the *Aplysia* neuron the only animal cells imaged (1) until recently; this was possible because of their relative large size (>250 microns in diameter).

Through the use of new microsurface coils (50-500 microns in diameter) to improve SNR, mammalian cells (<50um diameter) have now been imaged (2) at isotropic spatial resolutions down to 4.7 microns, and show a clear delineation between the cell body and surrounding tissue. Additionally, diffusion tensor imaging shows for the first time the ability of MR to perform tractography at the cellular level with direct histological correlation, which may be important for the validation of tractography. An example of this capability is illustrated in Figure 1 on excised fixed rat spinal cord tissue.

In this presentation we will summarize this progress, and then show the first direct MR images on fixed human brain tissue visualizing human brain cells with direct histological correlation. The cell bodies show as hypointense in the diffusion weighted images in a similar fashion to that observed in rat tissue. The potential of studies of mammalian cells on live perfused tissue will be discussed, and the impact of these data on the modeling of MR signals in tissues will be addressed.
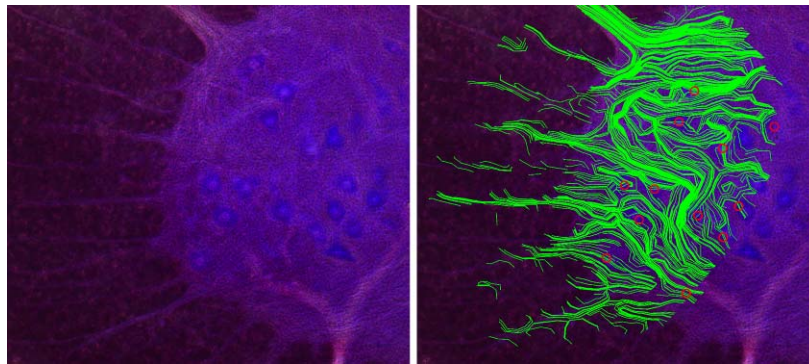
Figure 1. Example data on a fixed rat spinal cord. Left: histology. Right: tratography overlaid on the histology. Red circles indicate the positions of the cell bodies as identified on the diffusion weigthed image (not shown). A clear correlation between the cell locations on MRM and histology is evident, and also the tractorophy with histology.

References: (1) Aiken NR, Hsu EW, Blackband SJ. A Review of NMR Microimaging Studies of Single Cells. *J Magn Reson Anal*. 1:41-48 (1995). (2) Flint JJ et al, Magnetic resonance microscopy of mammalian neurons. Neuroimage 15;46(4):1037-40 (2009)

Characterization of tissue microstructure using porous media concepts

Evren Özarslan[1]

[1] Section on Tissue Biophysics and Biomimetics, NICHD, National Institutes of Health, Bethesda, MD, USA.

Abstract:

Magnetic resonance (MR) imaging or spectroscopy measurements have been widely employed to characterize the structure of materials and biological tissues. The noninvasive character of the MR acquisitions as well as the exquisite contrast obtained within soft tissue has made MR imaging (MRI) an indispensable tool in monitoring functional activation in the brain and the morphological changes associated with development and aging. Due to its sensitivity to numerous diseases, MRI is also employed in routine clinical practice for diagnostic purposes. Despite aforementioned advantages, conventional MRI scans suffer from limited resolution that prohibits the visualization of individual cells thus providing information at coarse length scales. To obtain information at smaller length scales, the MR signal can be sensitized to the diffusion of water molecules [1] whose motional history is influenced by the local structure. To exploit this phenomenon, it is necessary to develop models that link the geometric characteristics of the medium to the MR signal intensity. These models can then be used in the inverse problem of extracting the microstructural features of the specimen from the acquired MR signal.

In this talk, we will discuss several such models that we have developed over the years. Specifically, characterizing diffusion anisotropy enables the mapping of local axonal fiber orientation, which can be subsequently used to map the neural connections between different regions of the brain. Another novel application of anisotropic diffusion enables the mapping of directions perpendicular to macroscopic interfaces which could be used in generating a differential structure of the cortical surface. We will also discuss how an anomalous diffusion model for gray-matter structures can be employed to quantify the scaling characteristics of diffusion and an apparent fractal dimension for tissue. Finally, recent developments in the double pulsed field gradient MR acquisitions to infer the cell size, shape, and orientation distribution function will be discussed.

1. P.T. Callaghan, A. Coy, D. MacGowan, K.J. Packer, F.O. Zelaya, Diffraction-like effects in NMR diffusion studies of fluids in porous solids, Nature 351 (1991) 467–469.

T23

Electron Paramagnetic Resonance Imaging of Tumor Oxygen Status *In Vivo*

Murali Krishna Cherukuri, Shingo Matsumoto, Hironobu Yasui, Keita Saito, Nallathamby Devasahayam, James B. Mitchell, and Sankaran Subramanian

Radiation Biology Branch
Center for Cancer Research, National Cancer Institute
NIH, Bethesda, Maryland

Small animal such as mice are used in model studies with tumor xenografts or orthotopically growing tumors to assess treatment efficacy with drugs and radiation. In addition to looking at tumor growth kinetics and tissue analyses for specific markers, imaging studies are used. Most imaging modalities provide volumetric and morphological information on tumors and tumor response to treatment. However these changes manifest several days-weeks to manifest. Molecular/physiological changes in tumors appear within a day or two after treatment initiation in responding tumors. Imaging techniques which can determine molecular physiological properties in in vivo in tumors will be useful in drug discovery research or potentially for human use. Electron Paramagnetic Resonance Imaging is an emerging technique which has been implemented for in vivo applications using exogenous paramagnetic trityl-based free radicals which are non-toxic. The in vivo distribution of the trityl radicals can be assessed in EPR imaging from which the oxygen dependent line width provides information pertaining to tissue oxygen.

EPR Imaging studies in tumor bearing mice to specifically determine oxygen status and changes in response to treatment will be presented.

T24

^{2}H Double Quantum Filtered NMR Studies of Water Compartmentation in Sciatic and Optic Nerves

H. Shinar, T. Ben-David, U. Eliav and G. Navon

School of Chemistry, Tel Aviv University, Tel Aviv, Israel

The technique of ^{2}H double quantum filtered (DQF) NMR enables spectral separation of the different water compartments of biological tissues on the basis of their different residual dipolar interaction (1). In the study presented here we have used this technique to assign the different ^{2}H signals in sciatic and optic nerves to the nerve's anatomical compartments.

The ^{2}H in-phase DQF spectra (2) of rat sciatic nerve equilibrated in deuterated saline consists of 3 quadrupolar split satellites (approximate splittings: 1400, 500 and 200 Hz.) and a narrow central transition (Fig. 1). The overlap between signals B and C can be resolved by adding an inversion segment before the DQ filter. We have assigned signals A, B, C and D to the water in the epineurium, myelin, endoneurium and the intra-axonal water respectively. The assignment is based on a series of experiments: Upon addition of collagnease, an enzyme which degrades the collagen fibers and thus destroys their ordering, signal A is instantaneously decreased and signal C is abolished on a longer time scale. We have also found that signals A and C are shifted by various shift reagents such as Co-EDTA. In experiments where the nerve was stretched the quadrupolar splittings of signals A and C were considerably larger, an effect which is probably due to the loss of water from these compartments, while the effect on signal B was negligible. Moreover, during Wallerian degeneration of injured sciatic nerves, where the axons and the myelin are known to be affected, we have found a decrease in the intensity of signal B and D. The technique also enabled the study of the water exchange between the different compartments and the axons.

Fig. 1. ^{2}H in-phase DQF spectra of rat sciatic nerve. τ is the creation time of the 2nd rank tensors
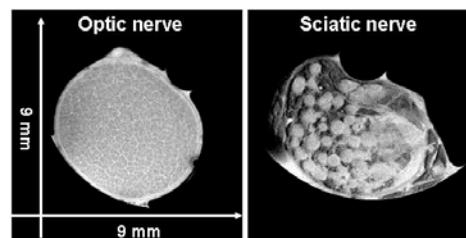
Fig 2. Gradient echo images of porcine sciatic and optic nerves

Similar results were obtained for porcine sciatic and optic nerves. The main differences in the ^{2}H DQF spectra of optic and sciatic nerves are the relative intensities of the signals corresponding to the different compartments. In the optic nerve, signal B which we have assigned to the water in the myelin sheaths is more enhanced and signal C which was assigned to the water in the collagen matrix of the endoneurium has a much lower intensity. This is due to the structural difference between the two nerves as can be seen in the high resolution ^{1}H images (Fig. 2).

References: 1. H. Shinar et al., JMR,**129** (1997),98. 2. U. Eliav et al. JMR, **137** (1999),295.

Wednesday September 2nd
Talks:

Mobile / Low Field I

Mobile / Low Field II

The NMR Machine: A Convenience Tool?

Bernhard Blümich,[1] Nadia Amor,[1] Federico Casanova,[1] Ernesto Danieli,[1] Agnes Haber,[1] Maxime Van Landeghem,[1,2] and Juan Perlo[1]

[1] Institute of Technical and Macromolecular Chemistry, RWTH Aachen University, Aachen, Germany
[2] Physico-chimie des Polymères et des Milieux Dispersés, UMR 7615 CNRS UPMC, ESPCI ParisTech, 10 rue Vauquelin, 75005 Paris, France

Abstract:

Mobile NMR devices are out for a while. Typically they are single-sided for nondestructive testing of large objects such as the borehole wall of an oil well or a historic building [1]. As such, mobile NMR is the counterpoint to laboratory NMR and clinical MRI with high-field magnets. Current NMR technology largely focuses on the development of stronger magnets with increasing demands for space, acquisition cost, and maintenance cost. The development of mobile NMR moves in the opposite direction. Magnets and hardware become smaller with more perfect fields not only for desktop relaxometry but also for desktop imaging and spectroscopy with the perspective of future micro NMR devices [2-5]. The three prominent application areas are high-throughput screening [4, 5], in-line monitoring, and NMR at extreme conditions. All of these types of application are expensive to serve or cannot be served with conventional high-field NMR instruments. In addition to that, small-molecule NMR at fields lower than 7 T is becoming obsolete lack of modern instrumentation, so that small-scale NMR not only offers new windows of opportunity in research and technology but is anticipated to reintroduce NMR to the analytical laboratory as a convenience instrument next to HPLC, IR, DSC and other instruments of analysis ready for use when needed at little to no maintenance cost. Progress in technology and applications of small-scale NMR will be reported addressing in particular desk-top magnets [3], low power excitation [6], and Laplace exchange NMR [7].

1. B. Blümich, F. Casanova, J. Perlo, Mobile Single-Sided NMR, *Progr. Nucl. Magn. Reson. Spectr.* **52** (2008) 197–269.
2. B. Blümich, J. Mauler, A. Haber, J. Perlo, E. Danieli, F. Casanova, Mobile NMR for geophysical analysis and materials testing, *Petroleum Science* **6** (2009) 1-7.
3. E. Danieli, J Mauler, J., Perlo, B. Blümich, F. Casanova, Mobile Sensor for High-Resolution NMR Spectroscopy and Imaging, *J. Magn. Reson.* **198** (2009) 80-87.
4. Lee, H., Sun, E., Ham, D., Weissleder http://www.nature.com/nm/journal/vaop/ncurrent/abs/nm.1711.html - a1, R., Chip–NMR biosensor for detection and molecular analysis of cells. Nature Medicine **14**, (2008) 869-874.
5. McDowell A., Fukushima, E., Ultracompact NMR: ^{1}H Spectroscopy in a Subkilogram Magnet. Appl. Magn. Reson. **35** (2008) 185–195.
6. B. Blümich, Q. Gong, E. Byrne, M. Greferath, NMR with excitation modulated by Frank sequences, *J. Magn. Reson.* **xxx** (2009) xxx – xxx.
7. M. Van Landeghem, A. Haber, F. Casanova, J.B. d'Espinose de Lacaillerie, B. Blümich, *Multi-Site Relaxation-Exchange NMR*, to be published

T26

Living with ultracompact NMR magnets

<u>Andrew McDowell</u>, Lana Chavez, Amanda McChesney, and Eiichi Fukushima

ABQMR, Inc., Albuquerque, New Mexico, USA

Abstract:

We have shown that is possible to build very small permanent magnets (few kilogram or even sub-kilogram) that achieve very high resolution (sub ppm) over volumes large enough to provide easy single-shot detection of NMR signals.[1]   Shown below is a 0.20 ppm line achieved in a 0.7 kg, 0.96 T magnet; the signal is a signal acquisition from a sample of volume of about 7 nL.

That magnet was unshimmed and the sample position was carefully adjusted to yield the narrowest line. We have since built shim coils for such magnets according to the designs of Anderson. The shim coils eliminate the need for careful sample placement and allow the routine achievement of line widths less than 100 ppb.

The combination of high resolution and small size presents some unusual challenges for those accustomed to permanent-magnet-based NMR systems. Most notably, the small magnet's field can change rapidly in response to temperature fluctuations, leading to limits on resolution and even spurious peaks in the spectra. Thermal fluctuations in the sample fluid can also reduce the spectral resolution when the detector volume is a very small fraction of the total volume of the fluid. In addition, the high magnetic field homogeneity of the shimmed magnets has the potential to place high demands on the materials and methods of probe construction.

We are pursuing a number of applications with our ultracompact NMR systems. One is the detection of single superparamagnetic beads in fluids. Experiments on beads immobilized in agarose gels show that single beads can readily be detected and that the contrast in the detection is due to both homogeneous and inhomogeneous broadening of the water resonances in the fluid near the bead. Spin dynamics simulations are consistent with our measurements.

We have also pursued MRI experiments in our ultracompact magnets. The image below is of three tubes (0.33 mm OD, 0.20mm ID) inside a 1 mm ID tube. The image is a single plane from a 3D spin echo image, 23µm x 23µm x 185µm resolution, 3.5 minutes experiment time.
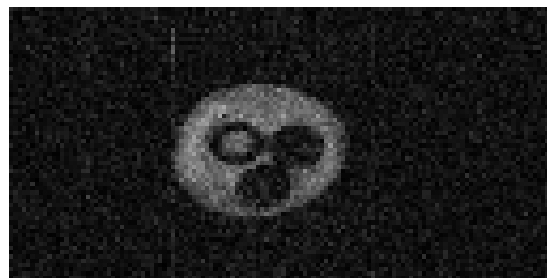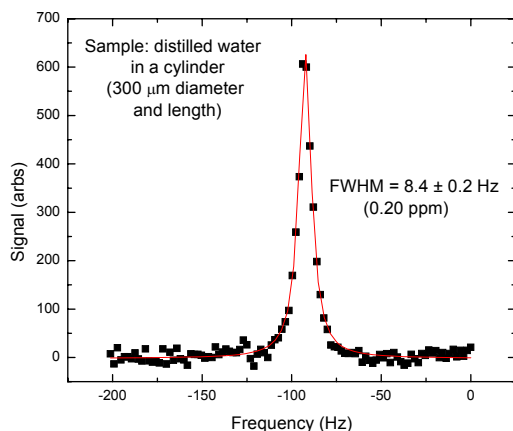
1.   McDowell and Fukushima, *Appl. Magn. Reson.* **35** (2008) 185-195.

T27

A Two-Dimensional NMR Method of Probing the Internal Field Gradients in Rocks

Lizhi Xiao   Ranhong Xie

China University of Petroleum, Beijing, China 102249

The internal field gradients in rocks have a big effect on nuclear magnetic resonance (NMR) transverse relaxation T_2 distribution. A two-dimensional NMR method of probing the internal field gradients of rocks is suggested and its inversion algorithms are developed using CPMG pulse sequence. Internal field gradient distributions of water-saturated sandstone and shaly sandstone with paramagnetic impurities are obtained. The result shows that internal field gradient of rocks increase with the increasing of content of paramagnetic impurities. The internal field gradients of sandstones with uniform grain show unimodal distributions. The T_2 distributions of water-saturated shaly sandstones with chlorite show bimodal feature with obvious irreducible water peak. The small pores with short T_2 have higher internal field gradients than that of the big pore with long T_2. When the content of chlorite is smaller than 15%, the short T_2 components corresponding to irreducible water peak increase with increasing the content of chlorite, T_2 distribution becomes wider. However, when the content of chlorite is more than 15%, the higher internal field gradients result in short relaxation component decaying quickly, the short T_2 components decrease, T_2 distribution becomes narrower with increasing the content of chlorite.

T28

Quantitative Analysis of Earth's Field NMR Spectra of Tightly-Coupled Heteronuclear Systems

Meghan E. Halse[1], Roderick E. Wasylishen[2], and Paul T. Callaghan[1]

[1] MacDiarmid Institute for Advanced Materials and Nanotechnology, Victoria University of Wellington, Wellington, New Zealand
[2] Department of Chemistry, University of Alberta, Edmonton, AB, Canada

Abstract:

One of the distinguishing features of ^{1}H NMR spectroscopy carried out in the relatively weak Earth's magnetic field ($B_E \sim 0.5$ G or 50 mT) is the observation of strong indirect spin-spin coupling between heteronuclei. While the NMR spectra of tightly coupled nuclei of the same species, so-called AB spectra, are commonly observed using high-field laboratory NMR spectrometers, the difference in Larmor frequency between heteronuclei in super-conducting magnets is such that the weak coupling condition is always satisfied for heteronuclear spin systems. Therefore, working in the Earth's magnetic field provides a unique opportunity to observe and analyze the spectra of tightly coupled nuclei of differing spin.

In this work we discuss the analysis of ^{1}H EFNMR spectra of systems where one spin is a quadrupolar nucleus ($I > \frac{1}{2}$) while the other nuclei in the spin system are spin-$\frac{1}{2}$. We will demonstrate the efficacy of perturbation theory for modeling and understanding these systems by comparing first-, second- and third-order perturbation theory calculations to exact calculations and to experiment. Two spin-systems are investigated: the ammonium cation, NH_4^+, which is well described by second-order perturbation theory and the tetraborohydrate anion, BH_4^-, for which a third-order perturbation energy term in required.

T29

ON-line coupling of capillary electrophoresis with portable NMR detection for pharmaceutical and environmental exposure applications

Kristl L. Adams[1], Joana Diekmann[2], Greg Klunder[1], Paul T. Steele[1], Christopher Harvey[1], Lee Evans[1], Julie Herberg[1]

[1] Lawrence Livermore National Laboratory, 7000 East Ave., Livermore, CA 94551, USA
[2] Leibniz University Hannover, Callinstr. 1, 30167 Hannover, Germany

Abstract:

Trifluoroacetic acid (TFA) is widely used in pharmaceutical peptide synthesis and purification; it is also a persistent atmospheric degradation product of hydrofluorocarbons and is increasingly used as an alternative to ozone-damaging chlorofluorocarbons. It is crucial to monitor for TFA in environmental risk assessments and in products intended for human use due to the toxicity effects of TFA binding to metabolic proteins in the kidney, liver, and other organs [*1*]. TFA content can be separated and measured by many techniques, including gas chromatography [*2*], ion chromatography [*3*], and capillary electrophoresis (CE) [*4*]. With the rising popularity of fluorinated pharmaceuticals [*5*], ^{19}F NMR offers an unsurpassed speciation method for determining compound chemistry and post purification TFA contamination. Currently purified peptides undergo a separation technique, followed by fractionation collection, NMR, and mass spectrometry analysis. Relatively large samples are needed for typical laboratory NMR measurements. The integration of CE with on-line portable NMR offers a low-cost high-throughput detection method for drug discovery that requires only nanoliter quantities for analysis. Time and reagent costs can be dramatically reduced by using small-scale methods for drug screening. In environmental applications, costs can again be reduced by screening samples on-site with portable technologies. We have coupled CE with a portable NMR system that uses lithographically patterned microcoils and a small 1.8T permanent magnet. We will present details on the integration of CE with the on-line ^{19}F NMR system with representative separations of TFA and perfluorinated organic acids from fluorinated compounds such as perfluorodecalin, a blood substitute.

1. A. Preiss, J. Kruppa, J. Buschmann, C. Mugge, *Journal of Pharmaceutical and Biomedical Analysis* **16**, (Apr, 1998) 1381.
2. C. E. Wujcik, T. M. Cahill, J. N. Seiber, *Analytical Chemistry* **70**, (Oct 1, 1998) 4074.
3. E. Kaiser, J. Rohrer, *Journal of Chromatography A* **1039**, (Jun 11, 2004) 113.
4. M. J. Little, N. Aubry, M. E. Beaudoin, N. Goudreau, S. R. LaPlante, *Journal of Pharmaceutical and Biomedical Analysis* **43**, (Mar 12, 2007) 1324.
5. J. P. Begue, D. Bonnet-Delpon, *Journal of Fluorine Chemistry* **127**, (Aug, 2006) 992.

T30

Portable Magnetic Resonance for Medical Diagnostics

Vasiliki Demas , James Chepin, Tom Lowery, Matthew Blanco

T2 Biosystems, 286 Cardinal Medeiros Ave, Cambridge MA 02141

Abstract:

Magnetic Resonance (MR) is a powerful tool for non-destructive evaluation of substances. On going innovations in portable MR have enabled new applications outside of the conventional high-field NMR laboratory. Non-conventional MR imaging and relaxation measurements are being attained with compact unilateral and portable sensors [1], and spectroscopy is conducted in one-sided and halbach type magnets [2]. As part of a an in-vitro medical diagnostics instrument, we have developed a prototype portable MR reader, which includes a permanent magnet, probe, spectrometer board, electronics, and computer for MR measurements of biological specimens.

T2 Biosystems is combining portable MR with magnetic relaxation switch technology to create a new class of magnetic resonance diagnostic sensors that provide sensitive, selective, molecular diagnostics in point of care settings. Magnetic relaxation switch assays consist of polymer-coated superparamagnetic nanoparticles that transition between dispersed and clustered states due to the presence of a target substance [3], and affect the T_2 relaxation times of surrounding water molecules in the specimen under investigation. Analyte sensitivity is achieved by functionalizing the nanoparticles with a binding agent, such as an antibody. To date, benchtop relaxometers and high-field MRI scanners have been used for MRSw measurements of a wide variety of analytes and specimen types. These include viruses, bacterial pathogens, proteins, nucleic acids, and small molecules in a variety of matrices such as buffer, whole blood, serum, plasma, urine, and crude cell lysate at concentration levels of picomolar or single virus particles [4].
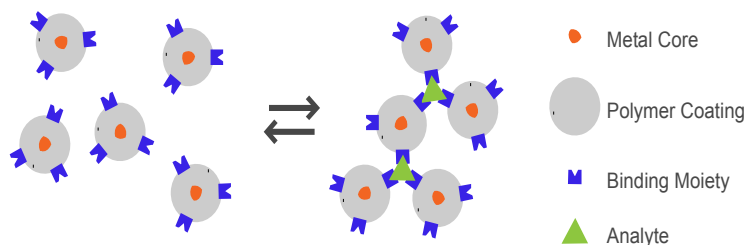
Fig. 1: Cartoon depicting particle clustering in the presence of analyte

1. Eidmann, G., Savelsberg, R., Blümler P., and Blümich, B *J. Magn. Reson. A* **122** (1996) 104-109; Prado, P.J., Blümich, B., and Schmitz, U., *J. Magn. Reson. A* **144** (1998) 200-206; Casanova, F. and Blümich, B., *J. Magn. Reson.* **163** (2003) 38-45; Prado, P.J. *Magn. Reson. Imaging* **21,** (2003) 397-400, and **19** (2001) 506-508; Murphy, D.P. *World Oil* **216**, no. 4 (1995) 65-70; Freedman, R., and Morriss, C.E. *70th SPE Annual Technical Conference and Exhibition, Dallas, Texas, USA.* (1995)
2. Meriles C.A., Sakellariou, D., Heise, H., Moule, A.J., and Pines, A., *Science* **293**, (2001) 82-85; Meriles, C.A., Sakellariou, D., and Pines, A., *J. Magn. Reson.* **164** (2003) 177-181; Demas, V., Sakellariou, D., Meriles, C., Han, S., Reimer, J., and Pines, A., *Proc. Natl. Acad. Sciences USA* **101** (24) (2004) 8845-8847; Perlo, J., Demas, V., Casanova, F., Meriles, C., Reimer, J., Pines, A., and B. Blümich *Science* **308** (2005) 1279; Perlo, J., Casanova, F., and B. Blümich *Science* **2007**; Demas V., Herberg J.L., Malba V., Bernhardt , A., Evans L., Harvey C., Chinn S.C., Maxwell R.S., Reimer J., *Journal of Magnetic Resonance* **189 (1)** (2007) 121-129.
3. Perez, J. M.; Joesphson, L.; Weissleder, R. *ChemBioChem* **5** (2004) 261-264.
4. Perez, J. M.; Simeone, F. J.; Saeki, Y.; Josephson, L.; Weissleder, R. *J. Amer. Chem. Soc.* **2003**, 125, 10192-10193; Kaittanis, C.; Naser, S. A.; Perez, J. M. *Nano Letters* **7** (2007**)** 380-383; Perez, J. M. Josephson, L. O'Loughlin, T. Hogemann, D. Weissleder, R. *Nature Biotech.* **20** (2002**)** 816-820; Sun, E.Y., Weissleder, R. and Josephson, L. *Small* **2** (2006) 1144-1147.

T31

Development of a portable MRI system for fruits and trees

Takeshi Kimura[1], Daiki Tamada[1], Shinya Handa[2], Katsumi Kose[3], Tomoyuki Haihsi[4], Kazuma Togashi[4], Hiroshi Gemma[5], Yoshihiko Sekozawa[5]

1. College of Engineering Sciences, University of Tsukuba, 2. Japan Society for the Promotion of Science,
3. Institute of Applied Physics, University of Tsukuba, 4. MRTechnology Inc.
5. Agricultural and Forestry Research Center, University of Tsukuba

Introduction: There are many papers that report postharvest fruits studied with laboratory MRI systems (1-3). However, if a portable MRI system for fruits or trees is developed, new MRI applications can be proposed. In this study, we have developed a portable MRI system for fruits and trees and evaluated its performance using phantoms and several pears.

Portable MRI system: The portable MRI system consists of a permanent magnet (field strength = 0.12 T, gap width = 170 mm, homogeneous region = 100 mm d.s.v., weight = 160 kg, Hitachi metals Co. Japan), a gradient coil set, RF probes, and a portable MRI console. The magnet was placed on a fork of a mobile lift (GL-4, Genie Industries, WA, USA) with a horizontal or a vertical gap space as shown in Fig.1. By using this lift, the height of the imaging region can be varied from 60 cm to 160 cm. Because the ratio of the pole piece diameter to the magnet gap was about 1.5, we designed the transverse gradient coil using the genetic algorithm as shown in Fig.2. We developed two RF probes with 68 mm and 113 mm clear bores for fruits as shown in Fig.3. The total power consumption of the MRI console was about 300 W.

Experiments: The MRI system was evaluated using a sphere water phantom (diameter = 96 mm) in our laboratory. After the laboratory experiments, the MRI system was operated in a pear orchard in our university as shown in Fig. 4. Several pears (Kousui, Japanese pear) were imaged using a 3D spin echo sequence (TR/TE = 200 ms/12 ms, matrix = 128^3, voxel size = $(1.2 \text{ mm})^3$, NEX = 1).

Results and discussion: Figure 5 shows a zx cross section of the phase image of the water phantom. Because the k-space origin was shifted from the spin-echo peak by 1 ms, this figure shows magnetic field distribution (about ±200 ppm in the 96 mm diameter sphere). Figure 6 shows contiguous vertical slices selected from a 3D image dataset of a pear acquired in the orchard. These images show a promise of our system. At present, several pears are measured every week and the ripening process is periodically monitored. Serial observation of fruits diseases will be another promising application.
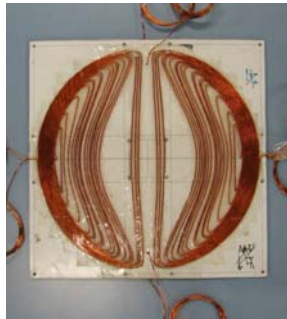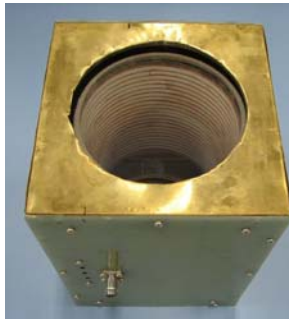
Fig.1   Fig.2   Fig.3   Fig.4
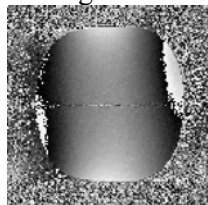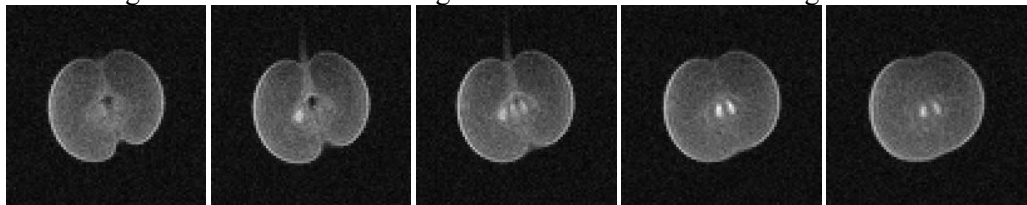
Fig. 5   Fig. 6

References:
(1) M. Koizumi, N. Ishida, H. Kano. Current topics in plant biology. **2**, 1-20 (200).
(2) G. Galed, M. E. Fernandez-Valle, A. Marinez, A. Heras. Mag. Reson. Imag. **22**, 127-137 (2004).
(3) M. Musse et al. Postharvest Biol. Technol. **53**, 22-35 (2009).

New developments of low field NMR

S. Appelt

Abstract:

We report about high resolution NMR experiments in the Gauss regime. The static magnetic field with an homogeneity of $\Delta B/B \sim 1$ ppm over 1 cm^3 is generated with a simple mobile open coil configuration without using any shim coils. Hyperpolarized ^{129}Xe NMR confirms this homogeneity.

^{1}H chemical shift differences in the ppm range of small organic molecules can be measured down to the ultimate limit of the static field, where the chemical shift differences correspond to the line width. We show that this limit can be broken if different hetero-nuclear J couplings for the corresponding chemical groups are present.

An exact theoretical condition is introduced, where the complex line splitting of NMR spectra due to the strong J-coupling starts to be observable. The experimental results and simulations of these complex NMR spectra strongly support the theoretical predictions.

Permanent Magnets for NMR and MRI

Cédric Hugon [1], Pedro M. Aguiar [1], Guy Aubert [1] and Dimitris Sakellariou[1]

[1]   DSM/IRAMIS/SIS2M/LSDRM CEA Saclay, Gif-sur-Yvette, France

Abstract:

Mobile NMR and MRI have been developed since the pioneering work on well logging, to reach modern high-resolution systems. Permanent magnets are key to such mobile systems and the development of rare earth NdFeB and SmCo materials allows us to generate magnets of important strength and homogeneity. Most current systems are based on bar magnets or Halbach designs and produce fields with poor homogeneity compared with high-field superconducting magnets.

Here we will introduce an approach for magnet design based on symmetry considerations as well as an analytical theory of magnetostatics that allows the design of arbitrary magnetic fields inside (in-situ) and outside (ex-situ) permanent magnets[1], having the required field homogeneity. The control of the field profiles can be mastered at any order, which leads to large sweet spots and deep object-penetration distances.

We revisit some previously proposed magnet structures[2] in the light of this new approach as well as present new homogeneous magnet structures which generate magnetic fields pointing at arbitrary orientations, in particular at the magic angle[3]. Applications to *in-situ* magnets and experimental results on small-scale prototypes will be presented, together with a discussion about imperfections and shimming.
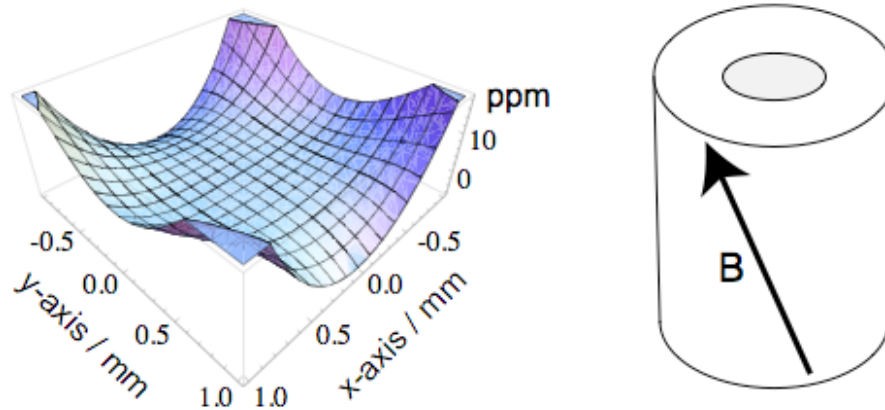
Fig. 1: Field map of the magnitude of the magnetic field in ppm, in a plane perpendicular to the z-axis of the magnet at z=0. The magnetic field points at an angle of ~54.7 degrees from this axis and reaches 0.25T.

1.   C. Hugon, P. Aguiar, G. Aubert, D. Sakellariou, *C. R. Chimie,* submitted (2009).
2.   G. Aubert, "Cylindrical Permanent Magnet with longitudinal induced Field", US Patent 5,014,032.
3.   D. Sakellariou, C. Meriles, R. W. Martin and A. Pines, Magn. Reson. Imag. **23,** (2005) 295-299.

The NMR-CUFF: from concept to portable plant imager

<u>Carel W. Windt</u>, Dagmar van Dusschoten and Peter Blümler

ICG-3, Forschungszentrum Jülich, Jülich, Germany

Abstract:

Plants are, in terms of geometry, terrible subjects for NMR. They are large and wide, whereas the objects of interest (stems, fruits, leaves) tend to be small. To fit a plant in a magnet the magnet bore either needs to be large enough to contain the whole plant, or the magnet needs to have an air gap that is wide and freely accessible. Both approaches are used in the laboratory, but are unsuitable for mobile applications: both wide bore and C-shaped magnets are too big and heavy. To facilitate portable plant NMR a magnet is needed that is lightweight, homogeneous enough to be able to measure long T_2's and allow imaging, open or openable to clamp it around stems, and small enough to fit between branches and leaves. In this contribution we present hand portable imagers based on the NMR-CUFF (Cut open, Uniform, Force Free) concept that meet these criteria.

An NMR-CUFF is composed of stacked Halbach type permanent magnet rings, spaced judiciously for optimal homogeneity. The assembly consists of two hinged halves and can be opened and closed with minimal force. Simple pole caps were used to counteract and smooth out field imperfections caused by spacers and flaws in the magnet elements of the Halbach rings. The prototype shown in fig. 1 weighed only 3.1 kg and provided a flux density of 0.57 T over a 3 cm bore, with a homogeneity <50 ppm over a 5 mm sphere after passive shimming, and <100ppm before. The homogeneity was maintained even after repeated opening and closing.

To allow imaging and q-space flow encoding, compact openable plane-parallel gradient coils were designed. The necessarily small gradients and RF coils here are advantageous, making it possible to drive the system with low cost, low powered and potentially battery operated RF- and gradient amplifiers. Because of space limitations only gradients for the X and Z direction were fitted. The gradient coils were laser-cut from 0.5 mm thick copper sheets, producing 630 mT/m at 40 A, and were positioned directly on the poles. The system was completed with a solenoid RF-coil wound on a split-able PTFE template plus an external broad band tuning circuit.

The NMR-CUFF was tested on various objects. It proved capable of acquiring echo trains several seconds in length and was suitable for multi-component T_2 analysis in botanical and industrial applications. Its quality and practical usefulness was further demonstrated by spin echo imaging and non-spatially resolved q-space sap flow measurements in trees.
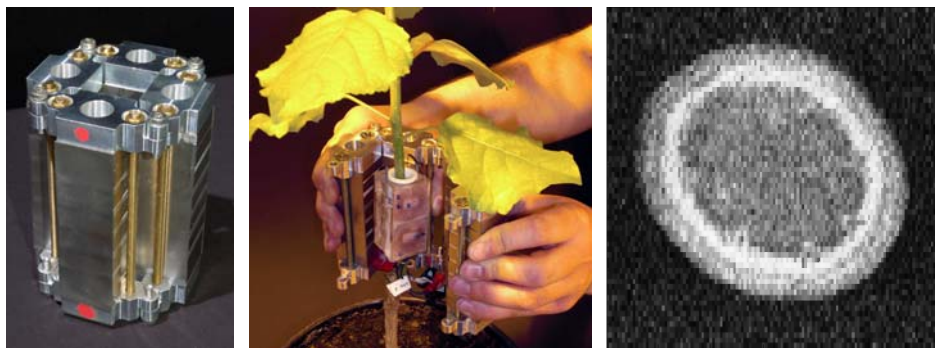
Fig. 1: NMR-CUFF (left), mounted around the stem of a tree (middle). Right: image of a stem slice.

Thursday September 3rd
Talks:

Young Investigators

Polarization Enhancement Techniques and Applications

2D Relaxation and Diffusion Correlation Experiments

T35

Characterization of complex cellular structures through displacement correlations measured using PGSE NMR

Tyler R. Brosten[1], Joseph D. Seymour[2], Robert S. Maier[3], Sarah L. Codd[1]

[1]Department of Mechanical and Industrial Engineering, Montana State University, USA
[2]Department of Chemical and Biological Engineering, Montana State University, USA
[3]U.S. Army Engineer Research and Development Center, Vicksburg, USA

Abstract:

Solid cellular structures are an important class of porous materials found throughout the industrial and natural world [1]. Previous techniques for measuring a characteristic length scale of these structures have relied upon *ad hoc* effective radii formulations. In this work a methodology is introduced in which the characteristic length scale is instead defined by a length scale inherent to the dynamics of dispersion within the pore space of the structure. Pulsed gradient spin-echo techniques are used probe the dispersion dynamics of water flow through the pore space of 97% porosity, fully-open, polymer foam. The short time dynamics of transverse dispersion, $D_\perp(t) = \sigma_\perp^2/t$, are found to be governed by coherent motion of fluid through the pore space. A correlation between axial displacement and transverse dispersion, $D_\perp(\zeta_\parallel)$, reveals a characteristic length scale, see figure 1. Similar 'memory' effects in transverse dispersion have been observed in flow through monodisperse packed beds [2-4].
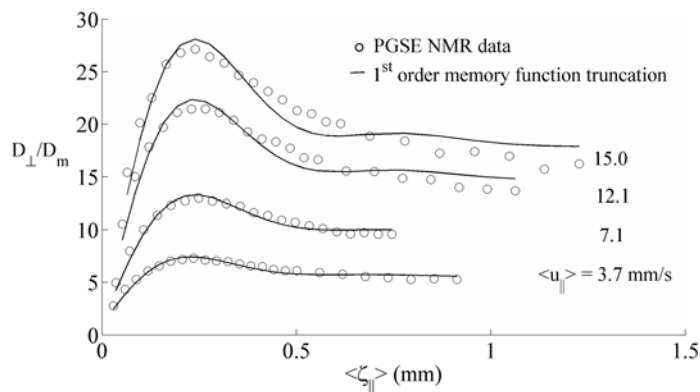
Fig. 1: Normalized effective transverse dispersion coefficient in a foam sample vs. mean displacement, also shown is an analytical fit using a first order truncation of the continued-fraction approach [5]; the maximum of these curves occurs at a fixed mean displacement of 250 μm

To better understand this stochastic process an analogy is made to molecular hydrodynamics. Theory from non-equilibrium statistical mechanics, which has been applied to nonlocal dispersion [6], provides a foundation for an analytical description of the memory effects found in transverse dispersion. The first order approximation to the memory function of the velocity autocorrelation function is adopted to model the experimental data in figure 1.

1. L. J. Gibson and M. F. Ashby, *Cellular solids : structure and properties, 2nd ed. Cambridge Press, (1997)*
2. S. Stapf, K. J. Packer, R. G. Graham, J. F. Thovert, and P. M. Adler *Phys. Rev. E* **58** (1998) 6206-6221
3. R. S. Maier, D. M. Kroll, R. S. Bernard, and H. T. Davis *Physics of Fluids* **12** (2000) 2065-2079
4. P. T. Callaghan and S. L. Codd, *Physics of Fluids, 13* (2001) *421-427*
5. H. Mori, *Progress of Theoretical Physics* **34** (1965) 399-&
6. J. H. Cushmann, X. Hu, T. R. Ginn, *Journal of Statistical Physics* **75** (1994) 859-&

T36

Compact Magnet Array for High-Resolution NMR and MRI with Portable Sensors

Ernesto Danieli , Juan Perlo, Federico Casanova, and Bernhard Blümich

ITMC, RWTH Aachen University, Worringerweg 1, D-52074, Aachen, Germany.

During the last years important progress has been reported in the development of mobile NMR sensors built from permanent magnets. These probes, unlike superconductor magnets, are small in size, low in cost, robust, and can achieve different degree of versatility at reasonable magnetic field intensity and homogeneity. Although, for years the lack of high resolution in such magnets was accepted to be the price paid for mobility of the sensor, we have recently demonstrated that the inhomogeneity of the magnetic field can be corrected by equipping the magnet with a suitable shim unit built from movable magnets. Setting the shim unit to generate a magnetic field that reproduces the spatial dependency of the main field, but in an opposing direction, a resultant field with high homogeneity has been achieved even in open sensors [1]. This strategy has proven to be also extremely efficient in shimming the field of closed magnet arrays where we successfully implemented fast MRI imaging techniques and proton spectroscopy in considerable large volumes [2].

In this work, we present a new magnet design where the movable pieces form part of the main unit to gain improved performance by additive instead of subtractive field correction. The movable magnets generate the different spherical harmonics terms needed to correct for the imperfection of the pieces forming the magnet. This strategy allowed us to obtain not only the desired homogeneity but also a higher magnetic field strength than the one achieved with the previous approach, since all magnet blocks contribute to the magnetic field in a constructive way. The higher performance of this approach enabled us to reduce the size of the magnet keeping the field strength and the sample volume constant. In particular, it was used to build a palm size magnet working in a volume large enough to fit conventional 5 mm NMR tubes where the high field homogeneity allowed us to measure proton NMR spectra of different solvents with a resolution better than 0.16 ppm at 30 MHz. By scaling the dimensions of the magnet the same geometry was optimized to build a portable MRI scanner for imaging of large cylindrical volumes of up to 5 cm long and 5 cm in diameter.
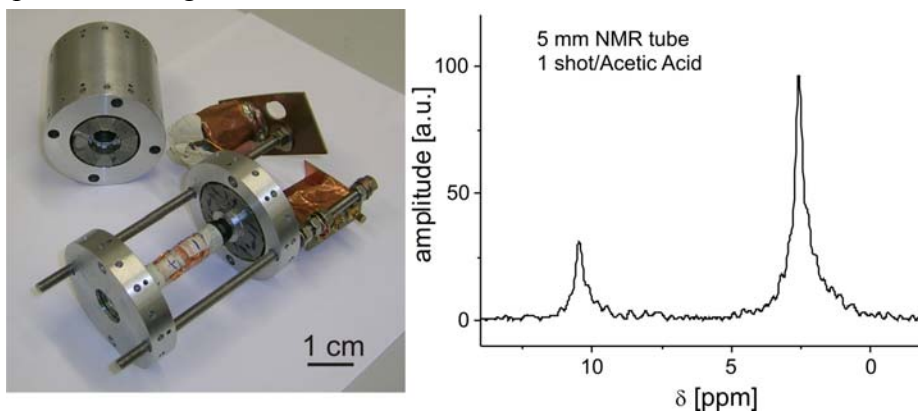
Fig. 1: Palm size magnet built from three Halbach rings made from SmCo (left). Acetic acid spectrum measured in a 5 mm. NMR tube at 0.7 T (right).

1.   J. Perlo, F. Casanova, and B. Blümich, *Science*, **315** (2007) 1110-1112.
2.   E. Danieli, J. Mauler, J. Perlo, B. Blumich, and F. Casanova, *J. Magn. Reson.*, **198** (2009) 80-87.

T37

High-Resolution-NMR below 200 kHz

Stefan Gloeggler[1] , Bernhard Bluemich[1] and Stephan Appelt[2]

[1] Institute of Technical and Macromolecular Chemistry, RWTH Aachen University, Aachen, Germany
[2] Central Institute for Electronics, Research Center Juelich, Juelich, Germany

Abstract:
We have built a new low-field NMR device based on electromagnets that operates with a B_0-field homogeneity of 1 ppm over $1 cm^3$ without shim coils.
To proof the homogeneity a spin-spin-relaxation experiment of ^{129}Xe was performed at 35 G, which corresponds to a ^{129}Xe-Larmorfrequency of 41.6 kHz.
As shown in figure 1 a T_2 of 7.5 seconds was obtained.

With this device it was possible to measure the chemical shift differences of protons in acetic acid for the first time at 9.8 G (^{1}H-Larmorfrequency of 41.6 kHz).
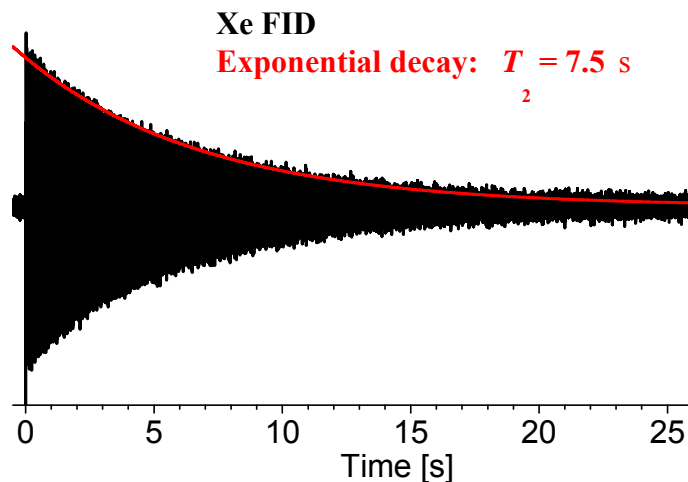
Fig.1: ^{129}Xenon FID at 35 G

T38

Velocity Imaging using Compressed Sensing

D.J. Holland[1], D.M. Malioutov[2], A. Blake[2], A.J. Sederman[1], L.F. Gladden[1]

[1] Department of Chemical Engineering and Biotechnology, University of Cambridge, Cambridge, United Kingdom.
[2] Microsoft Research Ltd., 7 J J Thomson Ave, Cambridge, CB3 0FB, UK.

Abstract:

In this work we show that compressed sensing can be successfully applied to phase encoded velocity MRI to decrease data acquisition times by up to an order of magnitude. Imaging velocity fields using Magnetic Resonance (MR) is time consuming. This is particularly problematic when studying multiphase flows. Compressed Sensing (CS) is a recent development from the signal processing field that utilizes the principles behind image compression technology to reconstruct images from sparse k-space sampling. We have developed a CS algorithm to measure the velocity distribution in both gas- and liquid-flows from significantly under-sampled data.

The image reconstruction method is based on maximizing the sparsity in a transform, Ψ, of the image. Examples of these sparse representations include the wavelet, and the spatial finite differences transforms. The reconstruction is obtained by solving the following constrained optimization problem:

$$\min \left\| \Psi \mathbf{x} \right\|_1$$

$$\text{subject to} \quad \left\| F\mathbf{x} - \mathbf{y} \right\|_2 < \varepsilon \tag{1}$$

where $\mathbf{x}$ is a vector representation of the image, F is the Fourier transform, and $\mathbf{y}$ is the vector of the measured k-space data points. The constraint, ε, is a threshold that can be set to the expected noise level. The l_1-norm acts as a proxy for sparsity – i.e. minimizing the objective in Eqn. 1 produces an image which has the sparsest representation in the transform domain while remaining consistent with the acquired measurements.

Figure 1 shows a velocity field reconstructed from a 30 % sampling of k-space using Eqn. 1. The CS reconstruction has been used, on both simulated and real data, to reconstruct images from only 30 % of the full k-space data set with less than 1 % error in the total flow measurement and less than 9 % error based on the l_2-norm. This CS approach is applicable to any imaging technique, and thus provides a general method for accelerating MR data acquisitions.
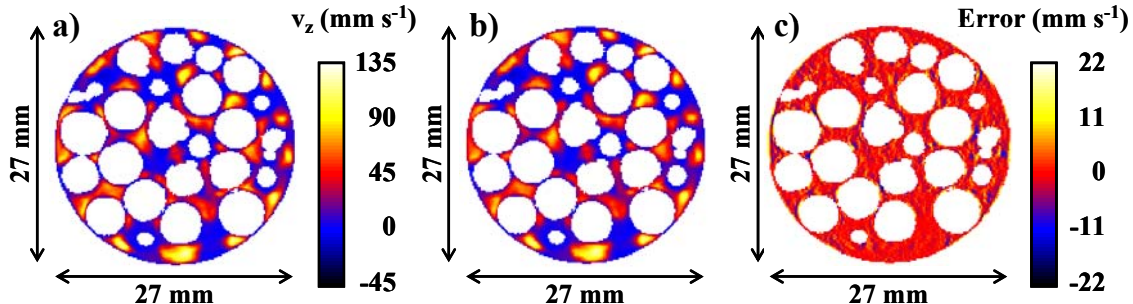
Fig. 1: a) MR map of the axial velocity of water flowing through a packed bed of 5 mm diameter spheres for full k-space sampling. b) Reconstruction of the velocity field in (a) with only 30 % sampling of the full k-space distribution. c) Absolute error in the reconstructed distribution.

Accurate Reconstruction of Under-sampled Images with Compressed Sensing and Dynamic Filtering

P. Parasoglou[1], D. Malioutov[2], A.J Sederman[1], J.Rasburn[3] and H. Powell[3], L. Gladden[1], A. Blake[2] and M.L Johns[1]

[1] Department of Chemical Engineering and Biotechnology, University of Cambridge, Cambridge, UK
[2] Microsoft Research Ltd, Cambridge, UK
[3] Nestec York Ltd, York, UK

Abstract:

Sparse *k*-space acquisitions when zero-filled and reconstructed with the use of a Fourier transform will exhibit artifacts and compromised quantification. In this study we compare the accuracy of reconstruction achieved when different methods are used, all of which essentially estimate the values of the un-sampled *k*-space points. The required experimental data was obtained by Single Point Imaging (SPI)[1] applied to determine the absorbed moisture distribution in a food wafer system, as described previously[2] this is a food conditioning process involving sample exposure to a humid air environment. A sample wafer image is shown in Figure 1(a). Seven wafer humidification experiments were performed at different air-flow conditions, each experiment consisted of 10 images of the wafer at increasing moisture content.. The norm of the difference of the under-sampled reconstructed images compared to the fully sampled case is presented in Figure 1(b) as a function of the % of *k*-space sampled for various reconstruction methods. Image reconstruction with the use of previously sampled points (hybrid image) performs slightly better than the usual practice of zero-filling[3]. Compressed sensing[4,5] improves reconstruction accuracy considerably (as shown in Figure 1(b)), by using an iterative optimization reconstruction that tries to calculate the missing *k*-space points by exploiting a sparse image domain. Further improvement can be achieved with the use of a dynamic filter (a Kalman filter in this case) and incorporation of prior knowledge of system dynamics.
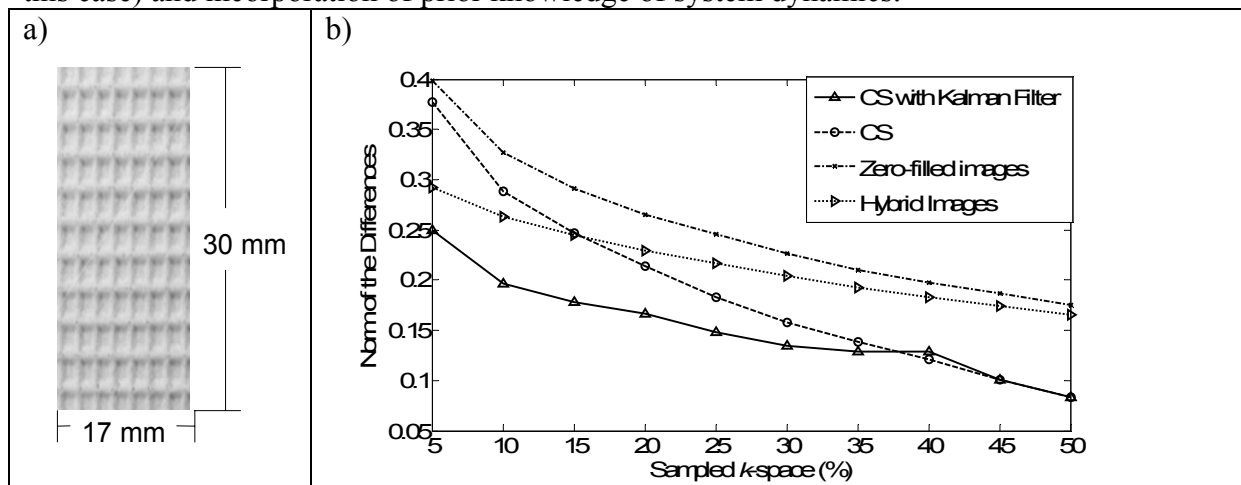
Fig. 1: Norm of the difference of the reconstructed images compared with the fully-sampled, as a function of the percentage of acquired *k*-space

(1)Emid, S.; Creyghton, J. H. N. *Physica B & C* **1985**, *128*, 81-83.
(2)Parasoglou, P.; Sederman, A. J.; Rasburn , J., Powel, H.; Johns, M. L. *Diffusion Fundamentals* **2009**, *10*, 1-3
(3)Parasoglou, P.; Sederman, A. J.; Rasburn, J.; Powell, H.; Johns, M. L. *Journal of Magnetic Resonance* **2008**, *194*, 99-107.
(4)Lustig, M.; Donoho, D. L.; Santos, J. M.; Pauly, J. M. *Ieee Signal Processing Magazine* **2008**, *25*, 72-82.
(5)Parasoglou, P.; Malioutov, D.; Sederman, A. J.; Rasburn , J.; Powel, H.; Gladden, L. F.; Blake, A.; Johns, M. L. *Journal of Magnetic Resonance*, (submitted).

Broadband volume coil for MR microscopy at 900 MHz

Chunqi Qian[1], Ihssan Masad[1,2], Samuel C. Grant[1,2], and Peter L. Gor'kov[1]

[1] National High Magnetic Field Laboratory, Tallahassee, FL 32310
[2] Chemical & Biochemical Engineering, Florida State University, Tallahassee, FL 32310

Abstract: The unique 900-MHz ultra-wide bore 21.1 T magnet in the National High Magnetic Field Lab provides great opportunities to the MRI community. To fully realize its potential, certain limitations of conventional RF hardware must be addressed. Among these is a necessity for the transmit/receive volume coil to tune over a broad range of sample loads. Frequency tuning in the standard birdcage coil is often achieved by adjusting the variable trimmer capacitor across one or two legs. This convenient tuning scheme, however, can disturb B_1 homogeneity. In this work, we show that a 900 MHz rat-size birdcage coil can achieve azimuthally symmetric tuning by mechanically varying the overlapping capacitance between the ring and the legs.
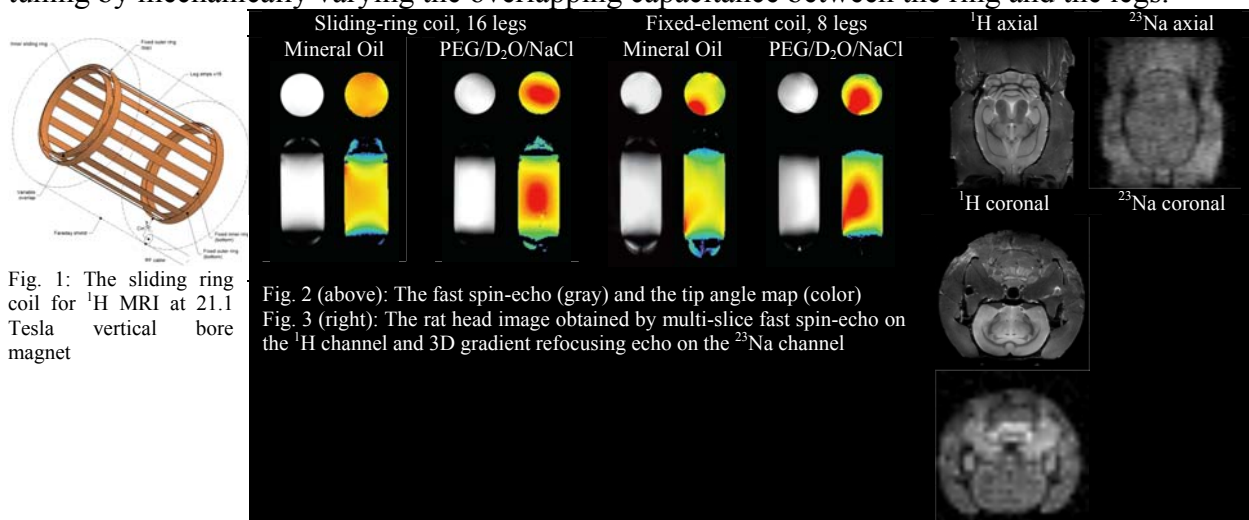
Fig. 1: The sliding ring coil for ^{1}H MRI at 21.1 Tesla vertical bore magnet

Fig. 2 (above): The fast spin-echo (gray) and the tip angle map (color)
Fig. 3 (right): The rat head image obtained by multi-slice fast spin-echo on the ^{1}H channel and 3D gradient refocusing echo on the [23]Na channel

Fig. 1 shows the physical implementation of the sliding ring birdcage coil. The coil has two fixed outer rings which help to retain a constant longitudinal FOV, and at least one inner ring that can slide up and down to maintain the azimuth symmetry during frequency tuning. The coil is fed at a single point located at the bottom end ring via a variable matching capacitor. The coupling between the legs and the coil's Faraday shield provides a return path to the ground.

Fig. 2 shows the image comparison under different sample loading conditions. To achieve impedance matching for both samples, the conventional fixed element coil cannot have more than 8 legs. But the sliding ring coil will have an increased tuning range with the increased number of legs. And as a result, the images from 16-leg sliding ring coil are more homogeneous than images from the 8-leg conventional coil.

This tuning approach can be extended to the double-resonant coil as well. Fig. 3 shows the multi-nuclei images obtained on an *ex-vivo* fixed rat head. The proton images have an in-plane resolution of 115 x 115 μm^2 (5 minutes acquisition time), which is sufficient to discern detailed anatomical structure. The sodium images have an isotropic resolution of 1 mm (34 minutes acquisition time). By combining both sets of images, structural and function information can be correlated. It is noteworthy to mention that when compared to the single resonance coils, this double-resonance birdcage retains 70% sensitivity in the proton channel and 90% sensitivity in the sodium channel. And the FOV only drops in the longitudinal direction of the proton channel to 70% that of a single resonance coil. All of these favorable properties can facilitate the unambiguous co-registration of multi-nuclei images.

1. J.C. Watkins, E. Fukushima, *Rev. Sci. Instru.* **59** (1988) 926-929

T41

Polarisation manipulation in MRI
by magnetic field-cycling and DNP

David J. Lurie, Lionel Broche, Chang Hoon Choi, Gareth R. Davies,
Saadiya R. Ismail, Dara Ó hÓgáin and Kerrin J. Pine

Aberdeen Biomedical Imaging Centre, University of Aberdeen, AB25 2ZD, Scotland, UK
www.ffc-mri.org

Dynamic Nuclear Polarisation (DNP) has been investigated as a method of detecting and imaging free radicals for more than 20 years. In the basic method of Proton-Electron Double-Resonance Imaging (PEDRI) the sample's EPR is irradiated during the acquisition of a proton NMR image. Parts of the sample containing unpaired electrons exhibit altered image intensity due to the Overhauser transfer of polarisation from electron to proton spins, revealing the location of the free radical under study [1]. In biological applications it is necessary to perform the experiment at very low field (~10 mT) so that the EPR irradiation is at sufficiently low frequency (<300 MHz) to penetrate into the sample without depositing excessive heat.

The disadvantage of PEDRI at low field is the inherently low SNR. To counter this, magnetic field-cycling can be employed. In Field-Cycled PEDRI (FC-PEDRI) the field is switched between a low value (B_0^E, the evolution field) and a high value (B_0^D, the detection field) during the pulse sequence. EPR irradiation takes place at B_0^E, typically 4 mT, at a correspondingly low frequency (~100 MHz). The field is then switched to B_0^D and the NMR detection pulse(s) and imaging magnetic field gradients are applied [1].

As well as using field-cycling for free radical imaging, we have explored its use in "pure" fast field-cycling MRI (FFC-MRI). The aim is to obtain spatially-resolved T_1-dispersion data, by collecting images at a variety of evolution field strengths. This has the potential to obtain new types of image contrast. Relaxometric imaging using field-cycling was first demonstrated by Carlson in 1992 [2], and since then relaxometric imaging methods have been implemented in Aberdeen [3], Stanford [4] and Western Ontario [5].

To date we have constructed two FFC-MRI systems. Both use the "field-compensation" method of field-cycling employing dual, coaxial magnets – one for signal detection at B_0^D and the other for partial field-cancellation. The first system employs a whole-body sized (60 cm bore) 59 mT permanent magnet [6] while the second employs a 450 mT superconducting primary magnet, with a coaxial resistive field-offset coil (15 cm bore) [7]. In this case an active shield coil is used, placed between the superconducting magnet and the field-offset coil, in order to prevent eddy currents in the superconducting magnet's cryostat.

1. Lurie D.J. In: "In Vivo EPR (ESR): Theory and Applications" Biological Magnetic Resonance, Vol. 18, ed: L.J. Berliner, Kluwer Academic / Plenum Publishers, New York., 547-578 (2003).
2. Carlson J.W., Goldhaber D.M., *et al*., Radiology **184**, 635-639 (1992).
3. Lurie D.J., 1st Symposium on Field-Cycling NMR Relaxometry, Berlin, p5, July 1998.
4. Ungersma S.E., Matter N.I., *et al*., Magn.Reson.Med. **55**, 1362-1371 (2006).
5. Handler W.B., Gilbert K.M., *et al*., Phys.Med.Biol. **51**, 2479-2491 (2006).
6. Lurie D.J., Foster M.A., Yeung D. and Hutchison J.M.S., Phys. Med. Biol. **43**, 1877-1886 (1998).
7. Lurie D.J., Davies G.R., *et al*., Magn.Reson.Imaging **23**, 175-181 (2005).

Enhancement of CEST and DNP by iDQC

Gil Navon,[1] Uzi Eliav[1] Mor Mishkovsky,[2] and Lucio Frydman[2]

[1] School of Chemistry, Tel Aviv University, 69978 Tel Aviv, Israel
[2] Chemical Physics Department, Weizmann Institute, 76100 Rehovot, Israel

Abstract:
Intermolecular Multiple-Quantum Coherences (iMQCs) provide a new type of contrast in MRI as a result of (a) their dependence on the intermolecular distance and (b) the non-linear dependence of the signal on the size of the magnetization. We have previously shown that iDQC gives enhanced effects of magnetization transfer (MTC) [1], chemical exchange saturation transfer (CEST) and nuclear Overhauser effect (NOE) [2], in agreement with the theoretical M^2 dependence of the signal. A major drawback of iMQC is their inherent low sensitivity. A recent study demonstrated that ex situ dynamic nuclear polarization (DNP) could assist in overcoming sensitivity problems for iDQC-based experiments on ^{13}C nuclei [3]. In the present work we show that although the DNP procedure enhances single-quantum ^{1}H signals only by about 600, which is significantly less than in optimized low- liquid-state counterparts, the nonlinear dependence of iDQC-derived signals on polarization can yield very large enhancements of the ^{1}H iDQC approaching 10^6. This enhancement allowed us to perform single-scan ^{1}H 2D iDQC imaging and spectroscopic experiments with SNR comparable to the single quantum counterparts (see Figure). The short times required to obtain ^{1}H hyperpolarization can be exploited for repetitive injections. This in turn opens up interesting possibilities of their own, both in terms of imaging applications as well as within spectroscopic setting.
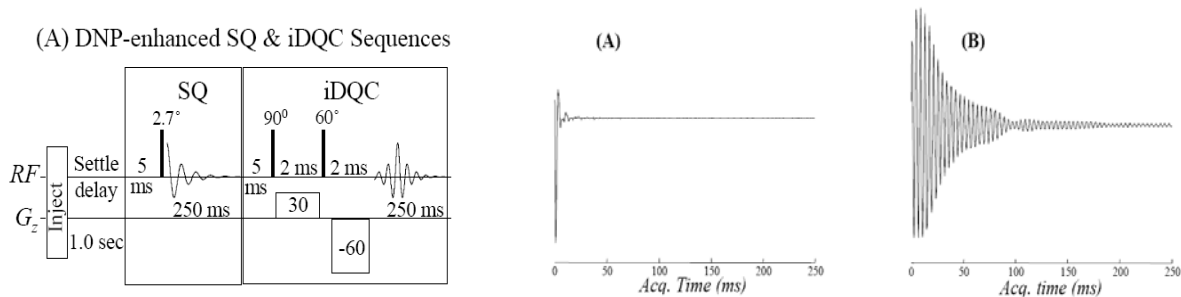
Fig. 1 Left side show the pulse sequence used to acquire the shown FIDs on the right hand side. Both SQ and iDQC measurements were done in a single shot. The tilt angle in the SQ segment of the sequence was set to 2.5^o in order to ensure that most of the magnetization is used for the iDQC experiment. The short T_2* of the SQ FID is a result of magnetic field inhomogeneity due to air bubbles.

1. U. Eliav, G. Navon, *J. Magn. Reson.* **190** (2008) 149-153
2. W. Ling, U. Eliav, G. Navon, A. Jerschow, *J. Magn. Reson.* **194** (2008) 29-32.
3. E. R. Jenista, R. T. Branca and W. S. Warren, *J. Magn. Reson.* **196** (2009) 74-77.

T43

Microtesla MRI with dynamic nuclear polarization

Vadim S. Zotev[1], Tuba Owens[1], Igor M. Savukov[1], Andrei N. Matlashov[1], John J. Gomez[1], and Michelle A. Espy[1]

[1] Los Alamos National Laboratory, Applied Modern Physics Group, Los Alamos, NM, USA

Abstract:

Magnetic resonance imaging at microtesla fields is a promising imaging method, which has seen significant developments over the past several years. This method combines the pre-polarization technique and signal detection by highly sensitive superconducting quantum interference device (SQUID) sensors to enable MRI at microtesla fields similar in strength to the Earth magnetic field. Recently, we demonstrated the first microtesla MRI of the human brain in combination with magnetoencephalography [1]. Despite this and other advances, microtesla MRI presently suffers from insufficiently high SNR due to low sample polarization, which limits its potential for biomedical imaging. One promising way to substantially increase SNR is to use the dynamic nuclear polarization (DNP) approach based on Overhauser effect. DNP of ^{13}C, performed at low temperatures with subsequent sample dissolution and injection, allows polarization enhancement by >10,000 times over polarization levels achieved in conventional high-field MRI systems [2]. Imaging of hyperpolarized substances labeled with ^{13}C has been successfully used for angiography, perfusion mapping, real-time metabolic imaging, and interventional MRI with unprecedented SNR levels. Because hyperpolarization of ^{13}C is performed outside a scanner, high magnetic fields of conventional MRI instruments offer little advantage for these applications. Moreover, hyperpolarized substances can be naturally imaged by microtesla MRI using specially designed multichannel SQUID systems with magnetic fields less than 1 mT. Here we describe our recent work on microtesla MRI with DNP. We demonstrate, for the first time, microtesla MR images acquired with Overhauser enhancement and SQUID signal detection. We also report the first NMR measurements of ^{13}C at low magnetic fields. The experiments were performed at 96 microtesla measurement field with pre-polarization at 3.5 - 5.7 mT and RF irradiation at 120 MHz. Room-temperature samples were doped with TEMPO free radicals. Our seven-channel SQUID MRI system was modified for DNP and used for the experiments. We achieved polarization enhancement by factor as high as 90 for protons and as high as 200 for ^{13}C. Our results demonstrate that DNP greatly improves SNR performance of microtesla NMR/MRI. They also suggest that SQUID-based microtesla MRI can be naturally combined with the ^{13}C hyperpolarization technique and successfully used for angiography and metabolic imaging.

1. V.S. Zotev et al, *J. Magn. Reson.* **194** (2008) 115-120.
2. J.H. Ardenkjaer-Larsen et al, *Proc. Natl. Acad. Sci. USA* **100** (2003) 10158-10163.

Continuous Flow Dynamic Nuclear Polarization of Water under Ambient Conditions for *in-vivo* Perfusion MRI

Mark D. Lingwood[1], Napapon Sailasuta[2], Ting Ann Siaw[3], Brian D. Ross[2], Pratip Bhattacharya[2], and Songi Han[1]

[1] Department of Chemistry and Biochemistry, University of California, Santa Barbara, USA
[2] Enhanced Magnetic Resonance Laboratory, Huntington Medical Research Institutes, Pasadena, CA, USA
[3] Department of Chemical Engineering, University of California, Santa Barbara, USA

Abstract:

We are developing the use of dynamic nuclear polarization (DNP) via the Overhauser effect to improve contrast for magnetic resonance imaging (MRI) by continuously generating DNP-enhanced water under ambient conditions. Many applications exist where visualizing the transport of water is desired, such as perfusion imaging of the brain, but separating the water of interest from the bulk signal is difficult. Paramagnetic agents are commonly used to enhance contrast, but these agents do not accurately reflect the function and transport of water in the system, and can have adverse physiological effects. To overcome these problems we use pure water or saline solution in a hyperpolarized state to visualize the transport of the water as distinct from the bulk signal of the system. The benefits of using the Overhauser effect at room temperature, as compared to dissolution DNP systems which hyperpolarize for hours at 1.2K before rapid thawing and injection, are that enhanced water can be continuously generated, and the stable organic radicals required for DNP can be covalently attached to a solid support and filtered from the flowing water [1], preventing the infusion of radical to the system of interest.

Previously we demonstrated this technique in model systems, to show the feasibility of using water hyperpolarized by the Overhauser effect as an imaging contrast agent [2]. We have also made the necessary DNP equipment portable [3], and since we use the fringe field of the magnet for the hyperpolarization process, we can perform our experiments with any MRI system using the standard spectrometer and imaging sequences.

We are now applying our methodology to *in-vivo* imaging studies. The experimental setup has been constructed, including a homebuilt microwave amplifier, resonant cavity and flow system. We have seen success in phantoms, an example of which can be seen in Fig. 1, where the hyperpolarized water entering a tube can easily be distinguished from thermally polarized water in a standard image from a clinical MRI. Hyperpolarized water flowing through a standing pool of water has also been visualized. The initial results of *in-vivo* tests are promising, and further experiments are ongoing.
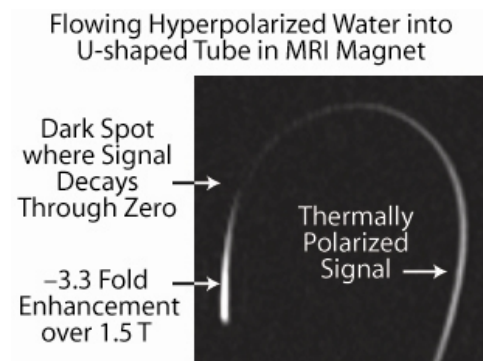
Fig. 1: Hyperpolarized water enters the tube on the left and flows clockwise to the right. Enhanced signal is visible for 1.4 seconds before the T_1 decay passes through zero.

1.   E.R. McCarney, S. Han, *J. Mag. Res.* **190** (2008) 307-315.
2.   E.R. McCarney, B.D. Armstrong, M.D. Lingwood, S. Han, *Proc. Nat. Acad. Sci. USA* **104** (2007) 1754-1759.
3.   B.D. Armstrong, M.D. Lingwood, et al., *J. Mag. Res.* **191** (2008) 273-281.

Overhauser Dynamic Nuclear Polarization at 0.04 T

Sandra Garcia[1], Brandon Armstrong,[2] Jeffrey Walton,[1] Songi Han[2] and Michael J. McCarthy[1]

[1] Food Science & Technology, University of California, Davis, Davis, USA
[2] Department of Chemistry and Biochemistry, University of California, Santa Barbara, Santa Barbara, USA

Abstract:

Several mechanisms for Dynamic Nuclear Polarization, DNP, are commonly used in current research. These include the Solid Effect, Thermal Mixing, Cross Effect and the Overhauser Effect. Out of these mechamisms, the Overhauser effect is most easily implemented because it does not require the sample to be frozen for polarization transfer to occur. In the presence of a magnetic field, electrons and nuclei in a solution are coupled. Nuclear signal enhancement occurs through a motion mediated relaxation process upon saturation of the electron spins.

Overhausser DNP has been employed at two extremes of the magnetic fields spectrum. At one end, it has been used for signal enhancement at Earth's field and the other end it has been used at 9.2 T where chemical shift resolution can be obtained.[1,2] Because the coupling factor between the electron and the nucleus (0.5) decreases with magnetic field, greater polarization enhancements can be obtained at lower fields at the cost of chemical shift resolution. Nonetheless, there is a great benefit in carrying out Overhauser DNP at low magnetic fields, mainly that the enhancement obtained from a system can be utilized to calculate translational correlation times and local viscosity parameters from the immediate surroundings of the electron and nuclear spins. Such an approach has been carried out by the Han group at UC Santa Barbara at 0.35 T, where we have measured a coupling factor of the electron and nucleus to be 0.22.[3] Here we report on the construction of a DNP setup that operates at 0.04 T and on the coupling factor we measured at this field, 0.4.

Large coupling constants are useful in analyzing local and surface (within 5 Angstrom) water's diffusion coefficients in the micelles or lipid bilayers as well as coacervate systems.[1] It is expected that the DNP signal at 0.04 T will provide higher contrast for measuring surface hydration dynamics of water than those observed at 0.35 T by the Han Group at UC Santa Barbara.

1. Meghan E. Halse, Paul T. Callaghan *J. Magn. Res.* **195** (2008) 162–168.
2. M. J. Prandolini, et al, *Appl. Magn. Res*. 34 (2008) 399-407.
3. B. Armstrong and S. Han, *J. Am. Chem. Soc*. **131** (2009), 4641–4647.

T46

A brief history of double wave-vector encoding

Paul T. Callaghan

MacDiarmid Institute for Advanced Materials and Nanotechnology, School of Chemical and Physical Sciences, Victoria University of Wellington, New Zealand.

The use of two pairs of magnetic field gradient pulses, applied in succession, allows for additional dimensionality in NMR diffusion and flow measurements. Obvious examples are the 2D velocity-velocity and diffusion-diffusion exchange experiments (1,2,3). And of course, where flow is present, it is possible to use double wave-vector encoding of opposite sign, to compensate for flow and reveal the underlying stochastic dispersion (4,5), a sophisticated variant of this being the measurement of the non-local dispersion tensor (6). But in fact the double-wave-vector experiment has an older vintage, dating back to a suggestion by Cory and Garroway in 1992 (7), verified in 2002 (8), that local pore anisotropy could be observed even in an isotropic distribution of pore orientations. A remarkable insight was provided by P.P. Mitra (9) who showed paradoxical dependence of the echo attenuation relative orientations of the wave-vector pair in porous media, work that has been extensively applied by Basser and co-workers (10) in medical imaging contrasts. This talk will present an overview and some prospects for the future.

(1) P.T. Callaghan and B. Manz, *J. Magn Reson* (1994) **A106**, 260
(2) P.T. Callaghan and I Fúro, , *J. Chem. Physics*, (2004) **120**, 4032
(3) Y. Qiao, P. Galvosas, T. Adalsteinsson, M. Schönhoff and P. T. Callaghan *J. Chem. Phys* (2005) **122**, 214912-1
(4) P.T. Callaghan, S.L. Codd and J.D. Seymour, *Concepts in Magnetic Resonance*, **11**, 181-202 (1999).
(5) A. A. Khrapitchev and P. T. Callaghan, *Phys. Fluids* **15**, 2649-2660 (2003)
(6) M.W. Hunter and P.T. Callaghan, *Phys. Rev. Lett.* **99**, 210602 (2007)
(7) D. G. Cory, A. N. Garroway, and J. B. Miller, Polym. Prepr. _Am. Chem. Soc. Div. Polym. Chem._ **31**, 149 (1990)_.
(8) P. T. Callaghan and M. E. Komlosh, Magn. Reson. Chem. **40**, S15 (2002).
(9) P. P. Mitra, Phys. Rev. B **51**, 15074 (1995)
(10) E. Özarslan and P. J. Basser, J. Chem. Phys**128**, 154511 (2008)

T47

2D NMR and Laplace Inversion

Yi-Qiao Song[1]

[1] Schlumberger-Doll Research, Cambridge MA USA

NMR has become one of the most important techniques for porous media studies in recent years. In particular, its application in petroleum exploration has been enhanced by the recent progress in NMR well-logging techniques for characterization of both rocks and fluids. Such advanced techniques are increasing being accepted as a valuable logging service especially in the technically challenging areas, such as deep-sea exploration. The continuous rise of global demand for energy and the difficulty of significantly increasing production capacity have made such oil reservoirs much more attractive. As a result, there is an urgent need of advanced technologies for better reservoir characterization and enhancing oil recovery. This talk will outline the recent MR development on two-dimensional NMR, MRI of rocks, and the mathematics of Laplace inversion.

T48

Determining Pore Sizes from T_2-T_2 Exchange Measurements

Jonathan Mitchell,[1] Thusara C. Chandrasekera,[1] Edmund J. Fordham,[2] Mike L. Johns,[1] and Lynn F. Gladden[1]

[1] Department of Chemical Engineering and Biotechnology, University of Cambridge, Cambridge, UK.
[2] Schlumberger Cambridge Research, Cambridge, UK.

Abstract:

T_2-T_2 relaxation exchange measurements have been used to observe molecular diffusive exchange in sedimentary reservoir rocks [3,4]. These experiments have been conducted, typically, at whatever magnetic field strength is available. However, we have acquired T_2-T_2 exchange data for water in a sandstone rock core across a range of field strengths and found a significant variation in the results, as highlighted in Fig. 1, where it can be seen that as magnetic field strength increases, both the number of discrete peaks on the T_2-T_2 diagonal and the number of off-diagonal peaks increases; the latter are associated with molecular diffusion between regions characterized by different relaxation times.
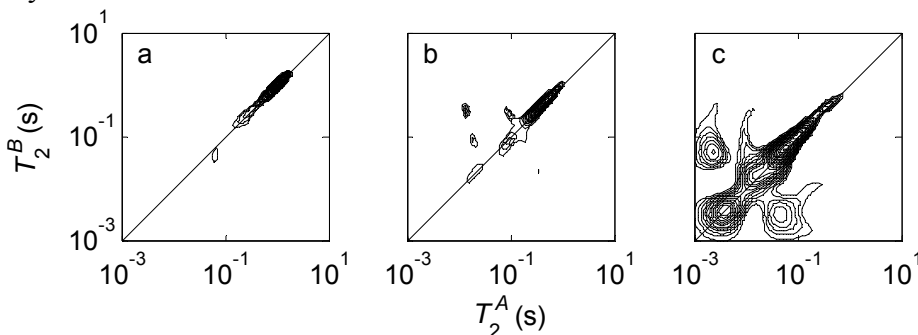
Fig 1. T_2-T_2 exchange plots of a water saturated sandstone core with an exchange time $t_S = 50$ ms, acquired at (a) low $B_0 = 0.05$ T, (b) intermediate $B_0 = 2$ T, and (c) high $B_0 = 9.4$ T magnetic field strengths. The diagonal lines indicate $T_2^A = T_2^B$ and the contour intervals are the same in each plot.

We have determined that the pores in this rock are large (radius $R > 10$ m) and that the pore size distribution is monomodal, so we assume the discrete peaks in the high field T_2 distribution do not correlate with pore size. We have therefore associated the variation in the T_2 data with the variation of internal magnetic field gradients that occur in the pores as a result of the susceptibility contrast between the liquid and the solid. These gradients are known to scale with magnetic field strength [5]. An overview of the information that can be reliably extracted from data acquired at different field strengths will be summarized. For example, for this rock sample, we will show that above a field strength $B_0 \sim 2$ T, diffusion in the pores is governed by the Localization regime [6], where magnetization is only observed from regions of local gradient minima (assumed to exist at pore centers) and near the pore walls. As such, exchange distances of R_X . ̃ ̃ m estimated from the high field data correspond to diffusive exchange between these local regions and lie in the range of the pore radii.

1. K. E. Washburn and P. T. Callaghan, *Phys. Rev. Lett.*, **97** (2006) 175502.
2. M. Fleury and J. Soualem, *J. Colloid Interf. Sci.*, **336** (2009) 250-259.
3. M. D. Hürlimann, *J. Magn. Reson.*, **131** (1998) 232-240.
4. T. M. de Swiet and P. N. Sen, *J. Chem. Phys.*, **100** (1994) 5597-5604.

Characterization of rock cores by Sodium NMR

Kathryn E. Washburn[1] , Guillaume Madelin[2] and Paul T. Callaghan[2]

[1] Weatherford Laboratories Norway, Trondheim, Norway
[2] MacDiarmid Institute for Advanced Materials, Victoria University of Wellington, Wellington, New Zealand

Abstract:

The ability to monitor the oil and water within rock cores is an aim of much porous media research. However, separation of the oil and water signal using proton NMR is nontrivial and many methods have been developed to attempt to isolate their signals. We present an alternative method to observe the behaviour of oil and water within a porous matrix. Rock cores from hydrocarbon reservoirs are typically saturated with water containing a high concentration of sodium chloride. Due to the polar nature of oil, salt will not be present in the oil phase. By monitoring the presence and amount of the sodium signal, the location and quantity of the water within the core can be inferred.

To test the ability to monitor movement of the differing fluids within the cores through the sodium signal, cleaned Bentheimer rock cores were saturated with mineral oil. Measurement of the sodium signal showed little or no sodium present in these cores. The cores were then placed in 100 kppm brine and allowed to spontaneous imbibe the liquid. Two dimensional images of the cores were then taken to show the influx of the salt water into the rock cores. These steps were repeated several times, showing the inflow of brine into the core over time. The patterns indicate an inhomogenous uptake of fluid into the core. Images taken on the cores several days after imbibition of the brine showed fluid redistribution throughout the core due to capillary forces. Calibration of image intensity against a fully saturated core of known pore volume allows us to determine the volume of brine that has been imbibed within the core.
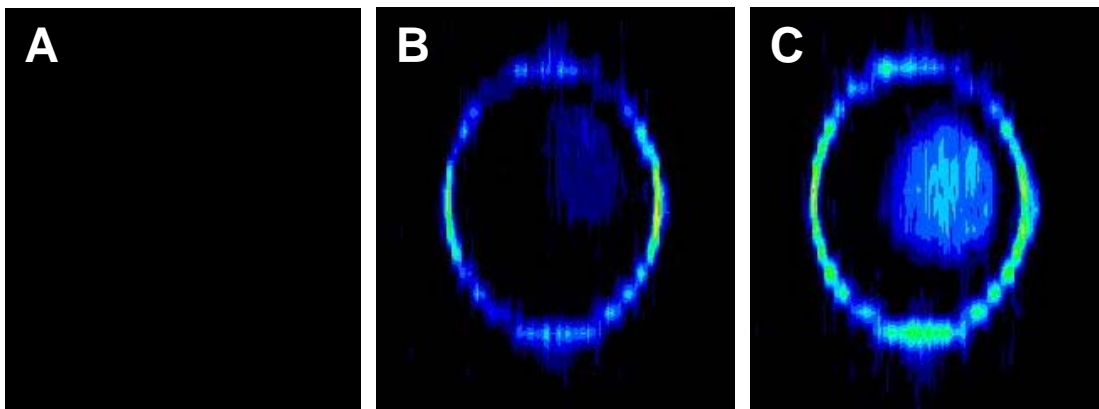
Fig. 1: a) Isopar L saturated b) 10 minutes brine imbibition c) 20 minutes brine imbibtition

For some cores, the sodium within the core can be located not only within the pore space, but in clay and the rock matrix itself. Multiple quantum filters can be applied to isolate the signal coming from the different populations of sodium.

Posters

Posters sorted by number

Poster #	Presenter	Title
P1	Muir, C.E.	Fluid Content Imaging of Porous Media - A Comparison of Methods
P2	Komlosh, M.E.	Pore diameter measured using d-PGSE-filtered MRI
P3	Adachi, S.	Visualization of liquid water distribution in wet snow using a compact MRI system
P4	Vogt, S.J.	Relaxation Measurements Determine Degree of Biofouling in Porous Media
P5	Haber, A.	Exchange in Natural Porous Media Investigated by NMR Relaxometry
P6	Leisen, J.	NMR Relaxometry of Layered Silicates containing Paramagnetic Impurities
P7	Olaru, A.M.	Physical and chemical changes in polymer/cement dispersions exposed to hydration
P8	Broadbent, A.L.	Magnetic resonance imaging and relaxometry to study rates of water uptake and diffusion in a commercially available gastrointestinal therapeutic system (GITS) tablet
P9	Bray, J.M.	Microstructure changes in a degradable bioceramic characterized in-vitro by NMR relaxation and diffusion mapping
P10	Van Landeghem, M	Multi-site relaxation exchange NMR
P11	Dvinskikh, S.	MRI of swelling, sedimenting, adsorbing and drying materials
P12	Valori, A.	Spatially resolved & Double Quantum Filter ^{1}H NMR studies of cementitious materials
P13	Zielinski, L.	Two-dimensional T_1-T_1 correlations between T_1 distributions at different Larmor frequencies
P14	Kolz, J.	Interactions of binary mixtures with polysaccharides investigated by 2D relaxation time measurements
P15	Fridjonsson, E.O.	Dynamic NMR study of colloidal particle deposition in a model porous media
P16	Fridjonsson, E.O.	Study of the flow dynamics of solid and liquid phases of a colloidal supsension in a microcapillary using NMR
P17	Rose, H.	Hydrodynamic Instabilities through Porous Media

P18	Rassi, E.M.	Influence of air on the hydrodynamics of water flow in porous media as investigated by magnetic resonance
P19	Brosten, T.R.	PGSE NMR measurements of colloidal particle transport through porous media - cellular foam
P20	Romanenko, K.V.	Flow imaging by magnetization prepared centric-scan SPRITE. Applications for core analysis.
P21	Kolz, J.	NMR velocity imaging of the extrudate flow profile at elevated temperatures and low liquid content
P22	Adair, A.	A Study of Cavitation in Fast Flow Using Motion-Sensitised SPRITE
P23	Kobayashi, K.	Visualization of the Rayleigh-Taylor instability in a soil liquefaction model system using magnetic resonance imaging
P24	Balcom, B.J.	MRI Velocity Mapping of Two-phase Flow in a Circular Capillary Tube
P25	Balcom, B.J.	Magnetic Resonance Imaging of Microfluidic Flow with a Parallel-Plate Resonator
P26	Feindel, K.W.	Rheo-NMR investigations of anomalous shear-banding: multidimensional dynamics under stick-slip conditions
P27	Altan, A.	Experimental evaluation of oil migration from almonds using MRI
P28	Halliday, N.	Magnetic Resonance Imaging of a Propagating Acidity Front in a Water-in-Oil Microemulsion
P29	Novak, J.	Magnetic Resonance Imaging of Chemistry in Flow
P30	Haber-Pohlmeier, S.	MRI Tracer Studies in Natural Soils
P31	Haber-Pohlmeier, S.	Waterflow Visualization by Tracer Transport in Root-Soil-Systems Using MRI
P32	Evertz, L.	Oscillatory Flow phenomena in simple fluids and complex fluids
P33	Paciok, E.	Ultrafast velocity mapping in planar micro-structures
P34	Utiu, L.	MRI for Investigations of Permeate Flow and Observation of the Cake-Layer Formation in Micro-Filtration Processes
P35	Broadbent, A.L.	Dynamic pulsed gradient spin echo nuclear magnetic resonance measurements and simulation of two-fluid mixing in Taylor vortex flow
P36	Shapley, N.C.	NMRI Characterization of Bimodal Suspension Flows
P37	Nevo, U.	Experimental models for studying the effect of shear-flow in biomedical DWI
P38	Brown, J.R.	Rheo-NMR Studies of Complex Spatiotemporal Dynamics in Wormlike Micelle Systems

P39	Reynaud, O.	Improved Flow ENhanced Signal Intensity (FENSI) perfusion imaging
P40	Creber, S.A.	Colloidal Acceleration in Porous Media Studied using NMR
P41	Creber, S.A.	Imaging and Quantification of Biofouling on Reverse Osmosis Membranes using NMR
P42	Renslow, R.	*In situ* effective diffusivity in biofilms
P43	Ogawa, K.	Development of a multi-layer planar gradient coil probe for a vertical bore superconducting magnet
P44	Handa, S.	Optimization of a planar gradient coil set using a genetic algorithm
P45	Balcom, B.J.	Three-Magnet Array for Unilateral Magnetic Resonance
P46	Horiga, M.	Development of a large bore planar gradient coil probe for a vertical bore superconducting magnet
P47	Wintzheimer, S.	A straightforward biplanar gradient design for mobile MR: Optimizing a modified maxwell/golay layout with simulated annealing
P48	Wintzheimer, S.	A novel gradient design for mobile MR: simultaneous generation of fast switchable linear and higher order field gradient for MR imaging
P49	Utsuzawa, S.	Design and construction of barrel magnets for unilateral NMR
P50	Steele, P.T.	Lithographically Produced Microcoils for Enhanced Portable NMR
P51	Hugon, C.	Single-sided magnets with controlled field profiles: high homogeneity on larger volumes
P52	Kochs, J.	Simple, high quality MRI r.f. coils for plants and other objects with a dumbell shape for use in supercons
P53	Blank, A.	Ex-situ Endorectdal MRI Probe for Prostate Imaging
P54	Aptaker, P.S.	Lexus: Laplacian 1-D exponential inversion software
P55	Minard, K.R.	Engineering & Performance of Magnetic Particle Imaging
P56	Gehrcke, J.-P.	Impact of local SPIO concentration on the Magnetic Particle Imaging signal
P57	Balcom, B.J.	Variable Bandwidth Filtering for Magnetic Resonance Imaging with Pure Phase Encoding
P58	Shigeki, R.	Static magnetic field shimming for MRI using a 3D geometrical phantom
P59	Van Dusschoten, D.	NMR microscopy T_2 mapping at high resolution
P60	Petrov, O.V.	Measuring spatially-resolved T_2 distributions in purely

		phase-encoded MRI applications
P61	Vogt, S.J.	Detection of Uranium Oxidation and Solubility using NMR
P62	Blank, A.	ESR Imaging in Solid Phase down to the Sub-Micron Resolution: Methodology and Applications
P63	Blank, A.	Direct Measurement of Diffusion in Liquid Phase by Electron Spin Resonance
P64	Subramanian, S.	Refinement of Oxygen resolution in Function EPR Imaging
P65	Chen, Y.Y.	Quantitative RARE imaging: applications to controlled drug delivery systems
P66	Kuethe, D.O.	Projection Imaging of Acrylic with FIDs *vs*. Solid Echos
P67	Kuethe, D.O.	Transient magnetization of permanent magnet pole pieces is trouble for projections imaging
P68	Muir, C.E.	Measuring Diffusion Using the Differential Form of Fick's Law and Magnetic Resonance Imaging
P69	Han, H.	Gradient waveform monitoring and adjustment with NMR microprobes
P70	Walton, J.H.	MR Thermal Imaging in the Presence of Motion
P71	Romanenko, K.V.	^{35}Cl profiling using centric scan SPRITE with variable flip angle excitation
P72	Nestle, N.	Diffusion effects in mm-scale spatlally selective excitation: more than just diffuse blurring
P73	Feindel, K.W.	Insights into knee cartilage degeneration: T_{1r} mapping at 4T and relevance to modern gait analysis
P74	Nakayama, T.	Measurement time reduction for trabecular bone volume fraction measurements of the calcaneus in the compact MRI system
P75	Saito, K.	Effects of rapamycin on tumor pO_2 and blood volume
P76	Munasinghe, J.P.	MRI of Kidney and Brain pathology in a mouse model of disseminated candidiasis
P77	Munasinghe, J.P.	Epileptogenesis leading to brief seizures do not cause MRI changes in brains of Rats
P78	Perles-Barbacaru	Mapping dopaminergic pathways by pharmacological MRI
P79	Kose, K.	3D MR microscopy of chemically fixed human embryos at 9.4 T
P80	Pope, J.M.	MR Micro-imaging of Articular Cartilage
P81	Beyea, S.D.	Quantifying High Concentrations of SPIO with TurboSPI
P82	Beyea, S.D.	High Resolution Asymmetric Spin-Echo (ASE) Spiral

		fMRI: An Examination of Functional Contrast & Specificity
P83	Mikac, U.	The use of magnetoliposomes as MRI contrast agents and for targeted drug delivery
P84	Zheng, S.	Influence of Relaxivity on Cartilage Glycosaminoglycan Imaging by Gadolinium Contrasts in MRI
P85	Sersa, I.	MR Microscopy Towards Detection of Neuronal Currents
P86	Milne, M.	Diffusion as a tool for understanding tissue differences in healthy and emphysematous lungs
P87	Minard, K.R.	^{3}He MR Microscopy of Pulmonary Airflow in Live Rats
P88	Oztop, M.H.	Diffusion of Water in Whey Protein Isolate Gels
P89	Oztop, M.H.	Investigation of different dehydration methods on proton environment in onions using ^{1}H-NMR relaxometry
P90	Melkus, G.	Non invasive imaging of ^{13}C labeled metabolites in barley seeds using geHMQC
P91	Wang, M.	Investigating embolism repair of xylem vessels in grape plants using proton magnetic resonance imaging
P92	Goudappel, G-J. W.	Water (re)distribution phenomena in savoury products - Understanding the effect of ingredients and processing on ageing
P93	Nestle, N.	Low-field integrated rheo-TD-NMR on industrial media - experiences and challenges
P94	Haber, A.	Non-Invasive Depth-Profiling of Walls by Portable Nuclear Magnetic Resonance
P95	Fabich, H.T.	Magnetic Resonance Analysis of Biopolymer Physically Crosslinked Gels
P96	Fukushima, E.	Magnetic Resonance Elastography of 3D force chains
P97	Utiu, L.	Hyperpolarized ^{129}Xe NMR Spectroscopy for Investigations of Porous Polymers
P98	Gong, Q.	*Para*-hydrogen-induced polarization in heterogeneous hydrogenation reactions
P99	Ma, Z.	Chemical Shift of Laser Polarized ^{129}Xe in BPTI Solution

Posters sorted by presenter

Poster #	Presenter	Title
P3	Adachi, S.	Visualization of liquid water distribution in wet snow using a compact MRI system
P22	Adair, A.	A Study of Cavitation in Fast Flow Using Motion-Sensitised SPRITE
P27	Altan, A.	Experimental evaluation of oil migration from almonds using MRI
P54	Aptaker, P.S.	Lexus: Laplacian 1-D exponential inversion software
p24	Balcom, B.J.	MRI Velocity Mapping of Two-phase Flow in a Circular Capillary Tube
P25	Balcom, B.J.	Magnetic Resonance Imaging of Microfluidic Flow with a Parallel-Plate Resonator
P45	Balcom, B.J.	Three-Magnet Array for Unilateral Magnetic Resonance
P57	Balcom, B.J.	Variable Bandwidth Filtering for Magnetic Resonance Imaging with Pure Phase Encoding
P81	Beyea, S.D.	Quantifying High Concentrations of SPIO with TurboSPI
P82	Beyea, S.D.	High Resolution Asymmetric Spin-Echo (ASE) Spiral fMRI: An Examination of Functional Contrast & Specificity
P53	Blank, A.	Ex-situ Endorectdal MRI Probe for Prostate Imaging
P62	Blank, A.	ESR Imaging in Solid Phase down to the Sub-Micron Resolution: Methodology and Applications
P63	Blank, A.	Direct Measurement of Diffusion in Liquid Phase by Electron Spin Resonance
P9	Bray, J.M.	Microstructure changes in a degradable bioceramic characterized in-vitro by NMR relaxation and diffusion mapping
P35	Broadbent, A.L.	Dynamic pulsed gradient spin echo nuclear magnetic resonance measurements and simulation of two-fluid mixing in Taylor vortex flow
P8	Broadbent, A.L.	Magnetic resonance imaging and relaxometry to study rates of water uptake and diffusion in a commercially available gastrointestinal therapeutic system (GITS) tablet

P19	Brosten, T.R.	PGSE NMR measurements of colloidal particle transport through porous media - cellular foam
P38	Brown, J.R.	Rheo-NMR Studies of Complex Spatiotemporal Dynamics in Wormlike Micelle Systems
P65	Chen, Y.Y.	Quantitative RARE imaging: applications to controlled drug delivery systems
P40	Creber, S.A.	Colloidal Acceleration in Porous Media Studied using NMR
P41	Creber, S.A.	Imaging and Quantification of Biofouling on Reverse Osmosis Membranes using NMR
P11	Dvinskikh, S.	MRI of swelling, sedimenting, adsorbing and drying materials
P32	Evertz, L.	Oscillatory Flow phenomena in simple fluids and complex fluids
P95	Fabich, H.T.	Magnetic Resonance Analysis of Biopolymer Physically Crosslinked Gels
P26	Feindel, K.W.	Rheo-NMR investigations of anomalous shear-banding: multidimensional dynamics under stick-slip conditions
P73	Feindel, K.W.	Insights into knee cartilage degeneration: T_{1r} mapping at 4T and relevance to modern gait analysis
P15	Fridjonsson, E.O.	Dynamic NMR study of colloidal particle deposition in a model porous media
P16	Fridjonsson, E.O.	Study of the flow dynamics of solid and liquid phases of a colloidal supsension in a microcapillary using NMR
P96	Fukushima, E.	Magnetic Resonance Elastography of 3D force chains
P56	Gehrcke, J.-P.	Impact of local SPIO concentration on the Magnetic Particle Imaging signal
P98	Gong, Q.	*Para*-hydrogen-induced polarization in heterogeneous hydrogenation reactions
P92	Goudappel, G-J. W.	Water (re)distribution phenomena in savoury products - Understanding the effect of ingredients and processing on ageing
P5	Haber, A.	Exchange in Natural Porous Media Investigated by NMR Relaxometry
P94	Haber, A.	Non-Invasive Depth-Profiling of Walls by Portable Nuclear Magnetic Resonance
P30	Haber-Pohlmeier, S.	MRI Tracer Studies in Natural Soils
P31	Haber-Pohlmeier, S.	Waterflow Visualization by Tracer Transport in Root-Soil-Systems Using MRI
P28	Halliday, N.	Magnetic Resonance Imaging of a Propagating Acidity Front in a Water-in-Oil Microemulsion

P69	Han, H.	Gradient waveform monitoring and adjustment with NMR microprobes
P44	Handa, S.	Optimization of a planar gradient coil set using a genetic algorithm
P46	Horiga, M.	Development of a large bore planar gradient coil probe for a vertical bore superconducting magnet
P51	Hugon, C.	Single-sided magnets with controlled field profiles: high homogeneity on larger volumes
P23	Kobayashi, K.	Visualization of the Rayleigh-Taylor instability in a soil liquefaction model system using magnetic resonance imaging
P52	Kochs, J.	Simple, high quality MRI r.f. coils for plants and other objects with a dumbell shape for use in supercons
P14	Kolz, J.	Interactions of binary mixtures with polysaccharides investigated by 2D relaxation time measurements
P21	Kolz, J.	NMR velocity imaging of the extrudate flow profile at elevated temperatures and low liquid content
P2	Komlosh, M.E.	Pore diameter measured using d-PGSE-filtered MRI
P79	Kose, K.	3D MR microscopy of chemically fixed human embryos at 9.4 T
P66	Kuethe, D.O.	Projection Imaging of Acrylic with FIDs *vs*. Solid Echos
P67	Kuethe, D.O.	Transient magnetization of permanent magnet pole pieces is trouble for projections imaging
P6	Leisen, J.	NMR Relaxometry of Layered Silicates containing Paramagnetic Impurities
P99	Ma, Z.	Chemical Shift of Laser Polarized ^{129}Xe in BPTI Solution
P90	Melkus, G.	Non invasive imaging of ^{13}C labeled metabolites in barley seeds using geHMQC
P83	Mikac, U.	The use of magnetoliposomes as MRI contrast agents and for targeted drug delivery
P86	Milne, M.	Diffusion as a tool for understanding tissue differences in healthy and emphysematous lungs
P55	Minard, K.R.	Engineering & Performance of Magnetic Particle Imaging
P87	Minard, K.R.	^{3}He MR Microscopy of Pulmonary Airflow in Live Rats
P1	Muir, C.E.	Fluid Content Imaging of Porous Media - A Comparison of Methods
P68	Muir, C.E.	Measuring Diffusion Using the Differential Form of Fick's Law and Magnetic Resonance Imaging
P76	Munasinghe, J.P.	MRI of Kidney and Brain pathology in a mouse model of disseminated candidiasis

P77	Munasinghe, J.P.	Epileptogenesis leading to brief seizures do not cause MRI changes in brains of Rats
P74	Nakayama, T.	Measurement time reduction for trabecular bone volume fraction measurements of the calcaneus in the compact MRI system
P72	Nestle, N.	Diffusion effects in mm-scale spatlally selective excitation: more than just diffuse blurring
P93	Nestle, N.	Low-field integrated rheo-TD-NMR on industrial media - experiences and challenges
P37	Nevo, U.	Experimental models for studying the effect of shear-flow in biomedical DWI
P29	Novak, J.	Magnetic Resonance Imaging of Chemistry in Flow
P43	Ogawa, K.	Development of a multi-layer planar gradient coil probe for a vertical bore superconducting magnet
P7	Olaru, A.M.	Physical and chemical changes in polymer/cement dispersions exposed to hydration
P88	Oztop, M.H.	Diffusion of Water in Whey Protein Isolate Gels
P89	Oztop, M.H.	Investigation of different dehydration methods on proton environment in onions using ^{1}H-NMR relaxometry
P33	Paciok, E.	Ultrafast velocity mapping in planar micro-structures
P78	Perles-Barbacaru	Mapping dopaminergic pathways by pharmacological MRI
P60	Petrov, O.V.	Measuring spatially-resolved T_2 distributions in purely phase-encoded MRI applications
P80	Pope, J.M.	MR Micro-imaging of Articular Cartilage
P18	Rassi, E.M.	Influence of air on the hydrodynamics of water flow in porous media as investigated by magnetic resonance
P42	Renslow, R.	*In situ* effective diffusivity in biofilms
P39	Reynaud, O.	Improved Flow ENhanced Signal Intensity (FENSI) perfusion imaging
P20	Romanenko, K.V.	Flow imaging by magnetization prepared centric-scan SPRITE. Applications for core analysis.
P71	Romanenko, K.V.	^{35}Cl profiling using centric scan SPRITE with variable flip angle excitation
P17	Rose, H.	Hydrodynamic Instabilities through Porous Media
P75	Saito, K.	Effects of rapamycin on tumor pO_2 and blood volume
P85	Sersa, I.	MR Microscopy Towards Detection of Neuronal Currents
P36	Shapley, N.C.	NMRI Characterization of Bimodal Suspension Flows
P58	Shigeki, R.	Static magnetic field shimming for MRI using a 3D geometrical phantom

P50	Steele, P.T.	Lithographically Produced Microcoils for Enhanced Portable NMR
P64	Subramanian, S.	Refinement of Oxygen resolution in Function EPR Imaging
P34	Utiu, L.	MRI for Investigations of Permeate Flow and Observation of the Cake-Layer Formation in Micro-Filtration Processes
P97	Utiu, L.	Hyperpolarized ^{129}Xe NMR Spectroscopy for Investigations of Porous Polymers
P49	Utsuzawa, S.	Design and construction of barrel magnets for unilateral NMR
P12	Valori, A.	Spatially resolved & Double Quantum Filter ^{1}H NMR studies of cementitious materials
P59	Van Dusschoten, D.	NMR microscopy T_2 mapping at high resolution
P10	Van Landeghem, M	Multi-site relaxation exchange NMR
P4	Vogt, S.J.	Relaxation Measurements Determine Degree of Biofouling in Porous Media
P61	Vogt, S.J.	Detection of Uranium Oxidation and Solubility using NMR
P70	Walton, J.H.	MR Thermal Imaging in the Presence of Motion
P91	Wang, M.	Investigating embolism repair of xylem vessels in grape plants using proton magnetic resonance imaging
P47	Wintzheimer, S.	A straightforward biplanar gradient design for mobile MR: Optimizing a modified maxwell/golay layout with simulated annealing
P48	Wintzheimer, S.	A novel gradient design for mobile MR: simultaneous generation of fast switchable linear and higher order field gradient for MR imaging
P84	Zheng, S.	Influence of Relaxivity on Cartilage Glycosaminoglycan Imaging by Gadolinium Contrasts in MRI
P13	Zielinski, L.	Two-dimensional T_1-T_1 correlations between T_1 distributions at different Larmor frequencies

Fluid Content Imaging of Porous Media – A Comparison of Methods

<u>Colleen E. Muir</u>[1,2], Oleg V. Petrov[1], and Bruce J. Balcom[1,2]

[1] UNB MRI Centre, Department of Physics, University of New Brunswick, Fredericton, Canada
[2] Department of Chemistry, University of New Brunswick, Fredericton, Canada

Abstract:

MRI is a powerful tool for the non-destructive imaging of fluid content and fluid behavior in porous media. The measurement of magnetic resonance relaxation times of fluids in porous media is commonly undertaken to measure the pore size distribution. MRI measurements of fluid content in porous media are often compromised by relaxation time contrast which yields apparent fluid content. In this work we compare four MRI techniques intended for quantitative fluid content imaging in realistic porous media: Frequency-encoded Spin Echo, SPRITE, Hybrid SE-SPI and T_2 mapping SE-SPI. Frequency-encoded Spin Echo is considered by many to be the "gold standard" for 1D imaging but often suffers from low SNR and is susceptible to image artifacts. SPRITE is a robust technique for samples with short signal lifetimes, such as rocks, but suffers from low sensitivity. Two recent techniques, Hybrid SE-SPI and T_2 mapping SE-SPI, show promise for fast, quantitative fluid content imaging [1]. Hybrid SE-SPI shows blurring in short T_2 samples, and T_2 mapping SE-SPI requires fitting to obtain the T_2 relaxation time distribution as a precursor to determining fluid content.

The four techniques are systematically compared with a cohort of water-saturated petroleum reservoir core plug samples. A comparison is made in terms of sensitivity, image quality and image quantification.

1. Li, L., Han, H., Balcom, B., *J. Mag. Res.* **198** (2009) 252-260.

Pore diameter measured using d-PGSE-filtered MRI

M. E. Komlosh[1], E. Özarslan[1], M. J. Lizak[,2], F. Horkay[1] and P. J. Basser[1]

[1] STBB, NICHD, NIH, Bethesda, MD, USA   [2] MIF, NINDS, NIH, Bethesda, MD, USA

Abstract:

Introduction: Double Pulsed Gradient Spin Echo (d-PGSE) filtered NMR is a powerful multiple scattering technique[1-2]. Recently, we applied it as a filter to an MRI sequence to detect microstructural differences within heterogeneous biological tissue[3]. A similar method was then used to measure pore diameter in radish and spinal cord specimens, and in packed-bead NMR phantoms[4,5]. However, these studies resulted in pore size estimates that were problematic due to the absence of an adequate model of the underlying microstructure and the absence of a well-characterized pore diameter with the NMR phantom. In this study we applied d-PGSE MRI to a well-characterized glass capillary array (GCA) NMR phantom and analyzed the data using a model that accounts for partial volume and all gradients within the d-PGSE MRI sequence.

Materials and Methods: The phantom consists of two water-filled GCA wafers (Photonis); nominal pore diameter=10 μm; thickness=500 μm. d-PGSE-filtered MRIs were performed by applying the two wave vectors sequentially (with no mixing period). The angle between them, ϕ, varied between 0 and 360°. A 7T vertical bore Bruker DRX system was used with δ=3.15ms, Δ=50ms, and G between 0 and 295 mT-m^{-1}. Simulations were performed that account for the shape of the array, partial volume effects, and all finite-width gradient pulses[6].

Results and Discussion: Fig. 1a shows a d-PGSE MRI of the phantom using G=295 mT-m^{-1} and ϕ=180°. Fig. 1b shows the experimental and simulated data for all G and ϕ. The measured pore diameter was the same with and without imaging gradients (between 8.9 and 9.2 μm). Optical microscopic measurements of a similar GCA yielded a pore diameter of 9.3 μm.

Conclusions: d-PGSE filtered MRI is a potentially powerful tool to determine pore diameter. We have demonstrated its application on a highly ordered pack of restricted cylinders with microscopic dimensions, and obtained what we believe are accurate estimates of the pore size by accounting for the effects of free diffusion and all gradients within the pulse sequence.

1. P. P. Mitra, *Phys Rev B* **51** (1995) 15074. 2. P. T. Callaghan, *et al. J. Chem. Phys.* **120** (2004) 4032

3. M. E. Komlosh, *et al. J. Magn. Res.* **189** (2007) 38 4. M. Koch, *et al. Magn Reson Med* **60** (2008) 90. 5. T. Webber, *et al Magn Reson Med* **61** (2009) 1001 6. E. Özarslan, *et al. J. Chem. Phys.* **130** (2009) 104702

a)

b)
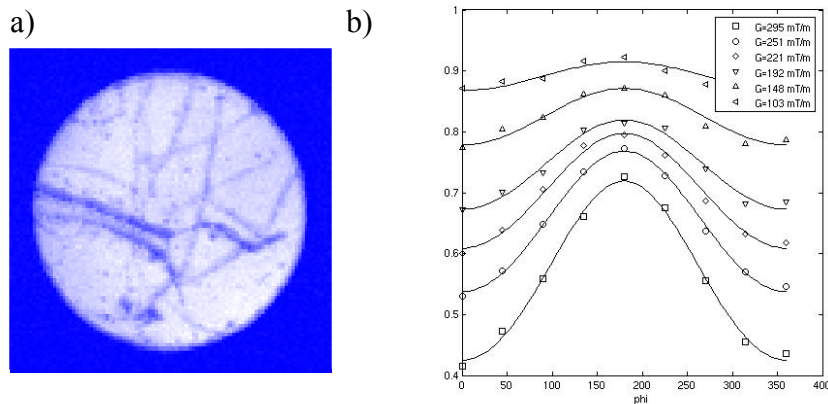
Figure 1a) d-PGSE MRI of GCA phantom at G=295 mT/m and ϕ=180°,
1b) Experimental (symbols) and simulated (solid lines) data vs. ϕ for G = 103, 148, 192, 221, 251 and 295 mT/m.

Visualization of liquid water distribution in wet snow using a compact MRI system

S.Adachi[1], T.Ozeki[2], S.Handa[3], R.Shigeki[1], K.Kose[1],

1: Institute of Applied Physics, University of Tsukuba
2: Hokkaido University of Education 3: Japan Society for the Promotion of Science

Introduction: We reported the first MRI system that was operated in a cold (~ -5 °C) room [1]. Although the system achieved a high spatial resolution (~(100 μm)^3) using a 1.0 T permanent magnet, the imaging region was limited to less than 30 mm diameter spherical volume. In this study we have installed a 0.2 T large gap (11.5cm) permanent magnet to extend MRI applications in the cold room.

Materials and method: The compact MRI system consisted of a permanent magnet, a gradient coil set, an RF probe, and a compact MRI console. The magnet, gradient coil set, RF probe were installed in a cold room and the MRI console was installed in a room at normal (20 ~ 25 °C) temperature, next to the cold room. The temperature of the cold room can be kept at any temperature between -5 and 10 °C. The control or signal lines for the gradient coils and RF coil were connected to the MRI console through a hole opened in the wall between the cold room and the operation room.

The specifications of the magnet are as follows: magnetic field strength = 0.2 T, gap space = 11.5 cm, homogeneous region = 6 cm diameter spherical volume, weight = 120 kg. The homogeneity of the magnet was adjusted with a passive shim technique using pieces of magnets in a temperature-regulated room (25°C) in the factory. The gradient coil elements were wound on circular FRP plates (diameter = 31.5 cm, thickness = 3 mm) using a 0.8 mm diameter polyethylene-coated Cu wire. The RF coil was a 8 turn solenoid wound on an acrylic pipe (outer diameter = 76 mm, inner diameter = 68 mm) using a 0.1 mm thick Cu foil and tuned to 8.6 MHz resonance frequency using three variable capacitors.

Granular snow specimens were sampled on May 23, 2009 in Tokachi-dake mountain in Hokkaido prefecture. Two samples were cut from the region from 15 to 35 cm (sample 1: grain diameter = 2 ~ 8 mm, mean density = 0.64 g/cm^3) and from the region from 38 to 52 cm (sample 2: grain diameter = 2 ~ 6 mm, mean density = 0.62 g/cm^3) as shown in Fig.1. The snow samples were inserted into cylindrical containers (ID = 6.5 cm, height = 18 cm) and 70 % NaCl solution (liquid at -5 °C) was poured to the containers to fill the lower region of the containers. The liquid water distribution in the granular snow was visualized using a 3D spin echo sequence (TR/TE = 200 ms/ 10 ms, NEX = 8, matrix = 128^3, voxel size = (0.6 mm)^3).

Results and discussion: Figures 2 and 3 show 2D cross sections selected from the 3D image datasets acquired with the above 3D sequence. The difference of the liquid water height was clearly visualized. Because the difference of the grain size and mean snow density between the two samples are small, the significant difference of the water height may be caused by the structural factor of the samples. To clarify the difference, much higher spatial resolution may be required.
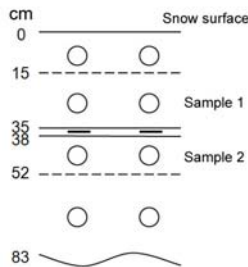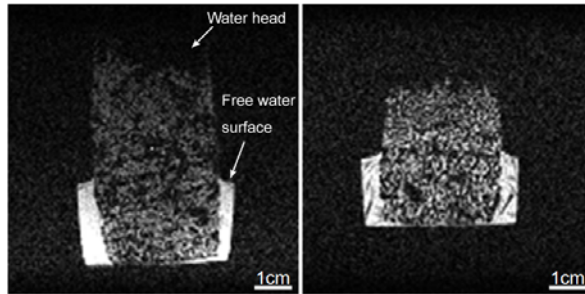
Fig. 1   Fig.2   Fig. 3

P3

References: [1] S. Adachi, T. Ozeki, R. Shigeki, S. Handa, K. Kose, T. Haishi, M. Aoki. Development of a compact magnetic resonance imaging system for a cold room. Rev. Sci. Instrum 80, 054701 (2009).

Relaxation Measurements Determine Degree of Biofouling in Porous Media

<u>Sarah J. Vogt</u>[1,3], Jennifer A. Hornemann[1,3], Konstantin V. Romanenko[2*], Sarah L. Codd[2,3], Joseph D. Seymour[1,3]

[1]Department of Chemical and Biological Engineering, Montana State University, Bozeman, MT, USA
[2]Department of Mechanical and Industrial Engineering, Montana State University, Bozeman, MT, USA
[3]Center for Biofilm Engineering, Montana State University, Bozeman, MT, USA

Abstract:

Recent 2D magnetic resonance (MR) correlation techniques have been able to access exchange in pore structures through surface and diffusion based relaxation measurements [1-5]. This research applies these techniques to measure pore and surface changes due to biofilm growth in various porous systems using T_2-T_2 relaxation maps. Biofilm growth involves the generation of a hydrogel, the extracellular polymeric substance (EPS), attached to the pore and occupying the pores. In considering the role of biofilms in altering T_2 relaxation behavior, the different diffusion and surface relaxation limiting regimes are considered [6, 7]. The impact of bacterial growth media and surface properties of spheres in the absence of biofilms is analyzed to establish a template against which to determine the role of biofilm growth. Model bead packs of various construction containing 100 μm borosilicate and soda lime glass beads were used to demonstrate how changes in the measured relaxation rates can be used to non-invasively verify and quantify biofilm growth in porous media [8]. Current research is continuing these studies to analyze biofilm growth in porous Berea sandstone. The bacteria chosen for these studies, *Bacillus mojavensis,* has shown resistance to super-critical carbon dioxide, and the non-invasive detection of biofilm growth throughout porous media could have important applications for carbon sequestration and storage.

1. Mitchell,J., J.D. Griffith, J.H.P. Collins, A.J. Sederman, L.F. Gladden, and M.L. Johns, *Journal of Chemical Physics*, **127** (2007) 234701-1-9.
2. Monteilhet, L., J.-P. Korb, J. Mitchell, and P.J. McDonald, *Physical Review E*, **74** (2006) 061404-1-9.
3. Song, Y.-Q., L. Zielinski, and S. Ryu, *Physical Review Letters,* **100** (2008) 248002-1-4.
4. Washburn, K.E. and P.T. Callaghan, *Physical Review Letters*, **97** (2006) 175502-1-4.
5. Fleury, M. and J. Soualem, *Journal of Colloid and Interface Science*, **336** (2009) 250-259.
6. Brownstein, K. R. and C.E. Tarr, *Physical Review A,* **19** (1979) 2446-2453.
7. Godefroy, S., J.-P. Korb, M. Fleury, and R.G. Bryant, *Physical Review E,* **64** (2001) 021605-1-13.
8. Hornemann, J.A., S.L. Codd and J.D. Seymour, *Env. Sci. Tech.,* submitted (2009).

*Present address: MRI Research Centre, University of New Brunswick, Fredericton Canada

Exchange in Natural Porous Media Investigated by NMR Relaxometry

A. Haber, S. Haber-Pohlmeier, B. Blümich

Institute of Technical and Macromolecular Chemistry, RWTH-Aachen University, Aachen, Germany

Natural porous media like soils have huge importance for food production and as first filter for water on its way to aquifers. The ability to fulfil these tasks is strongly controlled by the structure of their pore system, e.g. pore size distribution, connectivity, water content and water dynamics. The present work combines different methods of NMR relaxometry which are particularly convenient for the exploration of these properties. We applied these techniques on soil systems with increasing complexity: from medium sand to a Merzenhausen silt loam, composed of large fractions of small particles (clay and silt). Two further soils (Kaldenkirchen sandy loam and Selhausen silt loam) are intermediates between these extremes.

T_1 relaxometry is used for the determination of pore size distributions, since T_1 is unaffected by internal gradients, in contrast to T_2. Extending this by measurements at variable field strengths leads to so-called dispersion curves, from which the local dynamics of water near the pore walls can be determined. The next step is the determination of the ratio T_1/T_2 in a combined 2D correlation experiment. Finally, we obtained pore connectivites by measuring T_2-T_2 correlation exchange maps (Fig. 1). The diagonal peaks represent the T_2 relaxation in pores of differents size classes. In contrast to that, cross peaks indicate connections between pores and from their evolution with the exchange time mutual water exchange rates can be deduced.

In summary, we obtain from 1D relaxometry pore size distributions and local dynamics. From 2D experiments, which have been applied here for the first time on natural soil systems, information about pore connectivity is obtained which needs to be quantified with the help of simulated exchange maps.
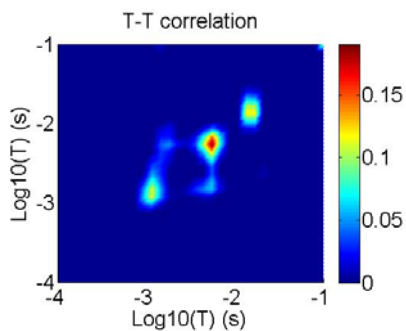
Fig. 1: T_2-T_2 correlation experiment of Kaldenkirchen sandy loam for an exchange time of 10 ms.

NMR Relaxometry of Layered Silicates containing Paramagnetic Impurities

Johannes Leisen, Bo Xu and Haskell W. Beckham

School of Polymer, Textile and Fiber Engineering, Georgia Institute of Technology, Atlanta/GA, USA

Abstract:
Naturally occurring layered silicates such as montmorillonite (MMT) contain small quantities of paramagnetic impurities (e.g., Fe^{3+}). These clay materials, composed of stacked layers called platelets, are used as additives in polymers to form nanocomposites in which performance depends on the homogeneity and morphology of the dispersed MMT. Paramagnetic-enhanced NMR relaxometry is an effective method for examining details of the MMT morphology.[1] For ^{1}H saturation-recovery at 300 MHz, initial portions of the magnetization build-up curves ($\leq$ ~20 ms) were found to depend on $\sqrt{t}$, indicative of diffusion-limited relaxation[2] and in agreement with calculations based on estimates of the spin-diffusion barrier radius surrounding the paramagnetic centers in the clay, the electron-nuclear coupling constant, and the spin-diffusion coefficient. Initial slopes of these magnetization recovery curves directly correlated with the fraction of clay/polymer interface (cf. Figure 1). Because the electron-nuclear coupling constant is larger at low magnetic fields, the time window for diffusion-limited relaxation should be broader. This was confirmed by ^{1}H saturation recovery experiments conducted at 23 and 300 MHz. New approaches for data analysis and presentation have been developed that allow for observation of the number of platelets/stack in layered silicates dispersed in polymeric matrices. This level of morphological detail, and how it changes with processing and deformation, is new information that should facilitate nanocomposite design and production.
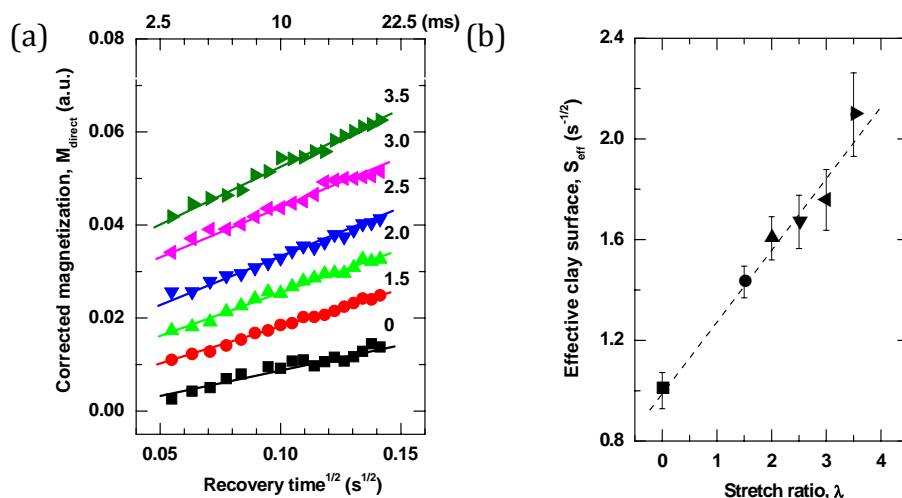
Figure 1. (a) Normalized and corrected magnetization vs square root of recovery time for polypropylene-MMT nanocomposites with stretch ratios (λ) from 0 to 3.5. Slopes of these lines, normalized to the slope for $\lambda = 0$ and proportional to the exposed clay surface or effective number of paramagnetic centers S_{eff}, are plotted in (b) as a function of stretch ratio.

1. Bourbigot et al., *Journal of Polymer Science B* **41**(2003)**,** 3188-3213.
2. Blumberg, W. E. *Physical Review* **119** (1960), 79-84.

Physical and chemical changes in polymer/cement dispersions exposed to hydration

Alexandra M. Olaru, Bernhard Blümich and Alina Adams

Institute for Technical and Macromolecular Chemistry, RWTH Aachen University, Aachen, Germany

Polymer/cement dispersions (p/c) are non-hydrated cement particles dispersed in water-soluble polymers [1], used in various demanding applications in the construction industry. The dispersions are prepared using small amounts of organic solvents. The formation of the cement matrix, which takes place upon hydration, is strongly influenced by the interaction between the different phases. The hardening of the cement and the chemical reactions of the organic components generate a system with extremely short relaxation times that cannot be analyzed by conventional frequency encoding MRI techniques.

Polymer/cement samples containing 30% and 40% polyvinyl acetate (PVAC) have been studied using Single Point Imaging (SPI). Data were extracted from 2D and 3D images to evaluate the changes in the sample upon hydration (swelling, water ingress speed, diffusion type) as well as the influence of the temperature and polymer amount on the hydration associated phenomena. T_1, T_2 and T_2^* maps have been acquired simultaneously with the hydration process using pulse sequences based on the SPI technique [2].
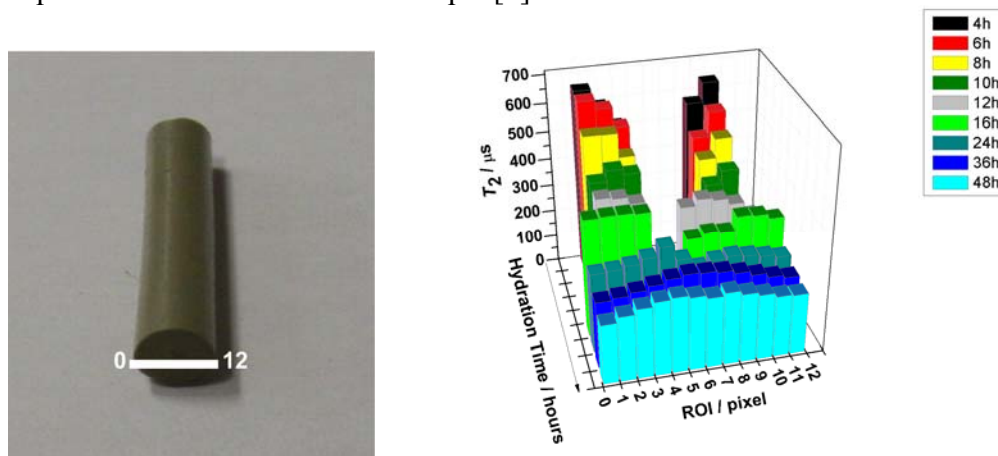
Fig 1. A selected region of interest in the sample cross-section (left) and the corresponding T_2 values as a function of the hydration time (right).

The measurements allowed the evaluation of the water spin density and of the cement hardening during the evolution of the hydration phenomenon. The results were correlated with the PVAC hydrolysis reaction kinetics obtained from ^{13}C NMR spectra and the silicate crystallization process, evaluated using ^{29}Si NMR. To the best of our knowledge, this is the first time the hydration of these materials and the associated phenomena have been monitored on-line and characterized by MRI and solid-state NMR methods.

References
[1] Y. Ohama, *Cement and Concrete Composites* **20** (1998) 189-212.
[2] S. D. Beyea et al., *Journal of Magnetic Resonance* **135** (1998) 156-164.

Magnetic resonance imaging and relaxometry to study rates of water uptake and diffusion in a commercially available gastrointestinal therapeutic system (GITS) tablet

Amber L. Broadbent[1,3], Rob J. Fell[1], Sarah L. Codd[2], Joseph D. Seymour[1], Dory G. Koehler-King[3], Sanjay J. Konagurthu[3], Kim A. Lightley[3], Erik M. Rassi[2]

[1] Department of Chemical and Biological Engineering, Montana State University, Bozeman, Montana
[2] Department of Mechanical and Industrial Engineering, Montana State University, Bozeman, Montana
[3] Bend Research, Inc., Bend, Oregon

The hydration of 4mg Cardura XL (Pfizer™), a commercially available gastrointestinal therapeutic system (GITS) tablet, was investigated using magnetic resonance imaging (MRI). Gastrointestinal therapeutic system tablets utilize osmotic pressure and polymer swelling to deliver active pharmaceutical ingredients in a controlled, steady and reproducible manner. Typically, these tablets consist of two osmotic layers - a drug layer and a water-swellable polymer layer, which are compressed to form a tablet core. The core is coated with a hard cellulosic membrane that is permeable to water but impermeable to ions, the drug and osmotic excipients. The coating contains one or more delivery ports through which the swelling polymer layer pushes the drug suspension after sufficient tablet hydration [1, 2]. MRI has been used previously to qualitatively evaluate GITS tablets which showed different release patterns of drug during quality control testing [3] and recently a benchtop-MRI system was used to characterize and compare various formulations for Isradipine push-pull tablets [4]. A large volume tablet holder for magnetic resonance studies within a vertical wide bore spectrometer was constructed. A short echo time (τ_e = 2.81 ms) technique for imaging the hydration of a GITS tablet was successfully implemented, and three separate imaging trials were conducted over a 16 hr. period. From the MR images, signal intensity profiles were generated and used to estimate rates of water uptake and diffusion coefficients for water in both the drug and polymer-sweller layers of the tablet. Spin-lattice T_1 and spin-spin T_2 relaxation times of the water signal from within the tablet were explored as a function of hydration time in order to consider the effects of relaxation on the signal intensity. As the tablet hydration time increased, the T_1 time of the water signal from within the tablet decreased and the T_2 time increased.

1. Theeuwes, F., *Elementary osmotic pump.* Journal of Pharmaceutical Sciences, 1975. **64**(12): p. 1987-1997.
2. Verma, R.K., B. Mishra, and S. Garg, *Osmotically controlled oral drug delivery.* Drug Development and Industrial Pharmacy, 2000. **26**(7): p. 695-708.
3. Shapiro, M., M.A. Jarema, and S. Gravina, *Magnetic resonanace imaging of an oral gastrointestinal therapeutic system (GITS) tablet.* Journal of Controlled Release, 1996. **38**: p. 123-127.
4. Malaterre, V., et al., *Benchtop-magnetic resonance imaging (BT-MRI) characterization of push-pull osmotic controlled release systems.* Journal of Controlled Release, 2009. **133**: p. 31-36.

Microstructure changes in a degradable bioceramic characterized in-vitro by NMR relaxation and diffusion mapping

Joshua M. Bray[1,3], Steven D. Beyea[1,2,3], and Mark J. Filiaggi[4]

Departments of [1] Physics & [2] Radiology, Dalhousie, Halifax, N.S., Canada
[3] Institute for Biodiagnostics, National Research Council, Halifax, N.S., Canada
[4] School of Biomedical Engineering, Dalhousie, Halifax, N.S., Canada

A modern approach to treating localized bone diseases involves direct implantation of a drug-loaded bioceramic at the affected site to achieve controlled delivery rates. Furthermore, degradable materials obviate the need for surgical removal and can reduce risks to the patient [1,2]. Drug release from this class of bioceramic is a complex function of the dynamic interplay between absorption of fluid from the surrounding environment and degradation of the microstructure in response to the fluid [3]. This paper describes the use of high-resolution MRI for non-destructive characterization of degradable calcium polyphosphate (CPP) bioceramics, utilizing spatially-resolved measurements of water distribution and of water mobility/transport parameters via the relaxation times (T_1, T_2) and the apparent diffusion coefficient (ADC).

CPP disks (4 mm o.d.) were fabricated using a gelling protocol (termed G1 disks) and a compaction-regelling protocol (termed G2 disks), each with a characteristic microstructure and drug release profile [4,5]. Using both types of disk provided a means to compare the effects of material processing on the MR parameters. Four samples of each type were secured in close-fitting NMR tubes, immersed in phosphate buffered saline (pH=7.2), and imaged at 24 hour intervals over a 14 day period. MR imaging was performed on a Bruker Avance spectrometer at 11.7 T with 35 μm resolution. Fluid density-weighted images were acquired using a spin-echo sequence (TE = 1.52 ms). Maps of T_1 and T_2 were acquired with Inversion Recovery and CPMG (τ = 1 ms) sequences. Because $T_1 >> T_2$ in CPP, maps of the ADC were acquired using a pulsed-gradient stimulated echo sequence (Δ/δ = 250 ms/2 ms).

The maps of T_1, T_2, and the ADC all revealed differences in G1 and G2 disks as a result of their respective microstructures. Additionally, the relaxation and diffusion parameters were characteristically biexponential, indicating the existence of water in exchange between at least 2 environments. One component may be attributed to freely-tumbling water in pores and void spaces, while the other is due to water more closely associated with the CPP matrix. Changes in the relative weighting of these components occurred throughout the experiment (see example timecourse, Fig. 1). This is thought to be an important mechanism for drug release, which depends on freely-diffusing water as a mode of transport from the CPP matrix. Future work will test this hypothesis by using simultaneous MRI and drug elution measurements to look for correlation between microstructural changes and drug release rates.

Fig. 1: Example timecourse. T_2 relaxation (top) and the relative weighting of the biexponential components (bottom) in a single voxel at the centre of a G1 disk. T_1 and ADC parameters exhibited similar trends.

1. K. Qiu et al., *J. Mater. Sci.* **41** (2006) 2429-2434.
2. D. Shi, Biomedical Devices and their Applications, Springer, Germany, 2004.
3. J. Bray et al., S*olid State Nucl. Magn. Reson.* **32** (2007) 118-128.
4. A. Dion et al., *Biomaterials* **26** (2005) 7276-7285.
5. C. Petrone et al., *Acta Biomater.* **4** (2008) 403-413.

P10

Multi-site relaxation exchange NMR

M. Van Landeghem[1,2], A. Haber[1], F. Casanova[1], Jean-Baptiste d'Espinose de Lacaillerie[2] and B. Blümich[1]

[1] Institute for Technical and Macromolecular Chemistry, RWTH Aachen University, D-52056 Aachen, Germany

[2] Physico-chimie des Polymères et des Milieux Dispersés, UMR 7615 CNRS UPMC, ESPCI ParisTech, 10 rue Vauquelin, 75005 Paris, France

Abstract:

Two-dimensional relaxation exchange NMR is in many ways similar to 2D frequency exchange NMR, except that the encoding times are comparable to the exchange time. In the case of exchange between more than two sites, this prevents the straightforward analysis of the cross peaks intensities in terms of join densities, and quantitative information can only be obtained by comparison with simulated spectra.

Relaxation-relaxation exchange experiments of water in inorganic porous media were performed at low and moderately inhomogeneous magnetic field with a simple, portable Halbach-Magnet. We were able to simulate the conditions for which T_2-T_2 cross peaks occur within a packing of spherical silica particles and thus we obtained both the true T_2 distribution and the characteristic exchange times. Moreover, we were able to show that in the case of exchange between three or more sites, interference between relaxation and exchange may lead to asymmetric 2D exchange maps, while the 2D exchange maps of a two sites system is always symmetric.
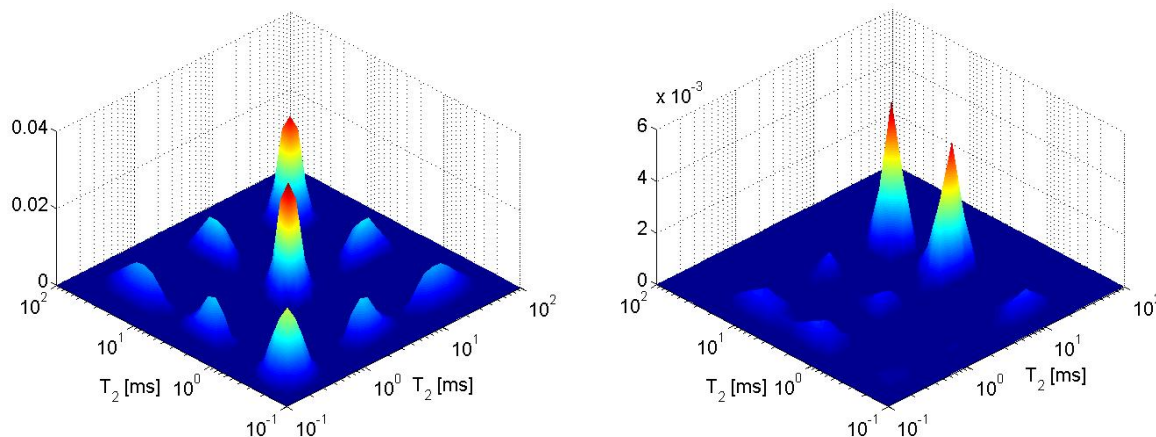
Fig. 1: T_2-T_2 exchange maps. Three exchange sites spectra symmetric (left) and non-symmetric (right)

1. K. E. Washburn, P.T. Callaghan, *Tracking pore to pore exchange using relaxation exchange spectroscopy,* **Phys. Rev. Lett. 97 (**2006) 175502.
2. A.D. Bain, *Chemical exchange in NMR*, **Progr. Nucl. Magn. Reson. Spectr. 43** (2003) 63-103.
3. J. Mitchell, J.D. Griffith, J.H. Collins, A.J. Sederman, L.F. Gladden, M.L. Johns, *Validation of NMR relaxation exchange time measurements in porous media*, **J. Chem. Phys. 127** (2007) 234701.
4. L. Monteilhet, J.-P. Korb, J. Mitchell, P.J. McDonald, *Observation of exchange of micropore water in cement pastes by two-dimensional T_2-T_2 nuclear magnetic resonance relaxometry*, **Physical Review E 74** (2006) 061404

NMR Linewidth Measurements of Petroleum Reservoir Rocks at Variable B_0 Strengths

Michael J. McAloon[1], Bruce J. Balcom[1]

[1] MRI Centre, Department of Physics, University of New Brunswick, Fredericton, Canada

The centric scan SPRITE MRI method has proven to be a very robust, general, and exceptionally quantitative measure of fluid content in a wide variety of porous media. The method works best for samples that exhibit single exponential FID decays. Our experience has been that single exponential T_2* decay is common, except at very low static fields, in some samples. In the present work we wish to examine the T_2* behavior more carefully by exploring the measurement of a larger range of rock samples.

When a uniform magnetic field is applied to fluid saturated porous rock, the internal magnetic field, within the pore space, is altered due to differences in magnetic susceptibility between the fluid and the solid matrix. Single exponential NMR free induction decays arise from a Lorentzian distribution of the internal field. A linear relationship between the NMR linewidth and applied magnetic field (with Larmor frequency) is observed in the sample cohort studied, Fig. 1 [1].

Inversion recovery (T_1) measurements were taken for these samples, as well as CPMG measurements to determine T_2 distribution, all as a function of static field.
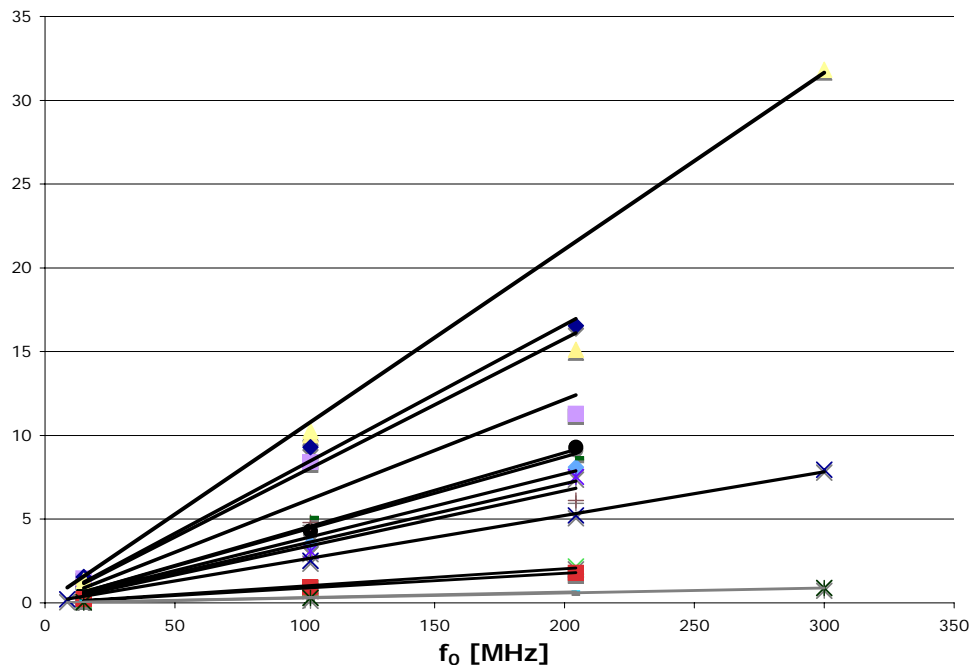
Fig. 1: NMR linewidths measured at four different magnetic fields (F_0 = 15, 100, 200, 300 [MHz]) for fourteen water-saturated rock samples. The slope is determined by susceptibility mismatch of matrix and fluid. Sample color aids in classifying sample behavior. Dark colored samples (red, black, dark grey) are indicative of significant metal content and have higher slope in Fig. 1, compared to lighter colored samples (light grey, beige), which suggest low metal content. Metal content is important because it strongly influences the susceptibility of the solid matrix and thereby the susceptibility differences with the pore fluids.

Quan Chen, Andrew E. Marble, Bruce G. Colpitts, Bruce J. Balcom, *Journal of Magnetic Resonance* 175 (2005) 306-308

Spatially resolved & Double Quantum Filter ^{1}H NMR studies of cementitious materials

<u>Andrea Valori</u>, Victor Rodin and Peter J. McDonald

Department of Physics, University of Surrey, Guildford, GU2 7XH United Kingdom

Abstract:

We report recent progress in the application of *in-situ* spatially resolved ^{1}H NMR and laboratory based Double Quantum Filter ^{1}H NMR to the study of cement based materials including concrete.

In the first part, we report the steps taken to achieve the first *in-situ* measurements of concrete drying on a construction site using a surface GARField portable magnet[1]. Results include those of tests that show that embedded steel reinforcements do not seriously degrade the surface GARField profiles.

In the second part we discuss steps taken to explore whether a meso-scale inhomogeneous distribution of Fe^{3+} impurities in cement gel structures is the determining structural inhomogeneity that gives rise to the "two-site exchange" witnessed in 2-D relaxation exchange experiments[2] or whether, as previously believed, it is exchange between two pores sizes. Using experiments on model materials including synthetic C-S-H and double quantum filtered measurements of ^{1}H mobility and anisotropy in cement we show that Fe^{3+} is important in determining the detailed NMR response. However, it is not the primary structural inhomogeneity underlying exchange experiments. Rather the normal and previous assumption of a bimodal two pore size distribution applies.

Moreover, we show that, as cement paste is dried, so the apparent fraction of immobile water increases, shedding light not only on the water distribution but also on the drying mechanism.

1. McDonald, P.J., et al., *Journal of Magnetic Resonance*, 2007. **185**(1): p. 1-11
2. Monteilhet, L., et al., *Physical Review E*, 2006. **74**(6) 061404

Two-dimensional T_1-T_1 correlations between T_1 distributions at different Larmor frequencies

Lukasz Zielinski and Martin Hürlimann

[1] Schlumberger-Doll Research, Cambridge, MA 02139, USA

Abstract:

In many complex fluids, such as polymers or gels, the dispersion of the relaxation rate as a function of the Larmor frequency deviates from the standard Lorentzian form derived from the assumption of an exponentially decaying correlation of the motions of the constituent molecules. Additionally, many such fluids are described by wide distributions of characteristic correlation times corresponding to motions of individual molecules or their segments, resulting in wide distributions of relaxation times T_1 and T_2. We find that in such fluids, different fluid components may be characterized by *different* dispersion relations, causing the distribution of relaxation times to change shape when measured at different Larmor frequencies.

We propose an experiment that directly probes these changes by measuring the correlations between T_1 distributions at different Larmor frequencies using the fast field cycling technique. T_1-T_1 correlations provide a novel probe of the dynamics of the system. An example of such a two-dimensional T_1-T_1 correlation experiment between Larmor frequencies of $\omega_o/2\pi$ = 15 MHz and 100 kHz is shown in Fig. 1. The sample is a crude oil characterized by a wide distribution of relaxation times. As is apparent from the Figure, we find that for different fluid components, the relaxation times at the two frequencies differ by a variable ratio. This leads to a flattening of the short-T_1 tail of the T_1-T_1 correlation map. This implies that the more rapidly relaxing protons (short-T_1 values) are more strongly affected by the change of the Larmor frequency than the more slowly relaxing protons (long-T_1 values). We propose a model of interactions that accounts for this behavior.
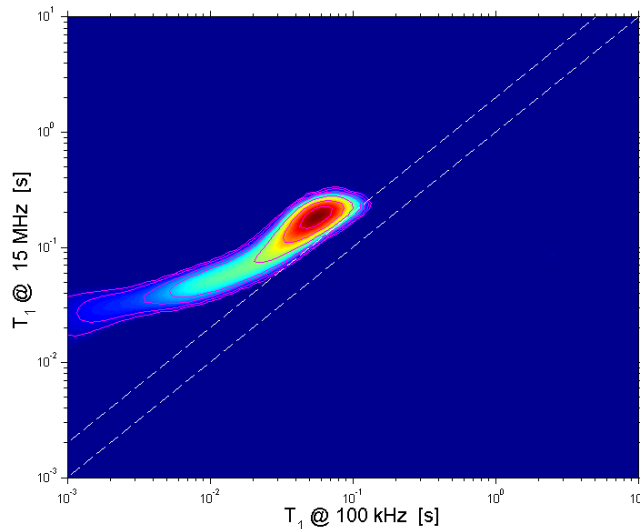
Fig. 1: T_1-T_1 correlation experiment at two Larmor frequencies of 15 MHz and 100 kHz for a crude oil sample. The lower and upper dashed lines indicate a constant ratio of 1 and 2, respectively.

P14

Interactions of binary mixtures with polysaccharides investigated by 2D relaxation time measurements

Jürgen Kolz[1], Yury Yarovoy[2], Mike L. Johns[1] and Lynn F. Gladden[1]

[1] Department of Chemical Engineering and Biotechnology, University of Cambridge, Cambridge, UK
[2] Unilever R&D, Trumbull, USA

Abstract:

Transverse relaxation time (T_2) has proven to be a valuable parameter to characterize liquid / polymer interactions [1-4]. However, many food, personnel care and cosmetic products contain multi-component liquid mixtures, where it is difficult to assign the different relaxation time components to a particular species when only a single relaxation time dimension is accessible.

In this study the interactions of corn starch with water/glycerol mixtures of different weight compositions were investigated by both chemical shift resolved T_2-measurements and 2D relaxation exchange experiments. The chemical shift resolved relaxation time measurements shown in Fig. 1 (a) and (b) reveal that for the hydroxy protons two relaxation regimes are present, while for the aliphatic glycerol protons three different relaxation regimes are observed. We associate these regimes with strongly bound, weakly bound and free liquid. The results were analysed and showed no preference for water occupation of strongly bound sites relative to glycerol.

T_2-T_2 exchange maps taken for different exchange times reveal rapid molecular exchange between strongly and weakly bound sites, with exchange between all three regimes emerging at longer exchange times (> 150 ms, as shown in Fig. 1c). The exchange distances between the different regimes are estimated from the areas of the off-diagonal peaks and are shown to be consistent with the size of the starch granules. Results for chemically shift resolved 2D exchange maps will also be presented, which allows the assignment of a particular species exchanging between the different sites.
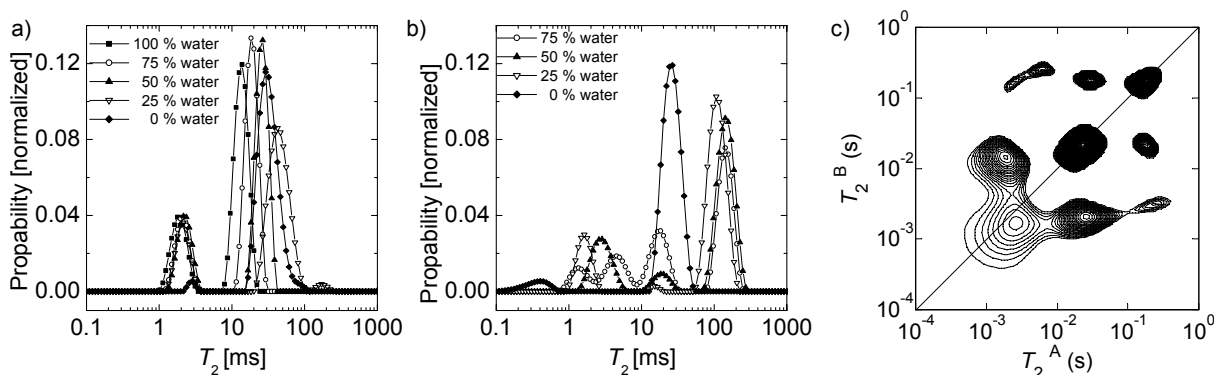
Fig. 1. T_2 distributions of a 50 wt% water / 50 wt % glycerol mixture in starch granules for a) the hydroxy protons and b) the aliphatic protons. c) T_2-T_2 exchange map for the system at an exchange time of 200 ms.

1. P. Y. Ghy *et al.*, *Biomacromolecule*s, **3** (2002) 991-997.
2. M. McCormick et al., *Macromolecules*, **36 (**2003) 3616–3625
3. B. MacMillan et al, *Polymer*, **40** (1999), 2471-2480.
4. J. D. Seymour et al., *Journal of Magnetic Resonance*, **167** (2004) 322-327.

Dynamic NMR study of colloidal particle deposition in a model porous media

Einar O. Fridjonsson[1], Sarah L. Codd[2] and Joseph D. Seymour[1]

[1]Department of Chemical and Biological Engineering, Montana State University, Bozeman, MT, USA
[2]Department of Industrial and Mechanical Engineering, Montana State University, Bozeman, MT, USA

Abstract:

The study of flow through porous media is a rich field of study where the non invasive nature of NMR allows for detailed study of the flow characteristics of complex fluids inside complex media. In this study we are interested in studying the deposition of hard sphere colloidal particles ($a = 2.49 \pm 0.92\mu m$) [1,2] in a model porous media (monodisperse 240μm diameter spheres in a 10 mm I.D. liquid chromatography column) and observe what effect the deposition has on the flow through the media. PGSE NMR techniques were used to characterize the flow of water through the media before and after deposition, these include the use of q-space as well as combined k-space and q-space methods. Increases in both the slow (holdup) and fast (backbone) components were observed after the first deposition (See Figure 1). Subsequent introduction of more particles to the porous media caused deposition that showed little change in the flow characteristics although increased deposit of particles was observed. This indicates that the particles have a tendency to be deposited in specific regions and it is in these regions that subsequent particle accumulation occurs.
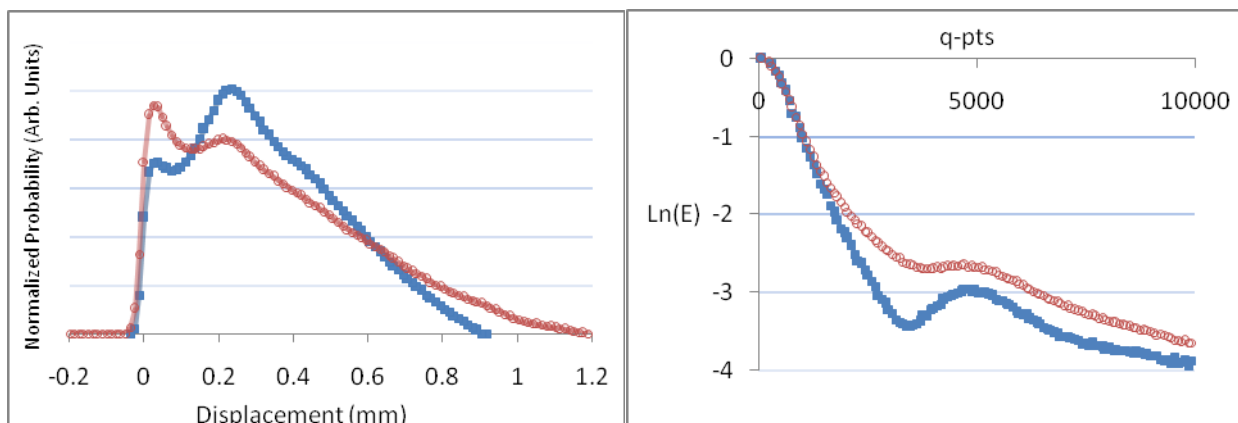
Fig 1. Shows the change in the probability of displacement and diffraction pattern at $\Delta = 200$ms for flow through the porous media before (solid squares) and after (open circles) the deposition of colloidal particles.

1.   A. Loxley, B.Vincent, *J. Colloid Interface Sci.* **208** (1998) 49.
2.   H. Wassenius, M. Nydén, B. Vincent, *J. Colloid Interface Sci.* **264** (2003) 538.

P16

Study of the flow dynamics of solid and liquid phases of a colloidal suspension in a microcapillary using NMR

Einar O. Fridjonsson[1], Sarah L. Codd[2], Joseph D. Seymour[1]

[1] Department of Chemical and Biological Engineering, Montana State University, Bozeman, MT, USA
[2] Department of Mechanical and Industrial Engineering, Montana State University, Bozeman, MT, USA

Abstract:

In this study the dynamics of solid and liquid phases of hard sphere poly methylmethacrylate (PMMA) colloidal suspensions (a = $1.25 \pm 0.46 \mu$m$^{\mu m}$, $\varphi = 0.22$) were studied in a $252 \mu^{\mu m}$ ID capillary for a/L > 2000 using dynamic NMR. Both phases were detected simultaneously by using oil (Hexadecane) filled colloidal particles allowing spectrally resolved Pulsed Gradient Spin Echo (PGSE) techniques to probe the motion of each phase at Pe_B = 410 and 820 over a time scale of Δ = 25ms to 500ms. By combining high resolution velocity map and propagator results the concentration profiles of the colloidal phase across the capillary was obtained, which was then fitted by the theoretical model of Morris and coworkers [1].

To obtain information about the microstructure of the colloidal system, the displacement scale dependence of both phases was probed by varying both the displacement time Δ and the flow rate through the capillary. This dependence was studied using single and double PGSE experiments to obtain the effective diffusion (dispersion) of each phase as well as obtaining both single and double PGSE Propagators. The low thermal motion of the colloids relative to the suspending fluid ($D_c/D_s \sim 10^{-4}$), allows the hydrodynamic dispersion of water in the colloidal suspension to probe the microstructure. Additionally, double PGSE experiments of the colloidal phase allow for the determination of interaction length scales in the system (see Figure 1).
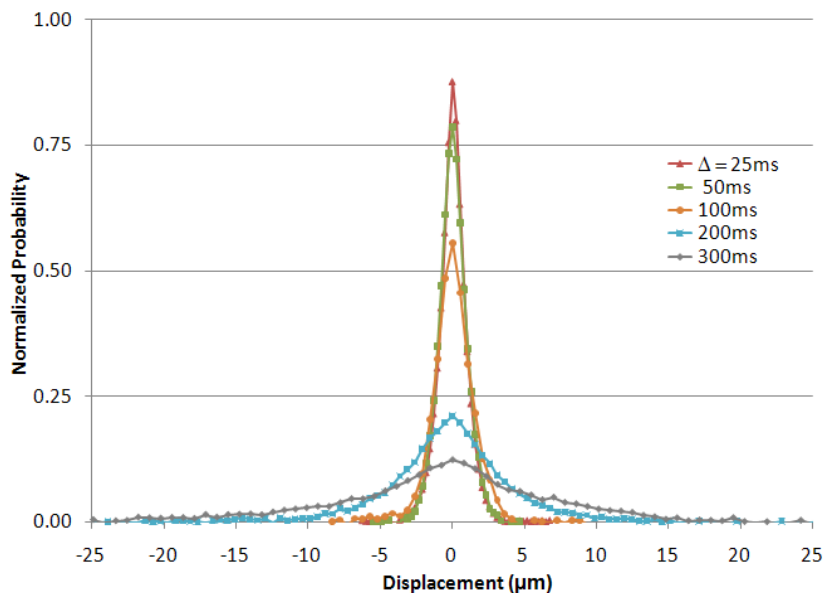
Figure 1. Shows the double PGSE propagator of the colloidal phase for the axial flow direction at V_{mean} = 1.4mm/sec, note the apparent restriction to displacement for $\Delta \leq$ 100ms.

1. M. Frank, D. Anderson, E.R. Weeks and J.F. Morris, *Journal of Fluid Mechanics*, **493** (2003), 363-378.

Hydrodynamic Instabilities through Porous Media

Heather Rose and Melanie Britton

School of Chemistry, University of Birmingham, Birmingham, B15 2TT, UK

Abstract:

Viscous fingering is a hydrodynamic instability that occurs when a fluid displaces another fluid of higher viscosity, under flow through a porous media. These instabilities are of interest in a variety of applications such as extraction of oil from pipes[1], instabilities in combustion[2] and growth of microorganism's colonies[3].

Most work in this area has focussed on non-reactive systems. In this research, we investigate the formation of these instabilities between two fluids of equal viscosity, which 'react' on contact, forming a third fluid of much higher viscosity. We have used aqueous solutions of cetyltrimethylammonium bromide (CTAB) and sodium salycilate (NaSal), which form wormlike micelles. Previous work on this system has investigated these instabilities optically using a Hele-Shaw cell[4,5]. This produces only 2D information about the system, and the 3D structure and behaviour in real porous media is not yet known. MRI is able to probe this, as well as the flow environment of the system. We have applied MRI to visualise the formation of viscous fingers in both an aqueous system and a model porous medium for the first time.

Images were collected using the fast spin-echo experiment (RARE[6]). A RARE factor of 32 was used, so that image contrast was produced by the differences in T_2 relaxation time between the water molecules in the CTAB and NaSal solutions. Methods for detecting the wormlike micelle layer were investigated. The formation of viscous fingers at a range of flow rates was studied.

1. G Pasa, O Titaud, *Transport in porous media* **58** (2005) 269
2. O Zik, Z Olami, *Phys Rev Lett.* **81**(1998) 3868
3. A Goriely, M Tabor, *Phys Rev Lett.* **90** (2003) 108101
4. Nagatsu, Y., A. Hayashi, et al, (2008) *Phys Rev E* **78** (2008) 026307
5. Podgorski, T., M. C. Sostarecz, et al. *Phys Rev E* **76** (2007) 016202
6. J Hennig et al, *Magn. Reson. Med.* (**1986**), 823.

Influence of air on the hydrodynamics of water flow in porous media as investigated by magnetic resonance

Erik M. Rassi[1], Sarah L. Codd[1], and Joseph D. Seymour[2]

[1]Mechanical and Industrial Engineering Dept., Montana State University, Bozeman, MT, USA
[2]Dept. of Chemical and Biological Engineering, Montana State University, Bozeman, MT, USA

Abstract:

Flow in porous media and the resultant hydrodynamics are important in fields including but not limited to hydrology, chemical, medical, and the petroleum industry. Observations and understanding of the hydrodynamics in porous media are critical to design and optimal utilization of porous media such as that seen in trickle bed reactors, medical filters, sub surface flows and carbon sequestration, to name a few. Magnetic resonance (MR) provides for a non-invasive technique that can probe the hydrodynamics on pore and bulk sample length scales and rapid imaging methods in particular have been applied to partially saturated flows [1-3]. We present time and ensemble averaged MR measurements to observe the effects of varying initial amounts of air imposed on a partially saturated bead pack under flowing conditions. The 10 mm internal diameter bead pack was filled with 100 μm borosilicate glass beads. Air was injected into the bead pack at flow rates of 0, 25, 50, 75, and 100ml/hr as water flowed simultaneously through the sample at 25ml/hr. The data is presented corresponding to gas to water flow rate ratios of 0:1 (water saturation), 1:1, 2:1, 3:1, and 4:1. After eight hours, the air was shut off and only the water remained flowing at 25 ml/hr until a steady state was reached. For each gas to water ratio initial condition MR images, free induction decay (FID) experiments, propagators, and velocity maps were taken as the water flow rate was increased to 500ml/hr. After the maximum flow rate of 500ml/hr, the MR images, FID experiments, propagators, and velocity maps were repeated and compared to the data taken before the maximum flow rate. The MR images indicate air was present before and was not present in significant quantity after the maximum flow rate was reached. This demonstrates that the increased flow rate had blown the air out and had changed the water saturation level of the bead pack. Propagators show very similar flow statistics before and after maximum flow rates regardless of initial gas to water ratios. All propagators for the gas ratios of 1:1, 2:1, 3:1, and 4:1 before maximum flow took on similar flow characteristics. After the maximum flow, all propagators returned to statistics of flow near those of the saturated condition. This further indicates that air in the bead pack has been blown out, but also shows that there exists a preferred distribution of dynamics for saturated flow. Although the propagators show the same dynamics, the spatially resolved velocity maps from before and after max flow are not identical. This demonstrates that although the global statistics of the dynamics before and after blowing air out are equivalent, local flow hydrodynamics are different.

1. M.L. Johns, A.J. Sederman, A.S. Bramley, and L.F. Gladden, *AIChE Journal* **Vol 46 No 11** (2000) 2151-2161.
2. M.H. Sankey, D.J. Holland, A.J. Sederman, and L.F. Gladden, *J. of Magnetic Resonance* **Vol 196** (2009) 142-148.
3. J.D. Seymour and P.T. Callaghan, *AIChE Journal* **Vol 43 No 8** (2096-2111).

PGSE NMR measurement of colloidal particle transport through porous media – cellular foam

Tyler R. Brosten[1], Einar O. Fridjohnsson[2], Sarah L. Codd[1], Joseph D. Seymour[2]

[1]Dept. of Mechanical and Industrial Engineering, Montana State University, Bozeman Montana USA
[2]Dept. of Chemical and Biological Engineering, Montana State University, Bozeman Montana USA

Abstract:

The flow and transport of a colloidal suspension through porous media is an important process found within a broad range of disciplines; spanning geophysics, engineering, and medicine. The purpose of this work is to present results from nuclear magnetic resonance (NMR) measurement of NMR-active core colloidal particle [1] transport through a high porosity media (open-cell polymer foam). The use of high porosity foam as the structural media allows one to observe transport dynamics with limited deposition of the colloidal particles on the structure. Transient and asymptotic transport dynamics of the liquid and solid phase are presented. Transport of both liquid and solid phase are shown to be governed by Fick's law, e.g. converging asymptotic dispersion coefficient; a phenomenon which has hitherto been implicitly assumed in colloidal particle transport in porous media theory. In addition it will be shown that deposition of the colloidal particles on and near the solid structure results in a reversible alteration of the pore structure. This micro or pore-scale phenomenon manifests within the macro-scale transport dynamics of the two phases as a separate scaling of the asymptotic dispersion coefficients with flow velocity, see Fig. 1.
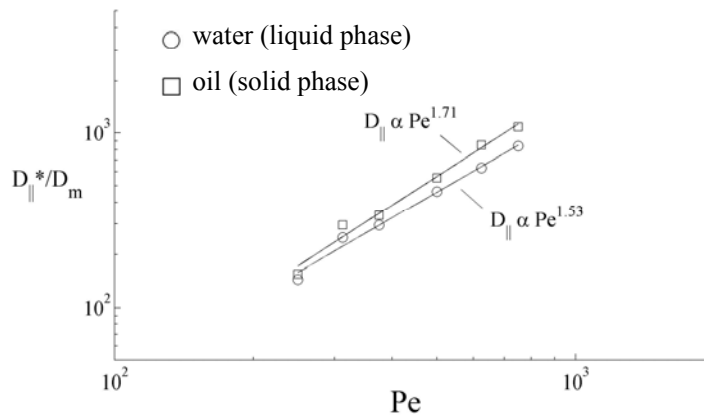
Fig 1. Scaling of the asymptotic axial dispersion coefficient with Peclet number (flow velocity) for a 15% concentration colloidal particle suspension flowing through a 97% porosity cellular foam, $D_m = 2 \times 10^{-9}\, m^2/s$

The cellular structure is a common framework for biological media [2] (e.g. sponges, trabecellular bone, etc.), thus in addition to addressing some general questions of colloid transport in porous media this work will serve as a model for colloid transport through these ubiquitous structures.

1. Brown JR, et. al, *Physical Review Letters* **24** (2007)
2. Gibson & Ashby, *Cellular solids : structure and properties*. 2nd ed. 1997.

P20

Flow imaging by magnetization prepared centric-scan SPRITE.
Application for core analysis.

Konstantin V. Romanenko, Bruce J. Balcom

MRI Centre, Department of Physics, University of New Brunswick, Fredericton, NB, Canada E3B 5A3

Abstract:

Permeability is one of the most basic and important characteristics of porous media. A variety of magnetic resonance methods has been employed for prediction of permeability in non-flowing systems. These measurements, through correlations, are particularly important for downhole NMR logging measurements in petroleum reservoirs. For complex objects with macroscopic heterogeneities, bulk measurements will be unreliable and we prefer flow based measurements with spatial resolution.

Single point imaging (SPI) MRI of porous media permits reliable quantification of local fluid content and flow [1-5]. Using magnetization prepared single point ramped imaging with T_1 enhancement (SPRITE) for flow characterization is particularly advantageous for reservoir rocks with short relaxation times of the saturating fluid. Velocity encoding using Cotts pulsed field gradient scheme [6] permits accurate mapping of flow parameters.

Spatially resolved 2D maps of propagator peak velocity, mean velocity, and standard deviation were acquired. The sensitivity of these parameters is examined with respect to heterogeneities in model porous objects and reservoir rocks. This method allows us to evaluate local permeability maps.

1. B.J. Balcom, Spatially Resolved Magnetic Resonance, Wiley-VCH, Toronto, 1998, pp. 75–86.
2. C.B. Kennedy, B.J. Balcom, I.V. Mastikhin, Can. J. Chem. 76 (1998) 1753–1765.
3. S.D. Beyea, B.J. Balcom, P.J. Prado, A.R. Cross, C.B. Kennedy, R.L. Armstrong, T.W. Bremner, J. Magn. Reson. 135 (1998) 156–164.
4. P.J. Prado, B.J. Balcom, I.V. Mastikhin, A.R. Cross, R.L. Armstrong, A. Logan, Magnetic resonance imaging of gases: a single-point ramped imaging with T_1 enhancement (SPRITE) study, J. Magn. Reson. 137 (1999) 324–332.
5. B.J. Balcom, R.P. MacGregor, S.D. Beyea, D.P. Green, R.L. Armstrong, T.W. Bremner, J. Magn. Reson. A 123
6. Linqing Li, Quan Chen, Andrew E. Marble, Laura Romero-Zeryn, Benedict Newling, Bruce J. Balcom, J. Magn. Reson. 197 (2009) 1-8.

NMR velocity imaging of the extrudate flow profile at elevated temperatures and low liquid content

<u>Jürgen Kolz</u>[1], Bart Hallmark[1], Yury Yarovoy[2], Mike L. Johns[1] and Lynn F. Gladden[1]

[1] Department of Chemical Engineering and Biotechnology, University of Cambridge, Cambridge, UK
[2] Unilever R&D, Trumbull, USA

Abstract:
Knowing the flow profile of materials in an extruder/plodder is essential for understanding and controlling the macroscopic properties of the extrudates. Previously in this laboratory, NMR imaging has been shown to provide in-situ velocity profiling in a ram extruder for representative industrial materials [1]. In this study the velocity profiles of materials having lower, more industrially relevant, liquid content (soap formulations) were measured inside a NMR-compatible PEEK ram extruder (barrel diameter = 25 mm) at elevated extrusion temperatures. A phase shift velocity imaging sequence applying two gradient increments has been used to provide velocity profiles at different positions and orientations with an adequate spatial resolution and sensitivity for these samples. In order to reach the desired extruder temperature (45 - 50º C) conventional NMR sample heating via air flow was insufficient due to the large thermal mass of the system. Appropriate heating was achieved by exploiting micro-capillary polymer films (MCFs). These are flexible poly(-ethylene) films containing an embedded array of parallel capillaries running along the length of the film [2] through which heating water was fed. The heating mantle consists of a double layer of MCFs that are wound around the barrel of the extruder as shown in Fig. 1(a), this is easily compatible with the geometric constraints of the magnet. Figure 1(b) shows radial distributions of axial velocities taken at different heights from the die entrance (diameter = 8 mm) for a formulation of shredded soap noodles at a temperature of 50° C. It can be seen that at positions further away from the die, plug flow is observed. Nearer to the die, the flow has converged towards the centre of the barrel and static zones are observed at the barrel walls. Figure 1(c) shows radial distributions of radial velocity. It can be seen that at positions near to the die entrance the material moves towards the centre of the barrel. Investigations performed with soap bar formulations containing different levels of solid and liquid fractions will be presented and their impact on spatially resolved velocity distributions will be discussed.
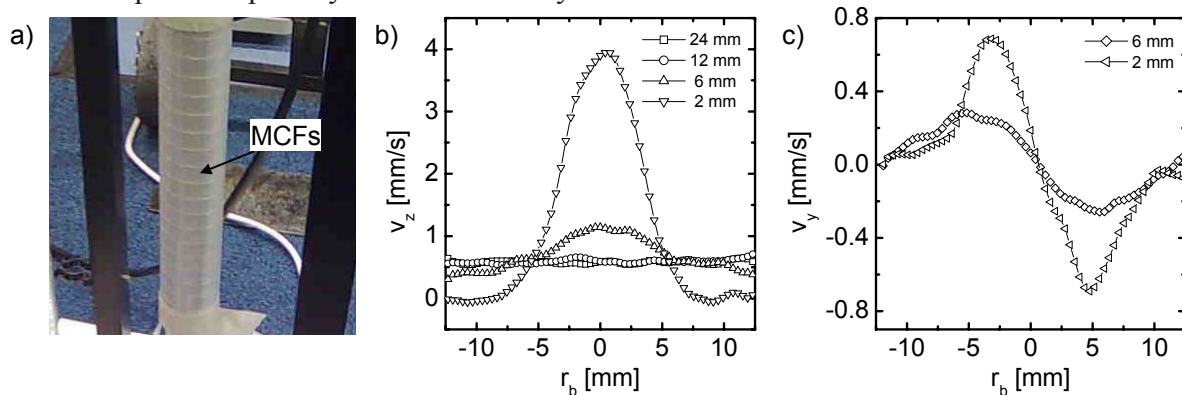
Fig. 1. a) Picture of the heating mantle made of micro capillary films wound around the extruder barrel. b) Radial distributions of axial velocity taken at different distances from the die entrance. c) Radial distributions of radial velocity taken at different distances from the die entrance.

1. E.C. Barnes et al., *Chemical Engineering Science,* **61** (2006) 1357-1367.
2. C.H. Hornung, et al., *J. Micromech. and Microeng.*, **16** (2006) 434-447.

A Study of Cavitation in Fast Flow Using Motion-Sensitised SPRITE

Alex Adair, Igor Mastikhin, Benedict Newling

MRI Research Centre, Department of Physics, University of New Brunswick, Fredericton, NB, Canada

Abstract:

Pressure variations in a flowing liquid due to system geometry can result in the formation of bubbles in areas where the local pressure drops below the vapour pressure of the liquid. The effect can readily be observed at pipe constrictions and at the tips of propellers. This process, known as hydrodynamic cavitation, is a concern in pipe flow as it can cause erosion of boundary surfaces. This study uses a motion-sensitised version of the SPRITE MRI technique [1] to measure cavitation in fast-flowing water. The technique of pure phase-encoding is ideal for the measurement of the complex nature of two-phase flow because the images it produces have no artefacts due to B_0 inhomogeneity and susceptibility variations [2,3]. SPRITE is well-equipped to image fast flows and samples with low T_2^*, and is suitable for measuring turbulent systems [4]. It has been used to estimate gas void fraction and to acquire 3D liquid velocity maps.
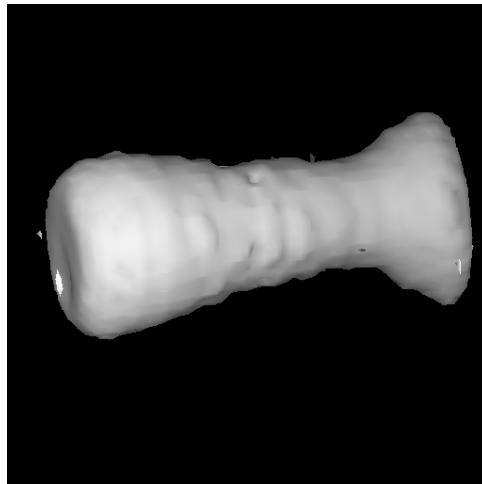
3D Conical SPRITE image of the cavitation zone

[1]   Halse, M. et al., *J. Mag. Res.*, **165**, 219-229 (2003)
[2]   Sankey, M. et al., *J. Mag. Res.*, **199**, 126-135 (2009)
[3]   Mastikhin, I., Newling, B., *Phys. Rev. E*, **78**, (2008)
[4]   Newling, B. et al., *Phys. Rev. Lett.*, **93**, 15 (2004)

P23

Visualization of the Rayleigh-Taylor instability in a soil liquefaction model system using magnetic resonance imaging

<u>K.Kobayashi</u>[1] , T.Ishikawa[1] and S.Handa[2], K.Kose[1], Y.Nohguchi[3]

[1] Institute of Applied Physics, University of Tsukuba, Tsukuba, Japan
[2] Japan Society for the Promotion of Science, Tokyo, Japan
[3] National Research Institute for Earth Science and Disaster Prevention, Tsukuba, Japan

Introduction: In 2001, a soil liquefaction model system constructed in a PET (polyethylene terephthalate) bottle was invented for scientific education and promotion of disaster prevention [1, 2]. This model, consisting of water and two kinds of sands with different grain sizes, had a layered structure resulting from mixing and sedimentation. When the bottle is mechanically shocked from outside like an earthquake, sand boiling induced by liquefaction is observed. In 2002, Nohguchi proposed a hypothesis that this sand boiling is caused by the Rayleigh-Taylor instability of the water film produced between the two sand layers and the liquefied intermediate sand layer [3]. In this work we applied MRI to the liquefaction model system to verify the hypothesis proposed by Nohguchi.

Materials and Methods: Two soil liquefaction model systems were constructed in PET bottles using two kinds of glass beads and a water (50 %) – ethanol (50 %) mixture. Figure 1 shows layered structures consisting of the glass beads: the bottom, intermediate, and top layers are a liquid saturated glass beads (diameter = 0.2 mm in average) layer, liquid saturated glass beads (diameter = 0.05 mm in average) layer, and bulk liquids, respectively. The thickness of the intermediate layer was controlled by the total weight of the smaller diameter glass beads, which was 25 and 50 g for the two bottles, corresponding to 5 and 10 mm thickness, respectively. The weight of the larger diameter glass beads was 187.0 g throughout for the bottles. We used a home-built MRI system with a 0.2 T permanent magnet. A 2D fast spin echo sequence (slice thickness = 7.5 mm, FOV = 64 mm × 128 mm, pixel size = 0.8 mm × 1.6 mm, echo spacing = 10 ms, echo train = 32, effective TE = 10 ms) was developed for MRI experiments. Cross sectional images were reconstructed from two successive echo-train datasets separated by 800 ms.

Results and Discussion: Figure 2 shows three cross-sectional images acquired with the FSE sequence. The left image had been acquired before it was shocked. The middle image was the state after 14.4 s from the left image. And the time interval between the middle and right images was 1.6 s. The middle image clearly shows formation of a bright thin layer (liquid layer) between the grass beads layers. This liquid layer shows wavy instability as shown in the right image. Because the density of the liqufied upper small glass bead layer is hevier than the density of the liquid layer, this condition is sufficient for generation of the Rayleigh-Taylor instability [4]. Therefore, we concluded that the sand boiling in the model system is caused by the Rayleigh-Taylor instability as predicted by Nohguchi.
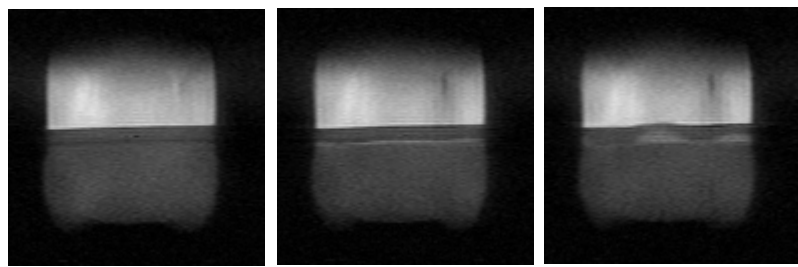
t = 0 s   t = 14.4 s   t = 16.0 s

Fig.1 Soil liquefaction model system   Fig.2 Vertical cross-sectional images of the model system

References: [1] Y. Miyachi, N. Kaneko, Japanese Patent, P2001-305952A, published Nov. 2, 2001. [2] Y. Miyachi, N. Kaneko, Chishitsu News **570**, 26 (2002). [3] Y. Nohguchi, Proceedings of the 37th Japan National Conference on Geotechnical Engineering 2003 (2002). [4] Chandrasekhar, *Hydrodynamic and Hydromagnetic Stability* (Oxford University Press, Oxford, 1961), Chapter X.

P24

MRI Velocity Mapping of Two-phase Flow in a Circular Capillary Tube

Bruce J. Balcom , Jing Zhang

Physics Department, University of New Brunswick, Fredericton, NB, Canada, E3B 5A3

Abstract:

Magnetic Resonance Imaging (MRI) can be used to visulize flow processes in optically opaque systems and has the potential to measure a wide variety of flow phenomena associated with microfluidics. Here, MRI has been used for cross-sectional velocity mapping of two-phase flow through a capillary tube. Images of 13μm x 13μm resolution were obtained for a channel of circular cross section (internal radius R = 400μm). The inflow comprised two small diameter tubes separated by a thin spacer upon entry to the sample space. Velocity mapping of both liquid systems has been studied using spin echo pure phase encoding techniques combined with chemical shift imaging (shown in Fig. 1). The results are in agreement with theoretical predictions of two-phase flow in microchannels [1]. These predictions are difficult to verify by any other experimental technique. The method is a versatile tool for the study of multicomponent flow in microfluidic systems.
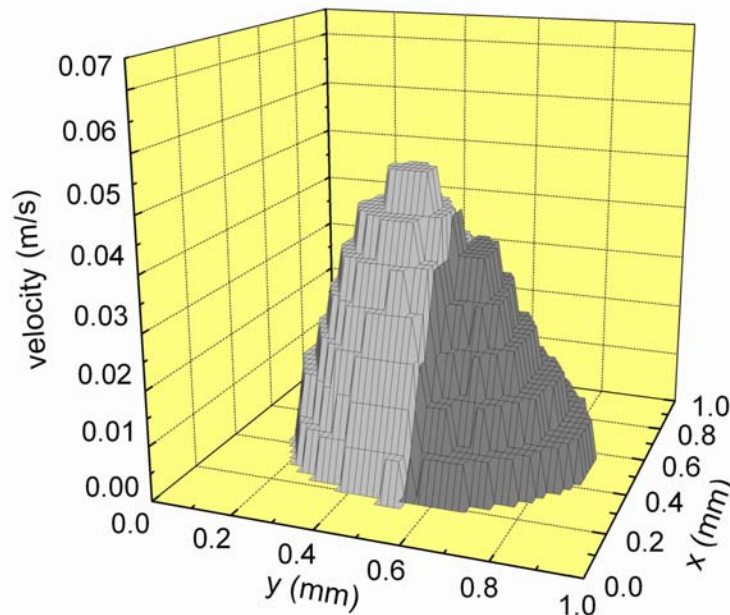
Fig. 1. Velocity mapping of two-phase flow in a circular channel versus image position. The internal radius of the channel is R=400 μm. The light gray region maps the velocity distribution of methanol, while the dark gray region represents the velocity distribution of water. The asymmetrical pattern is due to the higher inlet pressure of methanol.

1. Yecko, P., *International Journal of Multiphase Flow* 34 (2008) 272-282.

Magnetic Resonance Imaging of Microfluidic Flow with a Parallel-Plate Resonator

Bruce J. Balcom , Jing Zhang

Physics Department, University of New Brunswick, Fredericton, NB, Canada, E3B 5A3

Abstract:

Magnetic Resonance Imaging has been introduced to study flow in micro-channels using pure phase spatial encoding with a microfabricated parallel-plate NMR probe (shown in Fig. 1). The new NMR probe and pure phase spatial encoding enhance the sensitivity and resolution of the measurement. In this poster, ^{1}H NMR spectra and images were acquired at 100 MHz. The B_1 magnetic field is homogeneous and the probe is very sensitive, which enables velocity mapping of the fluids in the micro-channel with high signal to noise ratio. The parallel-plate probe with pure phase encoding spin echoes can also produce high resolution spectra, therefore chemical shift resolved velocity mapping was also undertaken. Results are presented which show separate velocity maps for water and methanol flowing through a straight circular micro-channel. The future performance of these techniques for the study of microfluidics is also extrapolated and discussed.
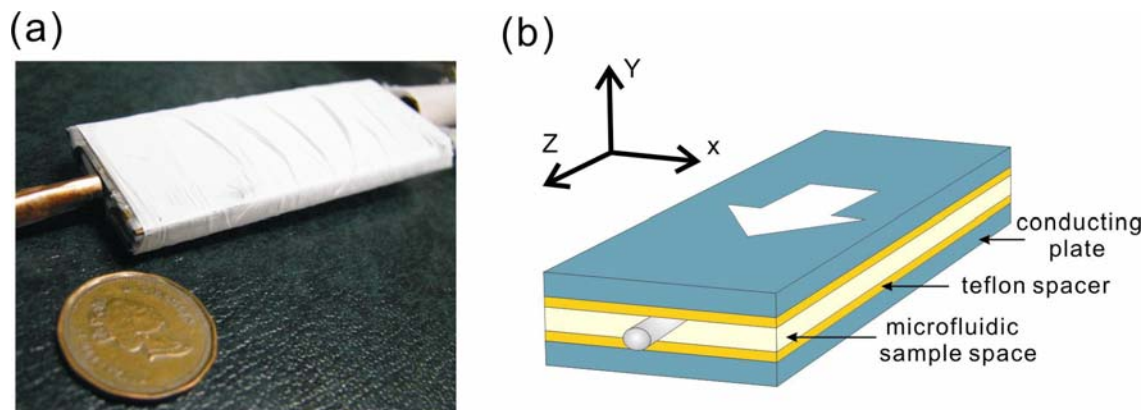
Fig. 1 (a) Picture of a micro-machined parallel-plate NMR probe. The plates are 7 cm x 2 cm. Signal from the inlet and outlet tubes is shielded from detection by a small diameter copper pipe. (b) Schematic illustration of the parallel-plate NMR resonator. The teflon spacers employed as a dielectric were 0.8 mm thick. Current flow is parallel to the long axis of the probe, oscillating at the resonance frequency.

P26

Rheo-NMR investigations of anomalous shear-banding: multidimensional dynamics under stick-slip conditions

<u>Kirk W. Feindel</u>[1] and Paul T. Callaghan[1]

[1] The MacDiarmid Institute for Advanced Materials and Nanotechnology, Victoria University of Wellington, Wellington, New Zealand

Abstract:

Complex fluids exhibit a combination of solid- and liquid-like properties. Such fluids are encountered everyday; common examples include foods, detergents, cosmetics, and biological fluids. By combining conventional rheological methodology with nuclear magnetic resonance techniques (rheo-NMR) [1], previously elusive information about flow and deformation of materials can be garnered. Some complex fluids display pathological flow behaviour, such as the spatial separation of the fluid into macroscopic regions of widely differing viscosity (i.e., shear banding) [2]. The relative proportions of the phases are postulated to satisfy a lever rule according to eqn. (1), with the shear bands maintaining fixed high ($\dot{\gamma}_H$) and low ($\dot{\gamma}_L$) shear rates with a mobile interface:

$$\dot{\gamma}_{applied} = \chi \dot{\gamma}_H + (1-\chi)\dot{\gamma}_L \qquad (1)$$

where χ is the total volume fraction.

Herein, the strain-controlled flow of a worm-like micellar solution in cylindrical Couette geometry is investigated using rapid 2D ^{1}H NMR velocimetry. We find anomalous shear banding in which stick-slip leads to an unusual lever rule behaviour where the interface position, *h/d*, remains constant while the high and low shear rates change, see Fig 1. Velocities are measured in the flow direction with the imaging plane oriented along the cell vorticity axis. The spatio-temporal resolution achieved reveals fluctuations in flow structure along the vorticity axis and instability of the high shear band.
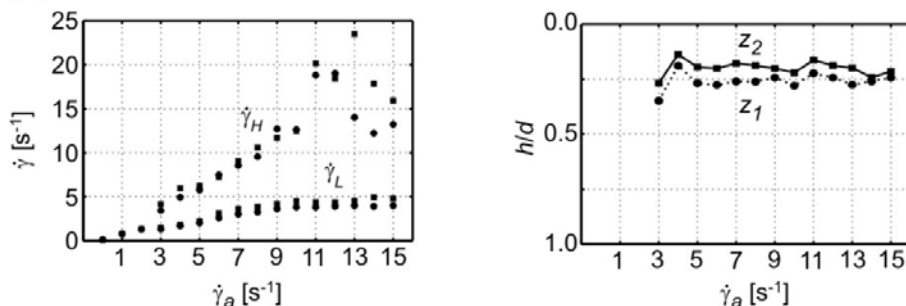
Fig. 1: Anomalous shear-banding with stationary interface, at two positions along the vorticity axis, z_1 and z_2.

1.   P. T. Callaghan, *Rheol. Acta.* **47** (2008) 243.
2.   H. Rehage and H. Hoffmann, *J. Phys. Chem.* **92** (1988) 4712.

Experimental evaluation of oil migration from almonds using MRI

<u>A. Altan</u>, D. Lavenson, K.L. McCarthy and M.J. McCarthy

Department of Food Science and Technology, University of California, Davis, CA 95616, USA

Abstract:

Release of oil in nuts due to damaged cellular structures can degrade the quality of products incorporating nuts. Therefore, the aim of this study was to evaluate migration of oil from almonds to chocolate and to investigate effects of type of roasting conditions and degree of roast.

Migration of almond oil into dark chocolate was studied by magnetic resonance imaging (MRI), using multi slice spin echo pulse sequence to acquire images with an 8 ms echo time and a 1000 ms repetition time. MRI measurements were performed on 1T Aspect AI MRI spectrometer. MRI images were acquired with a field of view of 68 mm, 128x128 and a slice thickness of 5 mm. A 2x3 factorial design was used for experimental design with factors of type of roasting (air roasting, cocoa butter roasting) and degree of roast (light, medium and heavy). The roasted almonds were enrobed in tempered dark chocolate and placed in sample holder. The holder included a raw almond, enrobed roasted almonds at each condition and degree of roast and a mixture of almond oil/cane sugar (50% w/w) as a reference. The sample holders were stored at 20 and 30°C over a period of 53 days. A calibration curve was prepared by mixing of almond oil (0-4.8%) and chocolate.

Mean signal intensity of images was standardized by mean signal intensity of a reference and plotted against the amount of added almond oil (% w/w). The equation of calibration curve was $y=0.0186x+0.1433$ ($R^2=0.9425$). The signal intensity increased linearly when the oil amount increased in chocolate. For the chocolate enrobed almond samples stored at 30°C, oil migration from almonds into chocolate was observed over the storage time. This study demonstrated that MRI can be used to evaluate the migration of oil from almond to chocolate.

P28

Magnetic Resonance Imaging of a Propagating Acidity Front in a Water-in-Oil Microemulsion

Nicola Halliday[1], A. F. Taylor[2] and M. M. Britton[1]

[1] School of Chemistry, University of Birmingham, Birmingham, UK
[2] School of Chemistry, University of Leeds, Leeds, UK

Abstract:

Microemulsions are thermodynamically stable, isotropic mixtures of water, oil and surfactant. For certain compositions, the mixture self organises to form reverse micelles (RM) of nanosized water droplets that are sequestered from the continuous oil phase by a monolayer of surfactant (and sometimes co-surfactant) molecules.

Properties observed for cellular water have been reported for water molecules in RMs and as such, reactions in reverse micellar systems serve as simplified models of reactions in biological cells [1]. Of particular interest is the effect that the aqueous microenvironment has on reaction rates. Autocatalytic reactions are particularly sensitive to their environment and are known to support propagating reaction fronts [2]. Our research uses nuclear magnetic resonance (NMR) techniques to study and image propagating acidity fronts of the bromate-sulfite reaction in a water-in-oil (w/o) microemulsion.

Our research shows that NMR relaxation times of water molecules in a cetyltrimethylammonium bromide/hexanol/aqueous w/o microemulsion are pH sensitive. T_2 relaxation times of the water change with pH as a consequence of differing rates of proton exchange between hexanol and water molecules. Associated with this exchange is a variation in chemical shift of the hexanol hydroxyl peak and the water peak. This phenomenon was exploited using a chemical shift selective (CHESS) sequence to gain MR contrast between reactant and product environments of the system. Magnetic resonance images were thus obtained of a propagating acidity front in a w/o microemulsion (Figure 1). This work may have wide spread application for the study and understanding of how microheterogeneous systems respond to pH, precluding the need for probe molecules.
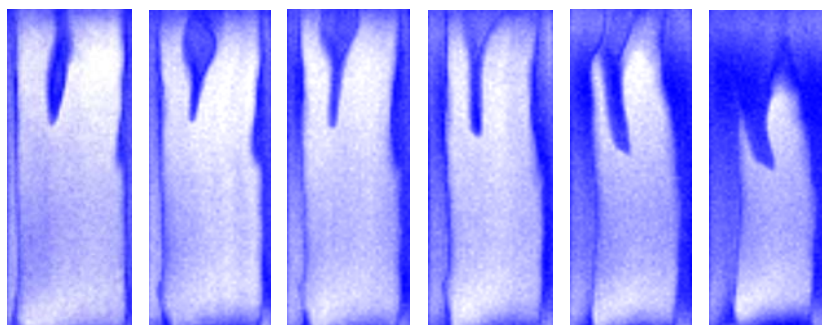
Figure 1: Magnetic resonance images of a propagating reaction front of the bromate-sulfite reaction in a water-in-oil microemulsion. Image slice thickness is 1 mm. The time interval between each image is approximately 6 minutes.

1. Bru, R., Sánchez-Ferrer, A., García-Carmona, F., *Biochem. J.* **310** (1995) 721-739
2. McIlwaine, R. E., Fenton, H., Scott, S. K., Taylor, A. F., *J. Phys. Chem. C* **112** (2008) 2499-2505

Magnetic Resonance Imaging of Chemistry in Flow

Jan Novak[1], Annette F Taylor[2] and Melanie M Britton[1]

[1]School of Chemistry, University of Birmingham, Birmingham, UK
[2]School of Chemistry, University of Leeds, Leeds, UK

Abstract:

The manganese-catalysed Belousov-Zhabotinsky (BZ) reaction has been studied under flow using Magnetic Resonance Imaging (MRI). The BZ reaction is known to form travelling waves and recently it has been shown that stationary waves form when the reaction is coupled with flow in a packed bed reactor [1,2]. We have extended the range of flow environments studied to include Taylor vortices in a couette cell and Poiseuille flow. The study of chemical waves under flow is of increasing interest as they provide alternative mechanisms for pattern formation in nature and in particular biology.

MRI visualisation of the chemical waves is made possible by a difference in the NMR relaxation times beween the two oxidative states of the metal catalyst [3]. In this study we look at chemical waves propagating through a series of Taylor vortices. Taylor vortices are a hydrodynamic instability produced in cylindrical Couette flow, comprising of torroidal counter-rotating vortices within the annulus of the cell. In our experiments, Taylor vortices are established and then the reaction is triggered at the bottom of the cell and the resulting wave propagates through the vortices (fig. 1).

Previous work has shown that MRI is able to produce velocity images of flow within Taylor vortices [4]. We have combined this capability with visualisation techniques to probe the coupling between the non-linear chemistry in flow. It has been found that at low shear rates, fronts propagate as single vortex packets, but at high shear fronts propagate as multiple packets.
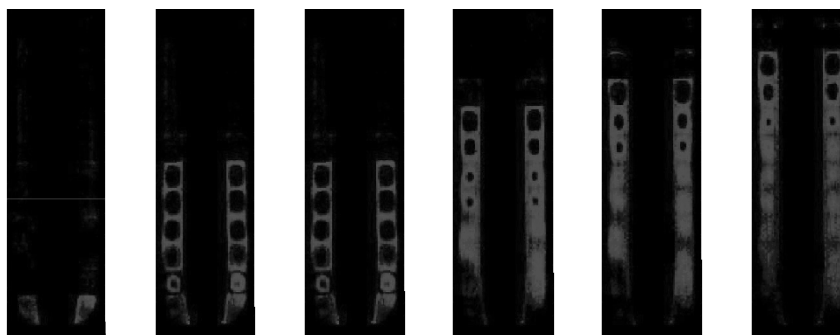
Fig.1: Images of the manganese-catalysed BZ reaction in a series of Taylor vortices, at six second intervals.

1. Bamforth, J. R.; Toth, R.; Gaspar, V.; Scott, S. K. *Phys. Chem. Chem. Phys.* **4** (2002) 1299-1306.
2. Britton, M. *et al*. *J. Phys. Chem. A* **109** (2005) 8306-8313.
3. Britton, M. M. *J. Phys. Chem. A* **110** (2006) 2579-2582.
4. Seymour, J. D.; Manz, B.; Callaghan, P. T. *Phys. Fluids* **11** (1999) 1104-1113.

MRI Tracer Studies in Natural Soils

S. Haber-Pohlmeier[1], S. Stapf[2], A. Pohlmeier[3]

[1] Institute of Technical and Macromolecular Chemistry, RWTH-Aachen University, Aachen, Germany
[2] Department of Technical Physics II, TU Ilmenau, Ilmenau, Germany
[3] Agrosphere Institute, Research Center Jülich, Jülich, Germany

Abstract:
Flow processes in soils control many important soil functions like water availability and transport of nutrients and contaminants. Natural soils are sensitive and complex systems. This requires non-invasive methods for the visualization of these processes. Since in most cases water flow velocites are too slow to be monitored directly by MRI flow imaging, they can be investigated conveniently by monitoring contrast agents. The purpose of this study is to investigate the usefulness of a paramagnetic contrast agent in aqueous solution. Therefore we have chosen Gd-DTPA for two reasons: i) it is anionically charged around pH = 7, so the probability to be adsorbed is low. ii) it is chemically stable, so no decomposition should be expected.

The MRI experiments have been performed on two scanners: first a 4.7T system with a 17 cm rf coil, secondly a 7T system with a 3.8 cm rf-coil. As sequences we used SEMS and FSEMS with relatively short repetition and echo times for T1-weighted imaging.

We started our investigations with a sand phantom consisting of an outer core of silt with low hydraulic conductivity and an inner core of medium sand with high conductivity. Under steady state irrigation the tracer plume moves homogenously only in the inner sand core without any preferential flow. The next system was a natural soil core, a sandy loam from Kaldenkirchen, Germany. In contrast to the first system we observed strong preferential flow, which is considerably faster than the average flow velocity. Finally, we conclude that with Gd-DTPA tracer water flow paths can be visualized and fast preferential flow processes can be detected non-invasively even in natural soil cores.

Waterflow Visualized by Tracer Transport in Root-Soil-Systems Using MRI

S. Haber-Pohlmeier[1], D. van Dusschoten[2], S. Stapf[3], A. Pohlmeier[4]

[1] Institute of Technical and Macromolecular Chemistry, RWTH-Aachen University, Aachen, Germany
[2] Phytosphere Institute, Research Center Jülich, Jülich, Germany
[3] Department of Technical Physics II, TU Ilmenau, Ilmenau, Germany
[4] Agrosphere Institute, Research Center Jülich, Jülich, Germany

Abstract:

Water supply for root and plant growth is one of the most important soil functions, which is mainly controlled by water fluxes in this unsaturated porous medium. Here, the rhizosphere i.e. the region directly between the rhizoplane and bulk soil is of special interest, since in this area the immediate root water uptake takes place. Using MRI as a powerful non-invasive method the water content can be visualized, but the water flow velocities themselves are too slow to be monitored directly by MRI flow imaging. Therefore indirect methods like monitoring the flux of paramagnetic tracers must be applied.

By means of infiltration experiments we have investigated for the first time the behaviour of a Gd-DTPA tracer solution in an unsaturated, heterogenous model soil that held maize and lupin plants, respectively.

1) In a first setup the tracer solution was infiltrated quickly from bottom and its content was imaged by a fast spin echo sequence over a period of 60 minutes. The infiltration process can be divided in several stages: i) While the plume moves homogeneously into the bulk soil, the tracer does not get into the immediate surrounding of the roots during the first six minutes. ii) After this initial period a continuously increasing enrichment of tracer in this region is observed for about twenty minutes, but not yet taken up by the plant.

2) In a second setup a small amount of tracer solution was injected from top directly in the root system of lupin in medium sand with low water content. The tracer plume was monitored for a period of several days. In contrast to the infiltration experiment, after several hours a motion of the tracer plume towards the tap root was observed. Simultanously high signal intensity appeared in the tap root and moved upwards in inner part of the root system until the tracer vanished eventually after 4 days.

The studies show that Gd-DTPA is a very convenient tracer for monitoring flow processes in soil − root systems and indicates and visualizes root activity directly. The investigations will be extended in future to natural soil cores and compared to model calculations for root water uptake.
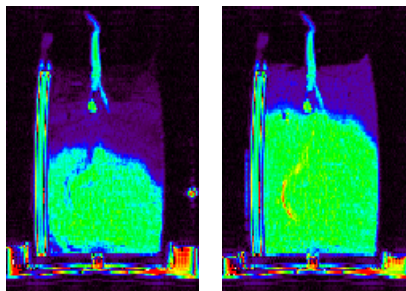
Fig. 1: Tracer distribution in maize root system 6 and 20 minutes after infiltration

Oscillatory Flow phenomena in simple fluids and complex fluids

Loribeth Evertz[1], Erik M. Rassi[1], Tyler R. Brosten[1], Keith B. Fisher[1], Sarah L. Codd[1] and Joseph D. Seymour[2]

[1] Dept. of Mechanical and Industrial Engineering, Montana State University, Bozeman, MT, USA
[2] Dept. of Chemical and Biological Engineering, Montana State University, Bozeman, MT, USA

Abstract:

This project is an undergraduate research experience funded by Montana INBRE and the Undergraduate Scholars Program (USP) at Montana State University. Blood is a complex fluid that can be classified as both a Newtonian and non-Newtonian fluid depending on the flow regime. Under normal conditions in the body, blood undergoes laminar flow, but oscillatory flow can induce diseased conditions at the wall of arteries [1]. If such diseased conditions are present, blood flow will become turbulent or even non-Newtonian. Detecting the altered flows, helps to locate the diseased condition before it has fatal consequences.

a controllable and predictable oscillatory flow has been established in order to gain a better understanding of the impact of such a flow on polymer solutions and colloidal suspensions. The oscillatory flow is generated by using a motor with an adapted shaft to drive an appropriately sized cylinder. By using the pressure oscillations in the flow to trigger the MR spectrometer, magnetic resonance techniques have been used to measure the velocity distributions and transport phenomena of various fluids undergoing oscillatory flows at specific points in the oscillation cycle.

1. Ku, DN. 1997. Blood Flow in Arteries. Ann. Rev. of Fluid Mechanics. 29: 399-434

Ultrafast velocity mapping in planar micro-structures

Eva Paciok , Federico Casanova and Bernhard Blümich

Institute for Technical and Macromolecular Chemistry, RWTH Aachen University, Aachen, Germany

NMR has proven to be a powerful tool for the characterization of flow in micro-fluidic setups like lab-on-a-chip mixers or reactors[1,2,3,4]. Such devices contain planar arrays of microscopic channels and chambers that need optimization to maximize throughput. The potential of NMR to monitor the flow pattern inside these structures has pushed the design of surface rf coils with geometries adapted to improve the sensitivity for each particular structure. Although the residence time of liquids inside these devices is relatively long, the significant variation of velocities of molecules, as they pass through the complex micro-structures, has hindered the implementation of fast velocity mapping techniques based on multi-echo generation (RARE). In fact, PGSE-RARE was proven to greatly suffer from B_1 inhomogeneities and to fail completely, even for slow velocities, if a planar surface coil is used[4]. In these conditions conventional PGSE sequences appear as the only alternative. In this work, we exploit the advantages of the FLIESSEN pulse sequence[5] (FLow Imaging Employing a Single Shot ENcoding), to overcome the limitation imposed by the inhomogeneity of the radiofrequency field generated by surface rf coils. While acquiring the complete information required to produce a 2D velocity map during a single CPMG echo train, the velocity information is frequently updated by independent velocity encoding of each individual echo.   The performance of this technique is demonstrated by measuring the velocity map of acetone flowing in a planar spiral phantom made from teflon tubing (OD 1.6 mm, ID 0.8 mm). The phantom was designed to ensure a sufficiently long residence time and, more importantly, drastic velocity changes during the measurement. Using a planar surface rf coil in combination with the FLIESSEN pulse sequence, high-fidelity velocity maps were obtained even though molecules pass through a whole winding during the experiment (Fig. 1).

(a)   (b)   (c)
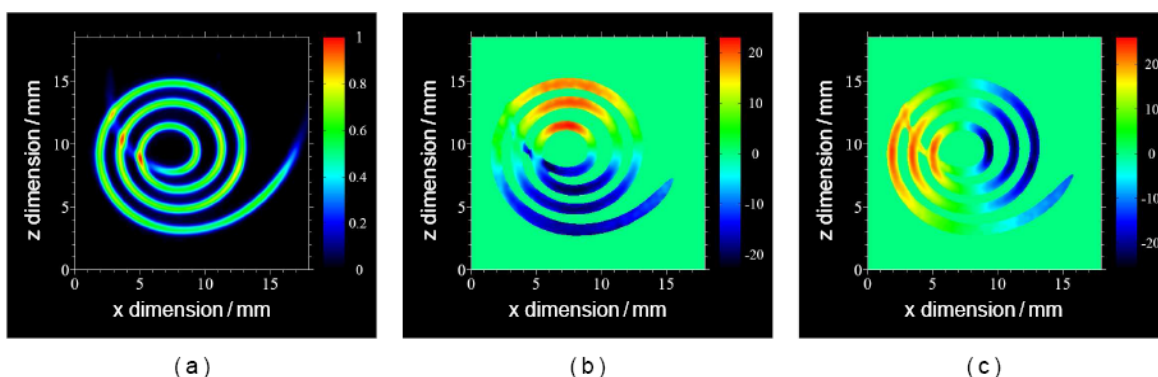
Fig. 1: Results of imaging and velocity mapping with FLIESSEN. (a) [1]H-spin density image of static acetone. (b) Map of the x velocity component and (c) map of the z component. Velocities up to 27 mm/s were measured, which means that spins in the inner rings complete at least a 360° -loop during the CPMG echo train.

[1]   S. Ahola *et al.*, *Lab Chip* **6** 2006 90-95.
[2]   B. S. Akpa *et al.*, *Annal Chem* **79** 2007 6128-6134.
[3]   E. Harel *et al.*, *JMR* **193** 2008 199-206.
[4]   S. Ahola *et al.*, *JMR* **182** 2006 143-151.
[5]   A. Amar, F. Casanova, B. Blümich, MRPM, Boston, 2008.

MRI for Investigations of Permeate Flow and Observation of the Cake-Layer Formation in Micro-Filtration Processes

L. Utiu[1] , M. Kueppers[1] , S. Buetehorn[2] and B. Bluemich[1]

[1] Institute of Technical and Macromolecular Chemistry, RWTH Aachen University, Germany
[2] Chemical Process Engineering, AVT, RWTH Aachen University, Germany

Abstract:

In recent years, the application of NMR imaging and microscopy techniques have been recognized to have great potential as an experimental tool for engineering research due to their versatility and accuracy [1,2].

In the framework of this study, a submerged micro-filtration process using a polymeric hollow-fibre membrane and silica suspensions of different solids concentration is investigated. Submerged hollow fibre membrane systems are used in municipal sewage treatment to separate the biologically purified water from the suspended solids. The overall objective is to evaluate the permeability distribution along the fibre and to determine the thickness of the layer of deposited matter (silica) continuously formed on the surface of the membrane. Characteristics like the permeability distribution along the membrane as well as the particle size distribution and rheology of a model suspension are of importance to understand the filtration behaviour.

In this work, the use of NMR imaging to simultaneously map and measure the flow in hollow fibre membranes was demonstrated. Dynamic NMR microscopy in terms of flow imaging was found to be robust and accurate in providing quantitative data of flow velocity, as compared to volume-flow rates obtained by direct measurements. NMR imaging has also been used to observe the silica particle layer formation at the surface of the membrane in response to a change in permeate flux and solids concentration [3]. The method is completely non-invasive and can be employed to optimise the operating conditions and to test the predictions of theoretical models for cake-layer formation and flow in hollow fibre membrane filtration modules, bio-reactors and membrane filtration systems.

1. P.T. Callaghan, Principles of Nuclear Magnetic Resonance Microscopy, Oxford University Press, Oxford (1991).
2. B. Bluemich and W. Kuhn (Eds.), Magnetic Resonance Microscopy: Methods and Applications in Materials Sciene, Agriculture and Biomedicine, VCH Press, Weinheim (1992).
3. V. Chen, H. Li and A.G. Fane, *J. Membr. Sci.* **241** (2004) 23-24.

Dynamic pulsed gradient spin echo nuclear magnetic resonance measurements and simulation of two-fluid mixing in Taylor vortex flow

Amber L. Broadbent[1, 3], Sarah L. Codd[2], Joseph D. Seymour[1], Jim M. Mullin[3]

[1] Department of Chemical and Biological Engineering, Montana State University, Bozeman, Montana
[2] Department of Mechanical and Industrial Engineering, Montana State University, Bozeman, Montana
[3] Bend Research, Inc., Bend, OR

The Couette flow system, which consists of two concentric cylinders with one or both cylinders rotating, is of practical interest in reaction engineering, filtration applications, mixing applications, including two-fluid dispersion formation, and rheological studies. The famous fluid dynamicist, G.I. Taylor, first investigated the onset of instability in such a flow system in 1923, and observed that for a given fluid when the inner cylinder rotation rate exceeded a critical value, pairs of counter-rotating, evenly spaced toroidal vortices appeared along the axial direction of the cylinder. Magnetic resonance is an ideal tool for classifying unstable Taylor vortex flow and for quantifying the transport processes that occur in these flows. Velocities and flow structures measured via MR techniques are extremely useful for designing mixing devices to enhance transport and for controlling structure formation in two-fluid systems. A RheoNMR Couette (Magritek Ltd. New Zealand) with a 1 mm gap d between the inner and outer cylinders was used to evaluate Taylor vortex flow in 1.65 cSt silicone oil, 1 cSt deionized water and 0.65 cSt silicone oil. The onset of instability in each of the single fluids was determined through dynamic PGSE experiments and Fluent CFD simulations. The rotation rate at which instability onset occurred agreed very well between the experiments and simulations, as did the wavelength of the unstable waveform. Axial direction velocity maps were obtained through dynamic PGSE experiments and Fluent CFD simulation for two two-fluid systems: 1.) 1.65 cSt silicone oil and water 2.) 0.65 cSt silicone oil and water. In the two-fluid experiments, water was placed in the lower portion of the axially oriented Couette and silicone oil was placed atop the water so that the two-fluids were axially stratified. Interestingly, in every two-fluid experiment conducted, the vortices in the axial direction velocity maps $v_z(r,z)$ were found to pair across the two-fluid interface. Even when the interface was asymmetric across the gap, the vortices paired across the interface. Apparently, the phenomenon of axial vortex pairing across the two-fluid interface is quite robust and may have potential for pinning molecules or cells between fluids. The ability to pin a biological cell at the interface in order to treat a portions the cell with different reagents has the prospect of supplying new capabilities for cellular biology [1-3].

1. Whitesides, G.M. and A.D. Stroock, *Flexible methods for microfluidics.* Physics Today, 2001. **54**(6): p. 42-48.
2. Takayama, S., et al., *Patterning cells and their environments using multiple laminar fluid flows in capillary networks.* Proceedings of the National Academy of Sciences of the United States of America, 1999. **96**: p. 5545-5548.
3. Takayama, S., et al., *Selective Chemical Treatment of Cellular Microdomains Using Multiple Laminar Streams.* Chemistry & Biology, 2003. **10**(2): p. 123-130.

NMRI Characterization of Bimodal Suspension Flows

Nina C. Shapley and Nancy F. Zeng

Department of Chemical and Biochemical Engineering, Rutgers University, Piscataway, NJ, USA

Abstract:

This investigation focuses on the flow behavior of a concentrated bimodal suspension (i.e. liquid containing particles of two sizes) through model geometries that mimic realistic systems in reinforced materials processing. One relevant example is the abrupt contraction-expansion geometry. Contraction-expansion flows arise in materials processing operations, such as injection molding or extrusion of ceramics and composites, and have the potential to significantly enhance particle size separation or mixing effects occurring in simple geometries such as tube flow. In previous studies of monomodal suspensions in the contraction-expansion geometry, we consistently observe the formation of distinct core-annular structures downstream of the expansion section.

In our experimental study, suspensions of neutrally buoyant, noncolloidal spheres in viscous, Newtonian liquids undergo pressure-driven flow in an abrupt, axisymmetric 4:1:4 contraction-expansion. Nuclear magnetic resonance imaging (NMRI) is used to measure the steady-state particle concentration distribution and flow field. By adopting varied particle materials (i.e. rigid polymer vs. hydrogel) we can monitor particle size separation through the contrast in the spin-spin (T_2) relaxation time among rigid solids, gels and suspending fluids acquired through CPMG scans. Figure 1 presents several maps of the fraction of T_2 relaxation due to alginate gel particles. Image analysis methods for obtaining quantitative concentration profiles of two particle types from NMRI data are under ongoing development. The role of relative large and small particle volume fractions and a comparison to results from monomodal suspensions will be presented.

(a)   (b)   (c)
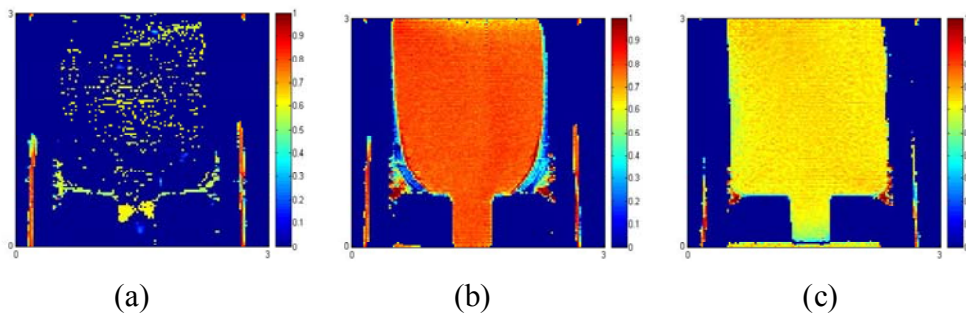
Fig. 1: Alginate gel (small) particle T_2 relaxation fraction maps from (a) ϕ=40% large/11% small bimodal suspension; (b) ϕ=15% large/35% small bimodal suspension; (c) ϕ=25% large/25% small bimodal suspension. Longitudinal view of expansion flow, FOV=3x3cm, slice thickness=1mm. Flow direction is upward.

Experimental models for studying the effect of shear-flow in biomedical DWI

Uri Nevo[1,2] , Peter J. Basser[2]

[1]Department of Biomedical Engineering, Tel Aviv University, Tel-Aviv, Israel
[2]Section on Tissue Biophysics and Biomimetics, NICHD, NIH, Bethesda, MD, USA

Abstract

Introduction: Diffusion weighted imaging (DWI) has a major clinical and research value. The DWI signal has been ascribed to multiple micro-structural sources but due to theoretical and experimental complexity, the relative contributions of these physical factors to the diffusion process and the DWI signal are poorly understood. **Our objective** is to quantify the contribution of an important, and yet overlooked mechanism that affects DWI: Incoherent micro-streaming of water molecules inside and around cells. Indeed, most models of fluid displacement and its effect on DWI treat diffusion in restricted or inhibited environments, but hardly treat the contribution of physiological flow. We report here our preliminary analysis and the use of two experimental models established for this purpose.

Methods: We derived the attenuation in DWI in the presence of the most basic flow patterns (See box 1). We used the Rheo-NMR with a Couette cell as a flow phantom to validate our derivation of micro-streaming inside a voxel. To complement the Rheo-NMR measurements we built a system and a protocol for measurement of DWI in the absence of physiological sources of artifacts (motion, blood-oxygenation). This system is based on the imaging of neuronal Organotypic cultures that are spontaneously active and are perfused during the MRI session.

Results: Fig. 1 describes the PGSE (spectroscopy) attenuation of a Couette cell, including the theoretical curve, and an erroneous fit to a bi-exponential curve. Fig. 2 displays a primary calculation of the possible contribution of micro-streaming in physiological conditions, relative to the contribution due to diffusion. Fig 3 presents a slide with a couple of Organotypic cultures and an ADC map.

Conclusions: Cellular micro-streaming is a mechanism of possible importance for our understanding of the biological DWI signal. The use of experimental biological model systems such as acute slices or organotypic cultures, and the use of flow phantoms, such as the Rheo-NMR can aid in resolving the significance of micro-streaming in clinical and biological scenarios.
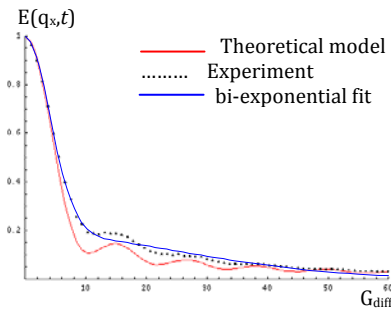
Fig. 1: Theoretical and experimental attenuation curves for a rotating Couette
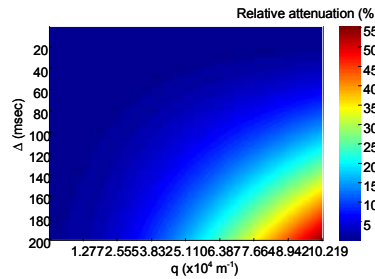
Fig. 2: The relative attenuation induced by linear shear for various values of experimental parameters (Δ, q) compared to that of a sample that diffuses freely with an average ADC of $1 \cdot 10^{-5}$ cm^2/sec, with the same experimental parameters. Notice that the relative contribution of shear-related attenuation increases with longer diffusion times (Δ) and q values.
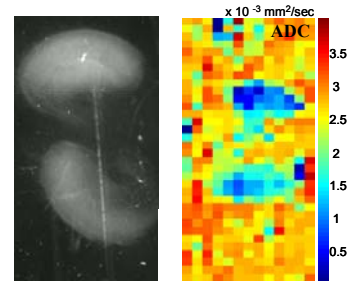
Fig 3: A slide with a couple of organotypic cultures (left); an ADC map of an organotypic culture.

Box 1: The attenuation in a PGSE experiment in a voxel of area a^2, with diffusion time Δ, over a sample under linear shear β (when Taylor dispersion is neglected) is: $E(\overline{q},\Delta) = E_{flow}(q_x,\Delta) \cdot E_{diff}(\overline{q},\Delta)$ where E_{diff} is the common diffusion attenuator, and E_{flow} corresponds to:

$$E_{flow}(q_x,\Delta) = e^{-2\pi i q_x v_{av}\Delta} \cdot sinc(\pi q_x \beta a \Delta)$$

In an axi-symmetric cylindrical flow the attenuation corresponds to:
Where $\omega(r)$ describes the radial velocity and J_0 is the 0th-order Bessel function of the first kind. A is the area A $= \pi \cdot (r_{ext}^2 - r_{int}^2)$, and:

$$E_{band}(\omega(r),t) = \frac{1}{A} \int_{r_{int}}^{r_{ext}} J_0(\kappa(\omega(r))) r \, dr.$$

$$\kappa(r) = 4\pi q_x r \sin\left(\frac{\omega(r) \cdot \Delta}{2}\right)$$

Rheo-NMR Studies of Complex Spatiotemporal Dynamics in Wormlike Micelle Systems

Jennifer R. Brown[1] and Paul T. Callaghan[1]

[1] School of Chemical and Physical Sciences, Victoria University of Wellington, Wellington, New Zealand

Abstract:

Recent experiment and simulation of wormlike micelle systems indicate complex spatiotemporal dynamics occur under shear flow. Surfactant systems under the correct conditions can self-assemble into long flexible cylindrical aggregates called wormlike micelles, which exhibit complex rheological behavior. Above a critical micelle concentration, a highly entangled network is formed with the additional complication of constant dissociation and recombination of micellar chains. Due to this, the linear mechanical response is viscoelastic and classically Maxwellian with a single relaxation time. A shear banding transition occurs in the nonlinear response, characterized by a plateau in the shear stress versus shear rate flow curve, where the flow field is inhomogeneous with macroscopic regions of varying shear rates. Instabilities at the band interface manifest as complex spatiotemporal dynamics of the three dimensional flow field. Nuclear Magnetic Resonance (NMR) techniques provide a unique perspective on the complex fluid flow behavior of wormlike micellar systems. NMR velocimetry measurements can probe flow structure in any direction. Improvements in rapid velocimetry techniques allows investigation of the temporal flow field fluctuations, which in combination with spatially localized information on molecular order obtained with deuterium NMR, provides information on the coupling between flow and microstructure. The semidilute surfactant system of cetyltrimethylammonium bromide (CTAB) and sodium nitrate in D_2O and H_2O at a concentration and temperature far from the isotropic to nematic phase transition exhibits complex behavior under shear, as revealed by spatially and spectrally resolved NMR measurements in the vorticity direction.

Improved Flow ENhanced Signal Intensity (FENSI) perfusion imaging

O. Reynaud[1], D. Le Bihan[1], A. Webb[2] and L. Ciobanu[1]

[1] NeuroSpin, CEA, Saclay, France
[2] Leiden University Medical Center, Leiden, The Netherlands

Introduction: Flow ENhanced Signal Intensity (FENSI) is a method for measuring blood flow changes during functional activation and cerebral perfusion [1]. As in DESIRE images [2], the signal enhancement is attained by measuring all protons that are present in, or pass through, a small region (tag slice) over a period of time (tag duration). For FENSI, this enhancement is related to the blood flow rate. However, in order to perform quantitative perfusion measurements one needs to estimate and account for other factors which can affect the signal enhancement such as magnetization transfer effects and signal increase due to repeated saturation. This is precisely the goal of the present study.

Methods: All experiments were performed on a 7T PharmaScan Bruker system. To analyze the MT and repeated saturation effects on the FENSI/DESIRE signal enhancement we used 2% agar phantom samples. We employed a FENSI-SE pulse sequence and measured the signal enhancement for six different tag thicknesses (from 200 – 450 μm). The MT effects was minimized by adding a train of MT pulses before the tag (30 pulses, Gaussian shape, 5 ms duration, flip angle 600° -2000°, 1.5 kHz off- resonance from water). Axial and coronal perfusion images were obtained on Sprague-Dawley male rats using a FENSI-EPI sequence with TE =15ms, TR=3s, thk =300 μm, in plane resolution 400 x 320 μm, 60 tags. Eight signal averages were acquired. Reference images were acquired with a single tag pulse.

Results and discussion: As expected, the MT effect due to the repeated tag pulses can lead to a signal increase of up to 40% (for our particular sample and experimental parameters). This effect can be minimized by placing a train of MT pulses before the FENSI tag. The idea behind this is to obtain the maximum magnetization transfer effect with this MT pre-pulse which will then render the tag pulse MT effect free. By varying the flip angle of the MT pulse we found that the maximum MT effect reduction is attained when the flip angle is higher than 1600° (Figure 1). After the MT removal, the difference between the experimentally obtained and the theoretically calculated signal enhancement due to diffusion [2] is caused by the repeated saturation pulses (between 1 to 15% for different slice thickness). While the repeated saturation effect cannot be removed its estimation is necessary for quantitative measurements.

Figure 2 shows *in vivo* perfusion images performed in the presence of the MT effect (a and b) and after the MT minimization (c and d). Figures 2e and 2f show further improved FENSI perfusion images obtained after CSF signal removal. The CSF was removed by acquiring a FENSI image with a very long TE (250 ms) and subtracting it from the FENSI perfusion image.
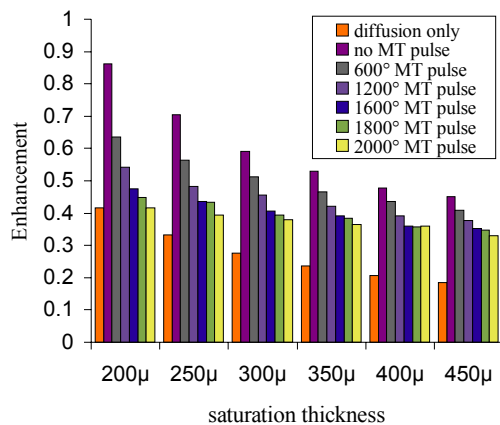
Fig 1. Evolution of signal enhancement with pre MT pulse application for different flip angles of the MT pulse.
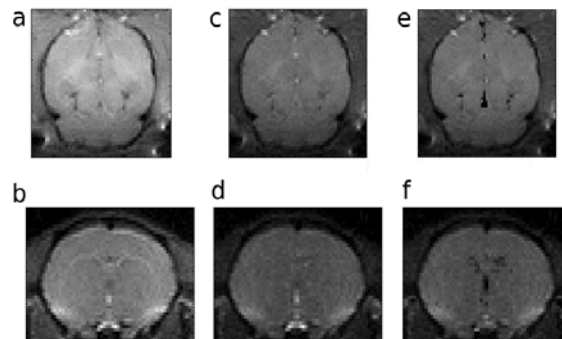
Fig 2. Coronal (a, c, e) and axial (b, d, f) FENSI perfusion images in a rat brain, without (a, b) and with (c, d) pre MT pulses and after CSF removal (e, f).

Conclusion: We present here the first perfusion images obtained with the FENSI technique. Our improved sequence is robust with respect to MT and repeated saturation effects and capable of providing quantitative flow information. We are currently in the process of validating our *in vivo* perfusion measurements by comparison with other perfusion techniques such as ASL and DSC. Once fully validated, the technique will be applied to perfusion studies in ischemic and brain tumor animal models.

References : [1] B.P. Sutton, C. Ouyang, B. L.Ching, L. Ciobanu, Magn.Reson.Med. (2007), 396:401; [2] L. Ciobanu, A. Webb, C. Pennington, J.Magn.Reson. (2004), 170:252.

Colloidal Acceleration in Porous Media Studied using NMR

<u>Sarah A. Creber</u>[1], Thomas R. R. Pintelon[1] and Michael L. Johns[1]

[1] Department of Chemical Engineering and Biotechnology, University of Cambridge, Cambridge, UK

Abstract:

Bioremediation, pathogen migration, and pollutant leaching in soil are all examples of colloidal transport in the natural environment; these transport processes are complex and often difficult to monitor [1]. In this work, the transport of colloids through porous media was studied using chemically-resolved pulsed field gradient NMR methods. Surfactant-stabilised decane in water emulsions were flowed through a randomly-packed glass bead column. Displacement (probability distribution) propagators of both the colloidal and continuous liquid phases were used to quantify both the colloidal entrapment and the velocities of the flowing colloids and continuous phase respectively. Representative displacement propagators in Fig. 1 (a) show the differences in transport behaviour of the colloidal and continuous phases, colloidal entrapment is immediately obvious. The (mobile) colloids flowed at a mean velocity 1.08 times that of the continuous phase (known as the velocity acceleration factor (VAF)), independent of displacement observation time and flowrate, as summarised in Fig. 1 (b). The finite size of the colloids restricted their flow path by a distance equal to their radius from the surrounding bead packing elements and thus effectively streamlined their flow; this phenomenon, known as radial exclusion was speculated to be the dominant factor in the observed VAF of the colloids. Simulations using a lattice Boltzmann platform and a Lagrangian particle-tracking algorithm incorporating radial exclusion confirmed this, as presented in Figure 1(b).
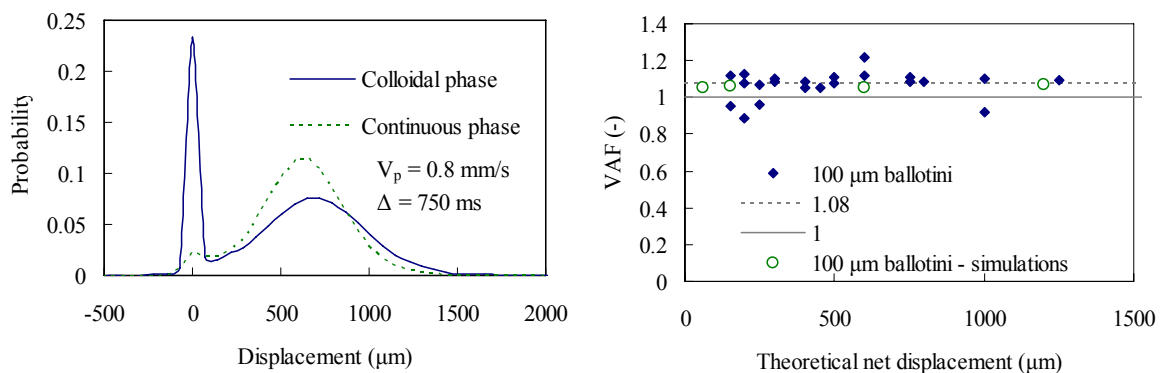
Fig. 1: (a) Representative displacement propagators showing colloid entrapment and relative acceleration and (b) summary of experimental and simulated velocity acceleration factors (VAFs).

1. Timothy R. Ginn, Brian D. Wood, Kirk E. Nelson, Timothy D. Scheibe, Ellyn M. Murphy, and T. Prabhakar Clement, *Advances in Water Resources* **25** (2002) 1017–1042.

Imaging and Quantification of Biofouling on Reverse Osmosis Membranes using NMR

Sarah A. Creber[1], Thomas R. R. Pintelon[1], Daniel A. W. Graf von der Schulenburg[1], and Michael L. Johns[1]

[1] Department of Chemical Engineering and Biotechnology, University of Cambridge, Cambridge, UK

Abstract:

Increasing global demand for freshwater has elucidated the need for effective, efficient water treatment technologies [1]. Reverse osmosis (RO) is one of these technologies in operation around the world, responsible for providing large populations with potable water. RO processes however are energy intensive with energy demands increasing dramatically as the RO membranes foul. Biofouling of RO membranes was studied using various NMR techniques. Small, representative RO membrane flow cells and a large, full-scale industrial spiral-wound RO membrane module were fouled under controlled conditions in the laboratory and compared with unfouled RO membranes. NMR spatial imaging showed good contrast between the biofilm and surrounding water by leveraging the short T_2 relaxation time of water in biofilm compared to bulk water. These images identified significant biofilm accumulation on the membrane spacer nodes, demonstrating that the spacers themselves have a large influence on membrane biofouling. Velocity imaging of flow through the RO membranes captured severely reduced flow channels across the RO membrane (as shown in Figure 1) due to biofouling and subsequent reduced effective surface area of the membrane. Thus, NMR techniques were proven an effective and non-invasive means to characterise biofouling in RO membranes. Lattice Boltzmann simulations of biofilm growth in the membranes were compared with the experimental results, showing excellent agreement.
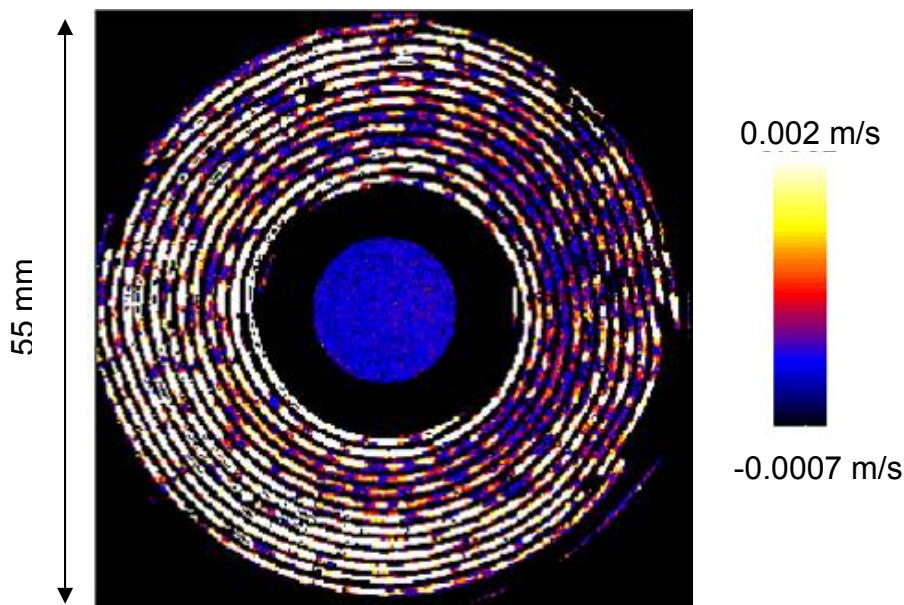
Fig. 1: 2D velocity image of a radial slice of the fouled industrial RO membrane module.

1. UNESCO, *The United Nations World Water Development Report 3*, 2009.

P42

In situ effective diffusivity in biofilms

Ryan Renslow[1], Paul Majors[2], Jeff McLean[3], Jim Fredrickson[2], and Haluk Beyenal[1]

[1] Washington State University, Pullman, WA, United States of America
[2] Pacific Northwest National Laboratory, Richland, WA, United States of America
[3] J. Craig Venter Institute, San Diego, CA, United States of America

Abstract:

The effective diffusivity (D_f) is generally assumed to be constant throughout biofilms. However, experimental evidence suggests that diffusivity decreases near the base of the biofilm and its value depends on biofilm structure. Most previous studies either kill the biofilm to measure D_f or measure the D_f in a single cluster of a living biofilm. The goal of our research is to quantify *in situ* depth-resolved D_f profiles in biofilms.

We used 4 different *Shewanella oneidensis* MR-1 biofilms grown in a constant depth film fermenter and quantified the depth-resolved self-diffusion of water at 30 °C. The diffusivities were reported as relative effective diffusivity by dividing measured diffusivity by bulk water diffusivity. Pulsed field gradient NMR imaging techniques were used to non-intrusively acquire the high-resolution (7.5 micron) diffusivity measurements [1, 2]. Multi-dimensional magnetic resonance imaging (MRI) was also used to help characterize the biofilm morphology.

Figure 1 shows multi-dimensional magnetic resonance imaging (MRI) of a selected biofilm. The yellow slices in the image show the location of the measurements. The measured D_f were averaged over the surface area of the slices (2000 μm × 2000 μm) and reported as surface averaged relative effective diffusivity (D_{fsa}) in Figure 2. The D_{fsa} dropped noticeably near the biofilm surface and increased near the middle of the biofilm showing heterogeneous D_{fsa} distribution in the biofilm. In repeated experiments we found a similar trend. Interestingly, the initial drop near the surface was reproducible in all our other biofilms. The D_{fsa} profiles overlaid with the corresponding MRI intensity image of the flow chamber (and biofilm on coverslip), shown in Fig. 3, demonstrates that D_{fsa} is constant in the bulk water and decreases in the biofilm. Finally, we calculated the average diffusivity for the bulk water (media free from the biofilm matrix) for all experiments as $2.33 \cdot 10^{-9}$ m^2 s^{-1}, which matched literature values for water at 30 °C [3]. The time series measurements demonstrated that D_{fsa} profiles decrease with time.
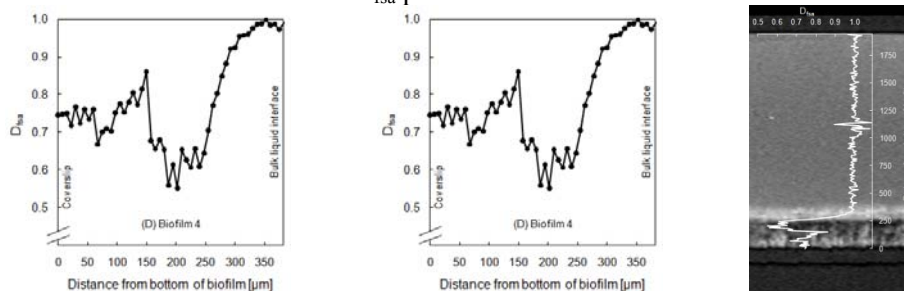
Fig. 1. 3D image of biofilm and slices depicting area averaged to obtain diffusivity measurements.
Fig. 2. Variation of D_{fsa} in a *Shewanella oneidensis* MR-1 biofilm.
Fig. 3. D_{fsa} profile overlaid with the corresponding MRI intensity image of the flow chamber (and biofilm on coverslip).

1. Beuling, E.E., et al., "Characterization of the diffusive properties of biofilms using pulsed field gradient-nuclear magnetic resonance." *Biotechnology and Bioengineering* **60**(3) (1998) p. 283-291.
2. Vogt, M., H.C. Flemming, and W.S. Veeman. "Diffusion in Pseudomonas aeruginosa biofilms: a pulsed field gradient NMR study." *Journal of Biotechnology* **77** (2000) p. 137-146.
3. Simpson, J.H. and H.Y. Carr, "Diffusion and Nuclear Spin Relaxation in Water." *Physical Review* **111** (1958) p. 1201.

Development of a multi-layer planar gradient coil probe for a vertical bore superconducting magnet

K.Ogawa[1], S.Handa[2], K.Kose[1]

1. Institute of Applied Physics, University of Tsukuba, 2. Japan Society for the Promotion of Science

Introduction: Intense magnetic field gradients are indispensable for high resolution MRI, MR microscopy, and molecular diffusion measurements. To obtain such intense field gradients, highly efficient gradient coils are desirable. Efficient gradient coils can be achieved through two approaches: the first one is to reduce the gradient coil size and the second is to icrease the current density in the coil plane. Because the first approach is limited by the sample size, the second approach should be considered. However, the current density in the coil plane is limited by the diameter and resistance (Jule heat) of the conducting wire. To solve this problem, Bowtell proposed a multilayer gradient coil and demonstrated its usefullness by a four-layer cylindrical gradient coil (1). In this study we have develped a multilayer planar gradient coil probe with a solenoid RF coil for vertical bore superconducting magnet.

Materials and method: Figure 1 shows gradient coil winding pattern developed in this study. The axial (z) gradient coil was designed as a combination of circular coils and the diameters were optimized using the genetic algorithm (2). The transverse (x, y) gradient coil was desgined using the target field method (3). These gradient coils were wound on 0.5 mm thick FRP plates using 0.3 mm diameter polyethyrene coated Cu wire. For the two-layer gradient coil, the gradient coils were wound on both sides of the FRP plates. The gradient coil plates were fixed on an octagonal RF shield box made of aluminum channel as shown in Fig. 2. A solenoid coil (inner diameter = 12 mm, length = 16 mm, number of turns = 3, wire diameter = 2.0 mm) was fixed in the center of the RF shield and tuned for the 202 MHz resoance frequency. The efficiencies of the gradient coils were measured using a water phantom (6.4 mm nylon sphere in a test tube filled with $NiSO_4$ solution). The linearity of the gradient coils was evaluated using another water phantom (37 capilleries (1.3 mm OD, 0.65 mm ID) in a test tube filled with $NiSO_4$ solution). A home-built MRI system using a vertical bore 4.74 T superconducting magnet was used throuhout the experiments.

Results and discussion: Table 1 summerizes efficiencies of the gradient coils. As shown in the table, efficiencies of the two-layer Gx, Gy, and Gz coils have about 50, 20, and 6 % larger than those of the one-layer gradient coils. Figure 3 shows a 2D cross sectional plane selected from the 3D image dataset of the capillery phantom. This image clearly shows the linearity of the gradient coils. Figure 4 shows a 2D cross sectional plane selected from the 3D image dataset of a chemically fixed child mouse brain (TR/TE = 1000 ms/40 ms, image matrix = $(128)^3$, voxel size = $(120 \ \mu m)^3$.). This image clearly shows the anatomical details of the mouse brain. In conclusion, although the increase of the gradient coil efficiency by the multilayer structure was limited because of the increase of the coil gap, the efficiency will be increased by thinning the coil thickness.

Reference: (1) R. Bowtell, P. Robyr. Multilayer gradient coil design. J. Magn. Reson. **131**, 286-294 (1998). (2) David E. Goldberg: Genetic Algorithms in Search, Optimization and Machine Learning, 1st edition, 1989 Addison-Wesley Longman Publishing Co., Inc. Boston, MA, USA.
(3) R. A. Turner, Target field approach to optimal coil design, J Phys D: Appl Phys **19**, 147-151 (1986).

	1-layer	2-layer
Gx	3.4	5.1
Gy	3.0	3.6
Gz	7.0	7.4

Table 1 G coil efficiency: G/cm/A

Fig.1

Fig. 2

Fig. 3

Fig. 4

Optimization of a planar gradient coil set using a genetic algorithm

Shinya Handa[1], Masafumi Horiga[2], Ryousuke Shigeki[2], Satoru Adachi[2] and Katsumi Kose[2]

[1] Japan Society for the Promotion of Science, Tokyo, Japan
[2] Institute of Applied Physics, University of Tsukuba, Tsukuba, Japan

INTRODUCTION: Planar gradient coil geometry has been used for compact MRI systems using permanent magnets. Because it assists on the basic gradient properties such as gradient strength, gradient field uniformity while maintaining sample or patient accessibility. Previous works on gradient coil design have been used analytical solutions based on Target field method [1,2]. Although those designs theoretically are having excellent performance, gradient coils obtained by those designs are extremely hard to build due to the current distribution concentrated in local regions. To overcome this problem, several studies have been employed stochastic optimizations such as stimulated annealing (SA)[3], genetic algorithm (GA)[4]. In this work, we have developed a planar gradient coil set optimized by GA considering capabilities of construction for the gradient coil set.

MATERIALS AND METHODS: Final goal of the optimization for the planar gradient coil was defined as minimized gradient field non-uniformity within user specified volume of interest (VOI). Considering the symmetry of transverse gradient coil, the coil loop was chosen as "D" shaped. Both shape of the loop and the combination of those loops were optimized simultaneously. In the axial gradient coil, the combination for the radius of circular coil was optimized. While optimization process, the gradient field distributions were calculated by the Biot-Savart law. Moreover, the GA can also take into account for the wire diameter so that wires are not overlap at all while optimization.

CONSTRUCTION AND EXPERIMENT: To test the design result, a gradient coil set was developed for a home-built MR microscope with a 4.74 T vertical bore superconducting magnet. The design parameters were as follows: gradient field homogeneity, below 10 % within 2.55 cm diameter of spherical volume (DSV); gap space, 3.8 cm; diameter of the current flowing region, 7.6 cm; and number of turns of wires, 16 turns for the transverse coil and 30 turns for the axial coil. Figure 1 shows the gradient coil set developed in this study. Linearity of the gradient field was measured using a 3D phantom (Fig. 2) composed of stacked 3 mm-thick plastic disks with grid-shaped square trenches (width and depth = 1 mm, inplane separation = 2 mm) and a cylindrical plastic container (outer diameter = 26 mm, length = 61 mm) filled with baby oil. The 3D phantom was measured using a 3D spin echo sequence (TR = 200 ms, TE = 10 ms, NEX = 2, image matrix = 256^3, voxel size = $(125 \ \mu m)^3$) with positive and negative readout gradients.

RESULTS AND DISCUSSION: Figure 3 shows a 2D cross-section selected from the 3D image dataset of the phantom. The measured gradient field homogeneity within 2.55 cm DSV is approximately 6 %. The calculated values of those gradient fields are found to be good agreement with the measured values in this experiment. In conclusion, a planar gradient coil design using a genetic algorithm was successfully developed and demonstrated its usefulness over conventional analytical designs.
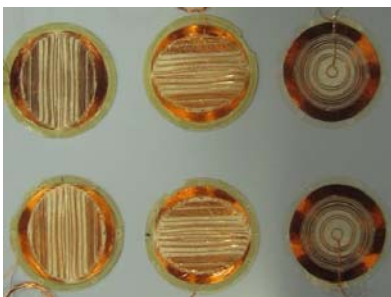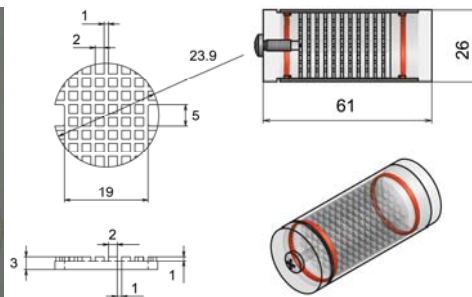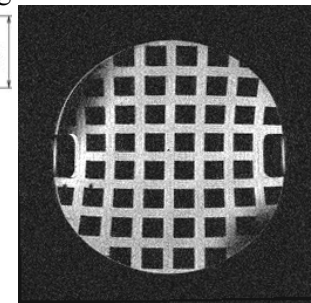
FIG 1.   FIG 2.   FIG 3.

1. R Turner, J. Phys. E: Scient. Instr., 21 (1988) 9482. 2. LS Petropoulos, Magn. Reson. Imag., 18 (2000) 615.
3. S Crozier et. al., J. Magn. Reson., A103 (1993), 354. 4. BJ Fisher et. al., Magn. Reson. Imag., 15 (1997) 369.

Three-Magnet Array for Unilateral Magnetic Resonance

Juan C. García-Naranjo [1,2], Bruce J. Balcom [1], Igor V. Mastikhin [1], Bruce G. Colpitts[2]

[1] MRI Centre, University of New Brunswick, Fredericton, Canada
[2] Department of Electrical and Computer Engineering. University of New Brunswick, Fredericton, Canada

Abstract:

Unilateral Magnetic Resonance (UMR) has emerged in recent years as a powerful tool to explore samples of arbitrary size. Marble et al [1] have recently proposed a very simple and powerful design employing a three magnet array. Two families of magnets for UMR employing this approach are presented.

The first magnet SA1 (Fig. 1), has a mass of less than 1 kg and a sensitive spot of 0.78 cm^3 ($\Delta B_0 < 5$ %) 0.8 cm displaced from its surface. The magnetic field is 763 G in the centre of the sensitive spot. By comparison to the array BA1 of [1], it is 75 % lighter and 80 % smaller. The signal amplitude obtained during a spin echo experiment is 60 % of the value with BA1 for the same acquisition parameters. The sensitivity is such that single shot CPMG decays from liquid samples may be readily measured. This magnet is light enough and small enough to permit hand-held UMR measurements.

The second approach introduces a moderate amplitude extremely linear gradient in the sensitive spot simply by manipulating the position of the central magnet block. A first magnet, similar in size to BA1, with linear gradient of 218 G/cm over 3 cm (Fig. 2), and another with 60 G/cm over 4 cm, are presented. Diffusion measurements to characterize the gradient and practical measurements employing these magnets are also included.
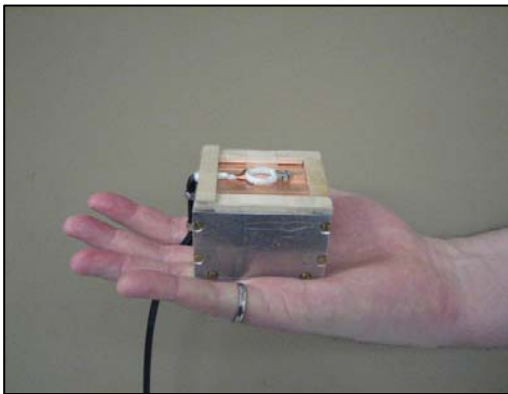
Figure1. Hand-held array SA1.
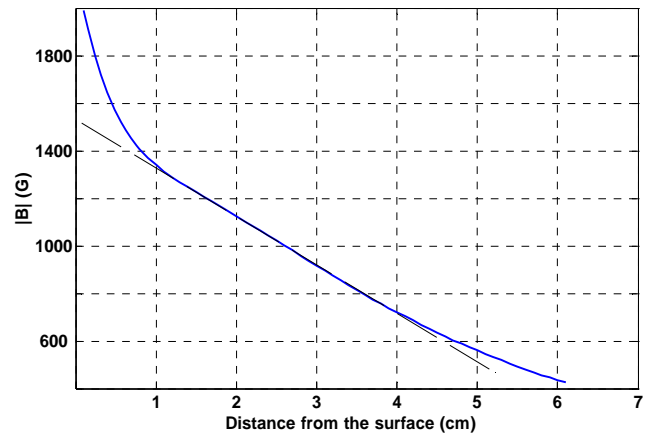
Figure 2. Linear gradient of 218 G/cm obtained with a three magnet array similar to BA1.

[1] A. Marble, I. Mastikhin, B. Colpitts and B. J. Balcom, *JMR* **186** (2007) 100–104.

Development of a large bore planar gradient coil probe for a vertical bore superconducting magnet

Masafumi HORIGA[1], Shinya HANDA[2], Ryousuke SHIGEKI[1], Katsumi KOSE[1]

1. Institute of Applied Physics, University of Tsukuba 2. Japan Society for the Promotion of Science

Introduction: Commercialized gradient probes for vertical bore superconducting magnets have a vertical sample bore to facilitate the sample exchange. However, solenoid coils, which have much better SNR than other RF volume coils (1), cannot be used for the vertical sample bore. Because high resolution MRI or MR microscopy requires high SNR as much as possible, use of solenoid coils is essential. In this work we have developed a large bore planar gradient coil probe with a solenoid RF coil for a 4.74 T vertical bore superconducting magnet and evaluated its performance using a 3D geometrical phantom.

Materials and Methods: The gradient probe consists of a planar gradient coil set and a solenoid RF coil. The planar gradient coils were designed using the genetic algorithm (2): the axial (z) gradient coil was designed as a combination of circular coils, and the transverse (x and y) gradient coil was designed as a combination of D shaped coils as shown in Fig.1. The design parameters of the gradient coils are: the gap space = 38 mm, diameter of the current plane = 76 mm, homogeneity = 10 % in 25.5 mm diameter spherical volume, number of turns = 30 (axial) and 16 (transverse). The gradient coils were wound using 0.4 mm diameter polyethylene coated Cu wire on 0.5 mm FRP plates. To increase the transverse gradient coil efficiency, two current planes were stacked together on both sides of a 0.5 mm thick FRP plate.

The RF coil was a 6 turn solenoid (inner diameter = 26.2 mm, length = 43 mm). The RF coil wire (2 mm diameter polyethylene coated wire) was divided into 6 elements connected with 6.8 pF ceramic chip capacitors to tune the tank circuit to 202 MHz as shown in Fig. 2.

Linearity of the gradient field was measured using a 3D phantom (Fig. 3) composed of stacked 3 mm-thick plastic disks with grid-shaped square trenches (width and depth = 1 mm, inplane separation = 2 mm) and a cylindrical plastic container (inner diameter = 23.9 mm, length = 40 mm) filled with baby oil. The 3D phantom was measured using a 3D spin echo sequence (TR = 200 ms, TE = 10 ms, NEX = 2, image matrix = 256^3, voxel size = $(125 \ \mu m)^3$) with positive and negative readout gradients. All the experiments were performed on a home-built MRI system using a vertical wide bore superconducting magnet (field strength = 4.74 T, Oxford Instruments, UK).

Results and Discussion: The efficiency of the gradient coils measured using a sphere phantom were 1.93, 1.71, and 2.19 G/cm/A for Gx, Gy, and Gz, respectively. These values are resonable for the 26 mm bore probe. Figure 4 shows a 2D cross-section of the 3D phantom selected from the 3D image dataset. The maximum nonlinearity of the gradient field and static magnetic field homogeneity calculated from the image datasets in a cylindrical region (diameter = 21mm, length = 22mm) were 6 % and 6.35 ppm, respectively.

In conclusion, we have developed a large bore gradient probe with a solenoid RF coil for a 4.74 T vertical bore superconducting magnet. This probe can be used for various MR microscopic applications.
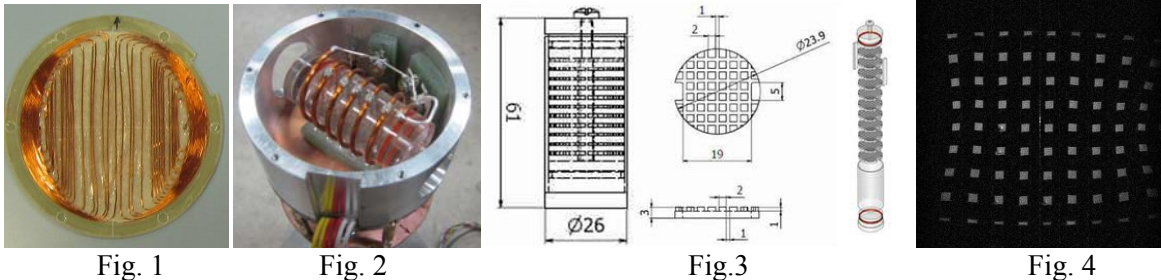
Fig. 1　　　　Fig. 2　　　　　　Fig.3　　　　　　Fig. 4

References:
(1) D. I. Hoult, R. E. Richards, J. Magn. Reson. 24(1976) 71-85
(2) S. Handa, M. Horiga, R. Shigeki, S. Adachi, K. Kose, Optimization of a planar gradient coil set using a genetic algorithm. 10th ICMRM, (2009) submitted.

P47

A straightforward biplanar gradient design for mobile MR: Optimizing a modified maxwell/golay layout with simulated annealing

S. Wintzheimer[1], M. Ledwig[1], T. Drießle[2], P. M. Jakob[1,2] and F. Fidler[1]

[1]MRB, Research Center Magnetic-Resonance-Bavaria, Würzburg, Germany
[2]Department of Experimental Physics 5, University of Würzburg, Würzburg, Germany

Introduction: During the last years, a number of methods for the design of gradient coils for MR imaging have been developed. Most of these methods try to find the maximum homogeneity at the expense of gradient strength and buildability. For many applications e.g. mobile MR imaging it is preferable to have a strong field gradient rather than perfect homogeneity. In this study, a modified Simulated Annealing algorithm was used to optimize a given gradient coil geometry.

The goal of this calculation was to obtain a simple biplanar coil layout which is capable of creating a strong and homogenous gradient fields for use in permanent magnets. This newly developed method was used to optimize a modified biplanar golay design as well as a modified maxwell design. The algorithm was adjusted to achieve maximum homogeneity and maximum gradient strength. Thereby it conserves the simple geometry given by the original golay/maxwell design as far as possible. Compared to other optimization methods, working e.g. with stream functions, this method is based on the real calculation of magnetic fields in each individual step.

Fig. 1: Simulation of optimized golay design: deviation from linear profile; contour line every percent

Methods: For demostration purposes a biplanar gradient system with a FOV of 1cm for a mobile MR system was calculated and built. Calculation is based on a modified version of Simulated Annealing, the Treshhold Accepting. The calculation of the magnetic field was done based on biot-savart's law. A set of coils either based on a modified golay design or a modified maxwell design with individual sizes and number of turns was optimized. In this special case the number of independently used golay/maxwell coils was varied to optimize the resulting design. All calculations were done in Matlab (MathWorks). The optimized gradient system was built and the resulting field was measured.

Fig. 2: Measured field of optimized maxwell design

Results: The optimal layout for the golay design is a combination of only two golay coils. Outer dimensions of the coils are approx. 4cm x 4cm. With this optimized system a gradient performance of 203 mT/m/A is achieved. The maximal deviation in a field of view of 1cm stays under 0.5%. For the maxwell design only three pairs of coils are the optimum. The max. diameter is 3.6cm. Thus a performance of 210 mT/m/A and a maximal deviation of 0.4% is archieved. The thickness of the complete system is only 6mm. Measurements show that the field predicted by simulations is reproduced by the constructed system. The simulated deviation of the calculated golay design is shown in figure 1. The measured gradient field created by

Fig. 3: FLASH-image of a garden been. Matrix size: 256x256; Resolution 9μm x 15μm; 256 Avgs.

the maxwell design is shown in figure 2. The measured linearity and gradient strength is sufficient for imaging. A FLASH-image of a garden been acquired with this gradient system at 0.5 T in a permanent magnet is shown in figure 3.

Conclusion: With this optimization method it was possible to calculate a both homogenous and effective biplanar gradient system for imaging small objects in a permanent magnet. This could be done while conserving a straightforward layout. Furthermore, a simple design for gradient coils, based on modified golay and maxwell designs, was found.

Kirkpatrick S., Gelatt C. D. and Vecchi M. P. Optimization by Sim. Annealing; Science. - 1983. - Vol. 220. - p. 671.

Dueck G. and Scheuer T. Threshold Accepting: A General Purpose Optimization Algorithm Appearing Superior to Simulated Annealing; Journal of Computational Physics. - 1990. - Vol. 90. - pp. 161-175.

Golay M. Field Homogenizing Coils for Nuclear Spin Resonance Instrumentation; Rev. Sci. Instr. - 1958. - Vol. 29. - p. 313.

P48

A novel gradient design for mobile MR: simultaneous generation of fast switchable linear and higher order field gradient for MR imaging

S. Wintzheimer[1], M. Ledwig[1], T. Drießle[2], P. M. Jakob[1,2] and F. Fidler[1]

[1]MRB, Research Center Magnetic-Resonance-Bavaria, Würzburg, Germany
[2]Department of Experimental Physics 5, University of Würzburg, Würzburg, Germany

Introduction: Shimming a magnetic field usually requires an additional set of complex coils which act independently from the linear gradient system used for MRI. Therefore a unique coil has to be developed for each field order, which is very extensive. Especially for permanents magnets used in mobile MR it is difficult to implement shim coils due to highly limited space between the pole pieces. In this study a novel matrix gradient design is presented, which is capable of generating both linear gradient fields for imaging and at the same time high order shim fields. The space requirements are equal to conventional biplanar gradient systems. The simultaneous generation of several orders can be achieved by using a set of individually driven coils. The complete gradient field results from the superposition of all these individual magnetic fields. This provides the possibility of creating a large variety of field profiles by driving each coil with a different current. Furthermore it grants the advantage of switching shim and gradient fields very fast due to low inductivity of each single coil.

Methods: In order to demonstrate the principle of the matrix gradients, a biplanar gradient system for a permanent magnet was simulated and built. It consists of 18 individual rectangular coils arranged in two opposite planes. For this special system we chose a distance of 2 cm between the planes and 4cm*4cm as dimension. The coils are arranged in each plane in two 3x3 matrices (figure 1). Each coil C_x is driven by the current I_x. Multiple field profiles have been measured and simulated. The simulations were done with a Matlab (MathWorks) script using biot-savart's law. In lack of 18 gradient amplifiers experiments were performed by adjusting the individual currents with potentiometers. By using this simple geometry it is possible to create linear as well as high order field profiles.

Results: Exemplarily a simulation of the linear gradient field in x-direction is shown in figure 2. The gradient strength is about 25mT/m/A in a FOV of 1cm. To
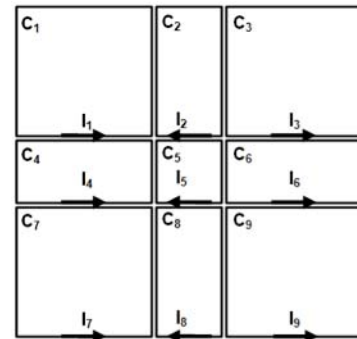
Fig. 1: One plane with 9 coils arranged in a 3x3 matrix. Each coil C_x is driven with a current I_x.
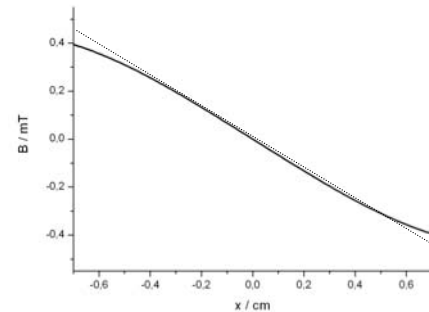
Fig. 2: Simulation of linear gradient field, exemplarily shown for the x-direction. Dashed lines mark the field of view, dotted line indicates the perfect linear gradient
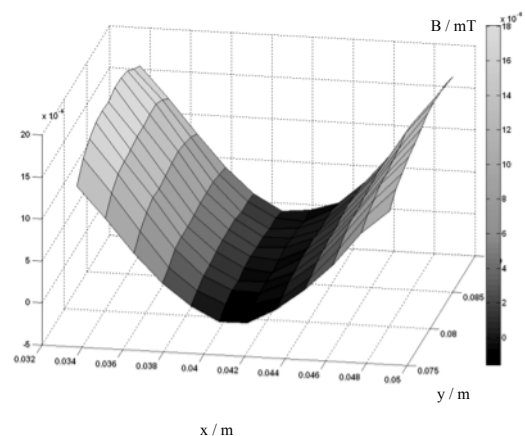
Fig. 3: Measured quadratic field profile

P48 - Continued

demonstrate the capability of creating higher field orders a measured quadratic shim field in x-direction is shown in figure 3. The field profile corresponds to the simulations. Thereby each coil has a low inductance of 1.4μH which makes very fast switching times of about 200ns possible. This short time applies to any arbitrary field profile, gradient as well as shim fields. Preliminary results are encouraging, since the novel design results in increased signal strength due to improved shimming capabilities while maintaing high performance linear gradients. Moreover it is possible to build an arbitrary matrix gradient system for almost every given geometry.

Conclusion: The proposed gradient system is able to create linear gradient fields as well as higher order shims simultaneously with fast switching times. The space requirements don't exceed the requirements for a standard biplanar gradient system. Furthermore, the possibility to switch high order shims as fast as linear gradients is advantageous e.g. for individual slice shim in multislice experiments. The geometry is not restricted to planar gradient systems and the number of coils and their arrangement is free of choice. The major drawback, however, is, that for each coil a separate gradient amplifier is required but it is possible to switch multiple field orders with optimal speed.

Patent Application DE1020080182656

P49

Design and construction of barrel magnets for unilateral NMR

Shin Utsuzawa[1], Eiichi Fukushima[2]

[1]New Mexico Resonance, Albuquerque, USA, [2]ABQMR, Albuquerque, USA

Abstract:

Unilateral, or inside-out, NMR to perform NMR measurements outside a magnet is gaining popularity [1-5]. It offers a major path to portable NMR. Some schemes, including NMR-MOUSE [1], do NMR in magnetic fields that decay with distance. Others use saddle points of magnetic field obtained at some distance. Both schemes have advantages and drawbacks, and users can choose an appropriate one according to their applications.

Barrel magnet, proposed by Fukushima and Jackson [6], is in the second group. It consists of a hollow cylinder magnetized in the axial direction, plus an optional bar magnet (or a smaller hollow cylinder magnet instead of a solid bar) inserted in the bore. It projects a saddle point (so called *sweet spot*) of magnetic field outside of itself, where magnetic field is relatively uniform over a region, with the consequence that the sample area is greatly enlarged over using a decaying field. Therefore, it is believed to increase the sensitivity at a large distance.

There are many freedoms in the selection of barrel and bar magnets to obtain the sweet spot at certain distances. However, size of the sweet spot and field strength at that point, both of which affect overall sensitivity, strongly depend on the dimensions of those magnets. For example, two barrel magnets with the same OD but different ID and height (Fig. 1) can provide sweet spots at the same distance (Fig. 2). In addition, the choice of the bar magnet, size and offset, significantly affect the overall field distribution. Thus, it is crucial to choose the right combination of those magnets among many possible to achieve good sensitivity and portability.

In this presentation, we will discuss the field distribution of barrel magnets with and without bar magnet inserts, and the resulting sensitivity. Also, we will provide an idea of how to build a barrel magnet of reasonable size using commercially available magnets. This information should be useful to people who want to construct a unilateral NMR apparatus by themselves.

OD 102 mm, ID 62 mm, H 82 mm, w ~ 3.1 kg   OD 102 mm, ID 50 mm, H 50 mm, w ~ 2.3 kg
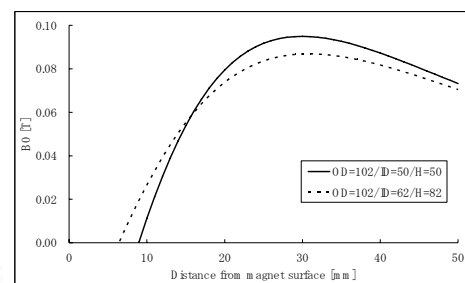
Fig. 1. Two barrel magnets with the same OD.   Fig. 2. Field profile of barrel magnets.

[1] G. Eidmann, *et al.*, *J. Magn. Reson. A* **122** (1996) 104-109.
[2] P. J. Prado, *Magn. Reson. Imag.* **21** (2003) 397-400.
[3] A. E. Marble, *et al.*, *J. Magn. Reson.* **174** (2005) 78-87.
[4] B. Manz, *et al.*, *J. Magn. Reson.* **183** (2006) 25-31.
[5] P. J. McDonald, *et al.*, *J. Magn. Reson.* **185** (2007) 1-11.
[6] E. Fukushima and J.A. Jackson. U.S.Patent **6,489,872** (2002).

Lithographically Produced Microcoils for Enhanced Portable NMR

Paul T. Steele, Kristl L. Adams, Christopher Harvey, Anthony Bernhardt, Julie Herberg

Lawrence Livermore National Laboratory, Livermore, CA, USA

Abstract:

To construct a portable NMR system, the bulky magnets of conventional systems must be abandoned in favor of more compact alternatives. Reductions in size and weight are made at the expense of field strength and uniformity. Microcoils, whether hand wound or fabricated by other means, are critical components in portable systems because their small size enhances sensitivity, partially compensating for lower field strength. New microcoils being developed at LLNL have the potential to further improve sensitivity by compensating for certain inhomogeneities in the magnetic field. Static field profiling, theoretical coil modeling, lithographic fabrication and real world testing of new microcoils will be described. Unshimmed static magnetic fields are easily mapped and the fields from arbitrary coils are rapidly and accurately predicted. This enables thousands of coil variations to be evaluated in automated searches for optimal designs. An LLNL developed photolithography technique can subsequently produce these designs on small capillaries. Designs can be fabricated that cannot be duplicated by other means such as hand winding. We expect to present data collected with a single NMR system using first standard and then optimized coils to directly demonstrate signal enhancement.

P51

Single-sided magnets with controlled field profiles : high homogeneity on larger volumes.

Cedric Hugon[1] , Guy Aubert[1] and Dimitris Sakellariou[1]

[1] DSM/IRAMIS/SIS2M/LSDRM CEA Saclay, Gif-sur-Yvette, France

Abstract:

Mobile NMR has been of interest since the 1950s with NMR well-logging, but it is only in 1995 that the first truly portable NMR system was proposed, the NMR-MOUSE[1] . This system provides an inhomogeneous field limiting the sample size and the resolution. Further recent developments have made possible high-resolution portable NMR[2] over sample volumes, which for current state of the art systems, are limited to a few mm3.

We propose a systematic method to build an intrinsically homogeneous magnet, which requires limited shimming to compensate for fabrication defects. This approach provides also with the ability to achieve different field profiles at will. Here we will present applications of this theory to one-sided magnets where the field is chosen to have a uniform gradient. The field profile properties can be theoretically extended to an arbitrarily large volume.

Based on this method, a magnet with constant gradient was designed and built. This magnet has a size of about 20 cm by 12 cm and delivers in theory more than 300 mT. The region of interest features a linear gradient of 3 T/m with a deviation of less than 10 ppm over 1 cm3 located 2 cm away from the surface of the magnet. Theoretical modeling of the magnet and of its shimming system will be presented, along with preliminary experimental results of the prototype. A homogenous field system was also designed and will be presented. Aspects of field measurements and simulation assessments will also be discussed.
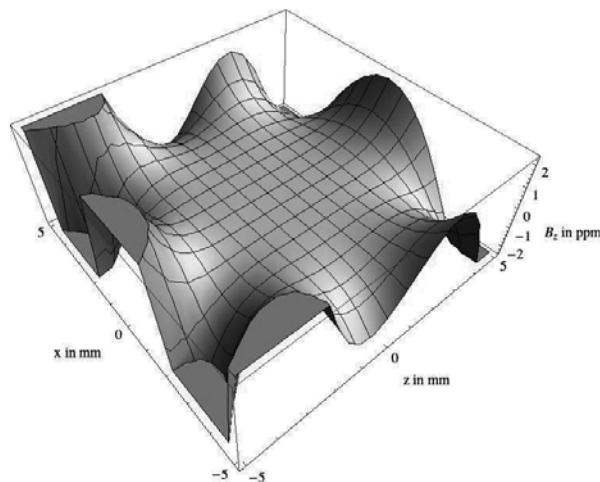
Fig. 1: Simulated variations of the gradient of B_z for a constant gradient single-sided magnet model designed according to our method. The nominal field is over 300 mT with variations within 1ppm in a sphere of diameter 8mm centered 2cm away from the surface.

---

[1] Eidmann, G., Savelsberg, R., Blümler, P., and Blümich, B., Journal of Magnetic Resonance A 122 (1996) 104.

[2] Perlo, J., Casanova, F., and Blümich, B., Science 315 (2007) 1110.

Simple, high quality MRI r.f. coils for plants and other objects with a dumbbell shape for use in supercons

Dagmar van Dusschoten[1], Normen Hermes[2] and Johannes Kochs[1]

[1] ICG-3, Research Center Jülich, Germany
[2] ICG-4, Research Center Jülich, Germany

Abstract:
NMR images of plants and other objects with a waist, a concave shape or narrow sections, are mostly obtained at a lower signal to noise ratio (SNR) than ideally possible due to the inefficient fitting of the r.f. coil. Although plants are rather flexible, forcing them through a narrow r.f. coil to improve SNR normally causes damage to the plant such that the non-invasive character of NMR is lost. For magnet systems with a magnetic field perpendicular to the plant axis, there exists an easy solution; closely wind a solenoid around the plant stem and connect it to a tuning circuit [1].

Here we demonstrate that the in-place construction of a r.f. coil can also be used for magnet types with a magnetic field direction parallel to the plant axis, like supercons, if the solenoid is placed under an angle with the main field, similar to solid state NMR probes. Since most plants that fit into a magnet have thin stems, they are easy to bend slightly without damaging the plant. Obviously, some signal is lost because the detectable xy-plane magnetisation is not perpendicular to the r.f. field of the coil, but at a 45° angle this amounts to a 30% loss. A splittable birdcage with a similar diameter would cause a 70 % signal loss compared to the ideally placed solenoid. This type of birdcage, however, is much harder to produce at much higher cost..

Here we compare two solenoid designs that can be wrapped around an object with a waist; the original design that is wound around a thin section and which is soldered in place, and a splittable solenoid. Both types of construction are used under a 45° angle with the main field. Thesecoils can simply be plugged on to a separate tuning circuit. One therefore needs only one tuning circuit for a multitude of similar r.f. coils, i.e they can be left on the plants for later use.

The splittable coil is the easiest in use, but the additional connectors cause aothert 3 dB signal loss compared to the wound in-place coil. Using a 10 mm coil diameter the latter design could be used to obtain images with a 30 μm resolution (0.5 mm slice thickness) within half an hour, at a magnetic field strength of 4.7 T.

1. T.W.J. Scheenen, D. van Dusschoten, P.A. de Jager and H. Van As, J. *Magn. Reson.* **142**, 207-215 (2000).

Ex-situ Endorectal MRI Probe for Prostate Imaging

Aharon Blank[1], Shlomo Ish-Shalom[1], Lazar Shtirberg[1], and Yuval Zur[2]

[1]Schulich Faculty of Chemistry, Technion – Israel Institute of Technology, Haifa, 32000, Israel
[2]TopSpin Medical (Israel) Ltd, Global Park, 2 Yodfat St. North Industrial Zone, Lod 71293, Israel

Abstract:

NMR and its descendant MRI are usually pursued in a setup based on a highly homogenous static magnetic field, B_0, with variance < 1 ppm, creating nuclear spin precession at a corresponding narrow band of frequencies. This requirement is one of the main reasons why clinical MRI systems often employ large magnet and corresponding large radio frequency (RF) and gradient coils, leading to their relatively high complexity and cost. However, if one is interested only in a specific small region within the body, it could be highly advantageous to obtain NMR information by using either a non-invasive hand-held probe or an intra-cavity self-contained (magnet +RF and gradient coils) NMR probe, thus avoiding the requirement for a large external magnet. Such an approach for NMR measurement or NMR imaging without a sample-surrounding magnet is termed "inside-out", or *ex-situ* NMR. Here we present a bench prototype of a new ex-situ MRI probe aimed at the imaging of the prostate (Fig. 1). The probe is designed for endorectal operation, combined with a provision for an ultrasound module which would direct the probe to the exact prostate region. The 60 mm high, 30 mm diameter probe demonstrated a relatively large field of view of ~ 50×50×20 mm, which is far beyond what was demonstrated to-date in the context of ex-situ MRI (scaled to the size of the probe). This capability was achieved by a unique magnet, RF coils and gradient coils design, along with sophisticated imaging and image correction algorithms. The clinical version of this probe prototype would be able to direct the physician during biopsy procedure, which is based today on "random biopsy" procedure, to specific suspicious areas. This should reduce the number of false negative biopsy readings and the number of unnecessary repetitions of the biopsy procedure.
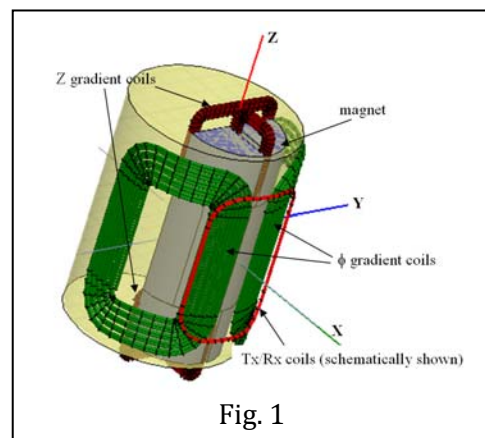
Fig. 1

Lexus: Laplacian 1-D exponential inversion software

P.S Aptaker[1]

[1] Laplacian Limited, Abingdon, UK

Abstract:

In NMR, both T1 and T2 data is often modelled by a discrete version of the Fredholm integral equation of the first kind,

$$\mathbf{g} = \mathbf{K.f} + \boldsymbol{\varepsilon}, \text{ with } f_j > 0 \tag{1}$$

where $\mathbf{K}$ is the kernel matrix, $\mathbf{g}$ is the measured data vector, $\mathbf{f}$ is the unknown input vector and $\boldsymbol{\varepsilon}$ is the noise. For T1 data, for example, $K_{ij} = \exp(-T_i / \tau_j)$.

Distributed exponential functions are, however, far from orthogonal and the problem is very ill-conditioned. While there are a number of algorithms commonly used, those based on Butler, Reeds and Dawson's algorithm (BRD) [1] have been particularly popular in the,"oil industry" e.g. *WinDXP,* which can be purchased, but generally only with the Maran Spectrometers. [2].,

Lexus [3] is a modern BRD implementation*, with some subtle improvements (see poster). The DLL can be called from, for example, Excel, via VBA, and could be, just as easily from any application with convenient DLL interfacing. With the addition of a C++ wrapper, it has also been integrated with Magritek's *Prospa* software. [4] (see Figure 1). The result can be run via any macro and the user can integrate it as they wish to their application.
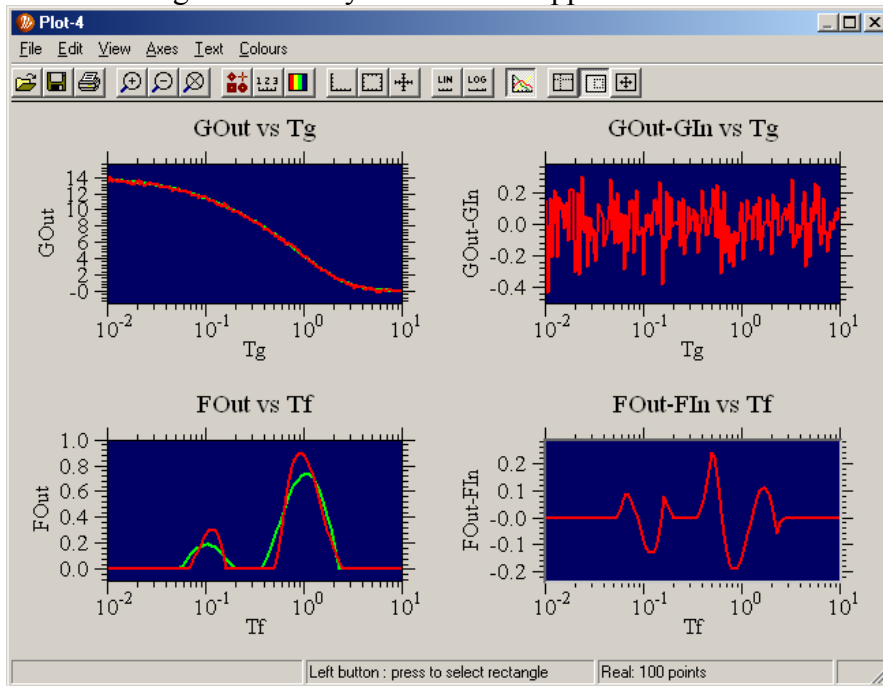
Figure 1 Lexus running, via a Macro, in *Prospa* .- Solution (green) from simulated input data (red).

1. Butler, Reeds and Dawson, Siam J. Numer. Anal **18 no. 3** (1981) 381-397.
2. *WinDXP* software http://www.oxford-instruments.com
3. *Lexus* software, www.laplacian.co.uk
4. *Prospa*, software, www.magritek.com

* Other algorithms have, and will be added

Engineering & Performance of Magnetic Particle Imaging

<u>Kevin R. Minard</u>[1], Matt Ferguson[2] and Kannan M. Krishnan[2]

[1] Pacific Northwest National Laboratory, Richland, WA 99352 USA
[2] University of Washington, Seattle, WA 98195 USA

Abstract:

Rapid advances in the synthesis of superparamagnetic nanoparticles has stimulated widespread interest in their use as contrast agents for visualizing biological processes with Magnetic Resonance Imaging (MRI). With this approach, strong particle magnetism shortens MRI relaxation times for nearby water protons and this, in turn, alters observed image contrast. Magnetic particle detection with MRI is therefore indirect and suffers from several associated problems, including – poor sensitivity and quantification, ambiguous contrast, and tissue-dependent performance. To overcome these limitations, scientists at Philips Research in Germany have recently developed a direct approach for Magnetic Particle Imaging (MPI) [1]. Unlike MRI, which requires a costly superconducting magnet, MPI utilizes relatively inexpensive components to directly quantify the amount of superparamagnetic material at each location. In practice, this is achieved with a weak oscillating magnetic field and exploits the nonlinear response of nanoparticle magnetization to generate harmonics detected using an inductively coupled receiver. Spatial localization is then realized using large static magnetic field gradients so particle magnetization outside a sensitive point quickly saturates and is non-responsive. By quickly sweeping the sensitive point through a live mouse, Philips has recently measured the biodistribution of magnetic moieties with high spatial resolution and video-rate imaging speeds [2]. In this presentation, our ongoing progress in constructing a 3D MPI system for live mice will be described, including - basic transceiver, magnet and particle design [3-4]. Initial results will also show that MPI performance is tissue independent, that signal varies linearly with nanomaterial amounts, that submillimeter spatial resolution is achievable, and that sensitivity is sufficient for MPI to serve as a quantitative dosimetry platform that overcomes many of the shortcomings currently associated with radio-tracer techniques. MPI is therefore expected to have widespread utility in diverse applications ranging from toxicology and drug development to clinical diagnostics.
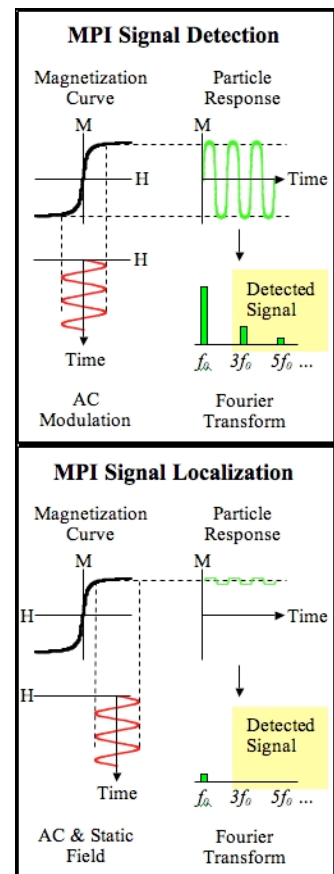
1. B. Gleich and J. Weizenencker, *Nature* **30** (2005), 1214-1217.
2. J. Weizenecker, B. Gleich, J. Rahmer, H. Dahnke and J. Borgert, *Phys. Med. Biol.* **54** (2009), L1-L10.
3. R.M. Ferguson, K.R. Minard and K.M. Krishnan, *J Magn. Magn. Mater.* **321** (2009), 1548-1541.
4. K.R. Minard, *Encyclopedia of Spectroscopy and Spectrometry 2nd Edn*, Elsevier, Edited by John C. Lindon, Accepted (2009).

P56

Impact of local SPIO concentration on the Magnetic Particle Imaging signal

J.-P. Gehrcke[1], M.A. Rückert[1,2], T. Kampf[1], W.H. Kullmann[2], P.M. Jakob[1] and V.C. Behr[1]

[1] Experimental Physics 5 (Biophysics), University of Würzburg, Würzburg, Germany
[2] Medical Technology, University of Applied Sciences Würzburg-Schweinfurt, Schweinfurt, Germany

Recently, Magnetic particle imaging (MPI) has been presented as a new imaging method that potentially offers 3D real-time imaging of the concentration distribution $c(x)$ of superparamagnetic iron oxide (SPIO) particles in biological systems at high spatial resolution [1].

A sample containing SPIOs at concentration c is exposed to a harmonically oscillating magnetic field $H(t)(O(10\,mT/\mu_0))$ at frequency ω_0. The MPI signal is the Fourier spectrum of the response field, which contains higher harmonics $N \cdot \omega_0$, due to the nonlinear magnetization curve $M(H,c)$ of the sample in the range of the field strength mentioned above.

In essence, $M(H,c)$ transposes input to output and therefore is the key quantity to calculate the MPI signal for a known configuration. For tomographic purposes, the quantity $c(x)$ has to be reconstructed from the MPI signal. Hence, the quality of the theory describing the impact of concentration c on the magnetization curve is essential for the image reconstruction.

Recent authors only considered Langevin's single particle model of paramagnetism (SPM) for reconstruction [e.g. 2]. Hence, magnetic inter particle coupling was neglected until now, which can be done for $c \ll 0.2\,mol/l$. When particles agglomerate in cell vesicles, as is the case for SPIO labeled markers, concentrations much higher than $0.2\,mol/l$ are reached.

Besides SPM, we use second order modified mean field theory (MMF2), which includes particle coupling in ferrofluids [3]. Magnetization curves $M(H,c)$ simulated with MMF2 theory are close to reality [4]. *Figure 1* particularly shows rising nonlinearity of the magnetization curve with increasing SPIO concentration. For $c \to 0$, MMF2 converges to SPM. *Figure 2* shows the variation of the single higher harmonics of the MPI signal in an 1D MPI experiment, while increasing the concentration of a rectangular sample of constant width: the MMF2 curves show that not only the amplitudes, but also the ratio of the harmonics change with increasing concentration. As expected, the SPM curves show no change. Hence, image reconstruction in MPI using Langevin's single particle model leads to deviations from the true distribution of concentrations.
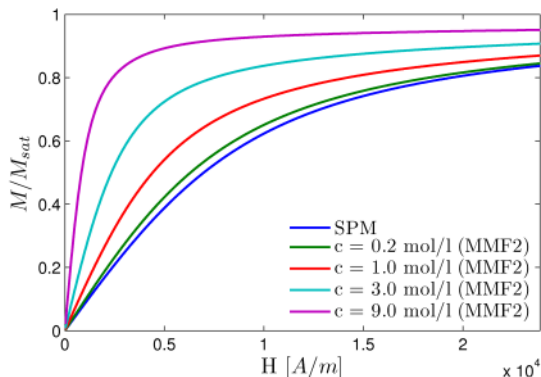
Figure 1: *Normalized Magnetization curves calculated for SPIO samples (consisting of Magnetite particles with diameter $d = 15\,nm$) with different concentrations c using MMF2 and SPM theory. M_{sat} is the saturation magnetization of the corresponding sample.*
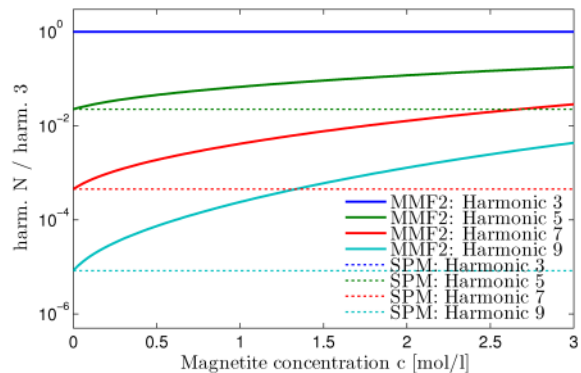
Figure 2: *Normalized MPI signal amplitudes of a simulated 1D experiment in dependence of c, which is the height of a rectangular SPIO sample $c(x)$ (consisting of Magnetite particles with $d = 15\,nm$). The amplitudes of harmonics $N = 3, 5, 7, 9$ are normalized to $N = 3$. The MPI signal was acquired and analyzed using MMF2 and SPM theory separately.*

P56 - Continued

[1] **B. Gleich, J. Weizenecker**: *Tomographic imaging using the nonlinear response of magnetic particles*; Nature 435 1214–7 (2005)
[2] **Rahmer et al**: *Signal encoding in magnetic particle imaging: properties of the system function*; BMC Medical Imaging 2009, 9:4
[3] **A. O. Ivanov, O. B. Kuznetsova**: *Magnetic properties of dense ferrofluids: An influence of interparticle correlations*; Phys. Rev. E 64, 041405 (2001)
[4] **Ivanov et al**: *Magnetic properties of polydisperse ferrofluids: A critical comparison between experiment, theory, and computer simulation*; Phys. Rev. E 75, 061405 (2007)

Variable Bandwidth Filtering for Magnetic Resonance Imaging with Pure Phase Encoding

Juan C. García-Naranjo[1], Paul M. Glover[2], Florin Marica[1], Bruce J. Balcom[2]

[1] MRI Centre, University of New Brunswick, Fredericton, Canada.
[2] The Sir Peter Mansfield Magnetic Resonance Centre. University of Nottingham, Nottingham, UK

Abstract:

Magnetic resonance imaging with pure phase encoding (sometimes known as single point or constant time imaging) has many desirable advantages, but is usually time consuming in comparison to frequency encoding methods. In single point imaging the maximum signal bandwidth is proportional to both the phase encoding gradient amplitude and the object size. It is usual practice to set the acquisition filter bandwidth to the maximum value expected during a measurement. Hence the filtering employed in this kind of measurement is not optimal for the low frequency k-space points.

An optimal way to set the filter bandwidth is presented in this study. By reducing the filter bandwidth to match the point sampled in k-space, the inherent SNR is improved and this, in turn, may be used to reduce the number of signal averages required for acceptable SNR. The variable bandwidth filter offers a theoretical SNR increase of 41%. This paper shows the results of its application and comparison with fixed low-pass filtering. Practical measurements show a gain of 20% in SNR, which would translate into a 31% reduction in averaging time required for a single image without any detrimental effects on the image quality.
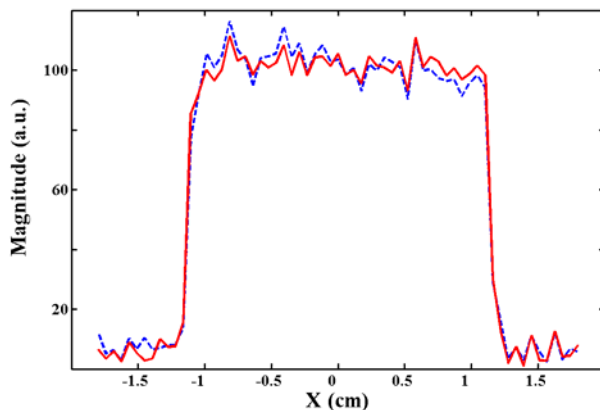
Figure1. 1D image with classical low-pass filter (--) and VBF (-).
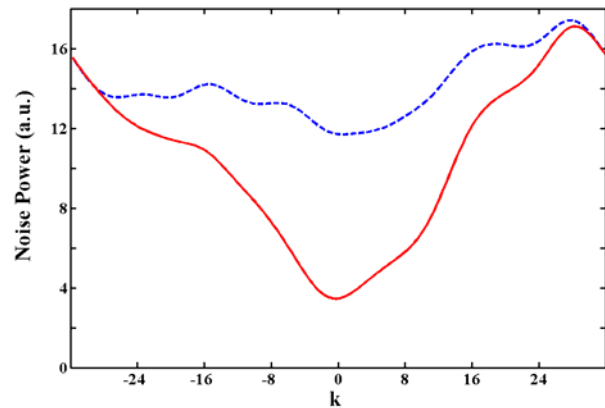
Figure2. K-space power spectral density with classical low-pass filter (--) and VBF(-).

Static magnetic field shimming for MRI using a 3D geometrical phantom

Ryosuke Shigeki[1], Satoru Adachi[1], Shinya Handa[2], Katsumi Kose[1]

1. Institute of Applied Physics, University of Tsukuba, Tsukuba, Japan
2. Japan Society for the Promotion of Science, Tokyo, Japan

Introduction: The "gradient shimming" technique, that utilizes phase images acquired with shim current offsets, is now routinely used to obtain homogeneous magnetic fields [1]. However, if nonlinearity of the magnetic field gradients generated by the gradient coils is not corrected, evaluation of the magnetic field homogeneity is not exact. To solve this problem, the magnetic field distribution should be measured in the correct (not distorted) spatial coordinates [2]. In this study, we measured the magnetic field distribution using a 3D geometrical phantom, developed a shimming method, and evaluated the magnetic field homogeneity of a permanent magnet.

Materials and methods: The 3D phantom used in this study consists of stacked 3 mm-thick plastic disks with grid-shaped square trenches (width and depth = 1 mm, inplane separation = 2 mm) and a cylindrical plastic container (inner diameter = 23.9 mm, length = 40 mm) filled with baby oil as shown in FIG 1. The coordinates of the control points are determined by the intersections of the trenches.

The compact MRI system consists of a permanent magnet (magnetic field strength = 1.0 T, gap width = 60 mm, homogeneous region = 30 mm dsv, weight = 350 kg) installed in a cold (-5 °C) room, a 2nd order shim-coil set, a gradient coil probe, and a compact MRI console. The spatial distributions of the magnetic field produced by the higher-order shim coils are proportional to xy, x^2-y^2, z^0, z^2, and z^3. MR images of the 3D phantom were acquired with a 3D driven-equilibrium SE sequence (TR =100 ms, TE = 10 ms, NEX = 4, matrix = 256^3, voxel size = $(100 \ \mu m)^3$) with full scale current (1 A) for one shim coil and no current for other shim coils. An MR image dataset with no shim current was also measured for the reference (base) image. The Cartesian coordinates of the control points visualized in the 3D phantom image datasets were semi-automatically measured [2] using a homebuilt GUI program. The magnetic field distribution was measured using the pixel shift along the readout direction [3]. To characterize the spatial distribution of the magnetic field generated by the shim coils, the magnetic field distribution was developed by the following polynomial:

$$f(x,y,z) = \sum_{l,m,n=0}^{N} a_{lmn} \varphi_{lmn}(x,y,z), \quad \varphi_{lmn}(x,y,z) = x^l y^m z^n, \quad (l+m+n) \le 3.$$

The optimum currents for the shim coils were numerically searched by using the polynomials to minimize root mean square (RMS) value of the pixel shift in the evaluated region (17 mm × 17 mm × 19 mm).

Result and discussion: FIG 2 shows 2D cross sections selected from 3D image datasets of the phantom. The left image was acquired with no shim coil current and the right image was acquired with optimum shim currents determined by the numerical search. In the evaluated region, the RMS value of the y coordinate shift of the control points from the real position was improved from 4.2 to 1.4 pixels. Therefore, it is concluded that the proposed shimming method worked well and the magnetic field homogeneity was successfully evaluated in the correct spatial coordinates.

FIG 1

FIG 2
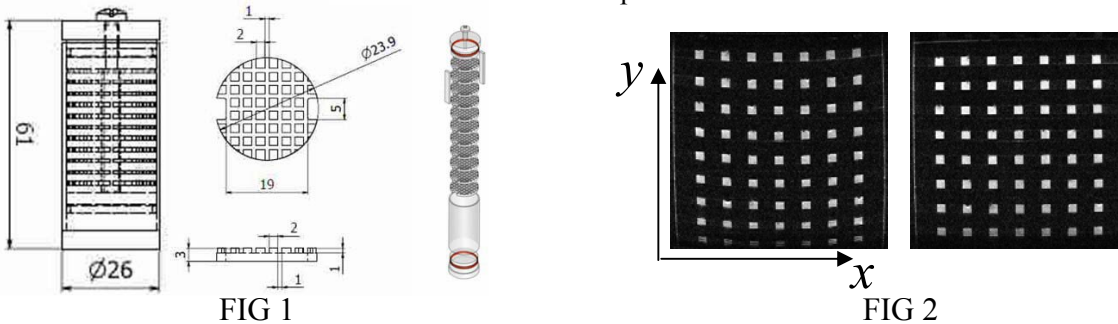
P58 - Continued

References: [1] P. Van Zijl, S. Sukumar, M. Johnson, P. Webb, R. E. Hurd. J. Magn. Reson. 1994; A111: 203-207. [2] D. Wang et al. Magn Reson Imag 2004; 22:529-42. [3] A. Kawanaka et al. J. Phys E: Sci. Instrum, 1986; 19:871-75.

High temperature ^{31}P NMR of chalcogenide glasses

E.L. Gjersing[1], S. Sen[1], H. Maekawa[2], and B.G. Aitken[3]

[1]*University of California at Davis, Davis, CA 95616*
[2]*Department of Metallurgy, Graduate School of Engineering, Tohoku University, Sendai 980-8579 Japan*
[3]*Glass Research Division, Corning Inc., Corning, NY 14831*

Chalcogenide glasses composed of arsenic (As), phosphorus (P), and one of the chalcogen elements (S, Se, and Te) have become the subject of recent interest due to their applications in infrared optics, non-volatile memory, and non-linear optics. While information is available about the short-range order in many chalcogenide glasses, very little is known about the relationship between their structure and transport properties such as diffusion and viscous flow. In this study, two glasses with novel molecular-like structures have been investigated using static, variable temperature ^{31}P NMR spectroscopy. The first glass system is a $Ge_3P_{1.3}As_{50.7}S_{45}$ glass which contains structural units like those shown in Figure 1a where the P-doped As-S molecules are bonded together by Van der Waals forces. The second glass, with composition $(As_2S_3)_{90}(P_2S_5)_{10}$, is thought to be composed of $As_2P_2S_9$ molecular units which are suspended in an As-S matrix, as shown in Figure 1b.

Static ^{31}P NMR spectra have been collected in the temperature range of 298-668K for the $(As_2S_3)_{90}(P_2S_5)_{10}$ glass ($T_g = 468K$) and 231K-319K for the $Ge_3P_{1.3}As_{50.7}S_{45}$ glass ($T_g = 312K$). NMR line shape simulations were performed to determine the timescale of molecular reorientation at each temperature which were then compared to corresponding timescales for viscous relaxation. For the $Ge_3P_{1.3}As_{50.7}S_{45}$ glass, isotropic tumbling of the molecules is observed at temperatures ~70K below the glass transition, indicating that motion is occurring despite the lack of viscous/shear relaxation. The $(As_2S_3)_{90}(P_2S_5)_{10}$ glass displays a region of lineshape narrowing from T_g up to 540K where the timescales for isotropic tumbling are decoupled from viscosity timescales. Above 540K the NMR measured time scale of bond breaking and reforming shows coupling with the time scales for viscous relaxation indicating that the motion of the P atoms are directly involved in the viscous relaxation process.
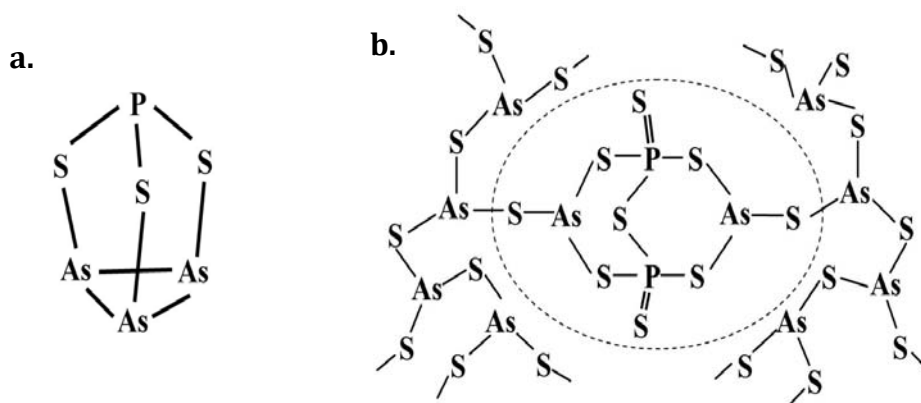
Figure 1. a. Phosphorous-doped As_4S_3 molecule. b. $As_2P_2S_9$ molecular units, surrounded by dashed line, within an As-S network.

P60

Measuring spatially-resolved T_2 distributions in purely phase-encode MRI applications

<u>Oleg V. Petrov</u> , Bruce J. Balcom

MRI Research Centre, University of New Brunswick, Fredericton, Canada

Abstract:

Most MRI implementations of T_2 mapping are focuced on clinical applications and employ multi-echo imaging pulse sequences with frequency-encoding (readout) gradients [1, 2]. Measurements in porous materials, however, present difficulties for using the frequency encoding. Susceptibility contrast in samples and sample holders can readily spoil the uniformity of the readout gradient and thus distort the image [3]. It is also hard to minimize the echo period due to restrictions on the readout gradient duration. Using a purely phase-encoding diminishes these problems, for the latter technique relies on a regular increment of the gradient's strength rather than on the gradient's uniformity [4].

Hence, we present two phase-encoding sequences for 1-D T_2 mapping. One is a CPMG-prepared SPRITE sequence and the other is multi-echo sequence with a single phase-encoding gradient. The test measurements were conducted on 0.35 T Maran DRX scanner (ν =15 MHz). Both sequences demonstrated a good ability to measure a single-exponential relaxation, providing the same T_2 values as a bulk CPMG measurement. Their ability to measure T_2 distribution is limited by the following factors. Due to its low sensitivity (hence a low SNR), the CPMG-prepared SPRITE method fails to measure long T_2 components behind the noise, so the resulting T_2 distribution may be truncated on the longer T_2 side. The multi-echo sequence cannot measure short T_2's (< 1-2ms) on the 0.35 T Maran, due to a hardware limited, finite-long, first echo interval containing the phase-encoding gradient (Fig. 1). This limitation is easily remedied with faster rise time gradients. Examples of the use of these T_2 mapping methods in porous media applications will be given.
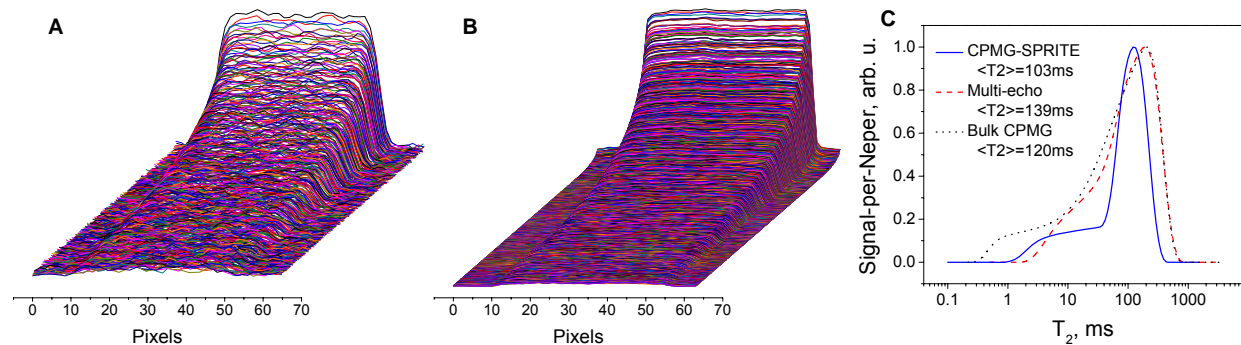
Fig. 1: Profiles of a Berea sandstone saturated with water, by CPMG-prepared SPRITE (A) and multi-echo MRI (B) sequences with an echo period TE = 0.4 ms. (C) T_2-distributions from central pixels of the profiles on (A) and (B), in comparison to a bulk CPMG measurement.

1.   Poon, C.S. and R.M. Henkelman, *Journal of Magnetic Resonance Imaging*, **2**(1992), 541-553.
2.   Mosher, T.J. and B.J. Dardzinski, *Seminars in Musculoskeletal Radiology*, **8**(2004), 355-368.
3.   Beuf, O., et al., *Journal Of Magnetic Resonance Series B*, **112**(1996), 111-118.
4.   Li, L., H. Han, and B.J. Balcom, *Journal Of Magnetic Resonance*, **198**(2009), 252–260.

Detection of Uranium Oxidation and Solubility using NMR

Sarah J. Vogt[1,2], Joseph D. Seymour[1,2], Brandy D. Stewart[1,2], Brent M. Peyton[1,2] and Sarah L. Codd[2,3]

[1]Department of Chemical and Biological Engineering, Montana State University, Bozeman, MT, USA
[2]Center for Biofilm Engineering, Montana State University, Bozeman, MT, USA
[3]Department of Mechanical and Industrial Engineering, Montana State University, Bozeman, MT, USA

Abstract:

The conversion of soluble uranyl ions (UO_2^{2+}) by bacterial reduction to insoluble uraninite (UO_2) is being studied as a way of immobilizing spent uranium waste [1-3]. Under anaerobic conditions, several known iron-reducing types of bacteria have been shown to also use the uranyl ion as an electron acceptor. Preliminary tests using a suspension of uraninite (UO_2) particles produced by *Shewanella putrefaciens* CN-32 bacteria show a dependence of the T_1 and T_2 on the oxidation state and solubility of the uranium. Gradient echo and spin echo images were compared to quantify the T_2^* effect caused by the magnetic field fluctuations of the uraninite particles and soluble uranyl ions. Since the precipitate studied is suspended in liquid water the effects of concentration and particle aggregation are also being explored. A suspension of uranium particles was injected into a polysaccharide gel, which simulates the precipitation of uraninite in the extracellular biofilm matrix. A reduction in the T_2 of the gel surrounding the particles was seen [4]. Therefore it may be possible to detect the presence of uraninite precipitate within a biofilm during the bacterial reduction reaction.

1. Abdelouas, A., Y. Lu, W. Lutze, H.E. Nuttall, *Journal of Contaminant Hydrology,* **35** (1998) 217-233.

2. Suzuki, Y., S.D. Kelly, K.M. Kemner, J.F. Banfield, *Nature,* **419** (2002) 134.

3. Sani, R.K., B.M. Peyton, A. Dohnalkova, *Water Research,* **42** (2008) 2993-3002.

4. Nestle, N. and R. Kimmich, *Colloids and Surfaces A: Physicochemical and Engineering Aspects,* **115** (1996) 141-147.

ESR Imaging in Solid Phase down to the Sub-Micron Resolution: Methodology and Applications

Aharon Blank, Ekaterina Suhovoy, Revital Halevy, Lazar Shtirberg

Schulich Faculty of Chemistry, Technion – Israel Institute of Technology, Haifa, 32000, Israel

Abstract:

Electron Spin Resonance Microcopy (ESRM) is an imaging method aimed at the observation of paramagnetic species in small samples with a micron-scale spatial resolution. At present, this technique is pursued mainly for biological applications at room temperature and in relatively low static magnetic fields. This work is focused on the use of ESRM for the measurement of solid samples. In the poster a brief comparison of various electron spin resonance (ESR) detection techniques will be provided, with an emphasis on conventional "induction detection" pursued in our work. Following that, some methodological details are provided along with experimental examples carried out at room temperature and in a static field of ~0.5 T. These examples show for the first time the imaging of solid samples measured by "induction detection" ESR with a resolution better than 1 μm. Based on these experimental examples and capabilities, an outlook for the future prospects of this methodology in terms of spin sensitivity and resolution is provided. It is estimated that single-spin sensitivity could be achieved for some samples at liquid-helium temperatures and static fields of ~2 T. Furthermore, under these conditions, spatial resolution could reach the nanometer scale. Descriptions and possible applications of this new methodology are also discussed.

Direct Measurement of Diffusion in Liquid Phase by Electron Spin Resonance

Yael Talmon, Michael Shklyar, Lazar Shtirberg and <u>Aharon Blank</u>

Schulich Faculty of Chemistry, Technion – Israel Institute of Technology, Haifa, 32000, Israel

Abstract:

The critical roll of diffusion in the mechanism of various biological and chemical processes has led researches to an ongoing search for methods to quantify the diffusion coefficient. The measurement of diffusion occurring over relatively long distances (of at least few microns) can be carried out with techniques such as nuclear magnetic resonance (NMR) or fluorescence recovery after photo-bleaching (FRAP), and are well-established. However, methods for the direct measurement of diffusion over short distances (in 10-100 nm range), occurring in the micro-sec time scale, have not yet been developed. Here we show that by utilizing the well known NMR pulse sequence pulse gradient spin echo (PGSE), in an electron spin resonance (ESR) experiment; one can measure the diffusion coefficients over such short distance and time scales. In order to adapt PGSE to ESR we had to develop high sensitivity micro-resonators and a capability to generate very intense and short gradient pulses of ~1 micro-sec in length and ~80 T/m in magnitude. Our preliminary work included the measurements of the non-restricted isotropic diffusion coefficient of three types of radical solutions: trityl radical in water, $N@C_{60}$ in chloronaphthalene and $N@C_{60}$ in CS_2. The experimental results were compared to the theoretical diffusion coefficient calculated by the Stocks-Einstein equation, and revealed an excellent agreement. This preliminary work is currently being further extended to the measurement and characterization of restricted diffusion of trityl water solution in nano-spheres.

Refinement of Oxygen resolution in Functional EPR Imaging

<u>Sankaran Subramanian</u>[1], Gadisetti V. R. Chandramouli[2], Shingo Matsumoto[1], Nallathamby Devasahayam[1] and Murali C. Krishna[1]

[1] Radiation Biology Branch, Center for Cancer Research, National Cancer Institute, NIH, Bethesda, MD 20892, USA
[2] College of Human Medicine, Michigan State University, Grand Rapids, MI 49503, USA

Abstract:
The definition of resolution is a fundamental concept in Magnetic Resonance Imaging. Since this technology depends on scanner's ability to spatially resolve spectral line, the resolution is defined in terms of the spectral linewidth. In EPR imaging, it is specified by one full width at half maximum height (FWHM) for Gaussian line shape where two point objects are considered as resolved. At this separation, the spectral lines from the objects overlap with each other, but their peak intensities are distinguishable. This definition is valid when the linewidth remains constant. In oximetric EPR imaging, the mapping of oxygen is carried out by monitoring the spatially resolved spectral line width of spin probes that show a linear dependence on the local oxygen concentration, reported in terms of the partial pressure of oxygen, pO_2, in mm of Hg. However, the linewidths vary *in vivo* not only with pO_2 levels, but with the local spin probe concentration as well. Since the linewidth that defines the resolution itself changes locally, the definition of natural linewidth as a factor of resolution is naïve for a pO_2 map. The resolution of pO_2 map is realistic only when corrected for the local spin concentration. Co-registration of EPR images with high resolution images from other modalities help enhance the digital resolution. In this scenario, the apparent high resolution of pO_2 levels is misleading and may lead to over-interpretation of the data. Specification of accurate resolution is important while studying the distinctions of pO_2 levels between organs and tissue boundaries.

In FT imaging techniques one can barter the resolution for the speed of scanning. FT imaging which scans *K*-space, offers better control on segregation of the *K*-space that adds to signal or to the resolution of the image. Therefore it is necessary to systematically study the parameters that affect the resolution of pO_2 maps and to specify the resolution explicitly with pO_2 map. FT-EPR images obtained by pure phase encoding of constant time points should have, in principle, linewidth-independent resolution, but they are subject to broadening by the point spread function of the instrument and these further affect the image and oxygen resolution. This 'blurring' modifies pO_2 levels at object boundaries. The effect of blurring can be examined by convolution of model point spread functions (such as Gaussian noise) on a hypothetical pO_2 image. When this is done hypoxic regions appear to have higher pO_2 levels while normoxic regions appear to be at lower pO_2 levels especially at object boundaries. Assessment of point spread function and deconvolution are difficult problems to achieve accurate quantitative pO_2 values. However, such assessment helps to estimate the limit of resolution. We are developing deconvolution schemes based on the point spread function derived from phantom measurements to achieve resolution enhancement both in spin and oxygen mapping. The goal is to add realistic resolution limits with measured pO_2 maps so that the interpretation of tumor physiology is more accurate. Results of ox metric EPR imaging on phantoms and in vivo will be presented and discussed.

Quantitative RARE imaging: applications to controlled drug delivery systems

Ya Ying Chen[1], L.P. Hughes[2], L.F. Gladden[1] and M.D. Mantle[1]

1. Department of Chemical Engineering & Biotechnology, University of Cambridge, Pembroke Street, Cambridge CB2 3RA, UK.
2. Pharmaceutical and Analytical R&D, AstraZeneca, Silk Road Business Park, Macclesfield SK10 2NA, UK.

Ultra-fast MRI imaging techniques such as EPI, FLASH and RARE have been used extensively as non-quantitative diagnostic tools in clinical medicine. The use of these techniques to study, *quantitatively,* fast and medium release controlled drug delivery systems with a spatial resolution of hundreds of microns has largely been ignored. Of these, RARE is most suited to study fast and medium release controlled drug delivery devices as, unlike EPI, it is tolerant of magnetic susceptibility differences and, unlike FLASH, produces images with a high signal-to-noise ratio. However, a major drawback of RARE imaging, is that the acquired k-space data is convolved with both T_1 and T_2 relaxation weighting and thus the image signal intensity is not a direct representation of the absolute spin density in the sample. Based on the work of Norris et al.[1], the talk describes the development and validation of two preconditioned RARE sequences that acquire quantitative images in less than 2 minutes: (i) a CPMG T_2-preconditioning sequence that gives quantitative T_2 relaxation time and water concentration images; (ii) a 13-interval bipolar pulse field gradient diffusion preconditioning sequence that provides images of the molecular self diffusion coefficient. The analysis of the data from a number of different phantom samples, with known relaxation and diffusion properties show this type of technique can quantitatively image systems with a minimum T_2 of 20 ms to within an error of approximately 5%. A description of the choice of RARE phase encoding, i.e. centric or linear, and how it affects the overall quality and quantitation of the resulting image will also be given.
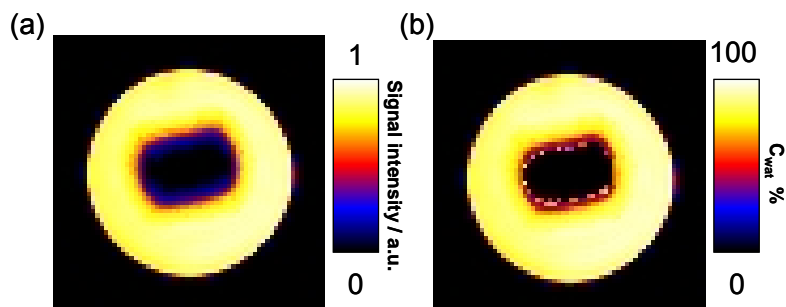
Fig. 1: Comparison of the images of swollen HPMC tablet in water after acquired with (a) conventional RARE and (b) quantitative RARE sequences.

We show, for the first time, how this technique can be used to quantify the dissolution process of a polymeric controlled drug release matrix, hydroxy-propylmethyl cellulose (HPMC) in water. Figure 1 shows the comparison between the images of a swollen HPMC tablet acquired with conventional RARE imaging and that obtained form the quantitative RARE imaging sequence developed in this work. A comparison of our quantitative RARE imaging with short echo-time FLASH imaging, for the HPMC/Water system, shows the superiority of the quantitative RARE method.

Projection Imaging of Acrylic with FIDs *vs*. Solid Echos

Dean O. Kuethe

New Mexico Resonance, Albuquerque, USA

Imaging short T_2 samples, such as polymethylmethacrylate with a T_2 of 14.5 µs, poses unpleasant trade offs for pulsed NMR. With FID-projection imaging, the dead time for the rf coil to ring down can cause one to miss substantial signal. One can make so-called "solid echos" with 90x-90y rf pulses   to cause an echo to form after the dead time, but it is difficult to make high-angle rf pulses short enough to avoid selective excitation in strong magnetic field gradients. [One excites spins in the presence of gradients because switching times of under 10 µs are generally impractical.]

This study compares the two techniques, using the same rf coil, scan time (75 min), gradient strength (240 mT/m), and number of projections (8100). The acrylic sample was a cylinder, 24.5 mm diameter and length, with 8 holes drilled parallel to the axis ranging from 1 mm diameter to 4.5 mm diameter in 0.5 mm increments. The coil was a 6-turn center-driven 30 mm diameter, 26 mm long, solenoid rf coil in an Oxford 80.35 MHz magnet with Resonance Research 120 mm ID shielded gradient coils that delivered 240 mT/m gradients at 18% duty cycle. The Tecmag Libra console provided 12-bit digitization of the received signal at 1 MHz. For FID-projection imaging, there were crossed signal diodes and a 7.5 Ohm resister to ground at ¼ wavelength from the coil. This junction was in turn ¾ wavelengths from the diodes that isolate the transmitter. So situated, the voltage-activated 7.5 Ohm device reduced the dead time from 13 to 7 µs at the expense of reducing the transmission efficiency. It was not used for forming solid echos, which are better served with high transmission efficiency. The solid echos formed 14 µs after the end of the second pulse, which avoided the dead time. The 240mT/m gradients restricted rf pulses to 4 µs or shorter. The excitation bandwidth, 300kHz, corresponds to 29 mm — enough to accommodate the sample length and diameter but insufficient for the 36 mm diagonal dimension. Even though the coil contained Johanson 56H01 and 59H01 high-voltage tuning and matching capacitors, 4 µs pulses could not provide 90x-90y pulses but were limited to 70x-70y. Nonetheless, with one 28dB ARR preamp, the digitizer's 12-bit range was filled by using a repetition time of 113 ms, which allowed 2 averages. For FID-projection imaging the repetition time (11 ms, which allowed 20 averages) was determined by the duty cycle of the gradient coils, and the signal-to-noise ratio was optimized by using the Ernst angle excitation pulse (19.5˚, 2.6 µs). The entire 70 µs of useful signal was collected so there was substantial point spread in the images, which was somewhat reduced by applying a Lorenzian line-narrowing filter to the time domain data.

Fig. 1: One 0.66 mm slice, perpendicular to the cylinder axis of the FID-projection image (left) and the 70x-70y solid echo image (right). The nominal resolution is isotropic. The FID-projection image is substantially better which is somewhat surprising because the 7.5 Ohm dead-time-shortening device merely shortened the dead time to the extent that FID imaging was possible.

1. J. G. Powles, P. Mansfield, Double pulse nuclear-resonance transients in solids. *Phys. Letters* **2** (1962) 58-59.
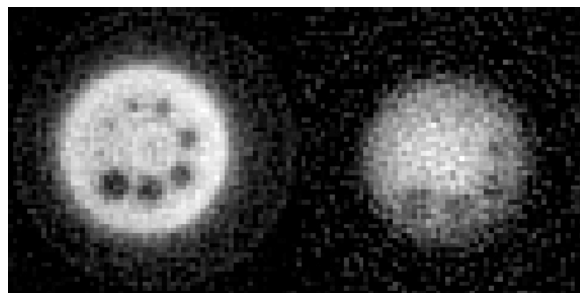
Transient magnetization of permanent magnet pole pieces is trouble for projection imaging

Dean O. Kuethe[1], Arvind Caprihan[2], Tomoyuki Haishi[3]

[1] New Mexico Resonance, Albuquerque, USA
[2] Mind Research Network, Albuquerque, USA
[3] MRTechnology Inc., Tsukuba, Japan

Permanent magnets offer inexpensive, low-maintenance alternatives to superconducting magnets for magnetic resonance imaging (MRI) and have performed fabulously with spin-warp imaging techniques [1]. We tried free induction decay (FID)-projection imaging with a permanent magnet and encountered a problem we had not experienced with superconducting MRI systems. It appears that the magnetic fields from the gradient coils induce transient alterations in the magnetization of the pole pieces. The transient magnetizations alter the directions of the gradients and have time constants on the order of milliseconds. For FID-projection imaging, it is important that the directions of the gradients are precisely known. Errors in the gradient directions hamper the ability to correctly locate objects in the image. For spin-warp imaging, if the phase- or frequency-encoding gradient direction is slightly different from specified, the images are fine so long as the error is consistent.

Lingering distortions in the field gradients cause changes in the time-domain data that resemble those caused by eddy currents in super conducting magnets. However, the effects of eddy currents are reduced if one uses slower gradient ramps and longer settling times before collecting data. In contrast, the distortions in data caused by transient magnetizations in the pole pieces are reduced by shortening the ramps and gradient pulses — it takes time for the alterations in magnetization to build up. When short gradient pulses are followed by equal and opposite ones, the transient magnetization is largely reversed and the resolution of the image is improved. However, residual transverse NMR signal is refocused so one can get image artifacts from incomplete spoiling. The figure shows an image of an apple, made without and with such compensating pulses.

Fig. 1: Apple with insect larva. The image on the left was made with a spoiled FID-projection pulse sequence. It is blurry because the gradient directions are altered by transient magnetization. The sharper image on the right was made with additional gradient pulses that reversed some of the transient magnetization at the expense of artifacts from unspoiled transverse NMR signal.
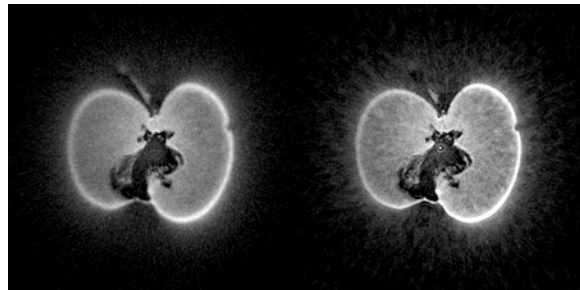
For eddy currents in superconducting magnets, one can precompensate or distort the gradient wave form to account for the time lag between the specified and actual field gradient. However, the success of precompensation depends on the eddy currents having similar symmetry to the current in the gradient coils. The transient magnetization of pole pieces is unlikely to have the necessary symmetry. It may be necessary to use shielded gradient coils to achieve good projection images with permanent magnets.

1. Y. Inoue, Y. Nomura, T. Haishi, K. Yoshikawa, T. Seki, K. Tuskiyama-Kohara, C. Kai, T. Okubo, K. Ohtomo, *J. Magn. Reson. Imag.* **24** (2006) 901-907.

Measuring Diffusion Using the Differential Form of Fick's Law and Magnetic Resonance Imaging

<u>Colleen E. Muir</u>[1], Brian J. Lowry[2], and Bruce J. Balcom [1]

[1] UNB MRI Centre, University of New Brunswick, Fredericton, Canada
[2] Department of Chemical Engineering, University of New Brunswick, Fredericton, Canada

Abstract:

Diffusion is an important process that occurs in many biological and industrial systems. Diffusive mass transfer in porous media and other systems is frequently measured in experiments where one controls or imposes well-known boundary conditions on samples and processes of interest. Ideal boundary conditions permit integration of Fick's law and fitting of either time or spatially varying concentration data to determine diffusion coefficients [1]. However, many practical mass transfer processes do not correspond to convenient boundary conditions and therefore have no integrated solution to Fick's law. In other cases, an integrated solution to Fick's law may exist but may be complex and challenging to fit to in order to solve for the diffusion coefficient. In either of these situations an alternative approach to measuring the diffusion coefficient is through the use of the differential form of Fick's second law.

The utility of the differential approach has been demonstrated by Karger et. al. in their recent study of the distribution of guest molecules in nanoporous host materials [2]. Interference microscopy was used to generate concentration profiles and determine diffusivity, but the method was limited to optically transparent samples. MRI is a non-invasive method that can be used to study transparent and opaque samples. In this work we use MRI to generate spatially and time-resolved profiles in which the measured signal is proportional to the concentration of H_2O. This naturally allows for easy use of the differential diffusion equation to determine the diffusion coefficient, D.

We employ double half k-space SPRITE to obtain profiles of the diffusion of H_2O from an agarose gel to a neighbouring D_2O reservoir. The differential form of Fick's second law was used to solve for the diffusion coefficient, $D = 1.3 \times 10^{-9}$ m^2/s. MRI is well-suited to this type of analysis as it naturally generates time and space resolved images. This technique is a simple alternative to a complicated integrated form of Fick's law.

1. Crank, J. *The Mathematics of Diffusion,* 2nd ed.; Oxford Science: Oxford, 1993.
2. Kärger, J; Kortunov, P; Vasenkov, S; Heinke, L; Shah, D. B.; Rakoczy, R. A.; Traa, Y.; Weitkamp, J. *Angew. Chem. Int. Ed. Engl.* **2006**, *45*, 7846-7849.

Gradient waveform monitoring and adjustment with NMR microprobes

Hui Han, Rodney P. MacGregor and Bruce J. Balcom

MRI Centre, Department of Physics, University of New Brunswick, Fredericton, N.B, Canada

Abstract:

MRI methods and PFG diffusion measurements rely on high fidelity large amplitude, fast slew-rate magnetic field gradients. Despite continuous advances in MR hardware, magnetic field gradient imperfections caused by eddy currents, group delay, gradient amplifier infidelity etc, render many advanced MR/MRI pulse sequences less than ideal.

Numerous methods have been developed to measure MRI gradient waveforms and k-space trajectories. The most widely used method to characterize gradient behavior is a slice selection method by Duyn [1]. The most promising new strategy appears to be magnetic field monitoring (MFM) with RF microprobes [2-3]. The two methods are based on measuring the time evolution of magnetization through frequency encode FIDs. Two critical problems remain. The k-space maxima are limited by gradient dephasing, while the gradient waveform duration is limited by the sample T_2^*.

We have developed a novel method to measure the magnetic field gradient using pure phase encode FIDs with an RF microprobe. A small doped water phantom (Dia 1 mm - 1 cm, T_1, T_2, $T_2^* < 100$ μs) within a microprobe is excited by a series of closely spaced broadband RF pulses each followed by single/multiple FID point acquisition.

The pure phase encode gradient monitor has solved the above two problems in addition to permitting measurement of high amplitude gradients for imaging and diffusion. The distinctive advantages of the new method are even more desirable for non-clinical MR applications, where larger amplitude gradients are often employed.

The new method is a point monitor with simple implementation and low cost hardware requirements, see Fig. 1. A trial waveform measured to illustrate the new method's ability to measure gradient waveforms with large net area and/or high amplitude is shown in Fig. 2. A gradient compensation strategy to eliminate eddy current effects is also presented. This is particularly important for systems where the experiment apparatus, containing the sample under study, supports eddy currents.

Fig. 1: Photo of probehead with water drop test sample
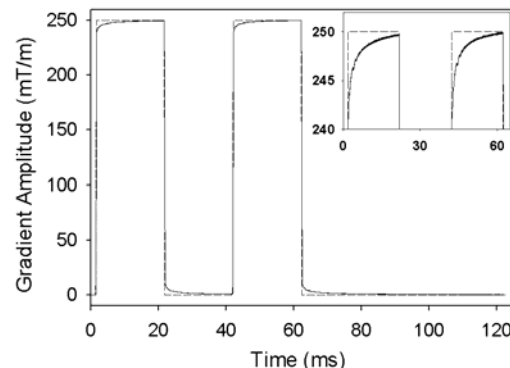
Fig. 2 Measured diffusion waveform, b = 100,000 s/mm^2

1. Duyn et al., JMR. 132 (1998) 150-153.
2. N. De Zanche et al., MRM. 60 (2008) 176-186.
3. C. Barmet et al., MRM. 60 (2008) 187-197.
4. H. Han et al., JMR. In revision.

P70

MR Thermal Imaging in the Presence of Motion

Youngseob Seo[1], Jacob Willig-Onwuachi[2], Jeffrey H. Walton[3]

[1]Department of Biomedical Engineering, UC Davis, Davis, CA, USA
[2]Department of Physics, Grinnell College, Grinnell, IW, USA
[3]NMR Facility & Biomedical Engineering Graduate Group, UC Davis, Davis, CA, USA

Magnetic resonance thermal imaging plays a crucial role in MRI-guided thermal therapy of cancer. Real-time *in vivo* temperature maps for monitoring and guiding thermal therapies such as radiofrequency ablation, laser ablation, focused ultrasound, and cryotherapy permit tailored treatments to meet specific endpoints for individual patients with immediate feedback. This ensures the coagulation of cancerous tissue to the margin while protecting adjacent normal tissues. These temperature maps, however, are easily corrupted by motion, meaning these techniques are limited to static organs. Previous methods of reducing motion artifacts have drawbacks that prevent them from being optimal for the application of the MR thermal imaging. The purpose of this research is to develop and optimize an MR thermometry method combined with parallel MRI techniques in mobile phantom experiments with respect to detecting and correcting the motion artifacts. Motion artifacts of the mobile phantoms were detected and corrected using SMASH navigators [1] while MR temperature maps were obtained using the proton resonance frequency (PRF) shift method[2] with complex image subtraction. Temperatures acquired by the MR thermal imaging was compared to that measured via thermocouples. MR thermal imaging combined with SMASH navigators resulted in accurate temperature maps of the mobile phantoms. The combination of MR thermometry and parallel MRI techniques will be an important tool for cancer thermal therapies in mobile organs.
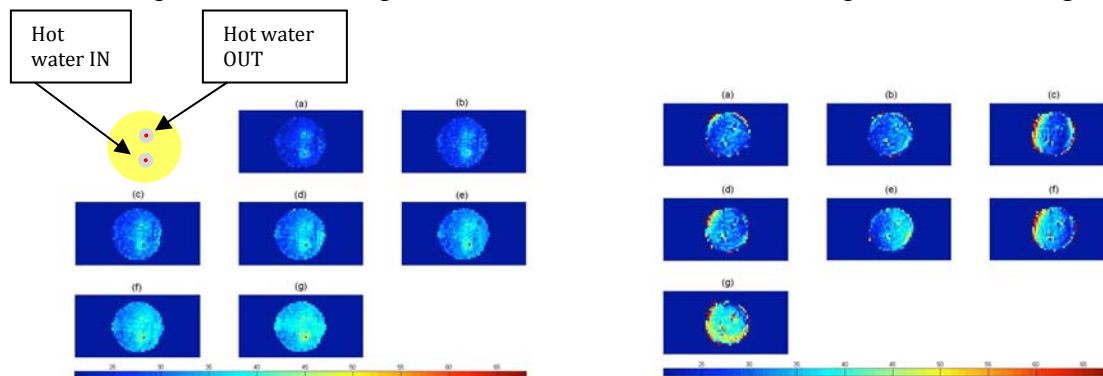
MR temperature maps at 10 min(a), 20 min(b), 30 min(c), 40 min(d), 50 min(e), 60 min(f), and 70 min(g) after heating. Left is a *static* phantom, Right is a mobile phantom. High temperatures at the edges are due to errors in the measured SMASH spatial harmonics.

1.Bydder, et al., Magnetic Resonance in Medicine, **49** (2003) 493-500
2.Ishihara, et al., Magnetic Resonance in Medicine, **34** (1995) 814-823

^{35}Cl profiling using centric scan SPRITE with variable flip angle excitation

Konstantin V. Romanenko[1], P.F. de J. Cano-Barrita[2], Bruce J. Balcom[1]

[1] MRI Centre, Department of Physics, University of New Brunswick, Fredericton, NB, Canada E3B 5A3
[2] CIIDIR IPN Unidad Oaxaca, Hornos No. 1003, Sta. Cruz Xoxocotlan, Oaxaca, Mexico

Abstract:

Single point imaging (SPI) is now widely accepted as a powerful quantitative technique for imaging objects with short spin-lattice, T_1, and spin-spin, T_2, relaxation times [1–4]. SPI and its later modification SPRITE (Single Point Ramped Imaging with T_1 Enhancement) [5] are pure phase encoding techniques. The gradient is increased stepwise, and a single point of the free induction decay (FID) is acquired at each step. Radio frequency (RF) excitation and signal acqusition are separated by a constant phase encoding delay, t_p. Magnetic field inhomogeneity and chemical shift artifacts, common for frequency encode imaging, are largely non-existent in SPI imaging [6]. MRI of low γ nuclei is not straightforward due to reduced signal-to-noise ratio and various hardware limitations. Our interest is focused primarily on objects with short T_2^* and low γ. In many cases of practical importance, such samples also feature short T_1. In order to reduce the encoding time t_p at a fixed field of view (FOV), usable gradients should reach very high magnitudes (~ 100 G$\times$cm^{-1}). This causes an additional limitation related to inhomogeneous excitation of the object by an RF pulse.

An efficient MRI technique for quantitative density profiling of samples with fast spin-lattice relaxation (T1 < 5 ms) is introduced. The pulse scheme is based on the 1D centric scan SPRITE technique [7]. Strong excitation of the sample at the k-space origin improves the sensitivity with respect to the original centric scan SPRITE technique. Radio frequency pulse durations are defined so as to provide uniform excitation of the sample at every k-space point. For a particular k-space point the pulse duration is required to be less than the inverse sample bandwidth. Simulations permit one to examine distortions from ideal profile geometry due to flip angle and spin-lattice relaxation effects. The proposed technique is especially suitable for the observation of low sensitivity samples, in particular, low γ nuclei like ^{35}Cl. In some cases, this strategy permits one to reduce the number of scans, i.e. the experiment time, by a factor of 100, depending on hardware, sample length and tolerable resolution loss. The designed pulse scheme is tested on cylindrical agar gel and type 1 Portland cement paste phantoms prepared to provide ^{1}H and ^{35}Cl signals, respectively.

1. B.J. Balcom, Spatially Resolved Magnetic Resonance, Wiley-VCH, Toronto, 1998, pp. 75–86.
2. C.B. Kennedy, B.J. Balcom, I.V. Mastikhin, Can. J. Chem. 76 (1998) 1753–1765.
3. S.D. Beyea, B.J. Balcom, P.J. Prado, A.R. Cross, C.B. Kennedy, R.L. Armstrong, T.W. Bremner, J. Magn. Reson. 135 (1998) 156–164.
4. P.J. Prado, B.J. Balcom, I.V. Mastikhin, A.R. Cross, R.L. Armstrong, A. Logan, Magnetic resonance imaging of gases: a single-point ramped imaging with T_1 enhancement (SPRITE) study, J. Magn. Reson. 137 (1999) 324–332.
5. B.J. Balcom, R.P. MacGregor, S.D. Beyea, D.P. Green, R.L. Armstrong, T.W. Bremner, J. Magn. Reson. A 123 (1996) 131–134.
6. S. Gravina, D.G. Cory, J. Magn. Reson. A 104 (1994) 53–61.
7. I. V. Mastikhin, H. Mullally, B. MacMillan, and B. J. Balcom, J. Magn. Reson. 156 (2002)122–130.

Diffusion effects in µm-scale spatially selective excitation: more than just diffuse blurring

Achim Gädke[1,2] and Nikolaus Nestle[1,3]

[1] Institute of Condensed Matter Physics, TU Darmstadt, Darmstadt, Germany
[2] present address: Victoria University of Wellington, New Zealand
[3] present address: BASF SE Ludwigshafen, Ludwigshafen, Germany

Abstract:

Diffusion has long been known as a source of artifacts and also as a possible contrast mechanism in NMR (micro-)imaging: Especially the attenuation of transverse magnetization due to diffusion in magnetic field gradients and the diffusive blurring of in-plane resolution by diffusion during the echo time have received attention in this context [1]. Furthermore, effects of barriers and susceptibility jumps were studied [2]. Much less attention was paid to possible diffusive migration of magnetization from and to selectively excited volume elements. Related effects were suggested as a possible approach to enhance contrast in MRI [3] and for a special technique to measure diffusion coefficients in fast-diffusing media [4].

The diffusion balance between the excited volume and its surroundings can be safely neglected for voxel dimensions larger than the typical length scales of diffusion relevant for the NMR experiment. The largest of these length scales is the saturation memory length $l_{sm} = \sqrt{2DT_1}$ describing the mean diffusive shift of excited magnetization during the bulk longitudinal relaxation time of the medium. First studies on the magnetization recovery behavior in selectively excited slices thinner than this length scale [5] indicated an effective longitudinal relaxation time orders of magnitude shorter than the bulk value for the magnetization recovery in the excited slice. Those experiments were conducted with rather poorly defined slice geometry and with full relaxation after each excitation cycle.

In order to mimmick the conditions in a conventional ultrahigh resolution NMR microscopy experiment or in mechanically detected NMR, periodically excited volumes instead of fully relaxed volumes are relevant. Such experiments were conducted using a novel experimental setup based on the spectrometer platform DAMARIS [6] with improved pulse shaping capabilities allowing slice-selective excitation down to 3 µm in a 73 T/m magnetic field gradient. Exact positioning of sample and excited slice is essential and was specially validated. Furthermore, the same excitation scenarios were also simulated using the Bloch-Torrey equation. Experimental and simulated results indicate that the diffusion effect also dominates the magnetization recovery behavior in the periodic excitation case and leads to effective signal enhancements of about 100 in comparison to the expectations for the bulk relaxation time. Consequences and implications for ultrahigh resolution MRI of biological structures are discussed, too.

[1] Callaghan, PT 1991 Principles of Magnetic Resonance Microscopy. Oxford, Clarendon Press; Haase A, Brandl M, Kuchenbrod E, Link A, *J Mag Res A* **105** (1993) 230-233

[2] Callaghan PT, Coy A, Forde LC, Rofe CJ, *J Mag Res, A* **101** (1993) 347-350; Nestle N, Rydyger K, Kimmich R, *J Mag Res* **125** (1997) 355-357

[3] P. C. Lauterbur, W. B. Hyslop, H. D. Morris, XI International Society of Magnetic Resonance Conference, 1992, Vancouver, BC.; L. Ciobanu, A.G. Webb , C. H. Pennington *J. Mag Res.* **170** (2004) 252–256.

[4] Kimmich, R., Simon, B., Köstler, H. *J. Mag Reson. A* **112** (1995), 7.

[5] Nestle N, Walaszek B, Nolte M *J Mag Res* **168** (2004) 46-52

[6] Gädke A, Rosenstihl M, Schmitt C, Stork H, Nestle N *Diffusion Fundamentals* **5** (2007) 5 6.1-6.9

Insights into knee cartilage degeneration: T_1 mapping at 4 T and relevance to modern gait analysis

Kirk W. Feindel[1], Janie L. Astephen Wilson[2], and Steven D. Beyea[1,2,3]

[1] NRC Institute for Biodiagnostics (Atlantic), Halifax, Canada
[2] School of Biomedical Engineering, Dalhousie University, Halifax, Canada
[3] Department of Physics and Atmospheric Science, Dalhousie University, Halifax, Canada

Abstract:

Mechanical factors during activities of daily living are associated with diseases of the musculoskeletal system, particularly osteoarthritis (OA) of the knee [1]. Modern gait analysis combined with electromyography can provide insight into joint dynamics and neuromuscular function during gait [2]. However, these studies do not provide a direct correlation between gait patterns and early degenerative joint changes (i.e., localization of structural and biochemical changes within the articular cartilage). Early diagnosis of knee cartilage degeneration and its correlation with joint mechanics may lead to strategies for alleviation and/or re-mediation of the condition.

Magnetic resonance imaging and spectroscopy techniques have previously been developed and applied to characterize the structure and biochemical composition of knee cartilage [3]. Of the ^{1}H NMR relaxation based contrast mechanisms (e.g., T_1, T_2, $T_{1\rho}$), rotating frame longitudinal relaxation ($T_{1\rho}$) contrast is closely related to biochemical changes in degenerating cartilage [4]. Traditionally, $T_{1\rho}$ contrast has been obtained by applying a continuous wave (CW) spin-lock pulse prior to the imaging sequence. However, for clinical applications on humans at higher magnetic fields (i.e., > 3 T) limitations on specific absorption rate (SAR) values preclude the utility of this methodology. Recent developments in hardware have led to a resurgence in the use of adiabatic pulses [5], and Michaeli and coworkers [6] have demonstrated the efficacy of hyperbolic secant (HSn) pulses for providing $T_{1\rho}$ contrast with reduced SAR values relative to CW methods.

The research presented herein demonstrates that with the use of HSn pulses, in-vivo $T_{1\rho}$ contrast of human articular knee cartilage can be obtained at 4 T within SAR limitations. The $T_{1\rho}$ maps are subsequently interpreted in conjunction with results from gait analyses to determine the relationship between joint dynamics and knee cartilage degeneration.

1. D. T. Felson, A. Naimark, J. Anderson, L. Kazis, W. Castelli, and R. F. Meenan, *Arthritis Rheum.* **30** (1987) 914.
2. J. L. Astephen, K. J. Deluzio, G. E. Caldwell, M. J. Dunbar, and C. L. Hubley-Kozey *J. Biomech.* **41** (2008) 868.
3. F. Eckstein, T. Mosher, and D. Hunter, *Curr. Opin. Rheumatol.* **19** (2007) 435.
4. S. V. S. Akella, R. R. Regatte, A. J. Gougoutas, A. Borthakur, E. M. Shapiro, J. B. Kneeland, J. S. Leigh, and R. Reddy. *Magn. Reson. Med.* **46** (2001) 419.
5. M Garwood and L. DelaBarre. *J. Magn. Reson.* **153** (2001) 155.
6. S. Michaeli, D. J. Sorce, C. S. Springer Jr., K. Ugurbil, and M. Garwood. *J. Magn. Reson.* **181** (2006) 135.

Measurement time reduction for trabecular bone volume fraction measurements of the calcaneus in the compact MRI system

T.Nakayama[1], K.Taniguchi[1], S.Handa[2], K.Kose[1]

1. Institute of Applied Physics, University of Tsukuba, 2. Japan Society for the Promotion of Science

Introduction: In 2004, we proposed a compact MRI system for trabecular bone volume fraction (TBVF) measuremnt of the calcaneus to diagnose osteoporosis [1]. In 2005, we reported TBVF measurements for a large number of subject (~400) to evaluate long term reproducibility of the system [2]. In 2009, we reported a shield-room free compact MRI system for the heel measurements to reduce the installation space [3]. However, problems in the measurement time (several minutes) and reproducibility of the TBVF measurements (more than several %) are remained unsolved. In this study we have shorten the spin-echo time as short as possible to reduce the effect of T_2 decay and evaluated the short term reproducibility using two male volunteers.

Material and methods: The compact MRI system consisted of a permanent magnet (0.21 T field strength, 160 mm vertical gap), a gradient coil set, an RF probe, a local RF shield, and a compact MRI console. To obtain homogeneous RF magnetic field, the RF coil wire distribution of an oval solenoid was optimized using a genetic algorithm. To evaluate the reproducibility of the TBVF, the right calcanei of two male subjects were measured 10 times repeatedly after repositioning using following two protocols: one single spin echo sequence (TE = 9 ms) and two single spin echo sequences with different echo times (TE = 16, 96 ms). As the second protocol required two separate scans, the measurement time of the second one (5.2 min.) was twice that of the first one (2.6 min.).

Results and discussion: The percentage CV (coefficient of variance (standard deviation divided by the mean) expressed as a percentage) calculated for the repeated measurements averaged over the two male subjects was 4.7 % and 7.9 % for the single SE sequence (TBVF corrected with mean T_2) and the dual single SE sequence (TBVF corrected with individual T_2) as shown in Fig.2. This result clearly shows the advantage of the TBVF by the single SE sequence over that by the dual SE sequence.

The correlation coefficient between TBVF by the single SE sequence and that by the dual SE sequence was 0.6. This was not very high. This may be due to T_2 measurement error caused by low SNR of the image acquired with the long echo time (96 ms). To conclude, we achieved measurement time reduction by 50 % with 40 % CV reduction. In future, we will improve the RF coil and other electronics, and measure a large number of subjects.
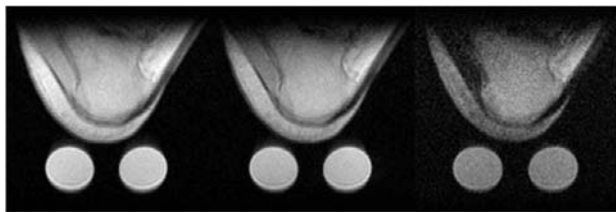
Fig.1
(left: TE = 9 ms, center: TE = 16 ms, right: TE = 96 ms)
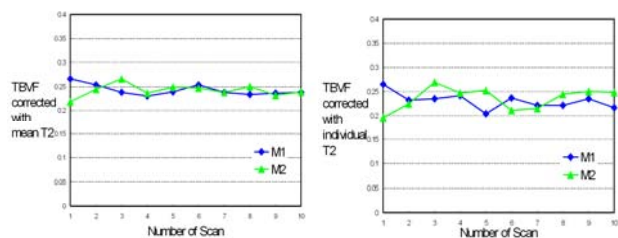
Fig.2

References: [1] K. Kose et al. Development of a compact MRI system for trabecular bone volume fraction measurements. Mag Reson Med **52**, 440-444 (2004). [2] S. Tomiha et al. Trabecular bone volume fraction measurements of a large number of subjects using a compact MRI. Mng Reson Imag. **23**, 1011-1015 (2005). [3] K. Taniguchi et al. Development of a Shield-Room Free Compact MRI System with a Highly Homogeneous RF Coil for Bone Density Measurements at the Calcaneus. Proc. ISMRM, 2009, p3097.

Effects of rapamycin on tumor pO_2 and blood volume

Keita Saito[1], Shingo Matsumoto[1], Nallathamby Devasahayam[1], Sankaran Subramanian[1], Jeeva Munasinghe[2], Murali C. Krishna[1]

[1] Radiation Biology Branch, Center for Cancer Research, National Cancer Institute,
[2] National Institute of Neurological Disorder and Stroke, National Institutes of Health, Bethesda, MD, U.S.A.

Abstract:

Rapamycin is an inhibitor of mammalian target of rapamycin (mTOR), and inhibits tumor growth and angiogenesis. Also rapamycin has radiosensitization effects on some tumors. In radiotherapy and chemotherapy of cancers, partial pressure of oxygen (pO_2) is an important factor to determine treatment outcome. Pulsed electron paramagnetic resonance imaging (EPRI) with triarylmethyl radical as a tracer gives us 3D maps of tissue pO_2 level in living animals, and magnetic resonance imaging (MRI) with ultrasmall superparamagnetic iron oxide gives us blood volume images [1]. In this study, we investigated effects of rapamycin on tumor pO_2 and blood volume of living mice by using EPRI and MRI.

Squamous cell carcinoma (SCC) cells (5×10^5 cells) were implanted s.c. into a right hind leg of female C3H Hen MTV mice. Treatments of rapamycin (10 mg/kg b.w./day) and measurements of pO_2 and blood volume were started after 8 days from implantation of the SCC tumor. EPRI measurements were done with a 300 MHz pulsed EPRI system, and MRI measurements were done with a 7 T scanner controlled with ParaVision 3.0.2 (Bruker Bio-Spin MRI GmbH).

Tumor growth in rapamycin treated mice was suppressed compared with non-treated mice, and body weights of mice were not changed by rapamycin treatments. Blood volume in tumor region was remarkably decreased even after 1 day from beginning of the rapamycin treatment. Tumor pO_2 did not drastically change but slightly increased after 2 days rapamycin treatments. These results suggest that rapamycin can normalize blood volume and suppress depletion of oxygen in the tumor region.

[1] Matsumoto S. et al., *J. Clin. Invest.* **118** (2008) 1965-1973.

MRI of Kidney and Brain pathology in a mouse model of disseminated candidiasis

Dhammika H.M.L.P. Navarathna[1], Jeeva. P. Munasinghe[2], Martin J. Lizak[2], David D. Roberts[1]

[1]Laboratory of Pathology, National Cancer Institute, [2]National Institute for Neurological Disorders and Stroke, National Institutes of Health, Bethesda. MD. USA.

Disseminated candidiasis is the fourth leading nosocomial infection in the United States, making it the most important human fungal pathogen. Candidiasis is most prevalent among immune compromised individuals (*e.g.* AIDS and chemotherapy patients). The limited number of antifungal antibiotics and their toxic side effects are an obstacle for effective therapy. As mortality is as high as 47% in candidiasis patients despite antifungal therapy, additional approaches are needed to target the pathogen. Kidney and brain are prime target organs of disseminated candida infection, with 50 % of candidiasis patients showing CNS invasion. *C. albicans* causes cerebral micro-abscesses with filamentous invasion during CNS infection (Fig-1). Histopathological studies suggest that *C.albicans* internalize in brain microvascular endothelial cell vacuoles and transmigrate across the blood brain barrier (BBB). However, damage caused to the BBB by candidia invasion in CNS as well as its pathogenesis in the kidney are poorly understood. This study addresses these questions in a mouse model using MRI.

MRI of Kidneys and Brain were performed on two different groups of mice at 7 Tesla. For brains, T_1-weighted axial slices encompassing the whole brain were acquired using a Gradient echo (GE) sequence before and 5 minutes after administration of a bolus of Gd-DTPA. Quantitative measurements of possible BBB breach was investigated with regions of interest (ROI) placed in the hippocampus, and cortices of both hemispheres to investigate any widespread BBB damage. Selected animals were then perfused and brain histology studied. Macrophage infiltration of the kidneys was observed using ultra small iron oxide particles (USPIO). T_2^*-weighted images of the kidneys were acquired 3 days post inoculation, 24 hours following administration of a USPIO contrast agent.

Signal increases due to possible Gd leakage to the brain in infected mice were seen in focal areas such as the frontal cortex and hippocampal regions (Fig-2B). As Gd-DTPA is a vascular contrast agent, no significant signal increase was observed in normal mice, where the BBB is intact (Fig-1A). We found significant amounts of macrophage infiltration in the kidney matrix compared to normal mice (Fig 3).

This study provides in-vivo evidence for breach in BBB during disseminated candida infections. These imaging methods could be useful tools to further study pathogenesis of *C.albicans* infection and to assess new therapeutic measures and drug development.
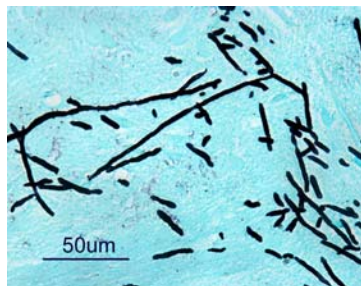
Fig.1. Light microscopic view of Candida infected brain from 8-week-old mice stained with fungal specific GMS stain. Candida filaments and yeast cells are stained in black.
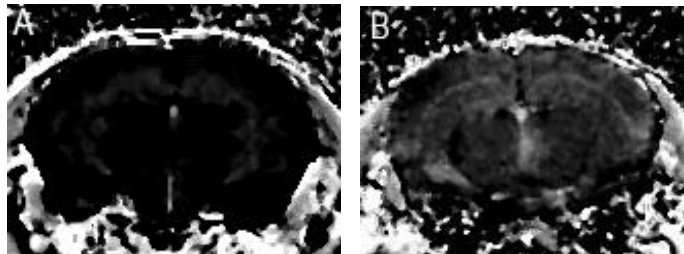
Fig-2 ([PostGd-PreGd]/Post Gd)% images of A) normal and B) infected mouse brain. The infected mouse brain has signal enhancement due to possible Gd leakage through the BBB in the brain cause by Candida.
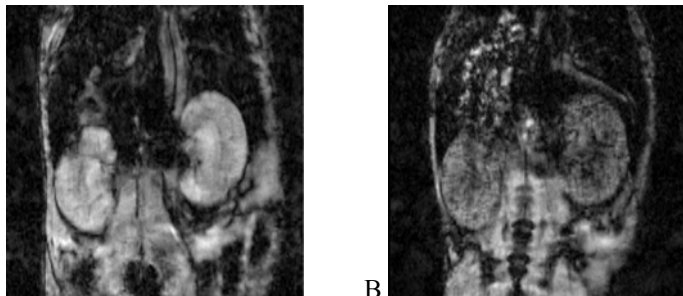
Fig. 2. Post USPIO images of A) Healthy and B) Infected mouse kidneys.

Epileptogenesis leading to brief seizures do not cause MRI changes in brains of Rats

Munasinghe J.P.[2], Acosta M.T.[4], Guerron D.A.[4], Zhang L.[3], Theodore W.H.[1]

[1] Epilepsy Research Laboratory, [2]Mouse Imaging Facility. National Institute of Neurological Diseases and Stroke, [3] National Cancer Institute. National Institutes for Health, Bethesda, MD. [4] Department of Neurology Children's National Medical Center, Washington DC. USA.

Glutamate receptors are implicated in altered excitation and inhibition leading to epileptogenesis. Increased excitatory neurotransmission may lead to lesions such as mesial temporal sclerosis that underlie epileptic foci. MRI studies in animal models of status epilepticus have shown significant structural changes and evolution of MTS-like lesions, but the effect of repeated single seizures without status is unknown. We used three different glutamate receptor agonists, ATPA, a specific KAr GluR5 subtype agonist, Kainic acid (KA), activating several receptor subtypes, and AMPA, agonist for AMPA gluR1-4 subtype, to evoke single seizures in rats . T_2, Apparent diffusion coefficient (ADC) and volumes of selected ROIs were evaluated to quantify acute and chronic regional changes in brain.

Rats were monitored with serial EEG and MRI at 24 hours, 1 week, 2 weeks, 4 weeks and 12 weeks post infusion. Rats anesthetized with 1.5% isoflurane had an MR-compatible cannula for EEG recordings placed stereotaxically in frontal lobe and rested. Single doses of each convulsant drug, and normal saline, each were given *i.v.* to four rats in doses that led to single seizures but not status epilepticus; valium (5 mg/kg) was administered if needed to stop progression. For each MRI, the rats were intubated, paralyzed with pancuronium, placed in a stereotaxic holder and mounted in a 72/25 mm, transmit/receive coil ensemble. Body core temperature was maintained at 37^0 C. MRI was performed on a horizontal 7 Tesla scanner. Eight 1 mm thick axial amygdale centered slices were acquired using a fast spin echo (8 echos) sequence for regional anatomical delineation (In-plane resolution = 150 μm. TE/TR = 10/2000 ms). Multi echo T_2 weighted (TE = 10 ms, 16 echoes, TR = 3 s, Matrix 128^2) and diffusion weighted (in three orthogonal directions) sequences (b = 4, from 0 to 3000 g/cm, TE/TR = 20/2500 ms, D = 32 ms, matrix = 64^2 or 128^2) with same geometry (FOV = 3.2 cm) were performed. Quantitative measurements were performed at each time point over 12 weeks, with regions of interest (ROI) placed in left and right amygdala, hippocampus, thalamic region, sensory and motor cortices of both hemispheres to investigate any widespread brain activation. All animals were then perfused and brain histology studied.

Ictal electrographic activity was present during drug infusion in the context of minimal clinical seizure activity; no animal developed SE at any time. Intermittent ictal and interictal EEG discharges persisted during the observation period for all convulsants (Fig-2). T_2, ADC showed local variation among drugs similar to saline during the course of the study (Table-1); differences were not statistically significant. We did not detect significant morphological changes (Fig-1).

Our study suggests that single intermittent seizures or abnormal electrographic seizure activity do not lead to structural or functional alterations in rats given ATPA, AMPA or KA. Transient variation in cortical or limbic structures due to convulsions induced by glutamatergic agonists may occur after one hour of seizure activity. However, in our chronic study, there was no evidence of neuronal injury from seizures not leading to SE.
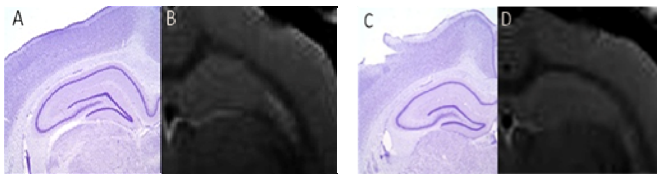
Fig-1 Histology and MRI images of the hippocampal regions of A &B) saline C &D KA treated rats
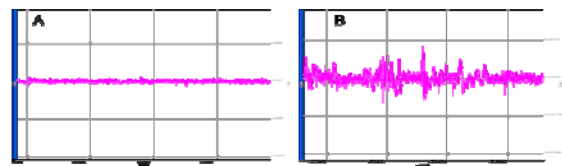
Fig-2- EEG discharges in A) saline and B) KA treated rats.

Parameter	saline		KA	
	Pre-infuse	week12	Pre-infuse	week12
ADC	1.12±0.05	1.08±0.05	1.07±0.03	1.11±0.02
T_2	60.5±2.75	57.03±0.88	60.6±1.14	59.65±1.2
Vol%	4.49	5.04	4.72	4.89

Table-1 Variations in 3 parameters for the Hippocampus for saline and KA over 12 weeks.

Mapping dopaminergic pathways by pharmacological MRI

A.T. Perles-Barbacaru, D. Procissi, A. V. Demyanenko, R. E. Jacobs

Caltech Brain Imaging Center, California Institute of Technology, Pasadena, CA

Abstract:

The specific aim of this project is to study monoamine neurotransmission abnormalities after cocaine administration in transgenic monoamine transporter knock out mouse models using non-invasive cerebral blood volume (CBV) weighted pharmacological magnetic resonance imaging (MRI).

All procedures are carried out in a 7T Bruker Biospec/Avance 30 cm horizontal bore magnet under general anesthesia using isoflurane. The MR signal is made sensitive to the CBV change accompanying neuronal activity, by overpowering the blood oxygenation level dependent effect [1] on T_2*-weighted images of the brain with the intravenous injection of a superparamagnetic contrast agent [2, 3]. Figure 1 shows: a) a coronal ΔR_2* map (= relative CBV map) obtained by an intravenous injection of 25 mg/kg P904, a new contrast agent from Guerbet Laboratories in France, and b) the corresponding pre-contrast fast gradient echo image of the mouse head.

Neuronal activity in specific pathways is elicited by a pharmacological challenge with cocaine injected intraperitoneally 30 min after P904 injection. Figure 2 shows the time course of the CBV-weighted signal from the nucleus accumbens (N. acc.) in a dopamine transporter deficient mouse, illustrating a CBV decrease after a 30 mg/kg cocaine dose. Figure 3 shows maps of the vascular response at different time points after cocaine administration depicting spatial differences.

No spatial or quantitative differences of the hemodynamic response to cocaine were found between dopamine transporter knock out mice and healthy control mice, which is probably due to the adaptations that occur in the monoamine neurotransmitter systems in these mice. Contrary to the vascular response in rats [4], acute intravenous cocaine administration leads to a general CBV decrease that has also been observed in monkeys [5] and humans [6] and is believed to reflect neuronal deactivation [7]. However, it is also possible that increased levels of dopamine have a direct vascular effect.

Figure 1: a) Relative cerebral blood volume (CBV) map of a coronal slice through a mouse brain before cocaine injection, and b) the corresponding T_1 weighted slice through the mouse head. Spatial resolution: $0.19 \times 0.19 \times 0.75$ mm^3.
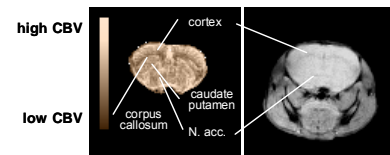
Figure 2: Signal time course in the N. acc. in a pharmacological MRI experiment involving contrast agent (CA) injection and a pharmacological challenge (cocaine). The gray plot is the original signal, the black plot is corrected for CA elimination (half life 5 hours). This signal is converted to relative CBV and the CBV change (ΔCBV) can be quantified by setting the signal drop upon CA injection to 100% (red plot, right axis). It shows the CBV decrease after cocaine administration with respect to the pre-cocaine baseline blood volume.
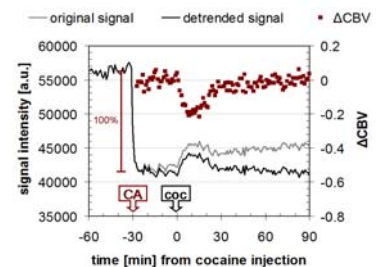
Figure 3: Maps of the CBV change at different time points after cocaine administration. The blue color corresponds to a CBV decrease. The vascular response in brain structures differ in amplitude and duration.
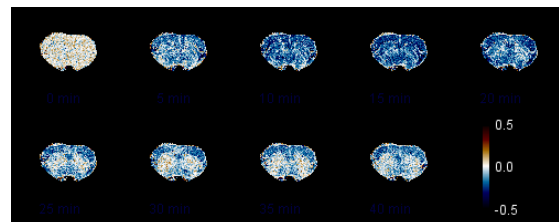
1. Ogawa, S., et al. *Magn Reson Med*, 1990. **14**(1): 68-78.
2. Berry, I., et al. *Magn Reson Med*, 1996. **36**(3): 415-9.
3. Mandeville, J.B., et al. *Magn Reson Med*, 1998. **39**(4): 615-24.
4. Marota, J., et al. *Proceedings of the International Society for Magnetic Resonance in Medicine*. 1997.
5. Mandeville, J.B., et al. *Proceedings of the International Society for Magnetic Resonance in Medicine*. 2005.
6. Kaufman, M.J., et al. *Psychopharmacology (Berl)*, 1998. **138**(1): 76-81.
7. Peoples, L.L., et al. *J Neurosci*, 1998. **18**(18): 7588-98.

3D MR microscopy of chemically fixed human embryos at 9.4 T

Yosuke Otake[1], Shinya Handa[2], Katsumi Kose[1], Kouhei Shiota[3], Shigeto Yamada[3]

1. Institute of Applied Physics, University of Tsukuba, 2. Japan Society for the Promotion of Science,
3. Center for Congenital Anatomy Research, Kyoto University

Introduction: In 2007, our group reported 3D MR microscopic images of 1,204 chemically fixed human embryos selected from the Kyoto Collection of Human Embryos (1). The number of the image voxels for these images was limited to $128 \times 128 \times 256$ voxels, primarily because of the magnetic field strength (2.34 T). In this study we developed a 9.4 T MR microscope with a wide dynamic range (~90dB), and acquired 3D MR microscopic images of chemically-fixed human embryos using a $256 \times 256 \times 512$ image matrix.

Materials and method: Carnegie Stage (CS) 17 to 22 human embryos were selected from the Kyoto Collection (2). The specimens were stored in NMR sample tubes filled with formalin solution and used for MR microscopy measurements. The MR microscope was developed using a 9.4 T vertical wide bore (89 mm) superconducting magnet (JASTEC, Kobe, Japan), a home-built gradient probe, and an MRI console developed in our laboratory (3). The MRI receiver system consisted of two parallel MRI receivers (DTRX4, MRTechnology, Tsukuba, Japan) with different gain (typically 30 dB difference). NMR signals were simultaneously acquired with the two receiver channels, and the MRI dataset in the k-space was synthesized from those acquired with the two channels. A 3D gradient echo pulse sequence (TR/TE = 100 ms/12 ms, FA = 90°, NEX = 12) was used for the $256 \times 256 \times 512$ voxel image acquisition.

Results and discussion: Figure 1 shows mid-sagittal sections of CS17 - CS22 human embryos selected from the 3D image datasets. The voxel size varied from 40 to 60 $(\mu m)^3$. Figure 2 shows maximum intensity projection (MIP) images made from the same 3D image datasets. Developments of internal structures are clearly visualized.

To obtain high resolution and large matrix MR microscopic images, high SNR and wide signal dynamic range are required (3). We solved these problems using a 9.4 T SCM and parallel receivers. The obtained results demonstrated the effectiveness of our aproach.

CS17: $(40\mu m)^3$ CS18: $(45\mu m)^3$ CS19: $(50\mu m)^3$ CS20: $(60\mu m)^3$ CS21: $(60\mu m)^3$ CS22: $(60\mu m)^3$
Fig. 1 Midsagittal cross-section
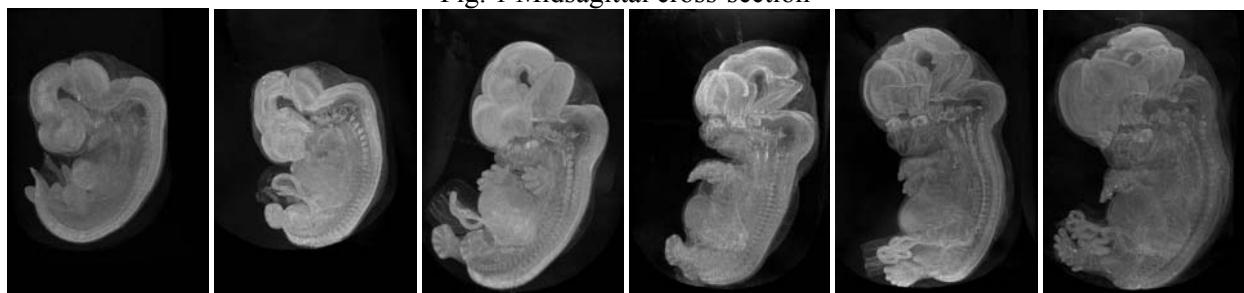
CS17   CS18   CS19   CS20   CS21   CS22
Fig. 2 Maximum intensity projection

P79 - Continued

References
1. Y. Matsuda et al. Magn. Reson. Med. Sci. **6**, 139-146 (2007).
2. Nishimura H et al. Teratology **1**, 281-290 (1968).
3. Y. Otake et al. Concepts Magn Reson (Magn Reson Engineerling) **29B,** 161-167 (2006).

MR Micro-imaging of Articular Cartilage

James M. Pope, Sally K. de Visser, R. Mark Wellard and Konstantin I. Momot

School of Physical & Chemical Sciences and Institute of Health and Biomedical Innovation
Queensland University of Technology, Brisbane, Qld 4001, Australia

Articular cartilage (AC) is a connective tissue covering the articulating surfaces of long bones. Its macromolecular scaffold consists primarily of collagen and proteoglycans. AC is anisotropic due to the alignment of collagen fibres, and non-uniform because the alignment varies between the three histological zones present in healthy AC. Its appearance in conventional MRI is complex, exhibiting orientation-dependent contrast that reflects both the anisotropy and heterogeneity. An understanding of the MR characteristics of AC is important clinically e.g. in osteoarthritis. However, a meaningful **interpretation of clinical MRI results from cartilage is currently complicated**, due to the complexity of the system and to the lack of parametric models to translate MRI parameters into quantitative information about the tissue. We aim to develop new micro-MRI methodologies for quantitatively probing the anisotropic microstructure of articular cartilage.

We have previously shown that the principal eigenvector of the diffusion tensor (DT) reflects the predominant alignment of collagen fibres in articular cartilage [1,2]. We have also shown that the DT principal eigenvector can be used to probe the reorganisation of collagen fibres under mechanical load (see Fig. 1) [3]. Here, we present the results of **Monte Carlo simulations of anisotropic diffusion** in AC [4], including a correlation between the magnitude of the fractional anisotropy of the DT and the volume fraction of collagen. In order to make possible *in vitro* micro-MRI of cartilage under controlled mechanical load, we have designed an **MRI-compatible cartilage consolidometer**; a prototype consolidometer is presented.

$T2$-weighted imaging complements the information obtained from DTI and is potentially better suited to clinical use due to its shorter acquisition time. We present a theoretical analysis of the **anisotropy in transverse relaxation** of water in tendon and cartilage. We show that the form of the experimentally observed anisotropy [5,6] is explained by a model where a water molecule hydrogen bonded to a collagen fibre undergoes rapid but restricted rotational diffusion (such that the intramolecular dipolar interaction is partially averaged), combined with a slow diffusional walk
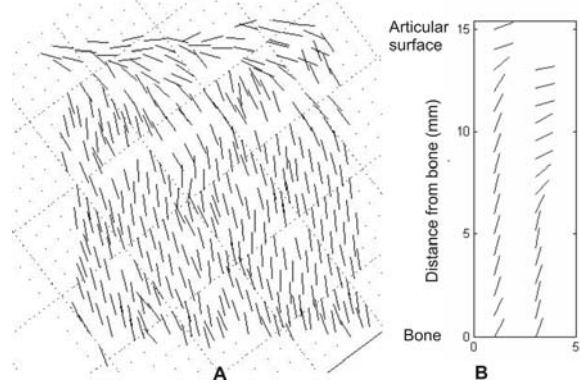
Figure 1. Effect of compression on DTI of cartilage [3]: (A) Typical orientation map of the principal diffusion eigenvector; (B) The average eigenvectors in uncompressed sample (left) and after 13% compression (right column).
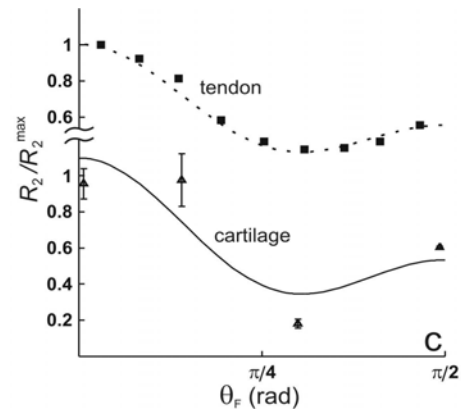
Figure 2. Comparison of the experimentally observed dependence of normalised transverse relaxation rates on the orientation of the collagen fibres in cartilage [6] and tendon [5] with the anisotropy calculated from our models. The curves which follow a relationship of the form:

$$R_2 = (1 - p_B)R_{2F} + p_B R_{2B}(0)\left(\frac{3\cos^2\theta_F - 1}{2}\right)^2$$

were calculated with the following parameters: cartilage, $p_B = 0.05$, $R_{2B}(0)/R_2^{max} = 15.0$, $R_{2F}/R_2^{max} = 0.363$; tendon, $p_B = 0.05$, $R_{2B}(0)/R_2^{max} = 11.9$, $R_{2F}/R_2^{max} = 0.427$.

P80-Continued

about the collagen fibre, (probably mediated by exchange with free water). This results in an anisotropic $R2$ of the bound species that exhibits a minimum at the magic-angle (see Fig. 2) [7].

References
[1]   R Meder et al, Osteoarthr. Cartilage 14 (2006) 875-881.
[2]   SK de Visser et al, Osteoarthr. Cartilage 16 (2008) 689-697.
[3]   SK de Visser, RW Crawford, JM Pope, Osteoarthr. Cartilage 16 (2008) 83-89.
[4]   KI Momot, Monte carlo analysis of anisotropic diffusion in articular cartilage. Work in progress (2009).
[5]   G Navon, U Eliav, DE Demco, B Bluemich, J. Magn. Reson. Imaging 25 (2007) 362-380.
[6]   Y Xia, JB Moody, H Alhadlaq, Magn. Reson. Med. 48 (2002) 460-469.
[7]   KI Momot et al, Anisotropy of spin relaxation of water protons in cartilage and tendon. Submitted to NMR in Biomedicine (2009).

P81

Quantifying High Concentrations of SPIO with TurboSPI

James A. Rioux[1,2], <u>Steven D. Beyea</u>[1,2,3], Chris V. Bowen[1,2,3]

[1] National Research Council – Institute for Biodiagnostics (Atlantic), Halifax, NS, Canada
[2] Department of Physics, Dalhousie University, Halifax, NS, Canada
[3] Departments of Radiology and Biomedical Engineering, Dalhousie University, Halifax, NS, Canada

Abstract:

MRI is a valuable tool in the non-invasive monitoring of cellular therapies, since cells labeled with super-paramagnetic iron oxide (SPIO) can be detected by a variety of MR techniques [1]. To evaluate the progress and effectiveness of cell therapies, quantitative information about cell density is necessary. When compartmentalized within cells, SPIO greatly increases the local R_2^*, with a far smaller effect on R_2, making R_2^* the parameter most sensitive to fluctuations in cell density [2]. However, at the densities required for cellular therapy, R_2^* is large enough to totally dephase signal even at very short echo times, making accurate quantification difficult.

We are exploring the use of TurboSPI [3] for quantifying the large R_2^* associated with high densities of SPIO. TurboSPI is a pure phase encoded sequence which samples the complete rise and fall of the spin echo at each k-space point (Fig. 1). The shape of this echo in the presence of small magnetic perturbers is well described [4] and can be fitted to extract an R_2^* value for each pixel in an image. Using this technique, we have quantified R_2^* for micron-sized SPIO particles suspended in gelatin, over a wide range of concentrations (Fig. 2). The highest concentration used corresponded to 7pg of SPIO per cell at a density of 4×10^6 cells/mL, which is a reasonable density and loading level for cellular therapies [5].
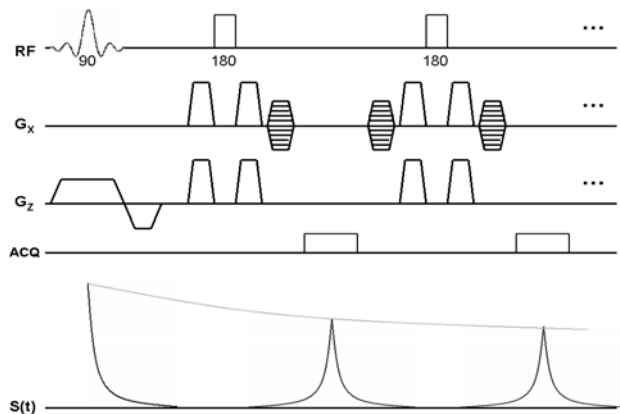
Fig. 1: TurboSPI pulse sequence showing the first 2 and echoes of the train. Signal decays with R_2 (grey) But rephases with R_2^* (black) during each echo. Images are purely phase encoded with no readout gradient.
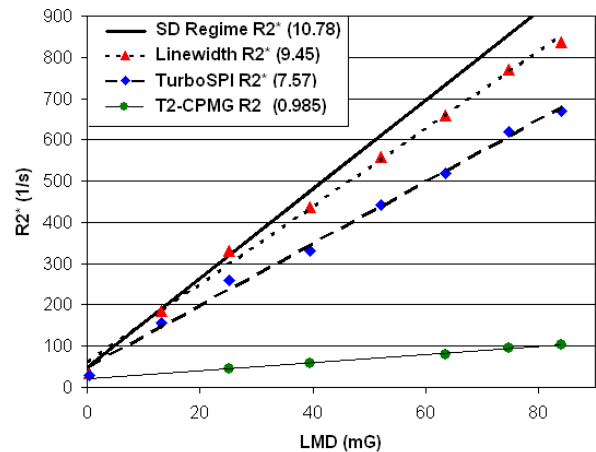
Fig. 2: Relaxation behaviour of SPIO particles in gelatin. R_2^* was measured by linewidth (red) TurboSPI (blue), and R_2 measured with a CPMG sequence (green). Slopes of lines are given in the legend; predicted slope is shown by the solid line.

1. J. Bulte et. al., *Current Pharmaceutical Biotechnology* **5** (2004) 567-584.
2. C. Bowen et. al., *Magnetic Resonance in Medicine* **48** (2002) 52-61.
3. S. Beyea et. al., *Journal of Magnetic Resonance* **144** (2000) 255–265.
4. D. Yablonskiy, *Magnetic Resonance in Medicine* **39** (1998) 417-428.
5. J. Frank et. al., *Radiology* **228** (2003) 480-487.

High Resolution Asymmetric Spin-Echo (ASE) Spiral fMRI: An Examination of Functional Contrast & Specificity

K. D. Brewer[1,3], L.A. Cherpak[1,3], R.C.N. D'Arcy[2,3], C. V. Bowen[1-3], and S. D. Beyea[1-3]

Department of [1]Physics & [2]Radiology, Dalhousie University, Halifax, NS, Canada,
[3]Institute for Biodiagnostics (Atlantic), National Research Council of Canada, Halifax, NS, Canada,

Introduction: Recently, our group developed a sequence, Asymmetric Spin-Echo (ASE) Spiral, for recovering signal and fMRI activation in regions of strong susceptibility-induced field gradients (SFG) [1]. This sequence acquires up to three images per excitation, each with spiral-in apodization, equivalent T_2'-weighting and increasing T_2-weighting. This is of particular interest, as studies have shown that T_2'-weighting increases BOLD sensitivity while T_2-weighting increases BOLD specificity to "true" neuronal activity [2]. In this work, we investigated the effect of increased T_2-weighting on activation using a visual fMRI task and have observed improved neurovascular coupling with activation patterns more specific to parenchyma, rather than with activation clusters co-located with large draining veins.

Methods: All data were acquired using a 4T whole body MRI system. Four 3-mm, high resolution (128x128) axial slices per volume (covering the primary visual cortex) were acquired using Spiral-In/Out (TE=30ms), Spin-Echo-In/Out (TE=105ms) and the ASE triple spiral sequence (TE=75ms, TE*=30ms). A venogram was also acquired for the same slices. FMRI experiments with an alternating radial checkerboard were used to elicit activation in the visual cortex. An activation map was calculated for each image (cluster threshold = $p<0.05$) using FSL [4] and overlaid on the venogram to examine whether activation was localized to veins.
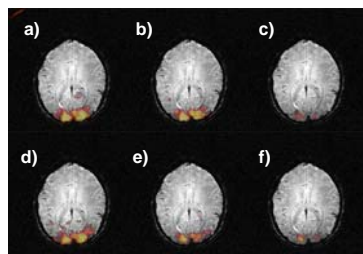
Figure 1 - fMRI activation from a visual checkboard stimulation, overlaid on a venogram. Images are shown for a) Spiral-In, b) Spiral-Out, c) Spin Echo Spiral-In/Out, as well as d) ASE Spiral Image 1, e) Image 2 and f) Image 3. Z-scores range from 2.3-12.

Results: Conventional T_2*-weighted Spiral-In (Fig 1a) and Spiral-Out acquisition (Fig 1b) have an activation pattern and extent that is similar to that of the first ASE image (Fig 1d). The latter ASE images (Fig 1e and f) were more heavily T_2-weighted, in addition to their matched T_2'-weighting, and the third ASE image (Fig. 1f) corresponded most closely to the purely T_2-weighted acquisition (Fig. 1c). It is noteworthy that the activation clusters remaining in Fig 1c and 1f were localized to the primary visual cortex. Recombined ASE images can also be expected to have improved specificity, through weighting of the combined data to the latter images. This is shown in Fig. 2, in which active draining vessels in the Spiral-In/Out acquisition exhibit little or no activation in the ASE Dual Spiral acquisition.

Figure 2 - fMRI activation maps acquired using a) Spiral-In/Out sequence, and b) ASE Spiral Sequence. Note the large draining vessels indicated by the black lines.

Conclusions: The ability to obtain images with matched BOLD-weighting and increasing T_2-weighting during the same acquisition is a novel feature of the ASE sequence. Control over the relative contribution of conventional T_2* BOLD contrast and T_2 dependent fMRI contrast permits the optimization of sensitivity and specificity in the final combined fMRI images.

References: **[1]** Brewer K.D., Rioux J.A., D'Arcy R.C.N., Bowen C.V. & Beyea S.D., *NMR in Biomed.* (2008). **[2]** Duong T.Q., Yacoub E., Adriany G., Hu X., Ugurbil K. & Kim S.G. *Magn. Reson. Med.* **49** 1019-1027 (2003).

The use of magnetoliposomes as MRI contrast agents and for targeted drug delivery

Urša Mikac[1], Ana Sepe[1], Georgy Mikhaylov[1], Anna A. Magaeva[2], Volya I. Itin[2], Sergej G. Psakhye[2], Boris Turk[1] and Olga Vasiljeva[1]

[1]J. Stefan Institute, Ljubljana, Slovenia
[2]Tomsk Scientific Center, Siberian Branch of Russian Academy of Sciences, Tomsk, Russia

Abstract:
The development of new effective drug delivery systems for the treatment of cancer is one of the top priority trends in the biomedical technology of the last decade. Among the different methods of drug delivery, magnetic drug targeting could be a promising approach by possibility of specific delivery of chemotherapeutic agents using magnetic nanoparticles and an external magnetic field which is focused on the tumor. Recently, magnetic nanoparticles have attracted additional attention because of their potential as contrast agents for magnetic resonance imaging and heat mediators for cancer therapy. Currently there are two approaches for the use of magnetic nanoparticles in targeted drug delivery: (i) chemotherapeutic agent is coupled directly to the nanoparticles or, (ii) both the drug and the magnetic nanoparticles are encapsulated into the lipid vesicle, forming magnetoliposomes [1, 2].

In our study super paramegnetic iron oxide nanoparticles (SPIO) with the average size of 7 nm were incorporated into the liposomes resulted in the bionanocomposites with the average size of 92 nm. The negative contrast on T_2-weighted MR images was proven on tumor samples *ex vivo*. The efficiency of the magnetoliposomes (potentially containing anti-cancer drug) for the targeted delivery to the specific tumor was tested *in vivo* using transgenic and transplanted mouse breast cancer models. First, pre-contrast T_2-weighted images were acquired. After the injection of magnetoliposomes the magnet (0.3 T) was attached to the skin over one tumor and MR images were taken after 1 hour and 48 hours. After 1 hour some darkening on the tumor exposed to the magnet was observed and 48 hours after injection a clear darkening was observed on the tumor exposed to the magnet indicating preferential accumulation of magnetoliposomes. The results proved the efficiency of the targeted delivery as well as magnetic contrast efficiency of the produced magnetoliposomes.

1. J. P. Fortin-Ripoche et al, *Radiologyl* **239** (2006) 415-424.
2. M. S. Martina et al, *J. Am Chem. Soc.* **127** (2005) 10676-10685.

Influence of Relaxivity on Cartilage Glycosaminoglycan Imaging by Gadolinium Contrast in MRI

ShaoKuan Zheng[1] , Yang Xia[2]

[1,2]Oakland University, Rochester, MI 48309, USA

As one of the three major molecular components (water, collagen, and proteoglycan) in articular cartilage, proteoglycans play a critical role in maintaining the mechanical stiffness of the tissue because they have heavily sulfated side-chains of glycosaminoglycan (GAG), which carry a high concentration of negative charges contributing to the stiffness of the tissue [1]. Since the loss of GAG is regarded as one of the early signs of the tissue degradation leading to the clinical diseases such as osteoarthritis, quantitative detection of GAG is invaluable. By the administration of a paramagnetic contrast agent, $Gd(DTPA)^{2-}$, the dGEMRIC procedure in MRI [2] can produce a GAG map via the T1 imaging.

This project concerns the experimental value of $Gd(DTPA)^{2-}$ ions' relaxivity (R-value) in cartilage, which is a critically important parameter in the quantification of GAG concentration in cartilage using dGEMRIC. A Bruker AVANCE II 7-Tesla/89-mm system was used. The R-value in a series of skim-milk solutions at 0-40% milk concentrations was measured using NMR spectroscopy and found to be approximately linearly proportional to the concentration of the solid component in the milk solution. Using the R-value at 20% solid component (which is the solid concentration of BNC), the GAG concentration in bovine articular cartilage (BNC) were quantified using the MRI dGEMRIC method at 26μm resolution **without** the customary scaling factor of two. We have also exhausted nearly all possible techniques that can be used to quantify the GAG concentration in BNC, including ^{23}Na NMR spectroscopy, ^{23}Na inductively-coupled-plasma (ICP) analysis, and biochemical assay. The GAG concentrations (mg/ml w.w.) in BNC by different methods are summarized in the following Table.

	dGEMRIC MRI		^{23}Na NMR Spectroscopy	^{23}Na ICP	Biochemical Assay
	Original [2] (R=4.17, SF=2)	**Our Method (R=5.77, SF=1)**			
Block 1	131.9±11.6 (n=4)	83.4±6.5 (n=4)	85.6±2.6 (n=4)	87.1±1.9 (n=3)	96.8±3.3 (n=8)
Block 2	107.9±4.9 (n=7)	70.1±2.7 (n=7)	69.6±3.0 (n=3)	68.1±5.9 (n=7)	86.7±7.6 (n=7)

We found that an appropriate definition for the concentration of Gd ions in macromolecule material is critically important in the calculation of GAG concentration by the MRI dGEMRIC method. **If** the R-value of the Gd ions was set to be the relaxivity of ions in the 20% solid milk solution, the GAG concentration in BNC can be quantified without the customary scaling factor of two in the original dGEMRIC technique [2], provided that the Gd concentration in the milk solution was defined as *millimole per volume of skim milk solution*. This result supports the quantitative determination of the GAG concentration in articular cartilage, if the R-value at 27.5% solid component (which is the solid % of articular cartilage) was used.

References: [1] Y Xia, *Investigative Radiology*, **35** (2000), 602-621.
[2] A Bashir, ML Gray, D Burstein, *Magn Reson Med*, 36 (1996), 665-673.

MR Microscopy Towards Detection of Neuronal Currents

Igor Serša[1]

[1] Jožef Stefan Institute, Jamova 39, 1000 Ljubljana, Slovenia

One of the greatest challenges of MRI is detection of weak electric currents in biological systems. The ultimate goal is MRI detection of neuronal currents, which would have enormous implication in neurology. However, present limitations of current density imaging (CDI) prevent its clinical use. Standard CDI techniques use phase encoding to store information on the magnetic field change that is caused by application of currents. The phase change is then used to calculate the current density using the Ampere law. For successful current detection phase shifts caused by currents must be large enough. This can be achieved either by increasing currents or by increasing time of their application. As biological tissues have normally relatively low conductivity and high voltage would damage the sample the only alternative is to prolog the encoding time, i.e., the current application time. However, the encoding time is again limited by the relaxation properties of the sample and it depends also on the imaging method used. In conventional imaging methods magnetic field gradients are evenly distributed throughout the imaging sequence. A consequence of that is the signal attenuation due to diffusion, which is quite apparent in MR microscopy experiments. In addition, long signal encoding times are often associated with a signal loss due to the T_2^* effect. Therefore, it is practically impossible to use signal encoding periods longer than 100 ms with the standard imaging approach.

A new CDI method is presented that extends the current encoding time up to one second in aqueous samples. The method uses a CPMG train of hard RF pulses that are synchronized with current pulses with alternating polarity [1], which is followed by the two-shot RARE based fast signal acquisition [2]. An increased sensitivity of the CDI sequence stems from a long current encoding period that is enabled by the CPMG RF pulse train without the use of imaging gradients, and from signal averaging enabled by the rapid signal acquisition. The CDI sequence was tested on a test sample consisting of two concentric cylinders (3 mm inner conductive cylinder and 10 mm outer reference cylinder) filled with a physiological solution (0.5% saline). The inner cylinder had electrodes at both ends and was connected to a 1 V voltage supply so that the current amplitude through the inner cylinder was 250 µA. The current encoding time, during the CPMG train of 20 refocusing RF pulses, was 800 ms long and 100 signal averages was used to increase the CDI sensitivity. Current density noise in the calculated CD image was equal to 0.1 A/m^2 which corresponds to the current noise per image pixel of 5 nA (image field of view was 15 mm and the image matrix was 64 by 64).

In summary, by increasing the current encoding time and by rapid imaging with several signal averages, CDI sensitivity was increased by a factor of 500 compared to the conventional CDI experiment. However, this promising method needs further testing on biologically relevant samples.

1.   Mikac, U., et al., Magn Reson Imaging, 2001. **19**(6): p. 845-56.
2.   Sersa, I., J Magn Reson, 2008. **190**(1): p. 86-94.

Diffusion as a tool for understanding tissue differences in healthy and emphysematous lungs

Michelle Milne[1], Mark Conradi[1]

[1] Washington University, St. Louis, MO, USA

Abstract:

In this study, diffusion NMR of ^{3}He and perfluorinated gases has been used to explore the structure of samples of excised human lung at a variety of length scales. In detail, perfluorinated gases are used to expore small length scales (smaller than can be imaged directly) to obtain information about surface-to-volume ratios, as suggested by Mitra et. al. [1]. Stimulated-echo diffusion NMR takes advantage of the long T_1 available with ^{3}He and this gas's large free diffusivity to probe lung connections across long distances. Tisssues from both healthy and emphysematous lungs were compared in order determine where the greatest disparity is found between the relative apparent diffusion coefficients.

1. Mitra et. al., *Phys Rev B* **Vol 37** (1993) 8565-8574.

³He MR Microscopy of Pulmonary Airflow in Live Rats

Kevin R. Minard[1], Richard E. Jacob[1], Gernot Laicher[2], Daniel R. Einstein[1], James P. Carson[1], Andrew P. Kuprat[1], H.T. Robertson[3] and Richard A. Corley[1]

[1] Pacific Northwest National Laboratory, Richland, WA 99352 USA
[2] University of Utah, Salt Lake City, UT 84112 USA
[3] University of Washington, Seattle, WA 98195 USA

Abstract:

Since describing our initial use of ³He MR for visualizing the three-dimensional (3D) vector flow of inhaled gas in live rats [1], we have developed powerful new post-processing techniques for rendering results in ParaView's open-source visualization environment [2]. Figure 1 illustrates how this enables the calculation of airstreams from measured gas velocity (A), facilitates assessment of local airspeed (B), and highlights air streaming along the trachea's outside radius of curvature (C). To assess the accuracy of our MR results, this presentation will describe validation studies performed using inhaled fluorescent microspheres. The general approach exploits data like that shown in Fig. 1 for measuring the fraction of inhaled air delivered to each of the rat's five lung lobes. Accuracy is then assessed by comparing MR results with the fraction of total inhaled fluorescence that is deposited in each lobe after aerosol administration in the same rats. Results establish the quantitative nature of MR flow measurements and provide a firm foundation for new applications. Possibilities that will be discussed include the use of ³He flow MR for measuring lobar lung compliance, and our ongoing efforts to develop, refine, and validate computational models of inhaled airflow and lung mechanics [3].
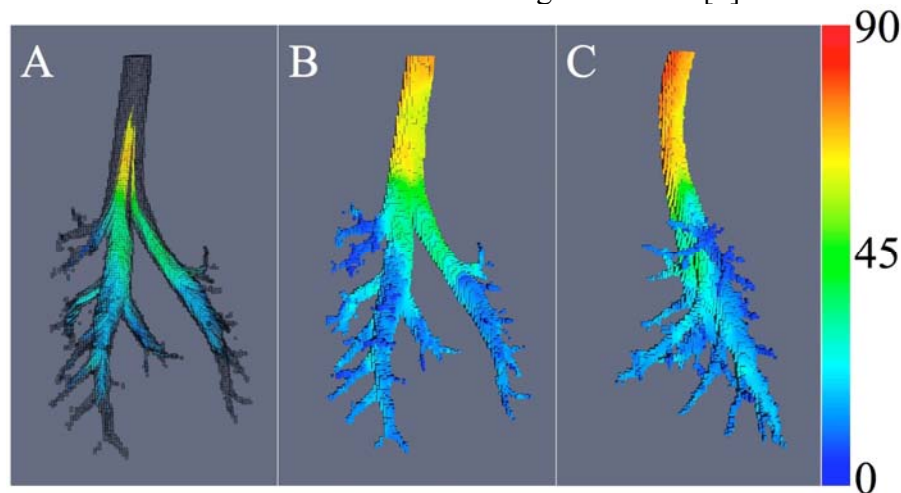
Figure 1: Typical in vivo ³He flow data acquired from a live, 250 g Sprague-Dawley rat. Calibrated color scale depicts gas speed in cm/s.

1. K.R. Minard et. al., *JMR* **194** (2008), 182-191.
2. http://www.paraview.org/
3. http://www.respiratorytract3d.org/

Diffusion of Water in Whey Protein Isolate Gels

Mecit Halil Oztop[1], Kathryn L. McCarthy, [2] Moshe Rosenberg[3,] Yael Rosenberg[4] and Michael J. McCarthy[5]

[1,2,5]   Biological & Agricultural Engineering, University of California/Davis, Davis, CA, USA
[2, 3, 4,5] Food Science & Technology, University of California/Davis, Davis, CA, USA

Abstract:
Whey protein-based gels absorbs water and exhibit pH-depended swelling when placed in a dispersing medium which makes them excellent devices for controlled release applications. Extent and rate of swelling affects the release of compounds of interest included in the gel. Understanding the physical principles that govern gel swelling is thus important when designing gel-based delivery platforms. The swelling rate of the gels is commonly monitored gravimetrically. **M**agnetic **R**esonance **I**maging (MRI) is a real-time non-invasive imaging technique that offers unique opportunities for monitoring changes, with time, in dimensions, geometry and water content of matrices. MRI can provide highly detailed information about swelling behavior of gels in continuous manner. Heat-set whey protein gels doped with $MnCl_2$ (0.075g/1000g solution) were prepared (with WPI solution containing 17% at 90 ^{o}C for 30 min) and swelling and diffusion of water was monitored in a solution of pH 7 by using a Multi Slice Spin Echo sequence (TE=20ms, TR=600ms) . Relative changes with time, in the total number of the voxels characterizing the gel in an image and the total signal intensity were compared with extent of swelling determined by gravimetric measurements. An excellent correlation (R^2=0.99) between results from the two methods was obtained. In addition, the images taken during swelling (Figure 1) gave us information about the mechanism of the swelling , the change in volume and how concentrations boundaries are changing which is useful for mathematical modelling of the process. It is also possible to calculate the velocity of the advancing front from the images which is necessary for the development of a mathematical model. The results demonstrated that monitoring swelling using MRI provided detailed information about swelling-related phenomena that was superior to that obtained gravimetrically and provides more information to develop mathematical models for the process.
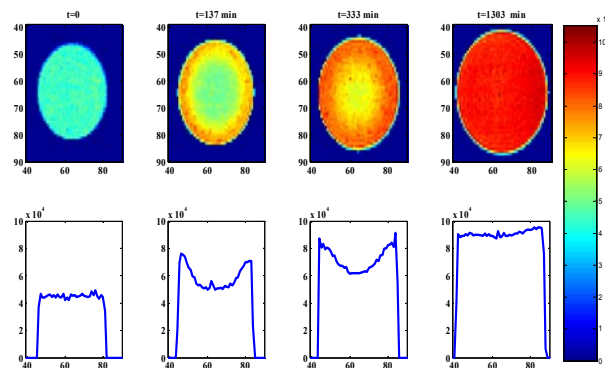
Figure 1. Diffusion/Swelling in whey protein gels with respect to time

Investigation of different dehydration methods on proton environment in onions using ^{1}H-NMR relaxometry

Maria E. Gonzalez[1], Mecit Oztop[2], Seda Ersus[1,3], Michael McCarthy[1,2] and Diane Barrett[1]

[1]Department of Food Science & Technology, University of California, Davis, Davis, CA
[2]Department of Biological & Agricultural Engineering, University of California, Davis, Davis, CA
[3]Department of Food Engineering, Ege University, Izmir, Turkey

The effect of different osmotic solutions and air drying on proton relaxation components in onion tissue was studied with ^{1}H-NMR relaxometry. Onion disks of 2 cm diameter and approx. 4mm thickness were immersed in 20 ml per disk of 0M (deionized water), 0.2M, 0.4M, 0.6M or 0.8M mannitol solutions for a period of 4 hours, after which T_2 measurements were obtained. For air drying experiments, onion disks were dehydrated in chambers of low relative humidity at 23 °C and the change in sample weight was recorded after 15, 30, 60 and 120 minutes. Decay curves due to transverse relaxation (T_2) were measured using the Carr-Purcell-Meiboom-Gill (CPMG) pulse sequence immediately after the dehydration experiments. T_2 distributions and relative peak areas were used to infer the effect of the different dehydration methods on the proton relaxation components in the onion tissue. T_2 distributions of osmotically tretaed onions were also compared with the results obtained from neutral red dye staining and light microscopy visualization. Relaxometry analysis gave five different proton relaxation components **(Figure 1)** inside the onion tissue. T_2 of the largest components decreased with increasing mannitol concentration which is consistent with gravimetric changes and the change in cell dimensions due to plasmolysis **(Figure 2)**. T_2 changes in air dried samples also indicated a T_2 decrease as dehydration time increased . The results showed that relaxation spectrums can be a good tool for monitoring dehydration in onions.
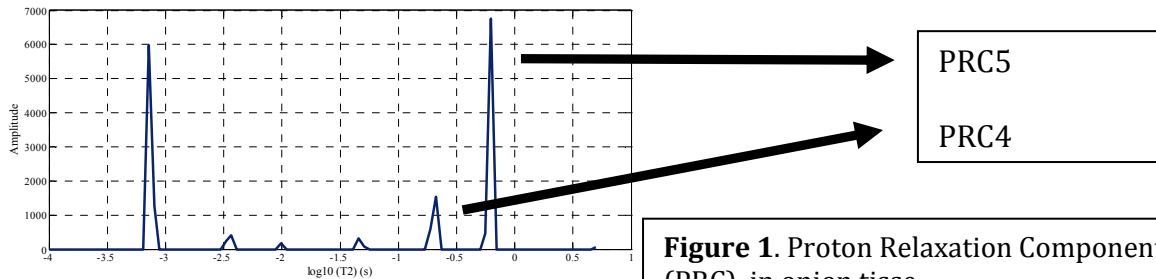
Figure 1. Proton Relaxation Components (PRC) in onion tisse
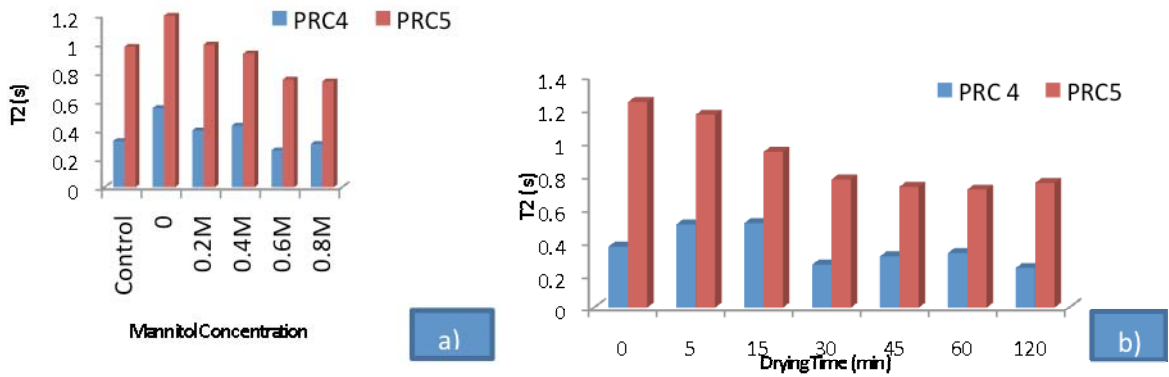
Figure 2. Effect of osmotic dehydration (a) and air drying (b) on proton relaxation components in

Non invasive imaging of ^{13}C labeled metabolites in barley seeds using geHMQC

Gerd Melkus[1,2], Johannes Fuchs[1,2], Hardy Rolletschek[2], Peter M. Jakob[1,3]
and Ljudmilla Borisjuk[2]

[1] Department of Experimental Physics 5 (Biophysics), University of Würzburg, Würzburg, Germany
[2] Institute of Plant Genetics and Crop Plant Research, Gatersleben, Germany
[3] Research Center for Magnetic Resonance Bavaria e.V., Würzburg, Germany

Abstract:

Interest in nutrient loading of seeds is fuelled by its central importance to plant reproductive success and human nutrition. The uptake of substrates, their time resolved distribution and the metabolic flux are important to understand the metabolism in crop seeds [1]. In this study 100 mM full labeled ^{13}C sucrose (Suc) solved in puffer solution was used in combination NMR methods to image its uptake, the spatial distribution and the metabolic products in barley seeds.

The experiments were performed on a 17.6 T WB Bruker spectrometer with a 1 T/m gradient system and a double resonant ^{1}H/^{13}C coil (inner diameter = 5 mm). For sensitive ^{13}C sucrose imaging a gradient enhanced Heteronuclear Multiple Quantum Coherence (geHMQC) editing scheme was used to detect the protons connected to ^{13}C carbons and the timing was adjusted to the ^{1}J-coupling constant of Suc ($\tau = 1/2J$) (see Fig. 1) [2]. For complete suppression of higher order coherences of the water resonance the sequence was extended with VAPOR presaturation scheme [3]. Parameters: TR = 1.5 s, number of experiments = 500 (hanning-weighted k-space acquisition), water suppression bandwidth = 500 Hz, MQC-Gradients G1 : G2 : G3 = 2 : 2 : -1, spatial resolution = 0.5 x 0.5 x 2.5 mm^3, duration for one experiment = 12 min 33s.

The indirect detection of the ^{13}C carbons improved the sensitivity of the experiment over direct ^{13}C detection (data not shown). Time resolved images of ^{13}C sucrose uptake and metabolic products could be acquired. Fig. 2 shows the barley reference image and the distribution of ^{13}C Suc and ^{13}C alanine (Ala) after 14 h administration of ^{13}C labeled sucrose. geHMQC spectra from the endospermal and the seed coat region can be seen in Fig. 3 showing sufficient SNR and optimal water suppression.

Fig.2 Reference and metabolic images from ^{1}H coupled to ^{13}C after 14 h administration of 100 mM ^{13}C labeled Suc

Fig.1 ge-HMQC spectroscopic imaging pulse sequence with water presaturation and ^{13}C decopuling

Fig.3 geHMQC spectra from (a) the endosperm and (b) the pericarp region (see Fig. 2).
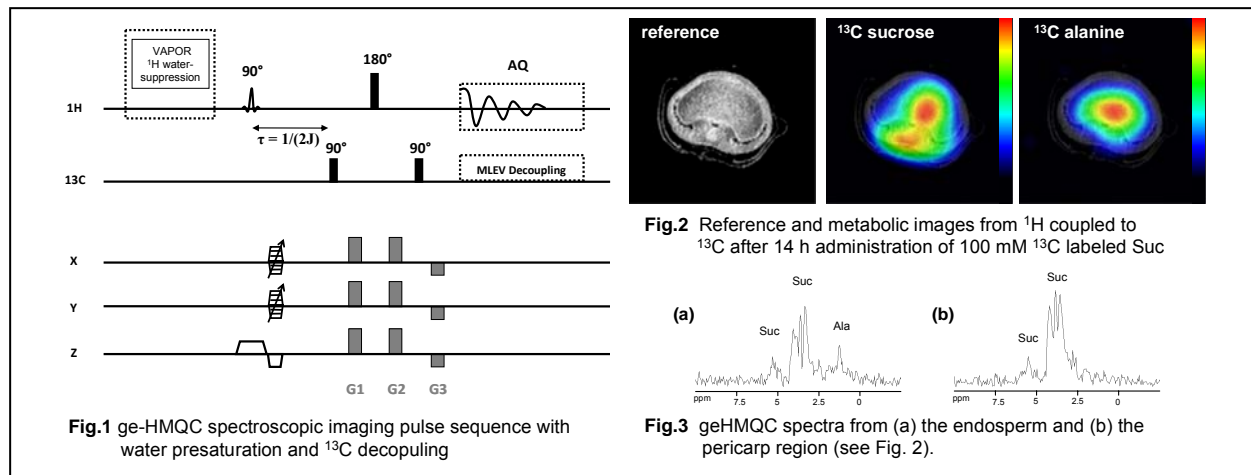
[1] Patrick and Offler, *J. Exp. Bot.* **52** (2001): 551-564.
[2] Tkác et al., *Magn Reson Med*. **41** (1999): 649-656.
[3] Ruiz-Cabello et al., *J Magn Reson*. **100** (1992): 282-302.

Investigating embolism repair of xylem vessels in grape plants using proton magnetic resonance imaging

Mingtao Wang[1], Uwe G. Hacke[2], Melvin T. Tyree[2] and Roderick E. Wasylishen[1]

[1] Department of Chemistry, University of Alberta, Edmonton, Canada
[2] Department of Renewable Resources, University of Alberta, Edmonton, Canada

Abstract:

Proton magnetic resonance imaging (MRI) experiments were used to visualize individual xylem vessels in the stems of grape plants. Proton MRI images of 20 μm resolution were acquired in ~3-6 minutes, allowing noninvasive *in situ* monitoring of changes in the functional status of individual vessels. The experiments were set so that the xylem pressure potential could be adjusted (Fig.1). The time required for recovery of all air-filled (embolised) vessels, and the rate of refilling individual embolised vessels, were investigated using multiple-slice FLASH MRI experiments. The progress of the meniscus for individual emboli was observed (Fig.2); the rate of the progress was found to be mainly controlled by the position of the vessel. This indicates that air diffusion through liquid from the surface of the bubble inside the plant to the surface of the stem, driven by the concentration gradient, is the predominant mechanism for movement of the dissolved gas during embolism repair.
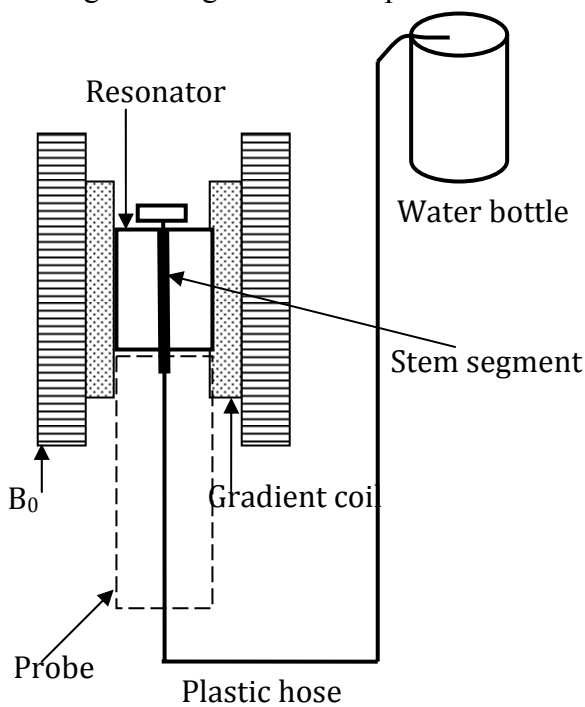
Fig.1 Schematic of the experimental setup.
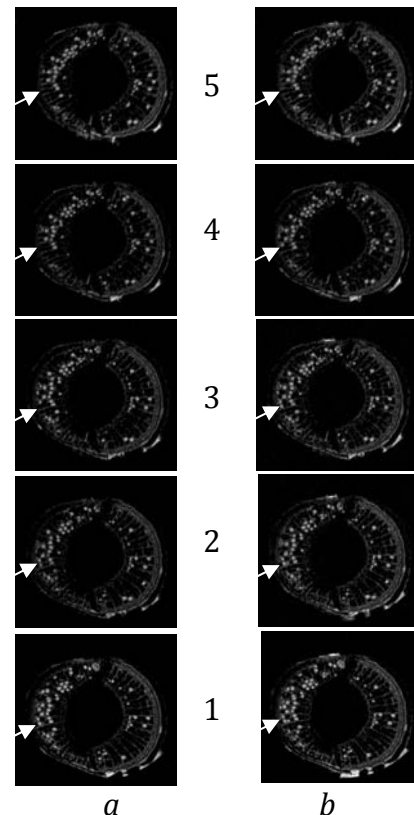
Fig.2 Progress in refilling of embolised vessels. Two experiments (*a* and *b*) were conducted 30 minutes apart. Images of slices 1 and 5 indicate the lowest and highest positions, respectively, along the stem. The white arrows highlight the progress of water in one vessel, from slice 2 in *a* to slice 3 in *b*, in 30 minutes.

Water (re)distribution phenomena in savoury products – Understanding the effect of ingredients and processing on ageing

Gert-Jan W. Goudappel[+], Song Miao[+], Andreas Mayr[++], Monika Schaenzel[++]

[+] Unilever R&D Vlaardingen, PO Box 114, 3130 AC Vlaardingen, The Netherlands
[++] Unilever Deutschland GmbH, Centre of Excellence Dry Foods, Knorrstr. 1, 74074 Heilbronn

Migration of water inside dry savoury products during (water based) processing and upon storage determines their physical properties and is the main driver of glassy – rubbery transitions and (re)crystallization phenomena. During processing these effects are responsible for processability of wet masses (e.g. stickiness) for powder forming and upon storage for (re)crystallization (e.g. caking).

This migration of the water during processing and upon storage is poorly understood and therefore hampers rational adjustment of the formulation and processing conditions of the wet mass to control these physical properties.

NMR T_2 relaxation studies were used in combination with A_w sorption isotherms and SEM analysis to investigate the water migration and morphology of the wet mass. The single raw ingredients corn starch, salt, sugar, MSG and respective ingredient mixtures as well as the full formulation were processed on lab-scale as function of stirring time and/or water content.

Results showed that the equilibrium time of the water migration is affected both by multiple water gradients between individual ingredients (A_w differences) as well as differences in water T_2 mobility. At longer storage time morphology change behaviour caused an increase in both A_w and T_2.

Low-field integrated rheo-TD-NMR on industrial media – experiences and challenges

Edme H. Hardy[1], Dirk Mertens[1,2], Karl-Heinz Wassmer[3], Nikolaus Nestle[3]

[1] Universität Karlsruhe, SRG 10-2 „Kombination von In-situ Messmethoden für die Prozessanalytik",
Karlsruhe, Germany
[2] present adress: Bruker Optics, Rheinstetten, Germany
[3] BASF SE Ludwigshafen, Ludwigshafen, Germany

Abstract:

Over the last few years, substantial progress was achieved in the implementation of pulsed-field-gradient (PFG)-NMR on low-field NMR systems with permanent magnets. Equipped with a flow-through probe head, such instruments can be used in capillary NMR-rheometry. In contrast to conventional capillary rheometry, the NMR experiment needs no variation of flow rates but measures the velocity probability density function (VPDF) under constant flow conditions. If the pressure drop over the capillary is known, the flow curve can be determined over the shear-rate range present in the flowing sample.

The possibility to work under constant flow conditions, without protruding sensor devices and on a closed flow-through tube makes the NMR-rheometry experiment very attractive for online and inline applications. The method was successfully demonstrated on a range of test samples as well as on some industrial polymer products. The diagram in Fig. 1 shows typical results (blue circles: olive oil, green triangles: acrylic-based technical polymer dispersion, red diamonds: poly-vinylpyrrolidone (PVP) solution, magenta squares: mayonnaise, black crosses: reference measurements by conventional rotation rheometry).
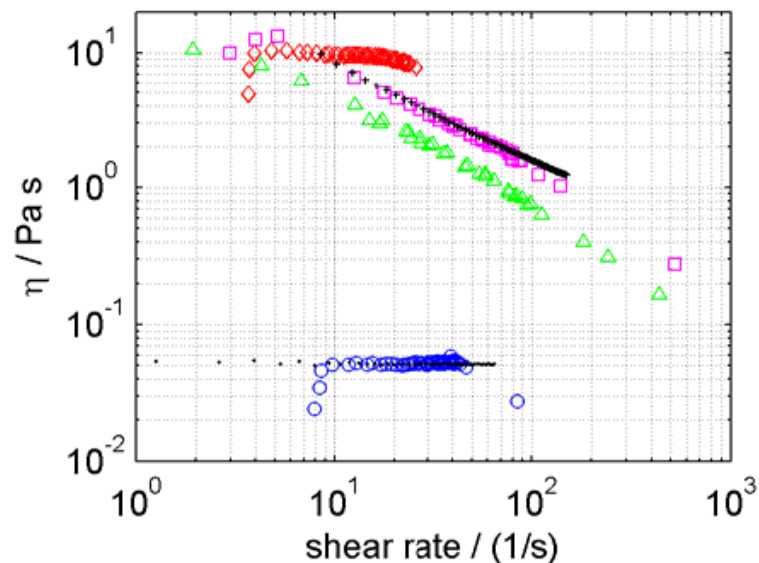
Fig. 1: Flow curves measured by low-field rheo-NMR.

Many industrial products exhibit complex magnetization decay curves which provide additional information about the sample from their relaxation times. The contribution explores possibilities and challenges in combining rheological and relaxation-time information in low-field NMR with a special emphasis on the sensitivity of CPMG curves to flow artifacts.

Non-Invasive Depth-Profiling of Walls by Portable Nuclear Magnetic Resonance

<u>A. Haber</u>[1], B. Blümich[1], F. Casanova[1], V. Boardman[2], A. de Vita[3], E. Del Federico[2]

[1] ITMC, RWTH Aachen University, D-52056 Aachen, Germany
[2] Pratt Institute, Department of Mathematics and Science, Brooklyn 11205, New York, USA
[3] British School of Rome, 00197 Rome, Italy

Abstract:

A compact and mobile single-sided ^{1}H NMR sensor, the NMR-MOUSE®, has been employed to characterize non-invasively the layer structure of historic walls. Following laboratory tests on a mock-up hidden painting, paint and mortar layers were studied at Villa Palagione and the Seminario Vascovile di Sant' Andrea in Volterra. Different paint and mortar layers could be identified. In the detached and restored fresco "Madonna di Carcere" from the Fortezza Medicea in Volterra, paint and mortar layers could be discriminated and differences in the adhesive that fixes the fresco to its support were found for restored and original sections. A newer and larger version of the NMR-MOUSE with 25 mm depth access was used in Herculaneum to measure moisture profiles through the Mosaic of Neptune and Amphitrite revealing large differences in moisture content of the tesserae and the same moisture content in the supporting mortar. These investigations of intact walls encourage the use of the portable and single-sided NMR technology for noninvasive studies of the layer structure and conservation state of historic walls.

1. Proietti, N., et al., *Fresco paintings studied by unilateral NMR..* Journal of Magnetic Resonance, **177 (**2005**)**: p. 111-117.
2. Bluemich, B., et al., Degradation of historical paper: nondesctructive analysis by the NMR-MOUSE. Journal of Magnetic Resonance, 161 (2003), p. 204-209.

Magnetic Resonance Analysis of Biopolymer Physically Crosslinked Gels

Hilary T. Fabich[1,2], Joseph D. Seymour[1,2] , Gill G. Geesey[2], and Sarah L. Codd[2,3]

[1] Dept. of Chemical and Biological Engineering, Montana State University, Bozeman, MT, USA
[2] Center for Biofilm Engineering, Montana State University, Bozeman, MT, USA
[3] Dept. of Mechanical and Industrial Engineering, Montana State University, Bozeman, MT, USA

Abstract:

This project is an undergraduate research experience funded by Montana INBRE and the Undergraduate Scholars Program (USP) at Montana State University. Using the non-invasive properties of nuclear magnetic resonance (NMR), the way water diffuses and relaxes in a biopolymer gel can be examined. Understanding the molecular role of water in physical gelation processes and water distribution impacts on gel material properties is a topic of long standing interest with potential to enhance applications such as drug delivery, tissue engineering [1] and understanding of biological function [2]. Two types of physically crosslinked gels are studied in this work; thermoreversible xanthan gum/locust bean gum (XG/LBG) gels and divalent cation mediated alginate gels. In previous studies on XG/LBG gels, the T_1 properties of the hydrogen molecules on the polymer backbone have been analyzed to characterize changes in dynamics due to thermoreversible gelation [3]. The water T_1, T_2, and diffusion measured in these gels as a function of temperature is near that of free water an indication of limited water restriction or binding due to gelation. The T_2 measurements follow a temperature dependence very similar to that of pure water. The T_1 and diffusion measurements, however, seem to show a slight, but distinct change from the data trend of pure water with temperature. That change is expected to become more prevalent as the weight percent of polymer is increased [4]. The second gel of interest, alginate, and the impact of Ca^{2+} on gelation has been extensively studied using NMR [1, 5-8]. Our interest in this system stems from the role of acetylated and deacetylated alginates in biofilm formation [2] and NMR data on the relaxation and diffusion of water in model alginates are providing baseline data for exploring the role of water in biofilm formation.

References
1. N.E. Simpson *et al.*, *Biomaterials* **24** 4941-4948 (2003).
2. D.E. Nivens *et al.*, *J. Bacteriology* **183**(3) 1047-1057 (2001).
3. S. Richter, T. Brand and S. Berger, *Macromol. Rapid Commun.* **26** 548-553 (2005).
4. T.D. Hart *et al. Enzyme and Microb. Technol.* **24** 339-347 (1999).
5. K. Potter, T.A. Carpenter and L.D. Hall, *Carbohydrate Research* **246** 43-49 (1993).
6. N. Nestle and R. Kimmich, *Colloids and Surfaces A* **115** 141-147 (1996).
7. J.M. Duez *et al.*, *Mag. Reson. Chem.* **38** 324-330 (2000).
8. B.P. Hills *et al.*, *Mag. Reson. Chem.* **38** 719-728 (2000).

Magnetic Resonance Elastography study of 3D force chains

Eiichi Fukushima[1] and Lori Sanfratello[2]

[1] ABQMR, Albuquerque, USA
[2] New Mexico Resonance, Albuquerque, USA

Abstract:

The issue of how force is transmitted through granular assemblies is a fertile area of research even in the 21st century. The basic problem is the lack of experimental methods to make measurements in 3D assemblies. Experiments in 2D and indirect evidence from 3D lead to the supposition that force is transmitted through the assembly in heterogeneous networks in which only a small fraction of the particles bear much of the force.
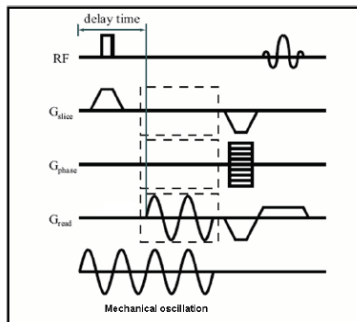
We developed a novel extension of Magnetic Resonance Elastograpy (MRE)[1] to image such force chains in 3D. An acoustic wave impinges on the granular assembly and an oscillating linear magnetic field gradient is imposed on the system in synchrony with the acoustic oscillation as shown at left. We hypothesized that the particles taking part in transmitting force through the system will oscillate with much larger amplitudes, thus accumulating more phase shifts, than those particles that are not involved in force transmission. The acoustic wavelength is chosen to be long compared to the sample. Our phase images (below, left) show such structures. Further, the structures at the boundaries (the lighter marks in the figure below, right) are consistent with force chains at boundaries as recorded with carbon paper (the darker marks).[2]

We developed computer codes and algorithms to determine the distribution of chain-lengths, where a chain is taken to be a relatively straight section between branching points. These tools were used to analyze both 2D photo-elastic data[3] and our 3D MRE data. Such analyses revealed that the distribution of chain-lengths decays exponentially with the characteristic decay length depending on the manner in which the system is stressed. For example, an isotropically compressed system has a smaller decay length than that of a system which is in a pure shear state (compression in one direction and expansion in the other). Therefore, decay lengths of chain-length distributions are meaningful quantitative measures that characterizes granular assemblies.
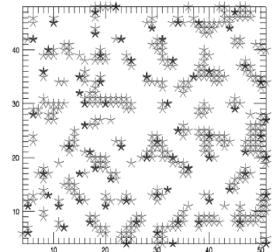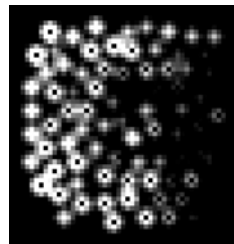
1. W. Denk, R. M. Keolian, S. Ogawa, and L. W. Jelinski. Proc. Natl. Acad. Sci. **90** (1993) 1595-1598; R. Muthupillai, D. J. Lomas, P. J. Rossman, J. F. Greenleaf, A. Manduca, and R. L. Ehman, Science **269** (1995) 1854-1857.
2. L. Sanfratello, E. Fukushima, and R. P. Behringer. Gran.Matt., **11**(2009) 1–6.
3. L. Sanfratello and E. Fukushima, "Distribution of Force Chain Lengths: A Useful Statistic that Characterizes Granular Assemblies," submitted to Granular Matter, June, 2009.

Hyperpolarized [129]Xe NMR Spectroscopy for Investigations of Porous Polymers

L. Utiu[1] , C. Melian[1] , S. Appelt[1,2] and B. Bluemich[1]

[1] Institute of Technical and Macromolecular Chemistry, RWTH Aachen University, Germany
[2] Central Institute for Electronics, Research Centre Jülich, Germany

Abstract:

The high sensitivity of the chemical shielding interaction of Xenon atoms to its local chemical environment and the large [129]Xe NMR signals attainable through Rubidium optical pumping [1] have motivated the use of the laser-hyperpolarized [129]Xe as a probe for porous materials. Porous polymers are of great interest in technological and scientific application [2,3]. For instance, they have many applications as oxygenating membranes, proton exchange membranes for fuel cells, and drug delivery systems.

The aim of this work is to show that Xenon can be used as a tracer for structure information and for direct observation of the exchange of hyperpolarized [129]Xe molecules penetrating in and out of the pore network. This study reports the application of one- and two-dimensional NMR spectroscopy with hyperpolarized [129]Xe to investigate the structure and the morphology of porous polymers.

1. M. Goodson, *J. Magn. Reson.* **155** (2002)157-216.
2. V-V. Telkki, J. Lounila and J. Jokisaari, *Phys. Chem. Chem. Phys.* **8** (2006) 2072-2076.
3. T.G. Walker and W. Harper, *Rev. Mod. Phys.* **69** (1997) 629-642.

P98

Para-hydrogen-induced polarization in heterogeneous hydrogenation reactions

Qingxia Gong, Walter Leitner, Jürgen Klankermayer, Bernhard Blümich

qgong@mc.rwth-aachen.de

Institut für Technische und Makromolekulare Chemie, RWTH Aachen University

Para-hydrogen induced polarization (PHIP) in NMR has become an established tool for the investigation of reaction mechanisms and kinetics of homogeneous catalysed hydrogenation reactions [1-3]. Recently, Igor V. Koptyug and co-workers demonstrated that PHIP effects can also be observed in heterogeneous catalytic systems [4-5]. Based on this investigation, the first signal enhanced gas-phase imaging was achieved with the use of supported Pd and Pt catalysts [6-7]. The application of PHIP NMR in heterogeneous systems offers the possibility to develop a novel powerful analytical tool for investigations on catalytic processes.

In a recent study we worked on the application of PHIP NMR in systems with supported ionic liquid phase (SILP) catalysts. As a model reaction we investigated the hydrogenation of propylene with various catalysts in a continuous micro-reactor setup. With the analytical setup, the catalyst's activation (Fig. 1) and the influence of variations of the reactions conditions (Fig. 2) were studied.
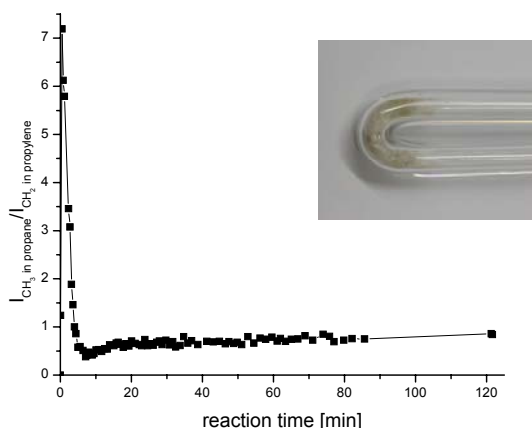
Figure 1. Activation of $[Rh(cod)(PPh_3)_2][NTf_2]$ in SILP using 30ml/min of p-H_2 and 20ml/min of propylene at 75°C
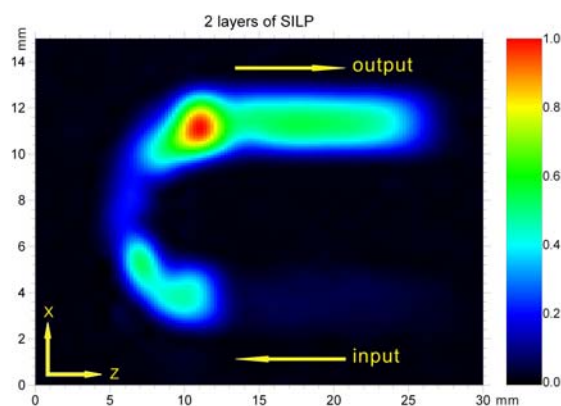
Figure 2. Chemical shift image of a 2-layer packed SILP reaction system after catalyst's activation

[1]   M. Stephan, O. Kohlmann, H. G. Niessen, A. Eichhorn, J. Bargon (2002) *Magn. Reson. Chem.,* **40**, 157-160.
[2]   P. Hübler, R. Giernoth, G. Kümmerle, J. Bargon (1999) *J. Am. Chem. Soc.,* **121**, 5311-5318.
[3]   R. W. Adams, J. A. Aguilar, K. D. Atkinson, M. J. Cowley, P. I. P. Elliott, S. B. Duckett, G. G. R. Green, I. G. Khazal, J. López-Serrano, D. C. Williamson (2009) *Science*, **323**, 1708-1711.
[4]   I. V. Koptyug, K. V. Kovtunov, S. R. Burt, M. S. Anwar, C. Hilty, S. Han, A. Pines, R. Z. Sagdeev (2007) *J. Am. Chem. Soc.,* **129**, 5580-5586.
[5]   K. V. Kovtunov, I. E. Beck, V. I. Bukhtiyarov, I. V. Koptyug (2008) *Angew. Chem. Int. Ed. Engl.,* **47(8)**, 492-1495.
[6]   L. S. Bouchard, K. V. Kovtunov, S. R. Burt, M. S. Anwar, I. V. Koptyug, R. Z. Sagdeev, A. Pines (2007) *Angew. Chem.,* **119**, 4142-4146.
[7]   L. S. Bouchard, S. R. Burt, M. S. Anwar, K. V. Kovtunov, I. V. Koptyug, A. Pines (2008) *Science*, **319**, 442-445.

Chemical Shift of Laser Polarized [129]Xe in BPTI Solution

Geoffry Schrank, Zayd Ma, Brian Saam

Department of Physics, University of Utah, Salt Lake City, USA

Abstract:

We measure the NMR chemical shift of laser polarized [129]Xe in wild type, Y35G, Y23A, and F45S BPTI (Bovine Pancreatic Trypsin Inhibitor) solutions of varying concentration. Our experimental technique uses [129]Xe in unprecedented low concentrations as a biosensor. The results provide structural information concerning the aforementioned proteins[5,6].

Xe reversibly binds to protein via weak van der Waals forces resulting in a chemical exchange between solution and protein-bound states. In the fast exchange limit, one detects a single peak that is chemically shifted as a function of protein concentration. Specific binding occurs at hydrophobic sites with high Xe affinity;

Figure 1: Chemical shift of [129]Xe resonance vs. protein concentration. Shifts are referenced to buffer solution. Data shows a linear dependence at low concentrations which is consistent with single site fast exchange interaction. The slopes are proportional to binding strength assuming the same chemical shifts for all bound states.

non-specific binding refers to all other interactions. BPTI is a good model system to study protein dynamics using [129]Xe NMR as a probe. It is extensively studied and has many well characterized mutants. Tilton *et al.* did the first NMR studies of Xe in hemoglobin and myoglobin solution in 1982 with 1-10 atm of thermally polarized Xe and ~1-10 mM concentration of protein[1]. Recently, Rubin *et al.* used 1 to 10 mM of dissolved laser polarized [129]Xe in maltose binding protein solution to study Xe binding affinity.[4]

We use a flow through polarizer that outputs 10 sccm of [129]Xe hyperpolarized to ~10%. Hyperpolarized gas boosts signal to noise and, coupled with a high resolution NMR spectrometer, enables us to measure sub-ppm chemical shifts to ±0.03 accuracy at very low Xe and protein concentrations (0-0.8 mM). To deliver the gas to the protein solution we employ a membrane system suggested by Baume *et al.*[2] This system allows gas to diffuse into solution without bubbling with concentration in solution estimated at 92-96 μM.

In accordance with the single-site fast exchange regime, we observe chemical shifts that are linear in protein concentration (Fig. 1). Consistent with a rigid lattice and a manufactured binding site, the mutants Y23A and F45S demonstrate strong binding (.56±.05 and .47±.07 ppm/mM, respectively) relative to wild type and Y35G (.15±.02 and .10±.07 ppm/mM, respectively). Wild type is believed not to have a specific binding site. Other experiments on Y35G have demonstrated both a hydrophobic cavity and extensive solution-phase motion[3]. The demonstrated weak binding supports the notion that only a small fraction of solution-phase Y35G is in a conformation such that the cavity is accessible to Xe.

References:
1. R. F. Tilton, Jr. and I. D. Kuntz, Jr. *Biochemistry* **21,** 6850 (1982)
2. Baume *Angew. Chem. Int. Ed.* 2006, **45**, 7282-7284
3. S. A. Beeser, *J. Mol. Biol.*, **269**, 154-164v
4. S. M. Rubin, S-Y. Lee, E. J. Ruiz, A. Pines, D. Wemmer, *J. Mol. Biol.* 2002, **322**, 425-440
5. W. M. Hanson *et al.*, *J. Mol. Biol.* 2007, **366**, 230-243
6. A. T. Danishefsky *et al.*, *Protein Sci.* 1993, **2**, 577-587

Author Index List

Author Index List

Author Index List

Author Index List

Author Index List

Author Index List

Author Index List

Participant List

Adachi, Satoru
University of Tsukuba
Ibaraki, Japan
adachi@mrlab.frsc.tsukuba.ac.jp

Adair, Alex
University of New Brunswick
Fredericton, NB, Canada
adair.alex@unb.ca

Adams, Kristl
Lawrence Livermore Nat'l Lab
Livermore, CA, USA
kristl@llnl.gov

Adolphi, Natalie
University of New Mexico
Albuquerque, NM, USA
NAdolphi@salud.unm.edu

Ailion, David
University of Utah
Salt Lake City, UT, USA
dailion@physics.utah.edu

Akpa, Belinda
University of Illinois
Chicago, IL, USA
akpa@uic.edu

Altan, Aylin
University of California
Davis, CA, USA
aaltan@ucdavis.edu

Altobelli, Stephen
New Mexico Resonance
Albuquerque, NM, USA
salto@nmr.org

Amor, Nadia
ITMC RWTH
Aachen, Germany
namor@mc.rwth-aachen.de

Appelt, Stephan
Forschungszentrum Juelich
Juelich, Germany
st.appelt@fz-juelich.de

Peter Aptaker
Laplacian Limited
Abingdon, Oxon, UK
psa@laplacian.co.uk

Balcom, Bruce
University of New Brunswick
Fredericton, NB, Canada
bjb@unb.ca

Baldo, John
Varian NMR Instruments
Fort Collins, CO, USA
john.baldo@varianinc.com

Basser, Peter
NIH
Bethesda, MD, USA
pjbasser@helix.nih.gov

Behr, Volker
University of Würzburg
Würzburg, Germany
behr@physik.uni-wuerzburg.de

Beyea, Steven
National Research Council
Halifax, NS, Canada
steven.beyea@nrc-cnrc.gc.ca

Bizunok, Sergey
Bruker Biospin
Natick, MA, USA
Sergey.Bizunok@bruker-biospin.com

Blackband, Stephen
University of Florida
Gainesville, FL, USA
blackie@mbi.ufl.edu

Blank, Aharon
Technion
Haifa, Israel
ab359@tx.technion.ac.il

Bluemler, Peter
Forschungszentrum Juelich
Juelich, Germany
p.bluemler@fz-juelich.de

Blümich, Bernhard
RWTH-Aachen/ITMC
Aachen, Germany
bluemich@mc.rwth-aachen.de

Bouchard, Louis
University of California
Los Angeles, CA, USA
bouchard@chem.ucla.edu

Bray, Joshua
Dalhousie University
Halifax, NS, Canada
jmbray@dal.ca

Britton, Melanie
University of Birmingham
Birmingham, UK
m.m.britton@bham.ac.uk

Broadbent, Amber
Montana State University
Bozeman, MT, USA
amber.broadbent@coe.montana.edu

Brosten, Tyler
Montana State University
Bozeman, MT, USA
tyler.brosten@coe.montana.edu

Brown, Jennifer
Montana State University
Whitehall, MT, USA
jbrown@coe.montana.edu

Busse, Scott
Montana State University
Bozeman, MT, USA
busse@chemistry.montana.edu

Callaghan, Paul
Victoria University
Wellington, New Zealand
paul.callaghan@vuw.ac.nz

Cassanova, Federico
ITMC - RWTH - Aachen
Aachen, Germany
fcasanova@mc.rwth-aachen.de

Chavez, Lana
ABQMR
Albuquerque, NM, USA
lchavez@abqmr.com

Chen, Ya Ying
University of Cambridge
Cambridge, United Kingdom
yyc27@cam.ac.uk

Ciobanu, Luisa
Neurospin/CEA
GIF/YVETTE, France
luisa.ciobanu@cea.fr

Participant List

Codd, Sarah
Montana State University
Bozeman, MT, USA
scodd@coe.montana.edu

Coy, Andrew
Magitek
Wellington, New Zealand
andrew@magritek.com

Creber, Sarah
University of Cambridge
Canbridge, United Kingdom
sarah.creber@gmail.com

Danieli, Ernesto
ITMC - RWTH - Aachen
Aachen, Germany
edanieli@mc.rwth-aachen.de

Demas, Vasiliki
T2 Biosystems
Cambridge, MA, USA
vdemas@t2biosystems.com

Driessle, Toni Michael
University Würzburg
Würzburg, Germany
toni@driessle.de

Dvinskikh, Sergey
Royal Institute of Technology
Stockholm, Sweden
sergey@physchem.kth.se

Evertz, Loribeth
Montana State University
Bozeman, MT, USA
loribeth.evertz@coe.montana.edu

Fabich, Hilary
Montana State University
Bozeman, MT, USA
hilary.fabich@coe.montana.edu

Feindel, Kirk
National Research Council
Halifax, NS, Canada
kirk.feindel@nrc-cnrc.gc.ca

Flint, Jeremy
University of Florida
Gainesville, FL, USA
jer1984@ufl.edu

Fridjonsson, Einar
Montana State University
Bozeman, MT, USA
einar.fridjonsson@coe.montana.edu

Fuchs, Johannes
University of Würzburg
Würzburg, Germany
fuchsj@physik.uni-wuerzburg.de

Fukushima, Eiichi
ABQMR
Albuquerque, NM, USA
eiichi@abqmr.com

Garcia, Sandra
University of California
Davis, CA, USA
spgarcia24@gmail.com

Gehrcke, Jan-Philip
University of Würzburg
Würzburg, Germany
jgehrcke@googlemail.com

Gjersing, Erica
University of California Davis
Davis, USA
elgjersing@ucdavis.edu

Gladden, Lynn
University of Cambridge
Cambridge, United Kingdom
gladden@cheng.cam.ac.uk

Gloeggler, Stefan
RWTH Aachen University
Aachen, Germany
stgloeggler@gmx.de

Goerke, Ute
CMRR University of Minnesota
St. Louis Park, MN, USA
ute@cmrr.umn.edu

Gong, Qingxia
RWTH Aachen University
Aachen, Germany
qgong@mc.rwth-aachen.de

Goudappel, Gert-Jan
Unilever Research
Vlaardingen, Netherlands
gert-jan.goudappel@unilever.com

Gross, Dieter
Bruker Biospin
75015 Bretten, Germany
dieter.gross@bruker-biospin.de

Haber, Agnes
RWTH Aachen University
Aachen, Germany
ahaber@mc.rwth-aachen.de

Haber-Pohlmeier, Sabina
RWTH Aachen University
Aachen, Germany
s.haber-pohlmeier@fz-juelich.de

Haishi, Tomoyuki
MRTechnology
Tsukuba, Japan
haishi@mrtechnology.co.jp

Halliday, Nicola
University of Birmingham
Birmingham, United Kingdom
nah136@bham.ac.uk

Halse, Meghan
Victoria University
Wellington, New Zealand
meghan.halse@vuw.ac.nz

Han, Hui
University of New Brunswick
Fredericton, NB, Canada
a023p@unb.ca

Handa, Shinya
National Institute for Environmental
Studies
Tsukuba, Japan
handa@mrlab.frsc.tsukuba.ac.jp

Henkelman, Mark
Hospital for Sick Children
Toronto, ON, Canada
mhenkel@phenogenomics.ca

Herberg, Julie
LLNL
Livermore, CA, USA
herberg1@llnl.gov

Hifumi, Hiroki
Daiichi Sankyo
Tokyo, Japan
hifumi.hiroki.px@daiichisankyo.co.jp

Participant List

Holland, Daniel
University of Cambridge
Cambridge, United Kingdom
djh79@cam.ac.uk

Holte, Laura
Doty Scientific, Inc.
Columbia, SC, USA
laura@dotynmr.com

Horiga, Masafumi
University of Tsukuba
Ibaraki, Japan
horiga@mrlab.frsc.tsukuba.ac.jp

Hugon, Cedric
LSDRM CEA Saclay
Gif sur Yvette, France
cedric.hugon@cea.fr

Hullihen, C. Richard
m2m Imaging Corp
Highland Hts, OH, USA
rhullihen@m2mimaging.com

Hunter, Mark
MacDiarmid VUW
Wellington, New Zealand
mark.hunter@vuw.ac.nz

Hurlimann, Martin
Schlumberger-Doll Research
Newton, MA, USA
hurlimann@slb.com

Jacobs, Austin
Montana State University
Bozeman, MT, USA
Austin.jacobs@coe.montana.edu

Jacobs, Russell
Caltech – Beckman Institute
Pasadena, CA, USA
rjacobs@caltech.edu

Johns, Mike
University of Cambridge
Cambridge, United Kingdom
mlj21@cam.ac.uk

Kampf, Thomas
University Würzburg
Würzburg, Germany
thomas.kampf@physik.uni-wuerzburg.de

Kanyha, Paul
Tecmag
Houston, TX, USA
info@tecmag.com

Kobayashi, Kyohei
University of Tsukuba
Ibaraki, Japan
kobayashi@mrlab.frsc.tsukuba.ac.jp

Kolz, Juergen
University of Cambridge
Cambridge, United Kingdom
jk463@cam.ac.uk

Komlosh, Michal
NICHD/NIH
Bethesda, MD, USA
komloshm@mail.nih.gov

Koptyug, Igor
Int. Tomography Center RAS
Novosibirsk, Russia
koptyug@tomo.nsc.ru

Kose, Katsumi
University of Tsukuba
Tsukuba, Japan
kose@bk.tsukuba.ac.jp

Kueppers, Markus
ITMC, RWTH Aachen
Aachen, Germany
mkueppers@mc.rwth-aachen.de

Kuethe, Dean
New Mexico Resonance
Albuquerque, NM, USA
dkuethe@nmr.org

Lee, Choong-Heon
UF McKnight Brain Institute
Gainesville, FL, USA
ldotcom@ufl.edu

Leisen, Johannes
Georgia Institute of Technology
Atlanta, GA, USA
johannes.leisen@ptfe.gatech.edu

Lingwood, Mark
University of California
Santa Barbara, CA, USA
mlingwood@chem.ucsb.edu

Lurie, David
University of Aberdeen
Aberdeen, United Kingdom
d.lurie@abdn.ac.uk

Ma, Zayd
University of Utah
Salt Lake, City, UT, USA
zayd.ma@utah.edu

Madelin, Guillaume
MacDiarmid Institute VUW
Wellington, New Zealand
guillaume.madelin@vuw.ac.nz

Magin, Richard
Univ. of Illinois at Chicago
Chicago, IL, USA
rmagin@uic.edu

Mair, Ross
Harvard University
Cambridge, MA, USA
rmair@fas.harvard.edu

Majors, Paul
Battelle Pacific Northwest Labs
Richland, WA, USA
paul.majors@pnl.gov

Maneval, James
Bucknell University
Lewisburg, PA
maneval@bucknell.edu

Manz, Bertram
Magritek Limited
Wellington, New Zealand
bertram@magritek.com

McAloon, Michael
University of New Brunswick
Fredericton, NB, Canada
y031m@unb.ca

McCarney, Evan
Magritek Limited
Wellington, New Zealand
andrew@magritek.com

McCarthy, Michael
University of California
Davis, CA, USA
mjmccarthy@ucdavis.edu

Participant List

McDowell, Andrew
ABQMR
Albuquerque, NM, USA
mcdowell@abqmr.com

Melkus, Gerd
University of Würzburg
Würzburg, Germany
melkus@physik.uni-wuerzburg.de

Mikac, Ursa
IJS
Ljubjana, Slovenia
urska.mikac@ijs.si

Milne, Michelle
Washington University
Saint Louis, MO, USA
mmilne@physics.wustl.ed

Minard, Kevin
Pacific Northwest National Lab
Richland, WA, USA
kevin.minard@pnl.gov

Mitchell, Jonathan
University of Cambridge
Cambridge, United Kingdom
jm600@cam.ac.uk

Muir, Colleen
University of New Brunswick
Fredericton, NB, Canada
colleen.muir@unb.ca

Munasinghe, Jeeva
National Institutes of Health
Bethesda, MD, USA
munasinj@mail.nih.gov

Nakayama, Tadaaki
University of Tsukuba
Ibaraki, Japan
nakayama@mrlab.frsc.tsukuba.ac.jp

Navon, Gil
Tel Aviv University
Tel Aviv, Israel
navon@post.tau.ac.il

Nestle, Nikolaus
BASF SE Ludwigshafen
Ludwigshafen, Germany
nikolaus.nestle@physik.tu-darmstadt.de

Nevo, Uri
Tel Aviv University
Tel Aviv, Israel
nevouri@eng.tau.ac.il

Newling, Benedict
University of New Brunswick
Fredericton, NB, Canada
bnewling@unb.ca

Novak, Jan
University of Birmingham
Birmingham, United Kingdom
jxn624@bham.ac.uk

Ogawa, Kyohei
University of Tsukuba
Ibaraki, Japan
kyo.mri@gmail.com

Olaru, Alexandra Maria
ITMC RWTH Aachen
Aachen, Germany
aolaru@mc.rwth-aachen.de

Ozarslan, Evren
National Institutes of Health
Bethesda, MD, USA
evren@helix.nih.gov

Oztop, Mecit Halil
University of California
Davis, CA, USA
hmoztop@ucdavis.edu

Paciok, Eva
ITMC RWTH Aachen
Aachen, Germany
epaciok@mc.rwth-aachen.de

Parasoglou, Prodromos
University of Cambridge
Cambridge, United Kingdom
pap31@cam.ac.uk

Perles-Barbacaru, Teodora-Adriana
Caltech
Pasadena, CA, USA
mflowers@caltech.edu

Petrov, Oleg
University of New Brunswick
Fredericton, NB, Canada
opetrov@unb.ca

Pitts, Simon
AWE
Reading, United Kingdom
simon.pitts@awe.co.uk

Pope, James
Queensland University of Technology
Brisbane, Australia
j.pope@qut.edu.au

Qian, Chunqi
National High Magnetic Field Lab
Tallahassee, FL, USA
qian@magnet.fsu.edu

Rassi, Erik
Montana State University
Bozeman, MT, USA
erik.rassi@coe.montana.edu

Reimer, Jeffery
University of California
Berkeley, CA, USA
reimer@berkeley.edu

Renslow, Ryan
WSU / PNNL
Pullman, WA, USA
rrenslow@gmail.com

Reynaud, Olivier
CEA / Neurospin
Antony, France
olivier.reynaud@cea.fr

Romanenko, Konstantin
University of New Brunswick
Fredericton, NB, Canada
kromanen@unb.ca

Rose, Heather
University of Birmingham
Birmingham, United Kingdom
her407@bham.ac.uk

Saito, Keita
National Cancer Institute
Bethesda, MD, USA
saitok3@mail.nih.gov

Sakellariou, Dimitrios
CEA Saclay
Gif-sur-Yvette, France
dsakellariou@cea.fr

Participant List

Sederman, Andy
MRRC
Cambridge, United Kingdom
ajs40@cam.ac.uk

Sersa, Igor
IJS
Ljubljana, Slovenia
igor.sersa@ijs.si

Seymour, Joseph
Montana State University
Bozeman, MT, USA
jseymour@coe.montana.edu

Shigeki, Ryosuke
University of Tsukuba
Ibaraki, Japan
shigeki@mrlab.frsc.tsukuba.ac.jp

Shinar, Hadassah
Tel Aviv University
Tel Aviv, Israel
shinar@post.tau.ac.il

Song, Yi-Qiao
Schlumberger-Doll Research
Newton, MA, USA
ysong@nmr.mgh.harvard.edu

Stapf, Siegfried
TU Ilmenau
Ilmenau, Germany
siegfried.stapf@tu-ilmenau.de

Steele, Paul
LLLNL
Livermore, CA, USA
psteele@llnl.gov

Subramanian, Sankaran
National Institutes of Health
Bethesda, MD, USA
subu@helix.nih.gov

Trail, John
Magritek
Wellington, New Zealand
johntrail@magritek.com

Utiu, Lavinia
ITMC RWTH Aachen
Aachen, Germany
lutiu@mc.rwth-aachen.de

Utsuzawa, Shin
New Mexico Resonance
Albuquerque, NM, USA
shin@nmr.org

Valori, Andrea
University of Surrey
Guildford, United Kingdom
a.valori@surrey.ac.uk

Van As, Henk
Wageningen University
Wageningen, Netherlands
henk.vanas@wur.nl

Van Dusschoten, Dagmar
ICG-3, Research Center Jülich
Jülich, Germany
d.van.dusschoten@fz-juelich.de

Van Landeghem, Maxime
ITMC RWTH Aachen
Aachen, Germany
Maxime.Van-Landeghem@espci.fr

Vogt, Sarah
Montana State University
Bozeman, MT, USA
sarah.vogt@coe.montana.edu

Walton, Jeffrey
University of California
Davis, CA, USA
jhwalton@ucdavis.edu

Wang, Mingtao
University of Alberta
Edmonton, AB, Canada
mingtao@ualberta.ca

Washburn, Kathryn
Weatherford Laboratories
Trondheim, Norway
kathryn.washburn@weatherfordlabs.com

Windt, Carel
Forschungszentrum Jülich
Jülich, Germany
c.windt@fz-juelich.de

Wintzheimer, Stefan
Research Center MRB
Wuerzburg, Germany
swintzheimer@physik.uni-wuerzburg.de

Xia, Yang
Oakland University
Rochester, MI, USA
xia@oakland.edu

Xiao, Lizhi
China University of Petroleum
Beijing, China
xiaolizhi@cup.edu.cn

Zhen, John
Magritek
Wellington, New Zealand
john@magritek.com

Zheng, Shaokuan
Oakland University
Rochester, MI, USA
zsk3699@hotmail.com

Zick, Klaus
Bruker Biospin
Rheinstetten, Germany
klaus.zick@bruker.de

Zotev, Vadim
Los Alamos National Laboratory
Los Alamos, NM, USA
vzotev@lanl.gov